Louisiana Tech University

Louisiana Tech Digital Commons

Summer 8-2019

Organically Modified Inorganic Nanoparticles for Halochromic Ionophores and Nucleic Acids

William Johnston
Louisiana Tech University

Recommended Citation

ORGANICALLY MODIFIED INORGANIC NANOPARTICLES

FOR HALOCHROMIC IONOPHORES

AND NUCLEIC ACIDS

by

William Johnston, B.S., M.S.

A Dissertation Presented in Partial Fulfillment
of the Requirements for the Degree
Doctor of Philosophy

COLLEGE OF ENGINEERING AND SCIENCE
LOUISIANA TECH UNIVERSITY

August 2019

LOUISIANA TECH UNIVERSITY

GRADUATE SCHOOL

June 27, 2019
Date of dissertation defense

We hereby recommend that the dissertation prepared by

William Johnston

entitled   **ORGANICALLY MODIFIED INORGANIC NANOPARTICLES**

FOR HALOCHROMIC IONOPHORES AND NUCLEIC ACIDS

be accepted in partial fulfillment of the requirements for the degree of

Doctor of Philosophy in Molecular Sciences and Nanotechnology

Dr. Sven Eklund, Supervisor of Dissertation Research

Dr. Gergana Nestorova,
Head of Molecular Sciences and Nanotechnology

Members of the Doctoral Committee:
Dr. Shauray Alam
Dr. Collin Wick
Dr. Patrick O'Neal
Dr. William Wolf

Approved:

Hisham Hegab
Dean of Engineering & Science

Approved:

Ramu Ramachandran
Dean of the Graduate School

ABSTRACT

In this dissertation, four nanoparticle reaction schemes were developed as substrates for halochromic dyes or nucleic acids. The reaction schemes include the use of two substrates: silica nanoparticles and halloysite nanotubes. The protocols can incorporate silica (SiO_2) nanoparticles and halloysite aluminosilicate (AlO_2SiO_2) nanotubes due to the presence of silane groups on the surface of either substrate. The reaction schemes are presented along with detailed protocols which were written to facilitate both reproducibility and to serve as an aid to further study and for easy modification of the protocol to suit a researcher's needs. The data is discussed in the materials section to annotate the stages of synthesis as well as the response of the nanoparticles to varying conditions of pH in both a broad range and a near neutral range.

The first particle scheme was designed to create a particle to measure pH using neutral red, a halochromic ionophore with sensitivity to near neutral pH values. Neutral red has a primary amine which is not required for its halochromic response but is suitable for covalent binding to an aldehyde. The particle synthesis involved functionalization of the inorganic silica surface with an amine. This amine was then covalently bound to a dialdehyde, glutaraldehyde, creating an imine and resulted in a terminal aldehyde functional group on the surface of the particle. The final step of the synthesis was to bind neutral red by its primary amine to the aldehyde functional group. This created a pH sensitive nanoparticle. The particles were stable and did not exhibit leaching or loss of

dye. The particles were sensitive to near neutral pH and observation of UV-vis spectra they could be used to discern changes in pH at a large range by observation of the spectral bands of the protonated and deprotonated states of the halochromic dye.

The second particle developed was a derivation of the first particle. Instead of using a dialdehyde to link two amines, a silane coupling agent was used to provide aldehydes to the surface of the particles. The aldehyde functional group was then linked to the amine functional group of the halochromic dye, neutral red. This protocol produced stable nanoparticles with pH sensitivity, was steps shorter, required fewer reagents, which reduced the cost of development and increased the facility of the protocol.

The third particle developed used an organosilane cross linking agent to produce nanoparticles made of covalently bound silica and the halochromic dyes, neutral red and Nile blue. The particles were highly responsive to changes in pH. Analysis of UV-vis spectral data showed a broad sensitivity to pH by changes in the spectral bands.

The fourth particle developed used the reaction scheme from the second particle. The surface of the inorganic particles was functionalized with aldehyde groups. The aldehyde modified particles were then shown to have the ability to covalently bind nucleic acids and nitrogenous bases.

The synthesis of these particles is presented along with the supporting data. Further areas of study and possible future work are discussed.

APPROVAL FOR SCHOLARLY DISSEMINATION

The author grants to the Prescott Memorial Library of Louisiana Tech University the right to reproduce, by appropriate methods, upon request, any or all portions of this Dissertation. It is understood that "proper request" consists of the agreement, on the part of the requesting party, that said reproduction is for his personal use and that subsequent reproduction will not occur without written approval of the author of this Dissertation. Further, any portions of the Dissertation used in books, papers, and other works must be appropriately referenced to this Dissertation.

Finally, the author of this Dissertation reserves the right to publish freely, in the literature, at any time, any or all portions of this Dissertation.

Author_____

Date _____

TABLE OF CONTENTS

LIST OF TABLES

LIST OF FIGURES

LIST OF SYMBOLS AND ACRONYMS

Silica nanoparticles	SiNPs
Halloysite nanotubes	HNTs
Silica NP core-APTES-Glutaraldehyde-Neutral red nps	SAGN
Halloysite core-APTES-Glutaraldehyde-Neutral red nps	HAGN
Silica-TSB-Neutral red nps	STNR
Halloysite-TSB-Neutral red nps	HTNR
Organosilane-neutral red nps	OSNR
Organosilane-Nile blue nps	OSNB
Silica nanoparticles with nucleic acids	SiNP-NA
Halloysite nanotubes with nucleic acids	HNT-NA
Tetraethoxysilane	TEOS
Aminopropyl triethoxysilane	APTES
Triethoxysilylbutyraldehyde	TSB
Neutral red	NA
Nile blue	NB

ACKNOWLEDGMENTS

First, I would like to thank my advisor, Sven Eklund, for talking me into switching to chemistry when I came back to school to complete a bachelor's degree. When I decided to apply to graduate school, he gave me the opportunity and space to do my research, as well as support and advice over all these years. Thanks as well for all the conversation and discussion over so many subjects. On an academic level this helped me to understand all the many details of science and research. On a personal level, it helped me to clarify my own opinions, respect the opinions of others and to maintain an open mind. I'm very grateful for all the dialogue.

I would like to thank Shaurav Alam, for the support and fellowship as well as the opportunity to work on projects that I otherwise would not have been able to. Thanks for all the advice on academic and nonacademic matters. He is truly someone who leads by good example.

I would like to express my gratitude to my professors and dissertation committee members Collin Wick, Bill Wolf and Patrick O'Neal. I truly appreciate their time, patience and advice.

I would like to thank the Chemistry Department of Louisiana Tech, especially Danny Eddy, for all the help and support. I have found that teaching a subject is the best way to learn it well and I'd like to extend my thanks for giving me that opportunity.

I would like to express my appreciation to Louisiana Tech for the funding and space to pursue research and a graduate education.

Finally, I would like to express my gratitude to family and friends. I want to thank my sister, Kathleen Johnston, for all the advice and reminding me that there is a light at the end of the tunnel. I'd like to thank Marge Zulaski for encouraging me to even think about the possibility of going back to school. I'd like to thank David Boyle for his insight and counsel. You have all made an unknowable difference.

CHAPTER 1

INTRODUCTION

In this dissertation, four nanoparticle reaction schemes were developed as substrates for halochromic dyes or nucleic acids. The reaction schemes include the use of two substrates: silica nanoparticles (SiNPs) and halloysite nanotubes (HNTs). The protocols can incorporate silica (SiO_2) nanoparticles and halloysite aluminosilicate (AlO_2SiO_2) nanotubes due to the presence of silane groups on the surface of either substrate. The reaction schemes are presented along with detailed protocols which were written to facilitate both reproducibility and to serve as an aid to further study and for easy modification of the protocol to suit a researcher's needs. The data is discussed in the materials section to annotate the stages of synthesis as well as the response of the nanoparticles to varying conditions of pH in both a broad range and a near neutral range.

The first particle scheme described was designed create a particle to measure pH using neutral red, an ionophore chosen because of its sensitivity to near neutral pH values. Neutral red has a pK_a of ~6.7 and contains a 1^0 amine, which is not required for its halochromic response. The first stage of the particle involves functionalization of the inorganic surface with a 1^0 amine. SiNPs and HNTs were used as substrates. The organosilane was aminopropyl triethoxysilane (APTES). The ionophore neutral red also contains a 1^0 amine. Glutaraldehyde, a ubiquitous dialdehyde used in many chemical and biological applications, was used as a crosslinker to attach the dye to the organically

modified nanoparticle. When used in particle synthesis glutaraldehyde tends to promote aggregation and large particle size. The pH of the reaction solutions was manipulated to increase the positive charge on the amine-labeled nanoparticles to decrease the favorability of large particles formed due the bridging capacity of glutaraldehyde. The result was the synthesis of particle labeled with dye, the results of which were readily apparent by visual observation as the pale yellow white particles became a red color. The dyes were stable and did not leach or wash off of the nanoparticles after repeated washes with organic solvents or solutions with pH values of <2.0 or >10.0. Changes in near neutral pH, between pH 6.0 and 8.0, could be seen with the eye. Observation with a spectrometer showed that the spectral data could be used to discern changes in pH at a large range by observation of the reflectance peaks of the protonated and deprotonated states of the dye.

The second particle developed was a derivation of the first particle. Instead of using a dialdehyde to link two 1^0 amines, the organosilane triethoxybutyraldeyde (TSB) was used to provide aldehydes to the surface of the SiNPs and HNTs. The aldehyde functional group was then linked to the 1^0 amine functional group of the neutral red dye. This process was similar in outcome to the first particle in range and sensitivity to response of pH. The protocol was steps shorter, thus requiring fewer reagents and time, reducing the cost of development and increasing the facility of the protocol.

The third particle developed used TSB as a organosilane cross linking agent to synthesize a silane organic dye matrix, which was grown into nanoparticles. The protocol was initially investigated using TSB and neutral red, but with two unproductive outcomes. Either no particles or an oily product were produced. When small amounts of

tetraethoxysilane (TEOS) and ammonia (NH_4) were added, in a modification borrowed from the Stöber process, spherical nanoparticles of dye-doped silane grew. The particles were highly responsive to changes in pH even at low concentrations. This protocol also used Nile blue, a halochromic dye with a pK_a of ~10. The color change at a range of pH 10.0-12.0 was easily visually apparent. Analysis of spectra showed that both the neutral red and Nile blue doped matrix nanoparticles could be used for sensing pH in a broad range by observing the changes in the reflection peaks of the protonated and deprotonated states of the respective dyes.

The fourth particle developed used the reaction scheme from the second particle. The inorganic SiNPs or HNTs were functionalized with TSB to provide aldehyde groups to the particle surfaces. The TSB-modified particles were then show to have the ability to covalently bind nucleic acids. Adenine, DNA, and RNA were used. The protocol used heat to denature the nucleic acids, rendering them into single strands. Aggregation was seen with the SiNPs, but the morphology of the HNTs was not seen to change with SEM images, suggesting that the HNTs may be a more suitable substrate. Further areas of study with this protocol that may be pursued as future work are discussed.

Sensors are generally defined as devices that can detect physical, chemical or biological changes in a study material or environment and can convert these changes into physical signals (Thevenot 2001). A biosensor can be construed as a device that is developed to observe the selectivity and to manage the particular requirements of biological components. A sensor consists of a transducer and a recognition element. The recognition element enables the detection of specific substances or environmental changes. The transducer converts the signal into a physical response which is then

collected by a signal processor and may be amplified or transformed into a suitable display. Common recognition elements are enzymes, antibodies, proteins, nucleic acids as well as cells and tissues. Biosensors can be divided into subclasses including electrochemical, piezoelectric and optical (Ronkainen 2010). This study is on the development of inorganic core nanoparticles functionalized with organosilane cross linking agents for use as a substrate for nucleic acids and organic halochromic ionophores. The protocols are discussed along with results and data and implications for future study.

CHAPTER 2

LITERATURE REVIEW

2.1   Silica Nanoparticles

Silica or silicon dioxide (SiO_2) is found commonly in nature as quartz, sand or in combination with metal ions in minerals called silicates. It is also found in living organisms such as diatoms, sponges and grasses (Iler 1979). It has a wide variety of synthetic applications such as fused quartz, glass, microelectronics and pharmaceuticals. Once considered toxic, silica has a low toxicity and is biocompatible and is even recognized as an essential trace element. Silicon ($23x10^{-6}\%$) is present in the human body after iron ($60\ x10^{-6}\%$) and zinc ($32\ x10^{-6}\%$) (E. Carlisle 1986). Silica has been utilized in a wide variety of biomedical applications such as nanoparticles, mesoporous materials, dendritic polymers, and biocompatible materials such as bioglass (Vallet-Regí 2006).

SiNPs are versatile scaffolds for constructing a wide variety of functional materials for biological systems. They are generally manufactured using the Stöber process, which can be easily tailored to adjust size, composition and desired moieties (Z. L. Kang 2010). The SiNPS can additionally be used to encapsulate and release drugs, reagents or dyes. The transparency of the silica is another feature that has been used to produce emissive particles used for applications such as bioprobes (Burns 2006).

Oral ingestion of silica has no associated health hazards and may have health benefits (Rondeau 2008). However, topical and lung exposure to crystalline silica can be

carcinogenic and lead to autoimmune and inflammation disorders such as silicosis and rheumatoid arthritis (Meyer 2017). Crystalline silica particles do not dissolve in physiological conditions and have been found to activate macrophages and dendritic cells by the production of interleukin, a pro-inflammatory cytokinin (Hornung 2008).

2.1.1 Chemical and Physical Structure

Silicon is a common element which is rarely found in a pure form, but in compounds due to reaction with oxygen and water. Silicon dioxide, SiO_2, comprises approximately 26% of the Earth's crust and is commonly found as sand (Agotegaray 2017). Silicates generally show a tetrahedral coordination with four oxygen atoms surrounding a central silicon atom. This is frequently seen in quartz and other silicates, which have a crystalline structure, but may also be found in glass, which has an amorphous structure. Silica occurs in several polymorphic crystalline structures as well as amorphous forms. The crystal forms generally have tetrahedral SiO_4 units, but the silicon-oxygen bond lengths will vary in a general range of $140\text{-}180^0$ (Holleman 2001). Most silica produced commercially is used in the construction industry as glass and Portland cement (Flörke 2008) and in the oil industry in hydraulic fracturing.

Silicic acid, $Si(OH)_4$, is a water-soluble form of silica. It is biologically relevant because of its higher solubility in water and is also an object of scientific interest. Silicic acid tends to easily polymerize in a wide variety of pH values and form colloidal silica. Synthetic compounds based on silica have been developed in areas such as microchips, paints and enamels, rubber alternatives, metallurgy, semiconductors and medical applications such as tissue engineering. Silicon is also used in the production of silicones, which are synthetic polymers with an organosiloxane system based on alternating oxygen

and silicon (Agotegaray 2017). Silica and organosilanes are extremely important in the manufacture of nanoparticles which are used in many industrial and scientific applications.

2.1.2 Biological Characteristics and Applications of Silica

Although once not considered essential for life, silica is found in many plants, marine life and single celled organisms. It can be found as a rigid microscale structure called a phytolith in most grasses and many dicotyledons, or flowering plants, and is integrated into the spicules of sponge skeletons and the skeletons of marine single celled organisms, diatoms and Radiolaria (Fernandez 2015). Single and multicellular organisms use silica and its formation can occur in the cell wall of an organism or in the extracellular matrix. Silicateins, a class of biosilica forming enzymes, are currently being studied for their purpose in biological systems (Muller 2011).

The role of silicon in human physiology is not clearly understood, but it is believed to play a role in the growth of connective tissue and bone as well as cellular enzyme pathways. Deficiencies of dietary silicon have been shown to cause abnormalities in tissue and skeletal structures (Jugdaohsingh 2007). Silicon is a trace element in mucopolysaccharides, carbohydrate polymers found in all collagenous tissues, and its presence is required for strength and stability in tissue architecture and formation.

Chemical structure is important in the use of silicon, or silica, in biological systems. There are various forms of silicic acid, ortho (H_4SiO_4), meta (H_2SiO_3), di ($H_2Si_2O_5$) and pyro ($H_6Si_2O_7$), but the ortho form is the most absorbable form in the human intestine (Reffitt 1999). At intestinal pH, the solubility of orthosilica is ~2-3 mmol/L (Iler 1979).

Silica based bioactive glasses are materials which have been developed for use in tissue healing and bone repair. They are biocompatible and can be incorporated into living tissue. Bioactive glasses contain silica as well as sodium, calcium and phosphorous, but it is thought that the silanol groups of silica may be responsible for the ability of bioglasses to act as nucleation sites (Vallet-Regi 2003). Silica can assume both crystalline and amorphous structures and the amorphous form allows incorporation of cations such as calcium, sodium and phosphorous. These dopants can modify the properties of bioglasses in vitro.

It is thought that when bioactive glasses are put in a physiological environment, they undergo a multiple stage process. The presence of modifier cations, in many cases sodium, Na^+, will ion exchange with biological solutions. Hydrolysis occurs in which silica-oxygen bonds are protonated and broken, forming silanol groups (Si-OH). This leads to changes in the morphology of the surface layer of the glass to form an outer gel surface. Calcium phosphate is precipitated onto the gel layer and undergoes mineralization into crystalline hydroxyapatite, mimicking natural bone structure (Nicholson 2002). Hybrid compounds of bioactive glass and hydroxyapatite have been investigated for bone tissue repair and regenerations. The developed glass has a low tendency to crystallize, avoiding adverse effects of the material such as hydroxyapatite decomposition. It has a higher strength than that of commercially available Bioglass® 45S5 and exhibits positive effects in cell viability and cell growth. This material could represent a useful application of modified silica for medical applications (Bellucci 2015).

Silica has been modified into organic-inorganic hybrid materials called dendritic polymers or star gels. These materials have characteristics of glasses and natural rubber.

They have a wide variety of tunable mechanical and chemical properties and have been used in industrial, scientific and medical applications (Vallet-Regí 2006). Star gels are quite promising, the polymers having organic sub-units with outer alkoxysilane groups, which enhance bio integration.

Mesoporous silica materials occur both naturally and may be synthesized. These materials have porous structures and tunable pore sizes that can be loaded with drugs or reagents. Additionally, they can be modified with secondary reagents to provide desired functional groups. Mesoporous silica nanoparticle synthesis usually uses a template-directed method with anionic or cationic surfactants (Wu 2013). Mesoporous silica frameworks have been reported with tunable pore sizes from 2-10 nm and have been evaluated as drug delivery systems (Y. e. Wang 2015). Mesoporous silica nanoparticles (MSNPs) are able to absorb molecules via the silanol groups exposed on their surface, but these characteristics can be altered depending on the drug or reagent of interest. MSNPs can be used to enable the bioavailability of hydrophobic drugs, improving absorption and delivery after oral dosage (Y. S. Wang 2014). A sustained drug delivery system using MSNPs was reported using both modified and non-modified silica structures. The modified structures were labeled with cross linking agents that provide specific functional groups to conjugate drug molecules within the pores of the nanoparticle. The system was found to have a even, sustained release over time (Tang 2013).

2.1.3   Advantages of Silica Nanoparticles

Nanoparticles are made from many materials and have a broad variety of sizes as seen in Figure 2-1, but silica presents multiple advantages. Silica's chemical structure is

easily manipulated to create nanostructures with distinct shapes, monodisperse sizes and tailored surface properties (Lin 2006). Silica is perhaps very well suited for biocompatibility and medical applications (Almeida, et al. 2011) and there is a sizeable realm of data devoted to the study of silica-based nanoparticles. Monodispersive amorphous silica nanoparticles were first synthesized by Gerhard Kolbe in 1956 (Kolbe 1956) and a process to synthesize SiNPs of controllable and uniform size was developed by Werner Stöber et al in 1968 (Stöber 1968). Stöber developed a method, still widely in use presently, which tunes the Si-np diameter by adjusting the ratio of catalyst to precursor (often ammonia and TEOS). The Stöber process is facile and reliable and can produce monodispersive SiNPs ranging from 10 nm in diameter to several micrometers. Subsequently, silica nanomaterials have been reported with different morphologies such as solid spheres, hollow spheres, mesoporous particles, rattle-typed spheres, foam-like nanoparticles and nanotubes (Chen 2018). Additionally, surface functionalization of SiNPs has been reported using functional moieties such as amine, thiol and carboxyl groups, antibodies, proteins, DNA, fluorophores, magnetic nanoparticles, polyethylene glycol (PEG), gating molecules and therapeutic drugs.
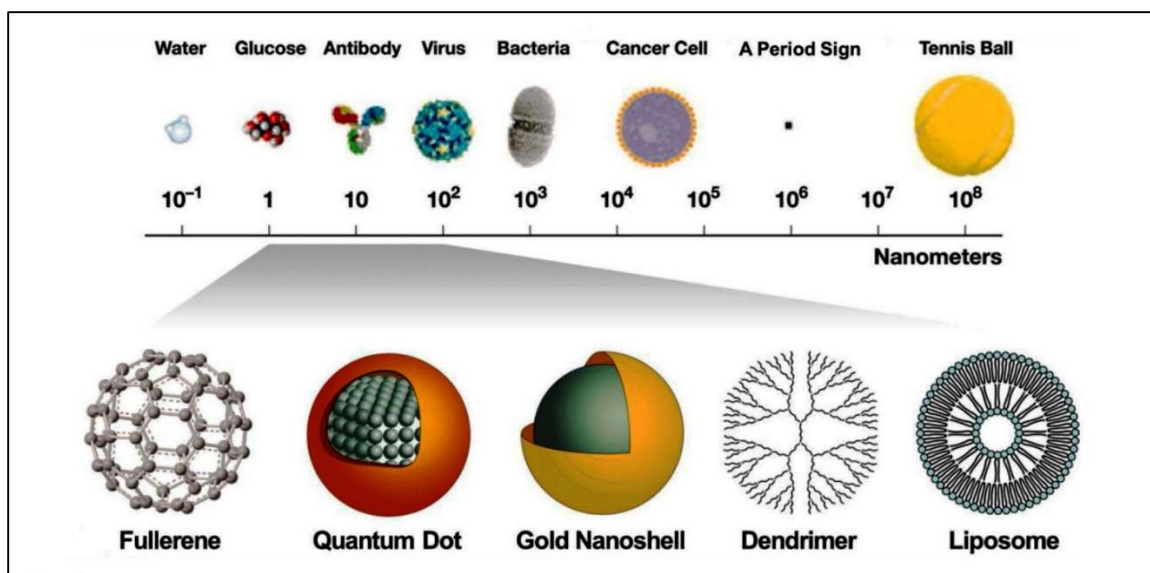
Figure 2-1. *The Sizes of Common Nanoparticles in Comparison to Biological Molecules and Organisms, in Nanometers (McNeil 2005)*

Silica based nanoparticles may be favored for biocompatibility because of their decomposition into silicic acid in vivo. Silicic acid has a very low toxicity and is found naturally in many human tissues. It can be metabolized and excreted by the kidneys (Park, et al. 2009). Silica toxicity, however, is dosage dependent and is also affected by particle size, surface properties and administration route. Crystal silica has a higher toxicity and has been implicated in silicosis, but amorphous silica has a more biocompatible profile and has been used as a food additive for decades (Liu, et al. 2011). The size and surface properties of SiNPs can be adjusted to increase biocompatibility. Since the nanoparticles will interact with immune cells as well as enzymes, proteins and other biomaterials in vivo, the route of delivery is very important. Oral administration has less immunotoxicity, but lower bioavailability, than intravenous, intraperitoneal or subcutaneous methods of administration (Elsabahy 2013).

SiNPs have a high degree of stability, but their degradation and circulation time can be tuned to meet the needs of the application (Labbaf, et al. 2011). Drugs or reagents can be carried within mesopores or the amorphous silica lattice of the nanoparticles and are released by diffusion. The stability of SiNPs is an important factor is sustained release of a drug or reagent as well as early undesired drug leakage. Generally, SiNPs are cleared by the human body in a short time, but surface modification can prolong circulation time. This has been reported using PEGylation, or surface adsorption by PEG, which increased circulation time compared to non-PEG functionalized nanoparticles (Jokerst, et al. 2011). Circulation and clearance rates can be decreased as well. Some biomaterials, such as contrast agents used in MRI scans, need to be cleared quickly to reduce background signal and noise, and to prevent interference with subsequent diagnostic procedures. An increase in clearance rates was accomplished by doping SiNPs with metal ions, which accelerated degradation, reduced circulation time and increased the clearance rate (Labbaf, et al. 2011).

The ubiquity of SiNPs is due to characteristics such as a large surface area and adjustable porosity and density, which provides large potential areas for sites of conjugation and non-covalent binding such as covalent, charge attraction and hydrogen bonding. As a tool for study and medical applications, SiNPs offer many morphologies, facile chemical modification, biocompatibility and low toxicity in addition to their tunable size, porosity, stability and biodegradability.

2.1.4   Synthesis of Silica Nanoparticles: Stöber Process

The Stöber process was developed by Werner Stöber et al in 1968 and is a widely used synthesis protocol to produce SiNPs with uniform and controllable size (Stöber

1968). A reaction scheme that details the Stöber process is presented in Figure 2-2. In this protocol, tetra-esters of silicic acid are reacted with water in an alcoholic solution, usually ethanol, containing ammonia as a catalyst. It is considered a sol-gel, or colloid to network, process. Depending on conditions such as pH, concentration of precursors or other reagents present, the process reliably produces SiNPs ranging from ~50 to 2000 nm. The process was developed to study hydrosols and aerosols, but its potential in research was quickly exploited. The Stöber process uses hydrolysis and condensation of alkoxysilanes, most commonly tetraethyl orthosilicate (TEOS). A solution containing silane precursors, water, an alcohol, often ethanol, and ammonia is mechanically stirred and allowed to react for an average of 12 hours. This facile protocol reliably produces durable SiNPs that can be washed and either dried or resuspended in solution for later use. The ratio of water to alcohol can be varied to adjust the size of nanoparticles. Additionally, TEOS can be added to increase the size of the SiNPs, or an organosilane, such as APTES can be added to modify the particles with desired functional groups.

SiNPs produced with the Stöber process ae used to study colloids, as delivery mechanisms for drugs and other materials into cells for in vivo studies, biosensor preparations, scaffolds for catalysts and for the production of aerogels (See Figure 2-2). SiNPs can be made with solid cores or with mesoporous structures using an ionic surfactant during particle aggregation (Boissière 2000).
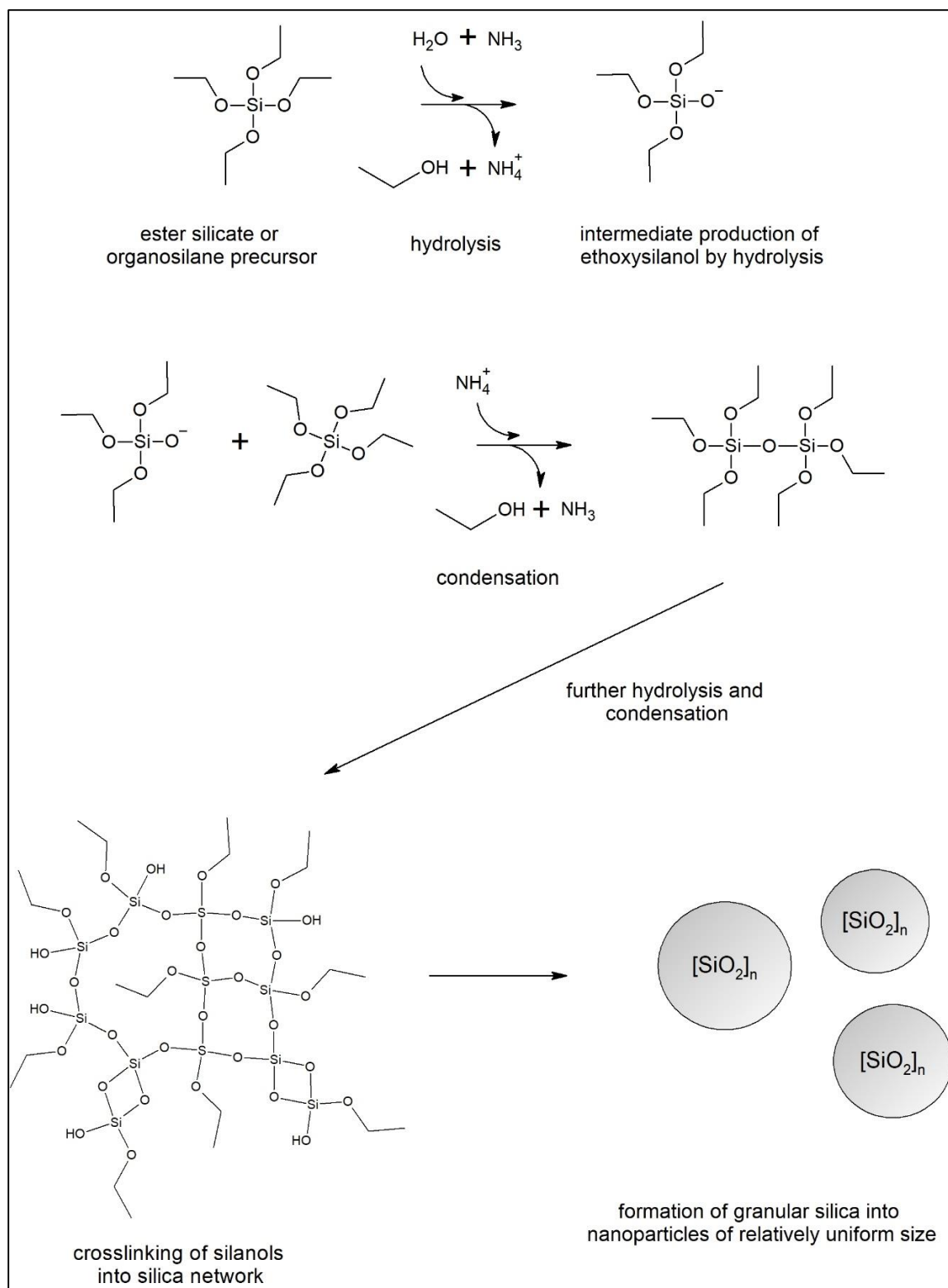
Figure 2-2. *A Representative Reaction Scheme of the Stöber Process*

2.1.5   **Modification Protocols of Silica Nanoparticles**

SiNPs can be produced by bottom-up or top-down methods. Top-down methods are far less common and more hazardous because they use hydrofluoric acid for electrochemical etching or high temperatures over 1500^0C for pyrolysis (Garrett 1992). Additionally, top-down methods are not as easily adapted to changes in morphology or functionalization. Fumed SiNPs produced by pyrolysis are nonporous and are not monodispersive but have a range of diameters. They are used as abrasives and desiccants. SiNPs produced by electrochemical etching have irregular structures and porosities. This method is more suited to produce porous silica films rather than nanoparticles.

Bottom-up methods for silica nanoparticle synthesis are more commonly used. These methods are much more approachable for most labs as they involve hydrolysis and condensation of silica in typically aqueous or alcohol-based solvents involving silica precursors and catalysts. Templates may also be incorporated into the process. The most familiar silica precursor is the silica alkoxide, tetraethyl orthosilicate (TEOS). The process proceeds by hydrolysis and condensation. Organosilanes are used to provide functional groups for additional conjugation sites on the particle surfaces. Popular reagents APTES to provide amino groups and mercaptopropyl methoxysilane (MPMS) to provide thiol groups. Hydrolysis of silica can be catalyzed by either an acid or a base, but ammonia is often used. In basic conditions, polymerization and condensation of silicate species are reversible, producing more homogeneous particles. Acidic conditions proceed at a much more rapid rate and more likely to produce polydispersive products (Wan 2007). Porous nanoparticles can be made by the use of templates such as surfactants that form micelles in solution and are incorporated into the silica matrix as it condenses.

Surfactants such as cetyltrimethylammonium bromide (CTAB) and sodium dodecyl

sulfate (or laurel sulfate), (SDS) are commonly used and can be removed by washing

with acidic ethanol or by sintering. This will produce mesopores smaller than 5 nm that

are useful for loading with small molecules. Larger pores are created with polymers to

load macromolecules, small metallic nanoparticles and quantum dots (Zhao, et al. 1998).

Cells and tissues have also been investigated as nanoparticle templates (Rosi 2004).

2.1.6   Surface Modification of Silica Nanoparticles

The surface of SiNPs has silanol (Si-OH) and siloxane (Si-O-Si) groups and lends

itself to facile conjugation protocols. Colloidal silica surfaces are almost completely

hydroxylated with -OH moieties while fumed silica has far less. Treatment with high

temperature can decrease the hydroxyl groups and increase the siloxanes, if that is needed

by the researcher (Zhang, et al. 2012). It can be modified by covalent bonding or

adsorption techniques. Both methods present advantages and disadvantages and can

dictate the use and purpose of the particle. Covalent bonding is more stable but can cause

alterations in the chemical and physical properties of the bound molecule. The use of

adsorption methods such as hydrogen bonding or charge attraction is usually more easily

reversible but is also much more unstable than covalent bonding. Some covalent bonds

are sensitive to environmental degradation by temperature, pH or interaction with

physiological factors and this can be exploited for the intended purpose of the constructed

nanoparticle (Cairns 2008).

Silanol groups are the key reason for the facile modification of SiNPs. Table 6-5

gives a list of commonly used functional groups. These groups react easily with many

other functional groups with simple and inexpensive laboratory protocols. Silane reagents

and crosslinking agents are abundant and commercially available. While some are too expensive to be considered for many researchers, most are within the economic reach of most labs. The most frequently used reagents are charged polymers or alkylsilanes that have amine or thiol groups attached. Amine and thiol moieties offer a facile linker chemistry with other reagents with isothiocyanate, maleimeide or epoxy groups among other options (Tsai, et al. 2009). In addition to providing reaction sites for bonding, these functional groups can change the zeta potential or surface charge of the nanoparticle. This can influence hydrophobicity or hydrophilicity, increase particle dispersion, stability in biological media, prolong circulation time.

Table 2-1. *Silane Cross Linking Agents and Their Functional Groups*

Functional Group	Silane
-NH$_2$ (amine)	(3-aminopropyl) trimethoxysilane
-SH (thiol)	(3-mercaptopropyl) triethoxysilane
-COOH (carbonyl)	carboxyethylsilanetriol
-PO$_3$ (phosphonate)	3-tridhydroxysilylpropyl methlylphosphonate
-NCO (isocyanate)	(3-isocyanotopropyl)-triethoxysilane

2.1.7   Formulations and Functions of Silica in Nanoparticles

The role of silica in particle construction can be as a core, shell or matrix. A silica core can be used to enhance light absorption, increase contrast or act as a reservoir for reagent or drug release. A silica shell can be used to facilitate surface functionalization, separate and stabilize the core, amplify signal, and to decrease the cytotoxicity of the core material. A nanoparticle matrix based on silica can provide a reservoir that can protect

reagents from environmental degradation, a doping structure, slow photobleaching and decrease toxicity (Chen 2018). The synthesis of a silica shell is similar to that of a silica core using hydrolysis, condensation and polymerization (Wan 2007). A core-shell structure is formed by growing a layer of silica on the surface of another material such as gold, iron oxide, carbon nanotubes or spheres and quantum dots. The surface must have the chemical or electrostatic affinity for silica in order for the reaction to occur. While some materials have a high affinity for silica, gold nanomaterials, for example, have a weak interaction and require stabilizers such as (3-mecaptopropyl)-trimethoxysilane (MPTMS) that has a thiol (-SH) group that bonds to the gold surface and an alkoxy group which serves as the scaffold to support silica shell formation (Liu, et al. 2011).

The deliberate introduction of impurities to a material is called doping. Silica can be doped with functional ions, groups and/or molecules to create additional functions or to modify characteristics. The methods generally used to produce doped silica nanostructures is by a one-pot sol-gel synthesis where silica precursors are mixed in solution with dyes, ions, quantum dots or other reagents or particles of interest (Pohaku-Mitchell 2012). The precipitation of hybrid particles proceeds from this. The other method is reverse microemulsion which is useful for doping with hydrophobic reagents. This method uses a combination of non-miscible host and guest solvents and a surfactant. The ratios of host:guest:surfactant can be adjusted to meet the needs of the protocol. An example of this would be hexane as a host solvent, water as a guest solvent and sodium dodecyl sulfate as a surfactant and the addition of a desired dopant such as a dye or ion (X. B. Zhao 2004).

Hybrid SiNPs may have complicated synthesis because of the difficulty of integrating the matrix with the desired cargo. This is currently difficult using one-pot synthesis. These protocols are influenced by the multiple components involved and their relative solubilities and compatibilities, especially concerning therapeutic or diagnostic molecules of interest. The general method is to attempt to load the SiNPs after their synthesis to preserve the biological activity of a therapeutic drug or the reactivity of a chemical reagent. These protocols tend to be inefficient and time-consuming, hindering their usefulness in industrial or medical applications (Rieter 2007).

SiNPs were used as scaffolds to support water soluble perfluorinated dendrimers based on polyhedral oligomeric silsesqioxane to monitor enzyme activity using regulation of F-NMR signals (Tanaka 2008). F-NMR signals may be suppressed in a solid state due to acceleration of transverse relaxation time and spin aniosotropy towards magnetic fields. When bound to SiNPs, the perfluorinated molecules exhibited restricted molecular rotation in an aqueous solution, and the F-NMR signal were reduced. The silica acted as an NMR quencher. The perfluorinated dendrimer was attached to the silica by an amino-phosphate linker that was susceptible to enzyme degradation. Once released from the SiNP by enzyme activity, the dendrimer NMR signals were detected.

2.2   Halloysite Nanotubes

2.2.1   Chemical and Physical Structure

Aluminosilicate clay minerals are naturally formed materials that are used in a broad variety of scientific, medical and industrial purposes. They have the general chemical formula of $Al_2Si_2O_5(OH)_4$ with an average composition of aluminum (20.9%), silicon (21.76%), oxygen (55.78%) and hydrogen (1.56%) but admixture of other

elements such as iron, magnesium and calcium are common (Yuan P. 2015). Clay minerals occur as many mineral types, but kaolinite and montmorillonite are commercially important varieties.

Halloysite is a type of aluminosilicate clay mineral that is found admixed into other clay subtypes such as montmorillonite and kaolin. It may form by hydrothermal alteration or in the presence of carbonate minerals such as feldspar, which decomposes in water and produces solutions containing ionic forms of silica, alumina, sodium and calcium from which aluminosilicate structures can precipitate (Kerr 1952). More complex micro and nanoscale structures such as plates and rolled tubes form when aluminosilicate clays are subjected to weathering and water flow, variations in temperature, volcanic rock formation or the conditions of glacially weathered regions (Wilson 1999). They are found in proximity to carbonate rock and layers of basaltic rock (Papke 1971). Halloysite is found with two microstructures: planar (halloysite nanoplates) and tubular (HNTs) (Sakiewicz, et al. 2016). The tubular structures are referred to as HNTs (HNT) and are the subject of a vast number of scientific studies and industrial applications. Commercial mining of halloysite is important in China, Poland, New Zealand and in the US mainly in the state of Utah. Halloysites were first characterized by Pierre Berthier in 1826 and named after the Belgian geologist Jean Baptiste d'Omalius d'Halloy, who found the material in Angleur, Liége, Belgium (Berthier 1826).

HNTs are di-octahedral structures with a cylindrical geometry. Initially the geometric structure of HNTs was believed to be a solid or perhaps porous cylindrical tube with a similar x to y axis ratio compared to a relatively large z axis. More analysis has

revealed that HNTs have a characteristic rolled scroll structure comprised of a series of folded alumina and silica walls with water molecules intercalated between the structural layers (Bates. T. 1950). The rolled tube geometry is formed due to a difference between the periodicity of the tetrahedral SiO_4 layer compared to the adjacent octahedral AlO_6 layer. The layers have a 1:1 composition in each sheet (Yuan P. 2015). A schematic of the aluminosilicate molecular structure and halloysite formation can be seen in Figure 2-3. The Al-O bond resulting from the shared oxygen of the tetrahedral and octahedral layers is stretched, further inducing structural stress in that plane (Rawtani 2012). The rolled scroll structure forms as a result of the strain caused by lattice mismatch between the adjacent silica and alumina layers (Du 2010).
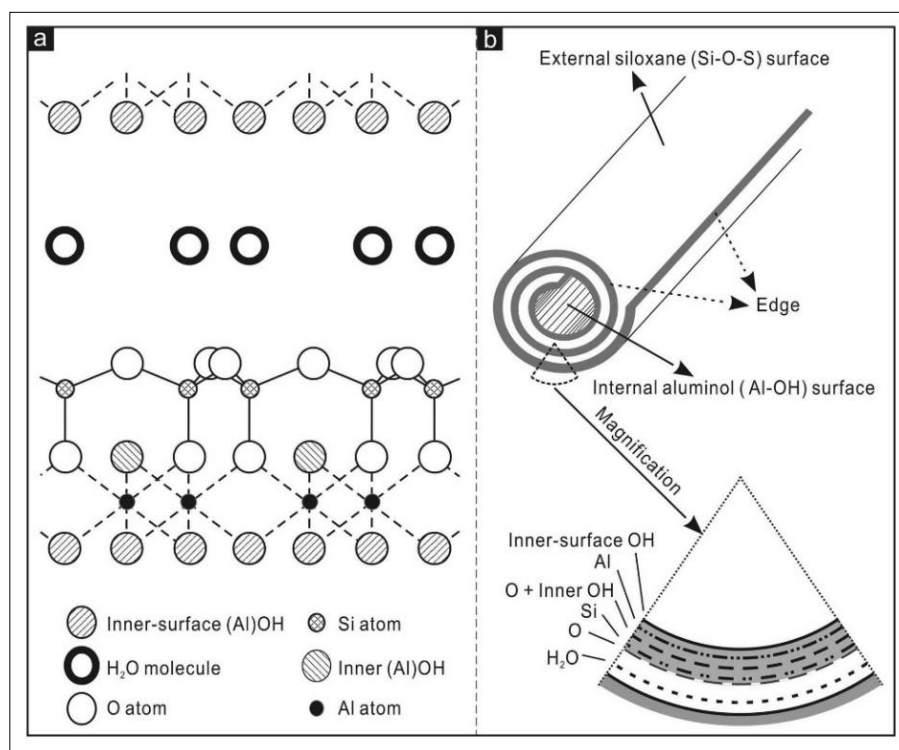
Figure 2-3. *Schematic Diagrams of (a) the Crystalline Structure of Halloysite-(10 Å), and (b) the Structure of a Halloysite Nanotube (Yuan 2008)*

The general molecular structure is $Al_2(OH)_4SI_2O_5 \cdot nH_2O$ and while it is mined in various states of hydration and dehydration, this characteristic can be easily altered to suit the researcher's needs. Values of n=2 describe the hydrated form, n=1 partially hydrated and n=0 dehydrated. The water molecules can be removed easily by either heating the HNTs or subjecting them to a vacuum chamber.

The outer surface of the roll contains siloxane (Si-O-Si) and silanol (S-OH) groups whereas the inner surface of the lumen contains alumina (Al-O-Al) and aluminol (Al-OH) groups. At a ph of <8, the silicon-based groups on the outer surface contribute to a negative zeta potential range, but the alumina lumen maintains a positive charge (Thanawala 2015). The zeta potential can be adjusted with surface modification (Veerabadran 2009). The charge disparity on the inner and outer surfaces creates the possibility of modification with electrostatic interaction of differently charged molecules. Cationic molecules can be used to modify the outer silica layer and anionic molecules can be used to modify the inner alumina lumen.

The walls or layers of HNTs have different structural forms such as zig-zag, arm-chair and chiral that are differentiated according to the rolling direction of the 2D lattice. The variant forms differ in stability as well as electrical and mechanical properties (Guimarães 2010). The Young's modulus of an HNT is approximately 230-340 GPa and the stiffness is similar to imogolite, gallium sulfide (GaS) and chrysolite nanotubes (Spyrnskyy 2011). The Young's modulus also decreases as the HNT radii increase due to an increase in structural defects. Unsurprisingly, as they are composed of aluminosilicates, HNTs are very good insulators and this property increases with the radii (De Silva 2015).

On average, HNT walls are composed of 10-15 aluminosilicate sheets with an outer diameter of 50-60 nm and an inner diameter of 12-15 nm. The length can vary from 500 nm to 2 μm. In the hydrated form, the layers of alumina and silica are associated with hydroxyl groups with the outer silica surface presenting a negative charge and the inner alumina surface a positive charge. Hydrated HNTs have a 1 nm distance between layers and dehydrated layers have a 0.7 nm distance. Although all nanoparticles have a high surface to volume ratio or specific surface area, the scroll like structure of HNTs greatly increases this aspect of their geometry. The typical specific surface area is 65 m^2/g, pore volume is 1.25 mL/g, refractive index is 1.54 and specific gravity is 2.3 g/cm^3 (Brindley 1952).

The HNT layers are a hybrid composition of adjacent silica and alumina. The charge and zeta potential of the outer silica surface of HNT is similar to silica (SiO_2) with a negative charge in a pH <8. The inner alumina core is similar to alumina (Al_2O_3), which is positive at the same pH range. The charges and surface area can change is response to pH, especially in strongly basic or acidic solutions (Yang 2016). It is due to this charge differential that cationic and anionic materials can be adsorbed onto HNTs, giving it a versatility that has interested many researchers.

2.2.2   Advantages and Disadvantages of HNTs

There are many concerns about the safety of nanomaterials. Many are toxic and are not considered safe for environmental use or human exposure. Clays have been used for millennia and have a generally well regarded as non-toxic profile. HNTs are extremely safe when compared to a similar well-studied structure, carbon nanotubes (Kamble 2012). HNTs are biologically safe, even in comparison to silica, graphene, and

other clay minerals such as montmorillonite, kaolin and bentonite (Kryuchkova 2016),

One example is the use of pristine HNT powder as a food additive for animals (pigs and

chickens) for the treatment of mycotoxin poisoning (Zhang 2015).

There are some caveats in the therapeutic use of HNTs however. HNTs are not

biodegradable in blood, which limits the use by intravenous injection due to a risk for

thrombosis (Yendluri 2017). Even if the HNTs were filtered for size, lengths in the

nanometer range could pose a hazard in capillary beds if aggregation were to occur.

There is little information on this but given the differential charge of the inner and outer

lumens of HNTs and that biological proteins are also charged; unforeseen interactions are

possible. There have been cautions against the potential inhalation exposure to HNTs

(Koivisto 2018). No significant exposure risk was suggested, but the fiber sampling tube

length was less than 2 μm. It was suggested that the samples used present a similar risk as

compared to aluminosilicate clay powder exposure, but caution is recommended until

further research on inhalation risks with nanotube lengths less than 1 μm are performed.

It has been found that HNTs are relatively safe in low concentrations. They have

been found to be natural, non-toxic, bio-compatible and are an EPA 4A listed material

(Vergaro 2010). Ahmed et al found that proliferation inhibition of human peripheral

lymphocytes was triggered in response to concentrations of HNTs greater than 1 mg/ml.

They suggest that HNT formulations may be suitable for oral drug delivery applications

in lower concentrations (Ahmed 2015). The consensus of current data suggests that

HNTs are a relatively safe nanomaterial and may be used for industrial and scientific

purposes as well as therapeutic biomaterials for human use without serious side effects.

There is always a caution that more studies should be done in vivo and with regards to

long term exposure. Additionally, since data suggests that toxicity to aluminosilicates is dependent on concentration, the prevalence of HNTs should be considered when designing safety standards.

2.2.3 Functionalization of HNTs

The dual surfaces of HNTs allow for a versatile range of modification schemes. Functional groups can be grafted on via the use of ormosils or organosilanes, allowing covalent bonding of materials of interest. A common approach is to modify HNTs with amine groups by covalently binding APTES (Yuan 2008). The molecular structure of APTES is shown in Figure 2-4. Once functionalized with APTES, the available amine groups can be the site of further covalent bonding or hydrogen bonding. Shi et al used this technique to increase the affinity of HNTs to oligonucleotides, allowing the conjugation of the short chain polymers to the outer surface of the HNTs (Shi 2011).
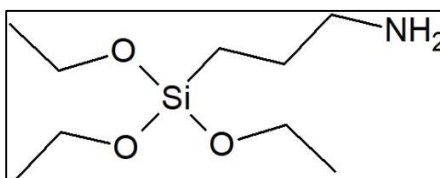
Figure 2-4. *APTES, One of the Most Common Crosslinking Ormosils, Used to Provide Functionalization with Amine Groups by a Variety of Facile Methods*

HNTs can be used for drug encapsulation and subsequent sustained release. This technique has been used to mitigate the toxicity of drugs by the shielding effects of the aluminosilicate composition of HNTs, which reduces toxic effects while improving biocompatibility. This process was used by Hu et al by functionalizing HNTs with (3-mercaptopropyl) trimethoxysilane (linear formula: $HS(CH_2)_3Si(OCH3)_3-$). This organosilane will attach a thiopropyl functional group ($HS(CH_2)_3-$) after hydrolytic

cleavage to a suitable substrate. After modification, the thiol-HNTs were loaded with doxorubicin and subsequently combined with per-thiol-β-cyclodextrin, which was bound via a redox reponsive disulfide bond. The drug loaded hybrid HNTs exhibited low toxicity in an extracellular environment, but a high drug release rate once the nanotubes were endocytosed by the metabolically active cancer cells (Y. C. Hu 2017).

Polymers can be grafted onto the surfaces of HNTs by a variety of techniques such as adsorption, electrostatic attraction, hydrogen or covalent bonding. In an example of this method, 2-bromoisobutyric acid was adsorbed onto HNTs by electrostatic attraction. The modified HNTs were blended with the initiator/monomer or inimer, 2-((bromoacetyl)oxy)ethyl acrylate and allowed to react, producing a highly branched polymer grown upon the halloysite surface. Functionalization of HNTs with dendritic polymers creates functional surfaces and interfacial materials which may have a wide variety of applications (Mu 2008).

2.2.4   Uses of HNTs

HNTs are already used in a diverse array of commercial and scientific applications from plastics and polymers to drug delivery and catalyst support matrices. HNTs have been shown to be stable and durable in multiple applications. The long-term stability has been studied at room temperature (22 ± 2^0C) in neutral, acidic and basic aqueous solutions. It was shown that in 1-3M H_2SO_4 solutions, the inner alumina surface begins to dissolve, leading to the formation of amorphous spherical SiNPs. In 1-3M NaOH solutions, the outer surface dissolved causing the formation of alumina nanosheets (Shamsi 2008).

HNTs have a high cation exchange capacity and maintain uniform sustained release rates with no initial rapid release peak. The release rate has been found to be predictable and tunable. Adsorption onto the inner lumen can protect sensitive materials during harsh processing (Kamble 2012). HNTs have been shown to be capable of loading multiple agents simultaneously and have superior loading rate speed and capacity in comparison to other materials. They have a high aspect ratio, high porosity and are non-swelling. These characteristics make HNTs a subject of great interest in scientific studies and industrial applications.

Some of the uses of HNTs include nanoreactors, or containers for enzymes or chemicals to react within, or as templates for the formation of other nanoscale structures. Nanocontainers use HNTs as vehicles for the incorporation of reagents into hybrid materials or for drug delivery with tunable release rates. The ability of HNTs to easily adsorb a variety of reagents via electrostatic attraction or hydrogen bonding has led to their use in environmental remediation as well as hybrid materials for many industrial and medical applications

Because of their multiwalled structure and dual layer composition, HNTs can act as containers or vessels to protect volatile or sensitive materials from external influences or to contain reagents within nanoreactors. HNTs were investigated as a nano-scale container for benzotriazole, a corrosion inhibitor (Y. S. Lvov 2008). The benzotriazole was readily adsorbed onto the HNT surface when mixed in a simple solution. When compared to non/encapsulated microcrystals, the loaded HNTs exhibited a release time 50-100 times longer.

The inner lumen of an HNT is a hollow core with diameters from 16-50 nm and is capable of entrapping active agents within the void spaces. Many applications have been developed using similar microtubes made from either carbon nanotubes or phospholipids, but these structures are often difficult to manufacture and may be cost prohibitive. HNTs have been found to be comparatively cost effective as well as less toxic. HNTs were found to readily adsorb a variety of reagents in multiple types of solutions: oxytetracyline HCL, a water soluble antibiotic, khellin, a lipophilic vasodialator dissolved in ethylene glycol to allow entrapment of the hydrophobic molecule, and nicotinamide adenine dinucleotide (NAD), a biochemical enzyme dissolved in water along with polyvinylpyrrolidone (PVP) to increase viscosity and aid NAD retention. Each of the adsorbed molecules showed slow release rate compared to controls. This study illustrates how the composition and structure of HNTs gives it a versatility that lends itself to use with many types of protocols and applications (Price 2001)

In addition to containment of reagents, HNTs can be used to immobilize enzymes. While powerful catalysts, enzymes are only effective in specific conditions such as temperature and pH. Manipulation of the peptide sequence of the enzymes or cross-linking the enzymes to a suitable matrix are possible delivery and functionalization techniques, but these often result in reduced efficiency of the enzyme. HNTs can provide a porous substrate that is less likely to reduce catalytic efficiency compared to zeolites, clays and natural or synthetic polymers. It was found that HNTs can immobilize laccase, glucose oxidase, lipase and pepsin, all of which are water soluble, by charge interactions between the aluminosilicate surfaces and the positive and negative charges of the amino acid residues of the polypeptide enzymes. The enzymes were found to retain their

catalytic activity. The HNTs were found to adsorb the proteins at a 4-8% wt and that 33% of the proteins will release after 10-30 hours. The remaining proteins will remain on the lumen surface creating a nano-scale reactor (Tully 2015).

Halloysite can be combined with natural and synthetic polymers to create hybrid materials for a wide variety of applications. A bone cement was developed and patented that combines poly-methylmethacrylate (PMMA) with HNTs loaded with therapeutic agents. The implantable ceramic composite involved a PMMA matrix with HNTs dispersed within it. The HNTs may be loaded with pharmaceuticals such as antibiotics, bone growth promoters and chemotherapeutic agents which can help overcome problems with infection, rejection and tissue adhesion. The hybrid material is comparable to a commonly used bone cement formulation, PMMA with zirconium oxide or barium oxide. The HNT-PMMA hybrid material has potential in orthopedic and dental applications. Since HNTs have been shown to readily adsorb a variety of therapeutic agents, they have an additional functionality that PMMA/ZrO_2 or BaO lack (Mills 2015).

2.2.5   Surface Modification Strategies of HNTs

2.2.5.1   *Inner Lumen*

Because of the structure and composition of HNTs, there are two approaches for modification: loading into the inner lumen or linkage to the outer surface (Y. D. Lvov 2016). The inner lumen of the nanotube generally occupies approximately 10% of the total volume and mainly consists of alumina groups. In pristine halloysite, this area is usually air filled, which may interfere with the total loading capacity. Various modification strategies have been reported, such as vacuum treatment and sonication, to

address this issue. Approaches to modifying the inner lumen are not as well studied as those directed towards modification of the outer surface.

Organosilanes are organically modified silicates, generally consisting of alkoxides of silicon with the addition of an organic functional group attached to the central silicon atom. APTES is commonly used to introduce primary amine groups, but organo-silane attachment to alumina is not as favored a reaction as to silica. In one study, however, the inner lumen was modified with APTES for the controlled loading and release of Acid Orange II dye, an anionic hydrophilic dye. Acid Orange II has a negatively charged sulfonate group, which was expected to have electrostatic interaction with positively charged amine groups. The study found that dye loading was increased by 32% compared to halloysite controls with poor tubular structure and that subsequent dye release in relation to pH performed as expected with a positive correlation to increase in pH (Yuan P 2012). This technique could be further used to increase loading of anionic reagents and would also exhibit a pH dependent drug release curve.

Treatment of HNTs with acids can increase the diameter of the inner lumen by etching due to the dissolution of the alumina groups. Sulfuric, hydrochloric, acrylic and acetic acids have been used for this technique. Temperature has been found to contribute to widening of the lumen with the acid etching process. Higher temperatures tend to produce non-uniform widening of the lumen while temperatures lower than 70^0C produced more uniform lumen (E. J. Abdullayev 2012). The possible mechanism proposed for the dissolution of the alumina layer occurred was diffusion of hydrogen ions into the lumen, followed by reaction with the alumina and subsequent removal of the

reaction products. They also found that loading capacity of a corrosion inhibitor increased by 400% as compared to conventional loading techniques.

Acid etching has been shown to be a valuable technique for HNT modification. When treated with sulfuric acid, a strong acid, HNTs show a large increase in porosity and surface area, but the distinctive scroll structure is almost lost. Treatment with weak acids like acetic and acrylic acids exhibited milder effects. The lumen increased in volume and the loading capacity increased by 77.8%. Measurement of the aluminum content of the treated HNTs by X-ray fluorescence and laser induced breakdown spectroscopy suggests a strong correlation between acid strength and aluminum reduction. The use of weak acids can give a more controlled and consistent increase in lumen volume, thus providing a larger loading capacity (Garcia-Garcia 2017).

HNTs can be used as a support matrix for catalysts. Silver nanoparticles were synthesized directly onto HNTs which were previously etched with sulfuric acid to increase the size of the inner lumen and to create vacancies within the crystal lattice of the aluminosilicate layers. The HNTs were dispersed into aqueous solutions of silver nitrate or silver acetate, then calcined to remove organic residue. The Ag nanoparticles formed on the outer surface when silver nitrate was the reagent, and in the inner lumen when silver acetate was used. This is postulated to be due to the higher electron affinity, ionization energy and steric configuration of the ionic radicals of the metal salts. The nitrate ion was more favored to attack the silica surface, versus the acetate ion which was more favored to attack the alumina surface. The Ag-HNT hybrid structures were then tested for catalytic activity by exposure to formaldehyde gas, which was subsequently decomposed into carbon dioxide (Ouyang 2016).

Motor exhaust purification relies on platinum-based exhaust catalysts, which are very expensive. Copper-nickel (Cu-Ni) alloy nanoparticles grown within HNT lumens have been developed that may offer a less expensive alternative to Pt-based catalysts. The nanocomposites were prepared by reducing chlorides of copper ($CuCl_2$) and nickel ($NiCl_2$) within HNTs using sodium citrate as a capping agent, resulting in bimetallic Cu-Ni nanoparticles forming within the HNT support structures. The synthesis was accomplished by dissolving the $CuCl_2$ and $NiCl_2$ in aqueous ethanol at pH 6-7. Sodium citrate, which is anionic, served to coordinate to the Cu^{2+} and Ni^{2+} ions and as a delivery agent to the positively charged alumina surface of the inner lumen. The ions were reduced to alloy nanoparticles with hydrazine, yielding a concentration inside the HNT lumen. In the absence of sodium citrate, the negatively charge silica outer surface adsorbed the metal cations and nanoparticles were only formed on the exterior. The composites with Cu-Ni nps in the inner lumen performed well in the catalytic conversion of nitrous oxide (NO) and carbon monoxide (CO) into nitrogen (N_2) and carbon dioxide (CO_2) respectively. An alternate synthesis produced Cu-Ni nps on the outer surface of the HNTs, but these performed poorly in comparison to both the HNTs with lumen festooned bimetallic nps or traditional Pt-based catalysts (Sanchez-Ballester N.M. 2015).

Nanomaterials can consist of nanoparticles, nanorods and nanodots and have been used to create hybrid structures with HNTs. Metallic nanoparticles such as iron, gold and silver have been used to increase the conductance capacity of HNTs, enabling them to be used for catalytic and electronic applications. While various nanomaterials have been immobilized on the outer surface of HNTs, they tend to exhibit fast separation and loss

due to leaching. Modification of the inner lumen with nanomaterials can potentially inhibit this loss and increase efficiency.

Functionalization of the inner lumen of HNT allows them to be used as a blending component for both natural and synthetic polymers. It can enhance compatibility and interfacial bonding of disparate materials or be used as a container to immobilize or protect enzymes or reagents. Polyethylene oxide (PEO) has been used to modify the inner lumen via hydrogen bonding with water between its ether groups and hydroxyl groups formed upon the inner alumina layer. This facile process confined PEO chains within the HNT lumen. The process was performed using acetonitrile, a common polar aprotic organic solvent, but residual water trapped in the HNT lumen was sufficient to provide hydrogen bonding. This process suggests that modification of the inner lumen with polymers capable of hydrogen bonding is facile and a potentially useful technique for many possible applications (S. e. Yang 2014).

Functionalization of the inner lumen can also be performed using dopamine. 3,4-dihydroxyphenylalanine, or dopamine, has been widely used to functionalize surfaces for biomedical applications (Yah 2012). It is a precursor catechol for melanin and mussel adhesive proteins and easily self-polymerizes. Dopamine has a higher affinity to metal surfaces compared to nonmetals but has a smaller binding energy required for metals in comparison to silica. The mechanism is postulated to be a monodentate-bidentate bond involving dopamine's two hydroxyl groups. Yah et al demonstrated that a dopamine derivative, 2-bromo-N-[2-(3,4-dihydroxyphenyl) ethyl]-isobutyryl amide, in an aqueous environment can be covalently linked to the alumina inner surface of HNTs, but not to the silica outer later. During the washing process, the dopamine derivative did not remain

on the silica surface but remained inside the alumina lumen. It was subsequently polymerized into a branching bottlebrush network inside the lumen. The presence of the dopamine-alumina bond was verified with C-NMR and XPS data. This study showed that the inner lumen can be modified with an organic reagent such as dopamine, which can then be used as a precursor to further modification.

HNTs can be functionalized by means of the disparate charges between the cationic inner layer and anionic outer layer. Consequently, it has been demonstrated that selective adsorption by oppositely charged surfactants alters the net charge, electrostatic repulsions and dispersion stability of halloysite in aqueous solutions. A facile method was developed to modify HNT surfaces with either decyltrimethylammonium bromide (DTAB) a cationic surfactant or sodium dodecanoate (NaL) an anionic surfactant. The resultant functionalized particles displayed modified behavior. The process was performed in an aqueous solution with appropriate pH values where the alumina inner surface was cationic and the silica outer surface was anionic. The DTAB sample adhered the cationic surfactant to the silica surface. The NaL sample adhered the anionic surfactant within the inner lumen on to the alumina surface. Adherence of the surfactants to the halloysite was verified with TGA and FTIR. Turbidity measurements revealed that over time, the cationic DTAB-HNTs precipitated from solution at a rate similar to pristine HNTs, while the anionic NaL-HNTs remain suspended in solution, indicating that they had become more water soluble. With adsorption of the negatively charged NaL, the HNT inner lumen became hydrophobic and was able to absorb decane with a sponge like effect. This process provided a novel strategy to tune the hydrophilic

characteristics of HNTs and to prepare nanotubes containing a hydrophobically enhanced lumen for future delivery applications (Cavallaro 2012).

2.2.5.2   *Outer Lumen*

The outer surface of the halloysite scroll structure contains silanol and siloxane groups, due to interaction with water. These are capable of interreacting with different functional groups by hydrogen bonding, electrostatic interaction, Van der Waal forces as well as covalent bonding. Guest molecules can be easily immobilized on the surface without suffering alterations of innate structure, as would be expected from covalent bonding. However, functional groups may be attached via covalent bonding in order to modify behavior such as hydrophobicity or hydrophilicity, alter the surface morphology, or to provide a cross linking agent to copolymerize HNTs with natural or synthetic polymers. Many modification strategies have been developed to provide custom HNTS for a plethora of applications.

The outer surface of HNTs is comprised of a tetrahedral sheet of silica and the inner surface of octahedral alumina. The silica layer (Si-O-Si) can be easily hydroxylated with a strong base such as sodium hydroxide (NaOH), producing external silanol groups (Si-OH) (S. D. Zhang 2011). The -OH of the base causes deprotonation of the silanol groups, increasing their reactivity. The alumina inner layer is more resistant to treatment with an alkaline agent, consequently this technique prepares the silica layer only. Base treated HNTs achieve a higher level of dispersion in water, organic polar solvents and epoxy matrixes, while also avoiding aggregation and interfacial adhesion. However, over time, treatment with bases at high pH values can lead to etching, which will increase loading capacity, but will result in wall thinning and ultimately degradation of the rolled

tubular structure. This treatment was used to create epoxy-HNT hybrid materials with a high dispersion of HNTs in epoxy, which greatly improved the stiffness and fracture toughness of a nanocomposite (Zeng. S. 2014). This material also had the advantage of low cost and facile preparation.

2.2.6   Polymer Hybrids

HNTs can be customized to prepare polymer hybrid materials. Methods have been developed to reduce HNT aggregation, alter the thermal and mechanical stability, induce electromagnetic properties and to produce polymer composites with modified mechanical strength, stiffness and impact resistance (Liu 2007).

In addition to producing composite materials, the polymer component can be chosen to provide a desired functional group. Polyethleneimine (PEI), a branched polymer with imine groups ([-C-NH-C-] and [-N(C-R)$_3$-]), was grafted onto HNTs to produce a hybrid complex for DNA delivery to cells. A reaction schematic can be seen in Figure 2-5. The HNTs were sonicated in a polyvinyl pyrrolidone solution in an ultrasonic cell disruptor to produce a sample of nanotubes with a length of ~200 nm. It had been earlier established that particles with lengths less than 200 nm are more likely to be ingested by cells via endocytosis rather than larger particles (S.E. Gratton 2008). The size standardized HNTs were functionalized with amine groups with APTES in ethanol, pH adjusted with acetic acid. The HNT-NH$_2$s were reacted with succinic anhydride in anhydrous dimethylformamide to graft carboxyl groups (-COOH). PEI was added to the solution and hybrid polymer-HNTs were obtained by covalent bonding between the carboxyl and imine/amine groups. The HNT-PEIs were found to be capable of adsorbing short segments of double-stranded DNA fragments labeled with green fluorescent protein

(GFP) by self-assembly. The hybrid nanotube-DNA complexes were up taken by endocytosis and once inside the cell, released their DNA cargo where it was absorbed into the nucleus and subsequently expressed GFP. The hybrid nanotube complexes were found to be effective for endocytosis and non-toxic (Long 2017).
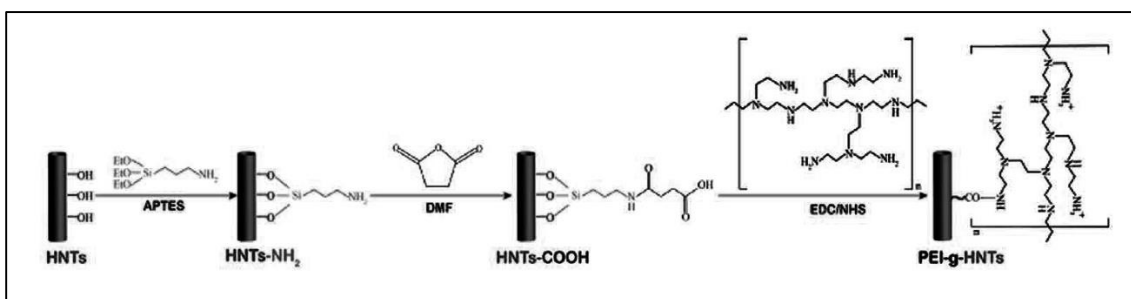
Figure 2-5. *Schematic Illustration of the Synthetic Procedures for PEI-g-HNTs Which Were Used for DNA Delivery (Long 2017)*

Halloysite can be hybridized to produce electrical conductivity for use in electrode fabrication. Polyaniline, a conductive organic polymer, was used to create a hybrid material with HNTs for an electrochemical sensor. The HNTs were first functionalized with APTES to create the presence of amine groups on the silica outer surface. The HNTs were then added to an acidic aqueous solution of aniline. Ammonium persulfate was used to initiate polymerization of polyaniline (PANI), using the HNTs as a template. The PANI-HNTs were electrically deposited on an electrode, since previous efforts have shown that other methods such as drop casting do not produce strong adherence of the PANI to an electrode surface (Tada 2005). This produced a uniform and compact film with a porous structure created by the three-dimensional network of the tubular structure of the HNTs. The PANI-HNTs sensor exhibited a sensitivity to ascorbic acid of 826.53 μA mM-1 cm-2 within a linear range of 0.005 to 5.5 mM with a low

detection limit of 0.21 μM. The sensor performance may be ascribed to the porous structure which may improve electron transport and interaction with solution. This study demonstrates that HNTs are promising materials for electrochemical applications (Shao 2017). However, the study unfortunately did not focus on reversibility or durability of the PANI-HNT electrodes.

Organic modification of glass or silica is a mature field. This is usually accomplished by a sol-gel process involving hydrolysis, condensation, hydrogen bond formation and then bond formation of a silane to the silica substrate. The general reaction scheme for the functionalization reaction of silanes can be seen in Figure 2-6. Organosilanes generally have alkoxy groups which hydrolyze and leave as alcohols, and silanol groups that hydrogen bond with hydroxyl groups on a prepared silica surface, which through condensation subsequently dehydrate to attach the organosilane to the silica. This process is usually performed in nonpolar solvents with low vapor pressure to decrease hydrolysis and self-condensation and increase the reaction to hydroxyl groups on the prepared surface, in this case HNTs (Arkles 1977).
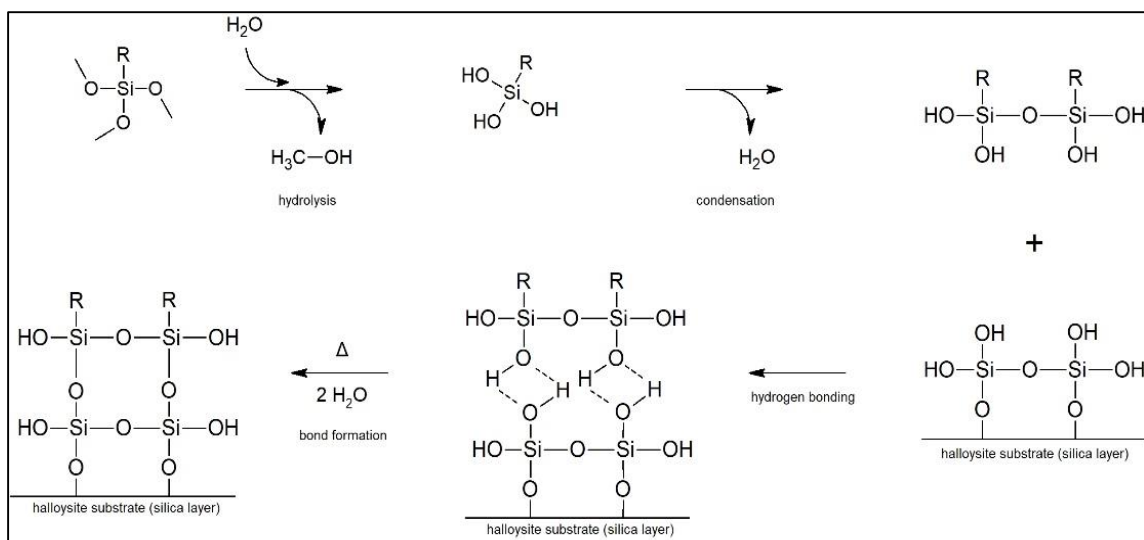
Figure 2-6. *Reaction Scheme for Functionalization of the Silica Surface of a HNT with an Organosilanes via Hydrolysis/Condensation*

Organosilane coupling requires the presence of hydroxyl groups on the silica surface. In pristine halloysite, they may not be abundant or may only be in areas with surface defect, depending on the history of the material and its state of hydration. The coupling reaction is dependent on sufficient density of hydroxyl groups. The surface can be prepared by activation of the HNTs silica surface with treatment by acids or bases. Treatment protocols using acids tend to be rapid and more likely to produce branching structures where basic treatment protocols are slower and tend to produce more compact structures. Alkali agents such as potassium hydroxide and sodium hydroxide are commonly used and typical acids are hydrochloric, acetic and sulfuric acids as well as piranha solution, which is a solution of sulfuric acid (H_2SO_4) and hydrogen peroxide (H_2O_2) (Sun 2015).

Organic modification of the outer silica surface of HNTs is a widely used procedure. It is generally facile and can be low toxicity depending on the solvent used. Silanes can act as the first step in modification strategies that allow the attachment of

other molecules or compounds such as enzymes, drugs, polymers and nanoparticles. A study was performed which produced a hybrid material from HNTs and cyclodextrins for drug loading. The procedure started with a first layer functionalization of the silica outer layer using 3-mercaptopropyltrimethoxysilane ($HS(CH_2)_3Si(OCH_3)_3$), a silane which has a mercaptopropyl group that would provide thiol groups (-SH). The thiol functionalized nanotubes were polymerized with heptakis-6-(tert-butyldimethylsilyl)-2-allyloxy-β-cyclodextrin, a compound containing a macrocyclic 7-glucose subunit. This created a hybrid system of HNTs and cyclodextrin structures. When mixed with clotrimazole, a drug used for the treatment of candidiasis, the drug interacted preferentially with the cyclodextrin cavity rather than the inner lumen of the HNTs. When tested in a system designed to mimic physiological conditions, the drug was released at a slow and sustained rate with ~60% released after 150 mins with no rapid initial release. Pristine HNTs, in comparison, showed a complete release of drug after 30 minutes (Massaro, Functionalized halloysite nanotubes: Efficient carrier systems for antifungine drugs. 2018). This hybrid system is biocompatible and made from readily available materials, provides not only slow, sustained release of drug, but may also protect the drug from degradation in a physiological environment.

Biological compounds can be used to functionalize or hybridize HNTs. Polymers based on saccharides, peptides, nucleotides and lipids have been used to create composite materials and particles. Biological polymers have a variety of functional groups such as hydroxyl (-OH), amine ($-NH_2$), and thiol (-SH) among others and can be attached to HNTs via adsorption, charge attraction, hydrogen bonding, Van der Waals and covalent binding (Bertolino 2017). Biomolecules can be attached to HNTs by many methods,

many of which are facile and inexpensive. Amylose, a polysaccharide made of α-D-glucose units, is a component of starch. It contains many hydroxyl groups, is very hydrophilic, but has a helical structure that renders it resistant to digestion. Amylose was hybridized with HNTs by a dry milling procedure and was dispersed in a solution of DMSO and water. The hybrid material showed a greatly enhanced dispersion compared to pristine HNTs. Subsequent observation overtime indicated the persistence of the interaction, which was speculated to be due to hydrogen bonding between the C-O-C and -OH groups of the amylose and the Si-O groups of the silica outer layer as the amylose helices wrapped around the HNTs (Chang 2011).

Polyphenols are biologically derived chemicals which have been widely studied in many applications. Tannic acid (TA), a low-cost environmentally friendly polyphenol is easily extracted from many plants, has gallol functional groups, is hydrophilic and exhibits strong solid-liquid interfacial properties. TA was used to modify HNTs by adsorption. Halloysite inner and outer surfaces consist of alumina and silica, but the overall net charge of HNTs is negative. Modification with the polyphenol TA increased the negative charge of the HNTs making it a better candidate to repel anions by electrostatic repulsion. TA has already been shown to enhance resistance to fouling by bacterial and mammalian cells (Q. A. Wei 2015). The adsorption was accomplished in an aqueous tris(hydroxymethyl)aminomethane (TRIS) buffer at pH 7.8. The functionalized HNT-TAs were added to a polysulfone membrane. Polysulfone is a common polymeric material containing phenol and sulfone modalities which is widely used for its thermal stability and tolerance to chemical conditions such as pH and chlorine. Unfortunately, it is prone to fouling during use with biologicals, which restricts lifespan and increases cost.

Once the HNT-TAs were polymerized in the polysulfone, the resulting membrane exhibited enhanced hydrophilicity and a negative surface charge. The hybrid membranes had a superior performance to unmodified polysulfone membranes and were hydrophilic, showed a high rejection of anionic dyes (reactive black 5 and reactive orange 16) and a low salt rejection (NaCl and Na_2SO_4), along with a high pure water flux of 92 L/m^2h (Ibrahim 2017). This material was developed as a possible candidate for wastewater purification, but the facile assembly protocol used demonstrates that incorporation of modified HNTs by chemicals such as polyphenols is a useful method of production to be explored.

Polypeptides and polynucleotides are important biomolecules consisting of polymeric chains of amino acids or nucleotides. In addition to their biological purposes as proteins, DNA and RNA, polypeptides and nucleotides have many scientific applications. HNTs were hybridized with polypeptides by a dry process described as "green" because no organic solvents were used and must therefore be environmentally safe. HNTs were mixed with DNA in an equal ratio and placed in a ball milling apparatus and milled for various increments of time at room temperature. The procedure not only produced HNT-DNA hybrid structures, but reduced nanotube length as well. The solvent free process is described as creating mechanical energy in the solid phase that enables interaction between the silica outer surface and the DNA phosphate backbone. FTIR data showed structural changes in the DNA backbone due to a reorientation of the phosphates, probably due to bending of the double helix during the wrapping of the DNA around the nanotubes (Shamsi 2008). The changes were expected from previous studies of the interaction of silica particles with DNA (Mao 1994). The HNT-DNA particles exhibited

enhanced hydrophilicity and dispersion in aqueous solutions. While this technique was interesting in its avoidance of solvents and ease of use, there were no attempts to ascertain the stability of the DNA wrapping. It is not clear that this would be a use for viable DNA. However, functionalization of HNTs with polypeptides was demonstrated to be easily accomplished and this technique may lead to further applications.

2.3 Chemistry of Color

The phenomenon of color is not described by one theory, but by multiple explanations. Color is produced when photons interact with atomic particles. Quantum theory investigates the aspect of excitation of electrons, energy level transitions and molecular vibrations. Ligand field theory deals with the effect of electronic energy levels upon colors produced by inorganic pigments, minerals and gems, as well as fluorescence, crystal lasers and phosphorescence. Molecular orbitals interact with light to produce the colors of most organic substances and some crystals and minerals as well. Energy band formalism, relevant to diodes and semiconductor lasers, leads to the color of metals, alloys, ores and minerals and some gemstones such as blue and yellow diamonds. The realms of geometry and physics cover colors produced through physical characteristics and phenomenon, such as Meis and Raleigh scattering, and explain colors produced by opals, sunset and sky colors, metallic sheens and some insect colors (Nassau 1983). All of these disparate theories combine to discuss aspects of color related phenomenon including dyes, pigments, bleaching and fading, glass and gemstones, biological coloration, fluorescence, phosphorescence, vision and many other aspects of what we refer to as color.

Molecular orbital theory is used to explain the color of organic molecules. These include naturally occurring substances such as animal and vegetable colorants, as well as synthetic dyes and pigments. Organic colorants involve electrons on one or multiple atoms within a molecule. Multi-atom or multi-molecular color producing materials usually involve charge transfer. Organic colorants are an extremely important aspect of chemistry and include the study and development of dyes and pigments used in industrial applications from textiles to lasers, and in biological applications ranging from lab studies to natural phenomenon such as vision and photosynthesis.

2.3.1   Organic Color

The first synthetic dye produced was aniline purple, or mauveine, by William Henry Perkin in 1856. Perkin's discovery was based on aniline, a coal tar derivative. Subsequently, intense research was applied to the study and development of coal-tar based dyes, many of which are still in use in modern times. An empirical approach was proposed by Otto Witt, which suggested that the molecular structure of dyes contain basic chromophore, or "color bearing" group, which may not itself produce color, but to which subsidiary groups he named auxochromes, or "color increasers", may be attached, thus producing color. Chromophores include carbon-carbon double bonds, often in conjugated systems with alternating single and double bonds. Other chromophores include the azo group (-N=N-), thiol group (R_2-C=S), nitroso group (R-N=O) and amines (1^0, 2^0, 3^0). Auxochrome groups can be composed of nitrate (-NO_2), hydroxyl (-OH), methyl (-CH_3), halogens (-X) as well as many others. It is now recognized that some auxochromes, such as primary amines, are electron donors, and some are electron acceptors, such as nitrate

or halogen groups. However, this approach is not universal, as some molecules with these characteristics do not produce color.

The curves in Figure 2-7 represent the concept of color dependent on concentration. The color of a dye can appear to change as the concentration is decreased or increased. The solid curve represents a higher concentration and has a stronger absorption in the violet as well as significant absorption in the blue and green wavelengths, resulting in an orange color. The lower dashed curve represents a solution with a lower concentration, showing a smaller absorption peak in violet and much lower absorption in the blue and green wavelengths, resulting in a yellow color. This phenomenon would not be an example of bathochromic or hypsochromic shifting, but of dichromatism. This is due to the concentration of the absorbing substance and the depth or thickness of the of the medium and is explained by the Beer-Lambert law which relates the attenuation of light to the material it is traveling through (Kreft 2009).
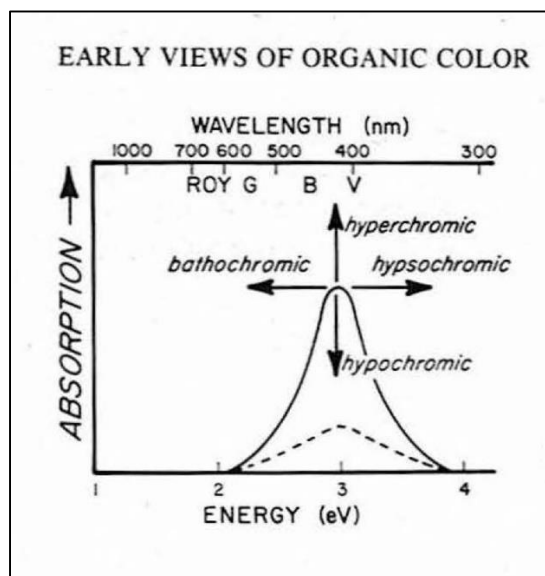
Figure 2-7. *The Absorption Band of an Organic Dye at Two Different Concentration Levels (Nassau 1983)*

It was proposed that the multiple resonance structures of dyes contribute to the magnitude of bathochromic and hyperchromic shifts. The greater number of resonance structures, the larger the shift (Pauling 1939). Subsequent publication of molecular orbital theory concerning color provided more understanding. Organic molecules may have electronic transitions that absorb in the ultraviolet region and do not display color in the visible range. The presence of conjugated systems or auxochromes groups may cause bathochromic shifts towards the red, contributing to the emergence of visible color. This involves bonding and antibonding orbitals, sigma (δ or $\delta*$) or pi (π or $\pi*$) types, and may involve n-type nonbinding orbitals. The increased addition of conjugated systems can increase the intensity of the bathochromic shift and produce colors in the visible range (Nassau 1983). This effect is seen in organic molecules with structures such as noncyclic polyenes, nonbenzoid ring systems and benzoid systems. A noncyclic system such as carotene has an absorption band in the blue-green region, giving it a yellow-orange color. A cyclic benzene based system like indigo has an absorption band in the orange-red region, causing a violet-blue color to be displayed.

A change in the molecular conformation due to pH levels can be seen in phenolphthalein. In acidic solutions, it has three benzene rings which only absorb in the ultraviolet region. In a basic solution, the lactone ring opens and the hydroxyl and carbonyl groups acquire negative charges. The structure now absorbs strongly at 555nm and presents a red color. This is also an example of halochromism. The addition of an oxygen bridge to the structure, linking two of the benzene rings creates fluorescein, which fluoresces, as it does not have a rapid path to dissipate absorbed energy.

The majority of organic dyes have conjugated chromophore systems with election donor or acceptor groups. Donor groups, which have neutral to positive charges, include amines ($-NH^2$, $-NRH$, NR^2), alkoxide ($-OR$), hydroxide ($-OH$) and acetate ($-OCOCH_3$). Acceptor groups, which have neutral to negative charges, consist of nitrate (NO_2), cyanide ($C\equiv N$), sulfite ($S=O-O-R$), carboxylate ($C=O=OH$), nitrite ($-N=O$) and carbonate ($-C=O-O$). Some dyes contain donor and acceptor groups, such as crystal violet which has three tertiary amine groups which can act as both donors and acceptors. As an organic molecule becomes larger and contains more complex structures, it will absorb light involving molecular orbitals. This is generally based on π-bonding in a conjugated system of alternating single and double bonds. Additionally, the attachment of electron donor and acceptor groups will influence the absorption spectra.

2.4   The Effect of pH Upon Spectra

The absorption spectra of a molecule can be obtained by plotting light absorption against wavelength. Spectra may be recorded in the range of visible light, 400-800 nm, or may extend into the ultraviolet or infrared, depending on the type of spectrum required. The resulting graph will present peaks where light is absorbed at distinct wavelengths, show minimum and maximum absorptions. The wavelength where the absorption (A) is highest is referred to as λ_{max} and along with the graph of the spectra, is characteristic of each specific molecule. This information is of particular importance with molecules that have color producing chromophores. It is used to identify the molecule.

The maximum absorption, or λ_{max} is generally a constant for a specific molecule, but it may change in response to interactions with the environment, such as when dissolved in various solvents or when the molecule is ionized. A shift towards a longer

wavelength is referred to as bathochromic or red shift. An example of this would be the

maximum absorption of a molecule shifting from 450 nm to 550 nm, or from a blue hue

to a green one. The absorption value moves towards the longer red wavelengths of the

spectrum, or ~635-800 nm, generating the reference of red-shifting. Bathochromic shifts

usually occur due to the auxochrome, or the functional group of the molecule that

influences the absorption of light by the chromophore. Examples of auxochromes are

amines ($-NH_2$), hydroxyls (-OH) and thiols (-SH), which are capable of protonation or

deprotonation in response to pH levels (Cairns 2008).

Examples environmental factors that may influence the λ_{max} are shown in Figure

2-8. Hypsochromic shifts are seen when the absorption maximum shifts towards the

shorter blue wavelengths, for example a shift from 600 nm to 500 nm. Like the

bathochromic shift, this may occur in response to ionization of the auxochrome but may

also be present from interaction with different solvents or temperature. The hypsochromic

effect may be useful in identifying aromatic groups. An increase in the light absorption

peak is termed as a hyperchromic effect, while a decrease in the absorption peaks is

called a hypochromic effect. Hyper and hypochromic shifts are related to concentration

of the chromophore and are useful for measuring a variety of phenomenon such binding,

uptake or degradation of the molecule of interest, for example.
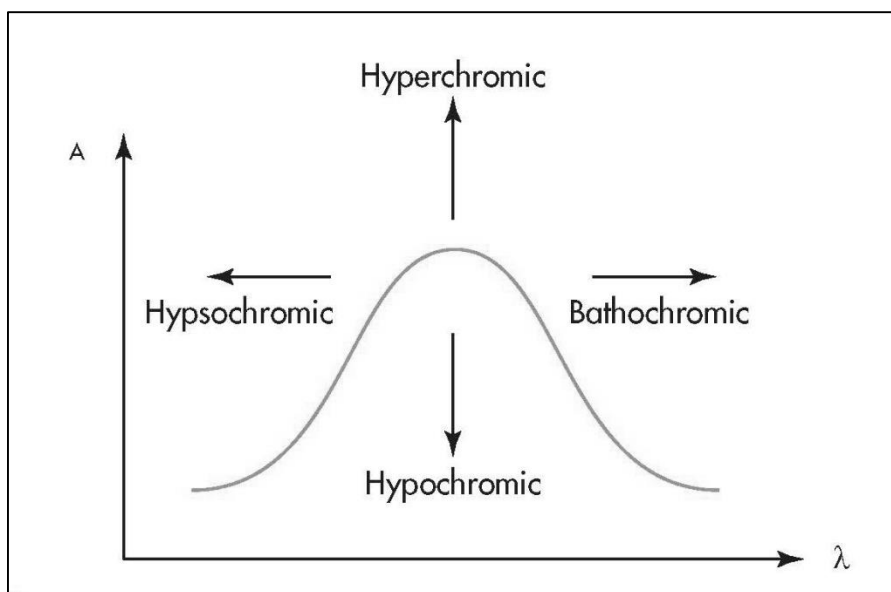
Figure 2-8. *A Model Graph of an Absorption Spectra Showing Shifts to the λ_{max} Due to Environmental Factors. (Cairns 2008)*

2.5 Ionochromism and Halochromism

A color change due to the interaction of a molecule with an ionic species is called ionochromism. Figure 2-9 illustrates the change in color of neutral red due to protonation and deprotonation. Neutral red is red in pH values >6.8 and yellow in basic conditions, showing a bathochromic shift when protonated and a hypsochromic shift when deprotonated. Chemical moieties that cause the change in color are called ionochromes or ionophores. The change can be from colorless to colored, or the reverse, and is usually reversible. Ionochromism can be separated into subdivisions based on the type of ion which prompts the change. Metallochromism applies when a metal cation causes the change. Chelating ligands such as crown ethers and cryptands covalently bound to chromophores are a common motif of these compounds. Halochromism refers to changes in color due to interaction with acids and bases, usually involving protonation and deprotonation (Bamfield 2010). Many compounds important to study undergo color

changes in response to protonation/deprotonation, including azo dyes, styryl dyes,

merocyanines and indophenols (Sabnis 2007). A wide variety of pH sensitive

compounds are commercially available with a extensive range of pH sensitivities.
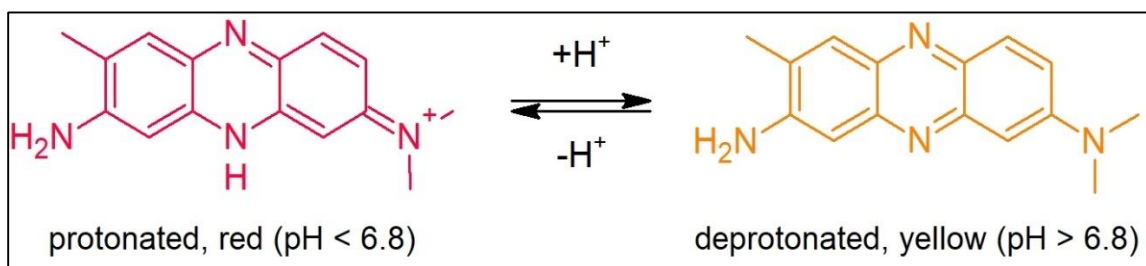
Figure 2-9. *The Neutral Red Molecule in Acidic and Basic Conditions, Showing the Rearrangement of Double Bonds with Protonationa Deprotonation*

Halochromic or pH sensitive dyes have many general structures. The phthalide

structure seen in phenolphthalein is a notable example. Phenolphthalein has a colorless

lactone form which converts to a mono- and diphenolate form when the lactone ring

opens to produce a red dianion. This process is reversible and is a common pH indicator

in the range of 8.5-9.0. Substitution in the phenolic rings of the phthaleins and

sulfophthaleins can produce a variety of colored dianions with different pK_a values, some

of which are fluorescent, such as the very important dye, fluorescein. These dyes do,

however, tend to be susceptible to photobleaching and photodegradation. Azo dyes (R-

N=N-R) and styryl dyes (N-R_3, N-R_2) with amine groups undergo protonation to give

azonium or ammonium tautomers. The azo dyes tend to become bathochromic and

hyperchromic, while the styryl dyes hypsochromic and hypochromic perhaps unto

colorless (Zollinger 2003).

2.6   Spectroscopy

Spectroscopy is an experimental application that is concerned with the absorption emission or scattering of electromagnetic radiation by atoms or molecules. Electromagnetic radiation covers a wide range from radio waves to γ-rays. The atoms or molecules can be in gas, liquid or solid phase (Hollas 2004). Isaac Newton performed an experiment in 1665 that dispersed white light into a spectra using a glass prism. In 1860 Bunsen and Kirchhoff developed the prism spectroscope as an analytical tool. Early applications were of the spectra of light produced by burning samples in a flame and of the sun. The visible spectra of hydrogen were observed in both of these methods. In 1885 Balmer correlated the spectral lines to a mathematical formula, bridging the relationship between experiment and theory in spectroscopy. Initially spectroscopy theory was based on classical Newtonian mechanics. Schrödinger developed quantum mechanics and from 1926 to the present, it has been of great importance. Emission spectroscopy is generally concerned with the ultraviolet and visible regions whereas absorption spectroscopy can be used in all regions of the spectrum.

To produce a spectrum, before the beam from the light source interacts with the sample, it is dispersed using a prism or a diffraction grating. Prisms are transparent objects with polished surfaces, often made from glass, quartz, plastics or fluorite. The refractive index of the prism is responsible for the dispersion of the light beam. A diffraction grating is a surface, glassy or metallic, which has been scored with a series of parallel grooves in an ordered spacing. The grated surface is usually coated with a reflective material such as aluminum to produce a mirror finish. Diffractive gratings can be planar or concave, in order to reflect or disperse the light beam.

Spectroscopy measures the level of interaction between light and matter. The earliest applications studied visible light diffracted by a prism into its component wavelengths. Further development included the interaction of a broader range of electromagnetic radiation and its interaction with matter. Spectroscopic data can be represented as an emission spectrum, which is a plot of the response data as a function of wavelength or frequency. Spectroscopy can be used to study physical and molecular composition and structure. Measurement devices range from spectrometers, spectrophotometers, spectrographs and spectral analyzers. It is of importance to chemistry because atoms and molecules have unique spectra which can be used to identify and quantify information about a known or unknown sample (Skoog 2007).

Each spectrum consists of either spectral lines or a plot of intensity vs. wavelength. Peaks and lines are spectral patterns which correspond to resonances between quantum states. Resonances can be plotted as amplitude to excitation frequency, with a peak at the resonance frequency. Many types of radiative energy can be used for spectroscopy, such as electromagnetic radiation (microwave, infrared, visible light, ultraviolet, x-ray), particles such as electrons and neutrons and even acoustic waves. In chemistry studies, spectroscopes focus mainly on Fourier transform infrared (FTIR) and ultraviolet-visible light (UV-vis).

Absorption spectroscopy studies the absorption of light or radiation by a material of interest. Absorption is determined by recording the percentage of light transmitted through the sample. Emission spectroscopy observes light or radiative energy emitted by the material. This can be used in studies of a sample's blackbody spectrum, or spontaneous emission spectra dictated by its temperature. Emissions studied can also be

from flames, as in atomic absorption spectroscopy, or in fluorescence where electrons are excited by UV into higher orbital states and subsequently decay back to their ground state. Raman spectroscopy is based on the observation of inelastic scattering of photons by matter and the subsequent vibrations and rotations of the atomic nuclei.

Molecular spectra will give information about electron spin rates, electronic states, molecular rotations and molecular vibrations.

2.6.1   Spectrophotometry

Spectrophotometry is an analytical tool that measures the light spectrum using near-ultraviolet, visible light and near-infrared. It is the quantitative measurement of the reflection or transmission properties of a material as a function of wavelength (Allen 2018). The amount of light that is absorbed by a compound can be measured as percent absorbed or transmitted. This can be measured by color, or by wavelength if the ultraviolet and infrared regions are of significance. Spectrophotometry is used for the measurement of solutions, gases, transparent objects and the surfaces of opaque materials. The observation of the visible spectrum (400-800 nm) is referred to as colorimetric analysis. However, the wavelength range can be 200-2500 nm, depending on the material studied and the equipment used.

This method is used by astronomers to measure the spectrum of celestial objects. It is commonly used in biochemistry to determine the equilibrium constant of a solution and in chemistry to characterize study materials. The absorption of light by a material or solution is due to the interaction of light with the electronic and vibrational modes of the component molecules. Every element or molecule has a distinct set of energy levels

related to its chemical bonds, electrons and nuclei. A material will absorb light of specific

wavelengths, producing a unique spectrum (Ninfa 2004).

Spectrophotometers have two designs containing a single or a double beam. A

single beam spectrophotometer measures the relative light intensity of a beam before and

after exposure to a material sample. A double beam instrument compares the intensity of

two light paths, one of which contains a reference sample and the other, material to be

measured. Spectrophotometers generally contain a light source, monochromator,

aperture, cuvette, photoresistors or a charged coupled device (CCD) and an amplifier.

The light source may be a broad spectrum source such as a halogen lamp that produces

visible and near ultraviolet light, or a limited spectrum source, such as narrow spectrum

LED which produces light in a known range. A monochromator contains a moveable or

fixed diffraction grating which produces a spectrum for analysis. In scanning

spectrophotometers, the detector measures light at stepped intervals until the proscribed

range is measured. CCDs are detector arrays that can be used to measure a light beam at

multiple wavelengths simultaneously.

When using the transmission mode of detection, the spectrophotometer measures

the beam that passes through a reference sample (or background) to a sample of interest.

The measurements are quantitatively compared, and the ratio is calculated giving the

percentage of transmission. If reflectance measurement is performed, the percentage of

light that is reflected from a reference sample and a study sample is measured and

compared. For any method used, the light from the source lamp is passed through the

monochromator and the light is diffracted into its component wavelengths. This light

passes through a rotating prism and the aperture. The photon flux density of the light,

reflected or transmitted, is then measured by a photodiode or light sensor. An array

spectrophotometer uses a light source which is diffracted with a reflection grating, which

passes through the sample and is measured by a detector array. Most infrared

spectrophotometers use Fourier transform spectroscopy to apply a logarithmic function to

the linear transmittance ratio to calculate the absorbency of the sample.

2.6.2   UV-Visible Spectrophotometry

Spectrophotometers can be used to measure in the ultraviolet and visible

spectrum. These instruments use light in the visible spectrum (400-700 nm) and the near

ultraviolet (200-400 nm). Ultraviolet light can induce electronic transitions. Fluorescence

measurements observe the transition from excited to ground state and absorption

measurements measure ground to excited state transitions (Skoog 2007). The electrons of

a molecule can absorb UV or visible light and become excited into a higher energy state.

The bonding and non-bonding electrons transition to the higher energy states of anti-

bonding molecular orbitals. The gap between the highest occupied molecular orbital

(HOMO) and the lowest unoccupied molecular orbital (LUMO) correlates to the length

of the wavelength of light absorbed. The possible types of transmission are $\sigma–\sigma^* > n–\sigma^*$

$> \pi–\pi^* > n–\pi^*$ in order of energy state (Griffith 1957).

UV-vis spectroscopy is used in the quantitative analysis of many materials such as

organic materials and biological compounds to inorganic materials like silicon and

transition metals. Metal ions can be colored due to transitions of their d shell electrons.

These cations are affected by coordination with anions or ligands, resulting in a change in

their maximum absorption (λ_{max}). Organic compounds absorb light in the UV and visible

range and this is affected by their degree of conjugation. The addition of alternating σ and π bonds will affect the absorption and may cause bathochromic or ipsochromic shifts.

When using UV-vis spectroscopy, care must be taken with protocols and methods. Organic solvents may have strong absorption curves which can obscure or compromise data collection. Ethanol is a common organic solvent used because of its weak absorption spectra. Ethanol is miscible with a wide variety of other organic solvents, but unfortunately is not universal. Additionally, solvent polarity, temperature, concentration, purity and pH can affect the spectra as well. and cuvettes. A sample to be measured must be loaded into expensive and fragile quartz cuvettes, rather than glass or plastic, so that the ultraviolet areas of the spectrum are not blocked by the material of the cuvette itself.

CHAPTER 3

PREPARATION OF HALOCHROMIC IONOPHORE FUNCTIONALIZED SILICA AND HALLOYSITE CORE NANOPARTICLES WITH GLUTARALDEHYDE

3.1 Introduction

Halochromic dyes react with protons and exhibit a physical change such as fluorescence or a chromatic shift in their spectral band. The difference can be seen between by observing the protonated and deprotonated states of the material. The use of a dye in solution to monitor pH can present problems since the dye may react with the study material and cause contamination. Covalently binding the dye to a nanoparticle can prevent the dye molecule from contaminating and altering the study material.

The particles in this chapter were functionalized with neutral red, a halochromic dye with a pK_a of ~6.8 that exhibits a colorimetric change at near neutral pH ranges. The cores of the particles consisted of either silica (SiO_2) nanoparticles or halloysite nanotubes. Halloysite consists of aluminosilicate (SiO_2AlO_2) layers with silica comprising the outer layer. Since silica and aluminosilicate contain silicate (n-Si-O-Si-n) groups, the protocol as developed was able to be used for either inorganic core with no modifications.

The dye was covalently bound to the nanoparticles by a multiple step process that is shown in the reaction scheme in Figure 3-1. In the first step, the particles were

57

functionalized with a 1^0 amine group (-NH2) using APTES, a widely used organosilane crosslinking agent. The silanol groups of the particles react with the ethoxy groups of the silane in an elimination reaction, forming a $-Si-O-Si(Ch_2)_3NH_2$ bond onto the nanoparticle surface with ethanol as a byproduct. In the second step, glutaraldehyde, a dialdehyde that is used in many biochemical applications, was added to the reaction mixture to link to the $-NH_2$.and to provide an aldehyde functional group for the addition of the NR. Aldehydes react with primary amines to produce imine bonds. In theory one aldehyde group of glutaraldehyde would react with the primary amine group attached by use of APTES, leaving the other aldehyde functional group on the surface of the particles.

In some early attempts after the addition of the glutaraldehyde, the particles began to agglomerate into much larger microparticles likely due to glutaraldehyde crosslinking the amine groups on neighboring NPs. Adjusting the amount of glutaraldehyde or the reaction solution volume did not remedy this issue. However, since the pK_a of the amine group of immobilized ATPEs is ~7.6 (Williams 2013), an acidic pH would impart a positive charge on the amine groups and the particles should repulse each other. Aliquots of SAGN and HNT-APTES were suspended in buffered solutions and measured at a range of pH solutions and their zeta potential was measured. At a pH value of 5.0 the zeta potential was 8 mV, implying that the particles had poor dispersion stability, but zeta potential is pH dependent and is a sum of the surface charges from all functional groups, including hydroxyls and amines.
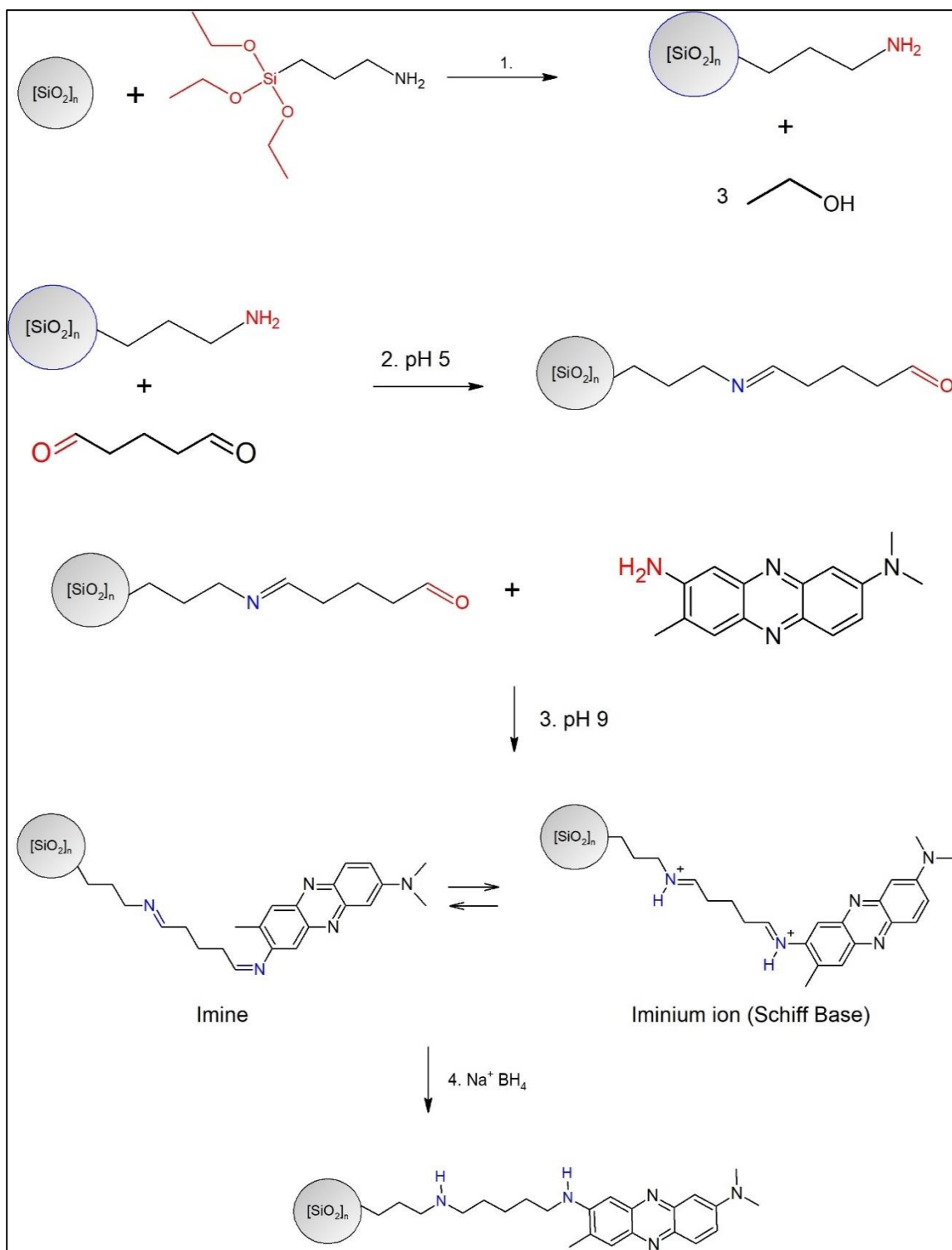
Figure 3-1. *The Reaction Scheme for the Modification of SiNPs or HNTs, with APTES, Glutaraldehyde and Neutral Red Followed by the Reduction of the Iminium Ions by Sodium Borohydride to Secondary Amines*

After adjusting the pH of the reaction solution to pH 5.0, the addition of glutaraldehyde did not lead to large microparticles, implying that crosslinking between the amine groups with glutaraldehyde was minimized.

The third step of this protocol was to bind the neutral red halochromic dye to the aldehyde functional group. Neutral red is a polyamine molecule with one primary amine functional group. The other amines are tertiary and should not react with aldehydes. The pH of the reaction solution was adjusted to pH 9 to reduce the likelihood of protonation of the dye's 1^0 or 3^0 amine groups. This allowed the 1^0 amine of the neutral red molecule to be covalently bound to the aldehyde group of the modified nanoparticles.

The aldehyde-amine reaction produces an imine bond that is reversible with an iminium ion. The fourth step of the protocol was a treatment with sodium borohydride to reduce the imine bond to a more stable secondary amine bond. This protocol produced nanoparticles with either silica or aluminosilicate cores that had covalently bound neutral red dye. The neutral red moiety was still pH sensitive as the molecule was covalently bound via its primary amine functional group, not the tertiary amine that is responsible for its halochromic response. The dye functionalized particles were also wash and leach resistant.

Even after multiple washings in both ethanol, 0.1M HCl, and 0.1M NaOH, the dye remained attached to the nanoparticles. As a control, SiNPs and HNTs were combined with neutral red alone, without APTES or glutaraldehyde. The product of this reaction was brownish-yellow particles that had no sensitivity to pH. Since silanols are capable of hydrogen bonding with 1^0, 2^0 and 3^0 amines (Baxter 1997) it may be due to the hydrogen bonding of the silanols to the tertiary amines of the neutral red that produced

the brown non-functional product. Although reaction of neutral red with HNTs produced red/yellow particles, the coloration diminished with successive washings until the HNTs returned to their original tone. It is supposed that the HNTs adsorbed the dye, rather than covalently attaching to the silanol groups, and gradually released it into the wash solutions, as adsorption and slow release is a well-studied characteristic of HNTs.

3.2   Experimental

3.2.1   Materials and Reagents

The SiNP cores were purchased from US Research Nanomaterials. The HNTs were purchased from Sigma Aldrich. The reagents neutral red (98.0%), APTES (99.0%), glutaraldehyde (50% wt. in water), and sodium borohydride (99.0%) were purchased from Sigma Aldrich. The solvents and other chemicals toluene (99.5%), ethanol (95.27%), isopropyl alcohol (95.27%), glacial acetic acid (99.0%), sodium hydroxide (97%) and phosphate buffered saline TAB (99.0%) were purchased from Sigma Aldrich and Fischer Scientific.

3.2.2   Protocol

The protocol was developed to be used with either silica SiNPs or aluminosilicate HNTs. The functionalization occurs upon the silica surface of the nanoparticles or the silica outer layer of the HNTs. All steps are identical for either core.

1. The HNTs and SiNPs were dried at 150^0C for 24 hours prior to use. A 200 mg sample of either HNTs or SiNPs was mixed with 50 mL of toluene and sonicated for 10 minutes to separate and disperse the particles into the toluene. The mixture was refluxed at 100^0C for 20 minutes, then cooled to 40^0C.

2. A 500μL aliquot of APTES was added to the solution and refluxed at 40^0C with magnetic stirring for 12 hours.

3. The particles were washed by centrifugation, the supernatant was removed, then the particles were re-suspended in ethanol using a vortex mixer, followed by another centrifugation. This was repeated two times to remove unreacted APTES and residual toluene.

4. The amine-functionalized particles were resuspended in 50 mL of 95% ethanol. The ethanol solution was sonicated for five minutes to evenly disperse the particles and then rapidly stirred in a round bottom flask. The pH was adjusted to pH 5.0 with glacial acetic acid.

5. A glutaraldehyde solution was prepared by dissolving 200 μL of 50% wt. glutaraldehyde in water into 2.0 mL of ethanol. The solution was slowly added dropwise to the nanoparticle solution. The reaction solution was stirred for 12 hours at room temperature. The glutaraldehyde functionalized particles were washed by the previous method of centrifugation and resuspension in 50 mL of ethanol. The pH was adjusted to pH 9.0 with 2M ethanolic sodium hydroxide.

6. A solution of neutral red was prepared by dissolving 118 mg of neutral red into 2.0 mL of ethanol. The solution was slowly added to the reaction solution. The reaction solution was stirred for 12 hours then washed three times with ethanol to remove unreacted neutral red.

7. The neutral red functionalized particles were resuspended in 50 mL of ethanol and rapidly stirred. A solution of sodium borohydride ($NaBH_4$) was freshly

prepared by dissolving 2.5 mg of sodium borohydride into 5 mL of isopropyl

alcohol. The $NaBH_4$ solution was rapidly added to the nanoparticle solution

and stirred for 15 minutes. 50 mL of DI H_2O was quickly added to the

solution to quench the unreacted $NaBH_4$. The particles were washed with

ethanol twice and DI H_2O twice then resuspended in DI H_2O or dried for

further use.

3.3   Instrumentation

The absorption/reflection spectra of the samples were obtained with an Ocean

Optics USB4000 spectroscope using a StellarNet LED driver equipped with a white

LED. The spectra were recorded and analyzed with Ocean View spectroscopic software.

The FTIR spectra were performed on a Thermo Scientific IR100 FTIR spectrometer with

an attenuated total reflectance (ATR) attachment. DLS and zeta potential measurements

were taken on a Brookhaven Instruments Zeta Plus analyzer. FESEM images were

obtained with a Hitachi S-4800 field emission scanning electron microscope. All

photographic images were taken with a Nikon D60 and processed with Photoshop.

3.4   Results and Discussion

3.4.1   Images

The silica core particles were synthesized following the protocol as previously

written. They were dispersed into buffered solutions at a concentration of 0.1 mg/ml. The

buffered solutions were adjusted to a range of pH levels prior to the addition of the

particles. Two series of solutions were prepared. One series contained a range of pH

values from 1.40 to 13.40 in increments of one, giving fourteen solutions in total. This

was to show colorimetric change over a broad pH range. The nanoparticle pH solutions

for this range can be seen in Figure 3-2. The second series of buffer solutions prepared

was from pH 6.0 to 8.0 in increments of 0.2, giving eleven solutions in total. The

solutions for the near neutral pH range can be seen in Figure 3-3. This was designed to

observe pH change in a near neutral range that spanned the isosbestic point of the silica-

APTES-glutaraldehyde-neutral red nanoparticles (SiAGN) and the halloysite-APTES-

glutaraldehyde-neutral red nanotubes (HAGN).

Figure 3-2. *SAGN Dispersed in Aqueous Buffer Solutions from Ph 1.4 to 13.40 Showing Color Change and Good Dispersion*

Figure 3-3. *SAGN Dispersed in Aqueous Buffer Solutions from pH 6.0-8.0 Showing Very Subtle Color Change but Good Dispersion*

After addition of the particles, minor adjustments to the pH of each solution were

made with 0.01M NaOH or 0.01M HCl. The particles exhibited rapid color change when

added to the solutions. The color change was apparent to visual observation, but the

particle solutions were measured with an Ocean Optics spectrometer. The particles

showed a good dispersion in the aqueous buffer solutions. The dispersion was seen to

persist for the duration of the measurements. Samples left overnight exhibited some

settling of nanoparticles to the bottom of the vessel.

The HNT core particles were synthesized according to the process used for SiNPs

with no modifications to the protocol. In the same methodology as the SiNPs, they were

dispersed into buffered solutions at a concentration of 0.1 mg/ml. The buffered solutions

were adjusted to a range of pH levels prior to the addition of the particles. Two series of

solutions were prepared. One series contained a range of pH values from 1.40 to 13.30 in

increments of one, giving fourteen solutions in total as seen in Figure 3-4. This was to

show colorimetric change over a broad pH range. The second series of buffer solutions

prepared was from pH 6.0 to 8.0 in increments of 0.2, giving eleven solutions in total as

seen in Figure 3-5.

Figure 3-4. HAGN *Dispersed in Aqueous Buffer Solutions from Ph 1.40 To 13.30 Showing Color Change and Dispersion*

Figure 3-5. *HAGN Dispersed in Aqueous Buffer Solutions from pH 6.0-8.0 Showing Color Change and Dispersion*

After addition of the particles, minor adjustments to the pH of each solution were made with 0.01M NaOH or 0.01M HCl. The particles exhibited rapid color change when added to the solutions. The color change was apparent to visual observation, but the particle solutions were measured with an Ocean Optics spectrometer. The particles showed a good dispersion in the aqueous buffer solutions. The dispersion was seen to persist for the duration of the measurements. Samples left overnight exhibited some settling of nanoparticles to the bottom of the vessel.

3.4.2   FESEM

To prepare the particles for FESEM, they were dispersed in ethanol at a low concentration, sonicated for ten minutes, then drop cast onto aluminum foil and dried in a fume hood. The aluminum foil provided an inexpensive and conductive surface to prepare the particles for the SEM. Particles prepared for SEM are subject to clumping during drying, but surface morphology can be observed. The unmodified SiNPs can be seen in Figure 3-6 and exhibit clusters of spherical particles. The SiNPs functionalized with APTES can be seen in Figure 3-7. The particles do not show much change in morphology from the unmodified SiNPs. The glutaraldehyde modified particles can be

seen in Figure 3-8. There is no change in the surface morphology. The particles from the

final stage of the synthesis protocol can be seen in Figure 3-9. Again, there is no change

to the surface features, but when visually observed, the particles have a red color,

indicating that the dye has been bound to the particle surface. As the particles were

modified in each step, they did not show changes in structure or morphology. This was

expected because the functionalization layers only consist of a one molecule thick layer

and should not substantially change the morphology. The SEM data confirms this

observation.
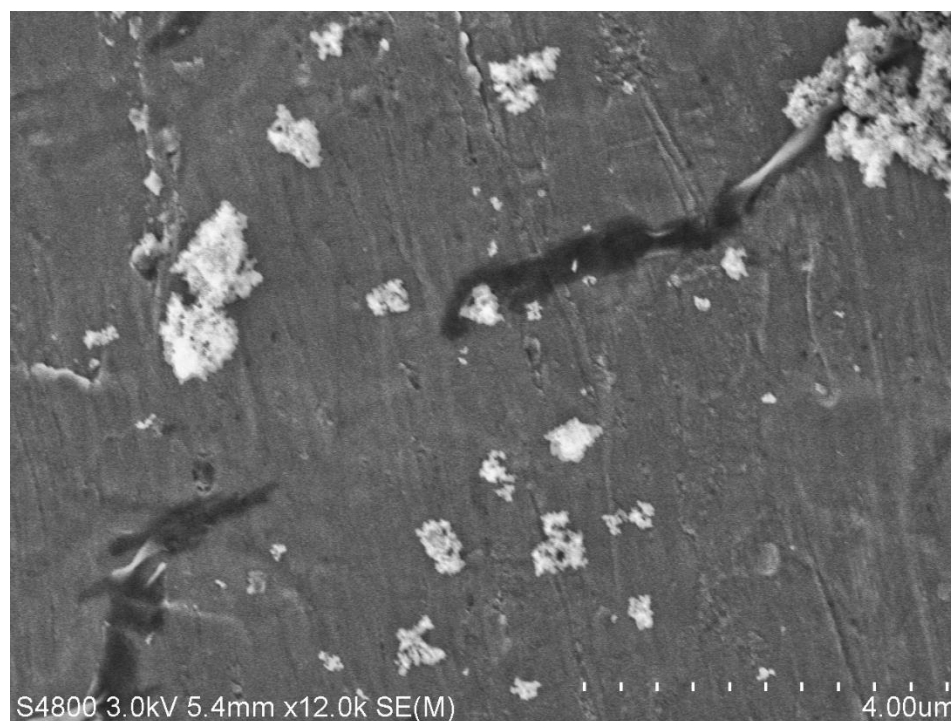
Figure 3-6. *Unmodified SiNPs Showing Clusters of Dried Particles*
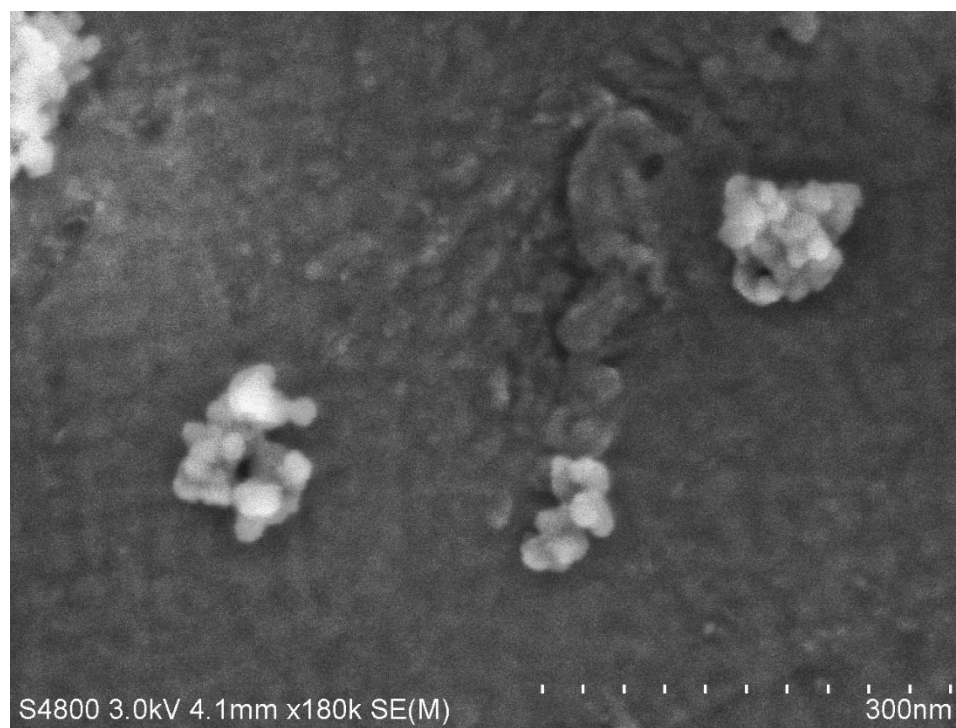
Figure 3-7. *SiNPs Functionalized with APTES*
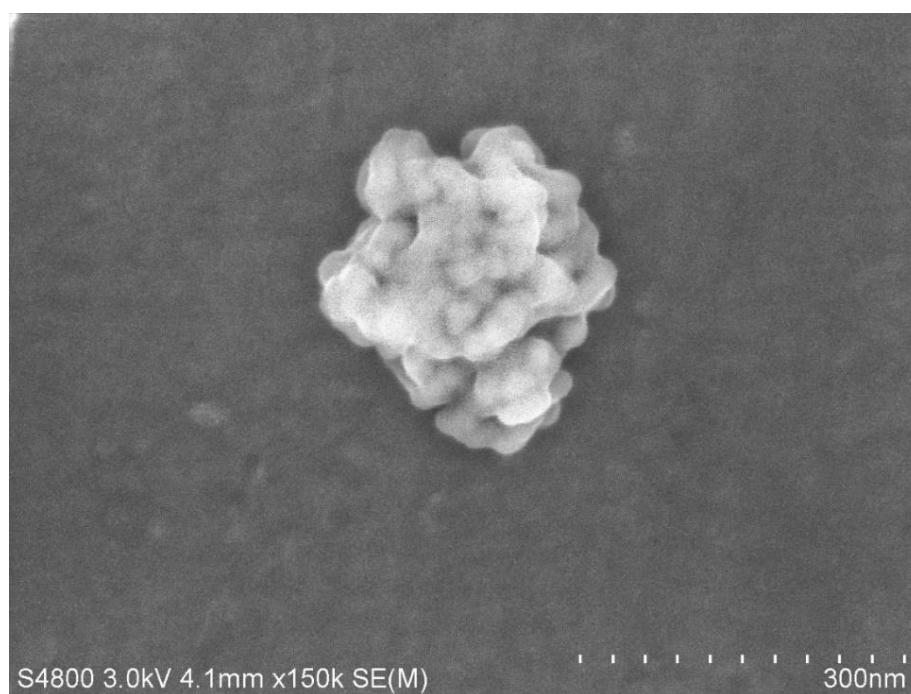
Figure 3-8. *SiNPs Functionalized with APTES and Glutaraldehyde*
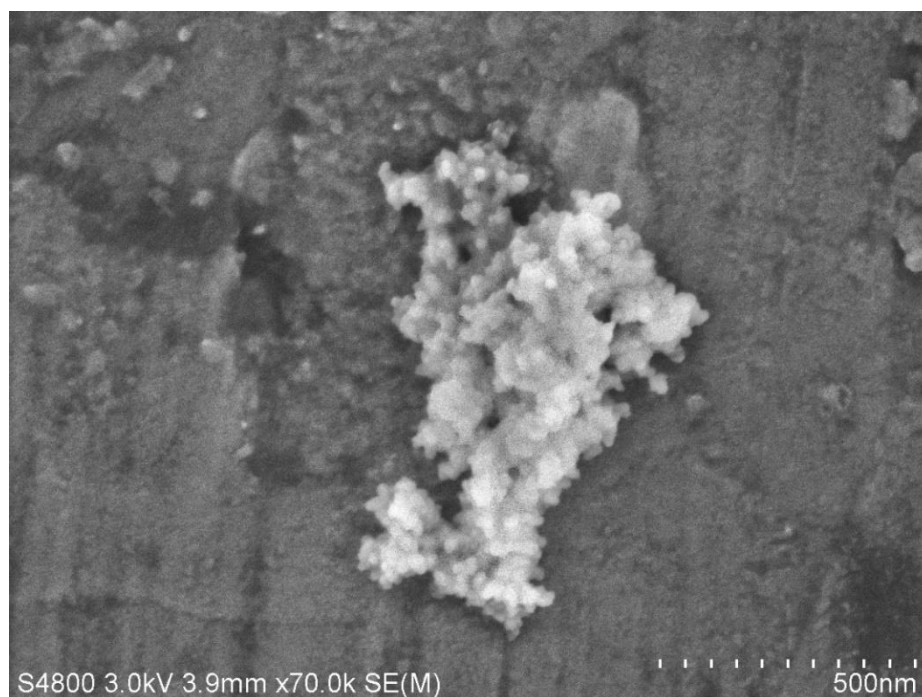
Figure 3-9. *SAGN NPS Functionalized with APTES, Glutaraldehyde and Neutral Red*

FESEM images of HNTs were taken in an original state and in stages of modification. The nanotubes were measured and showed a greater variability in size with compared with the SiNPs. This may be due to the fact that HNTs are a naturally produced material where SiNPs are synthesized using the well-known Stöber process which has been shown to reliably produce monodispersive particles. The unmodified HNTs can be seen in Figure 3-10 and exhibit the rolled scroll like tubes typical of HNTs. The HNTs functionalized with APTES can be seen in Figure 3-11. The particles do not show much change in morphology from the unmodified HNTs. The glutaraldehyde modified nanotubes can be seen in Figure 3-12. There is no change in the surface morphology. The particles from the final stage of the synthesis protocol can be seen in Figure 3-13. The HNTs do show a loss of surface detail and similar to the SiNPs, they exhibit a red color,

indicating that the dye has been bound to the particle surface. The loss of surface detail

may be due to the organic layers or from focus issues of the SEM.

Figure 3-10. *Unmodified HNTs*
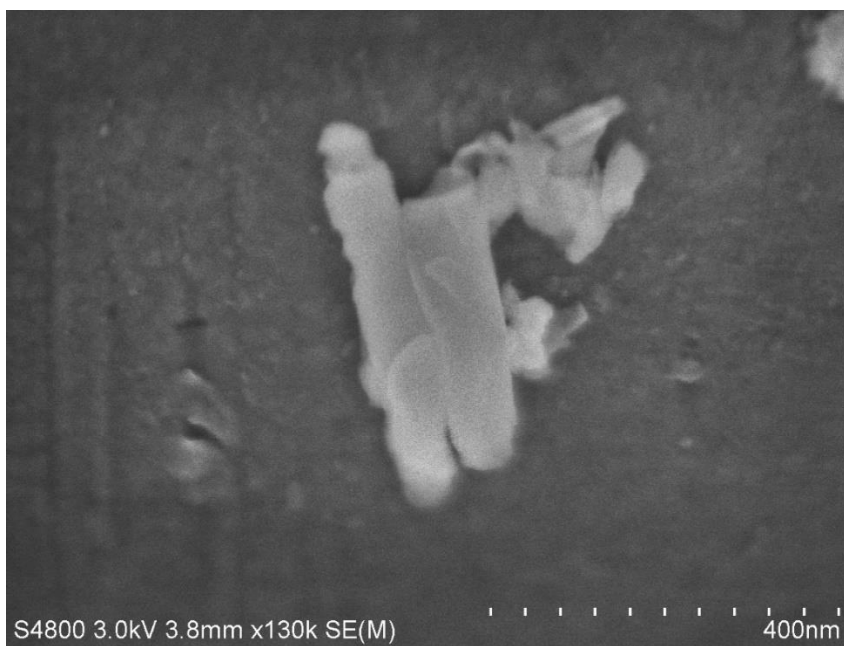
Figure 3-11. *HNTs Functionalized with APTES*
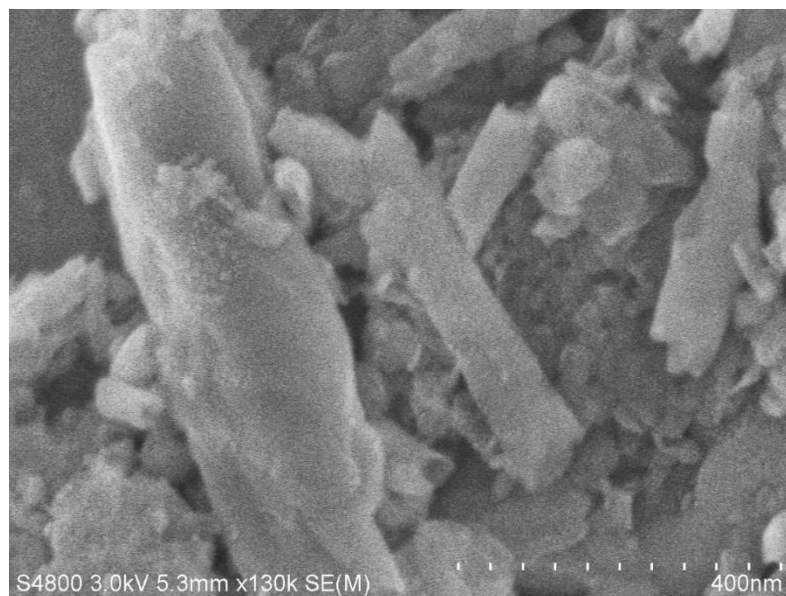
Figure 3-12. *HNTs Functionalized with APTES and Glutaraldehyde*
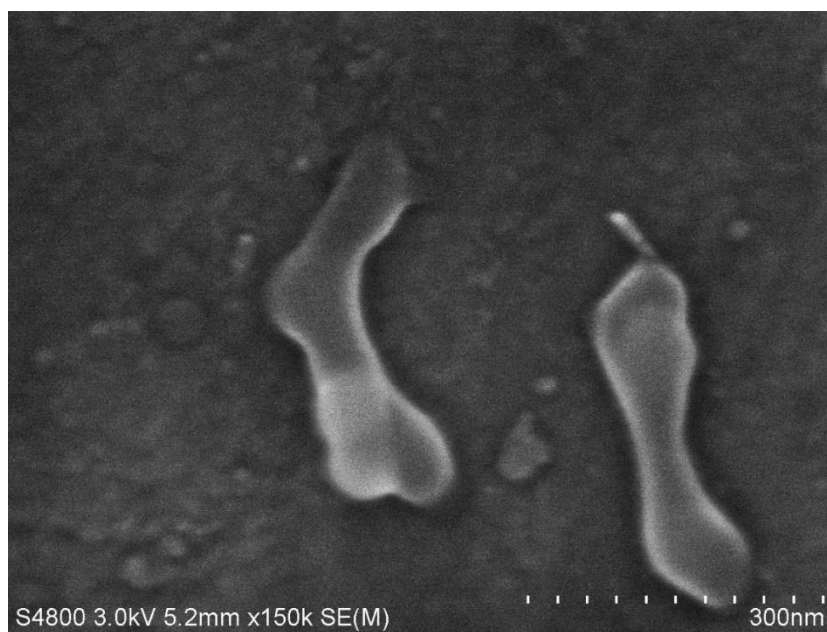
Figure 3-13. *HAGN Functionalized with APTES, Glutaraldehyde and Neutral Red Showing Some Loss of Surface Detail*

3.4.3　　　　DLS

The particles were measured with dynamic light scattering (DLS) by dilution with ethanol and sonication to separate the particles. With each successive layer, the SiNPs showed an increase in size from ~206 nm for SiNPs to ~296 nm for the SAGN, an increase of 43.7%, as can be seen in Figure 3-14. This effect may be due to flocculation in solution or loss of smaller particles during the purification and washing steps. The functionalized HNTs followed a similar pattern, as seen in Figure 3-15. With each successive layer, the HNTs showed an increase in size from ~351.4 nm for HNTs to ~522.8 nm for the HAGN, an increase of 48.8%, as can be seen in Figure 3-14. This effect may be due to the loss of smaller particles during the purification and washing steps.
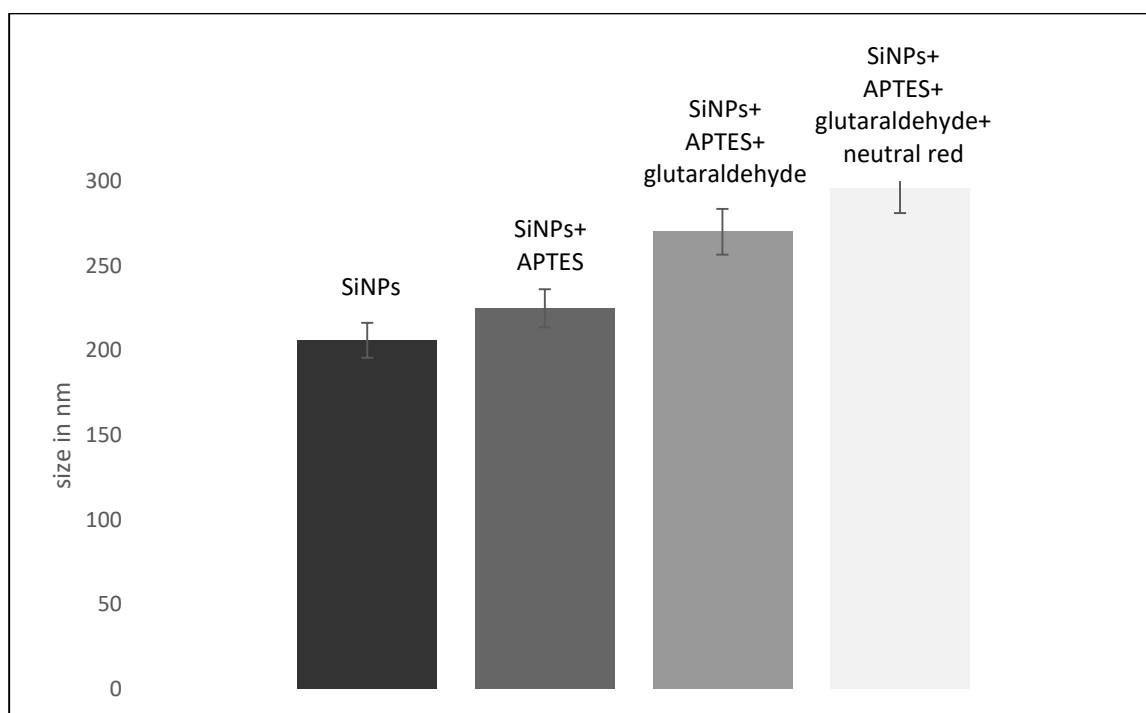
Figure 3-14. *DLS Data of the Steps of Synthesis of the SAGN Showing Particle Siz*e
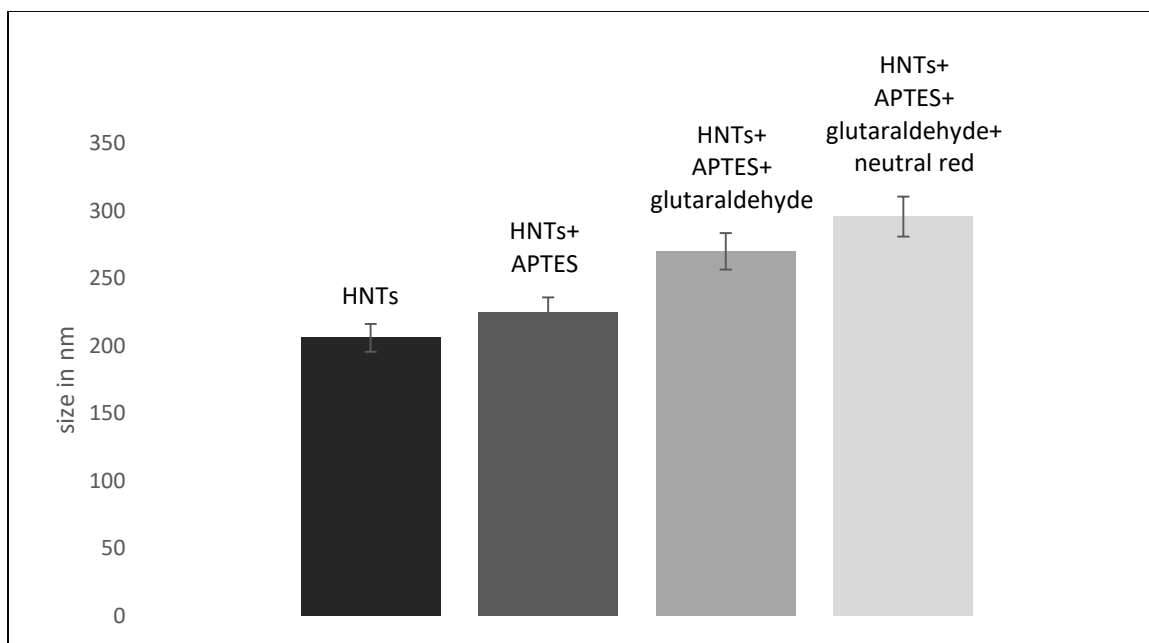
Figure 3-15. *DLS Data of the Steps of Synthesis of the HAGN Showing Particle Size*

3.4.4 FTIR Spectra

The graph in Figure 3-16 shows FTIR data recorded the reagents and for each stage of the synthesis of the SAGN NPS. The first spectrum is of the SiNPs. The second spectrum is of the SiNPS after functionalization with APTES to provide an amine group.
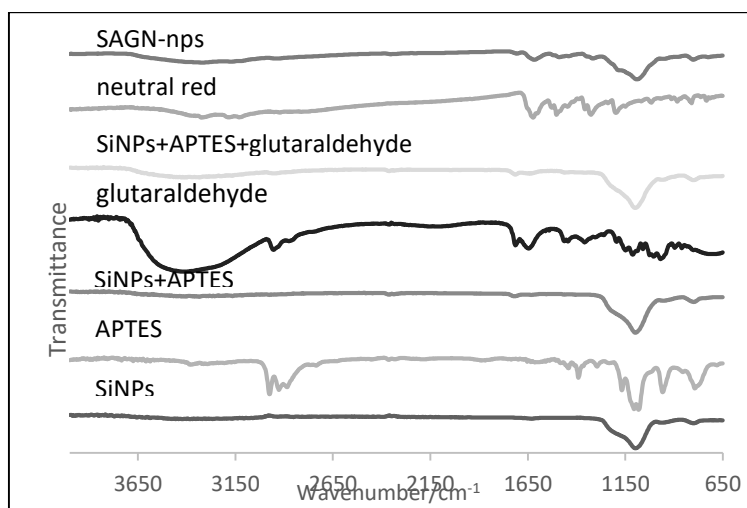
Figure 3-16. *A Comparison of IR Spectra of Modification Layers of SAGN and Reagents*

Figure 3-17 shows a comparison of the SiNPs+APTES with unmodified SiNPs. The two spectra both show a strong peak at 1100 cm^{-1} representing the Si-O stretch of silica. The SiNPs+APTES shows peaks at 1722 and 1633 cm^{-1} which may be from -NH$_2$ scissoring from the amine group of APTES. The peaks at 1465 and 1409 cm^{-1} may be from CH$_2$ bending from the alkanes. This data would suggest that the protocols may be modified by increasing the amount of the reagent or reaction time. The lack of a sharp peak may be due to the relatively small percentage of amine groups that were bound to the surface of the particle.
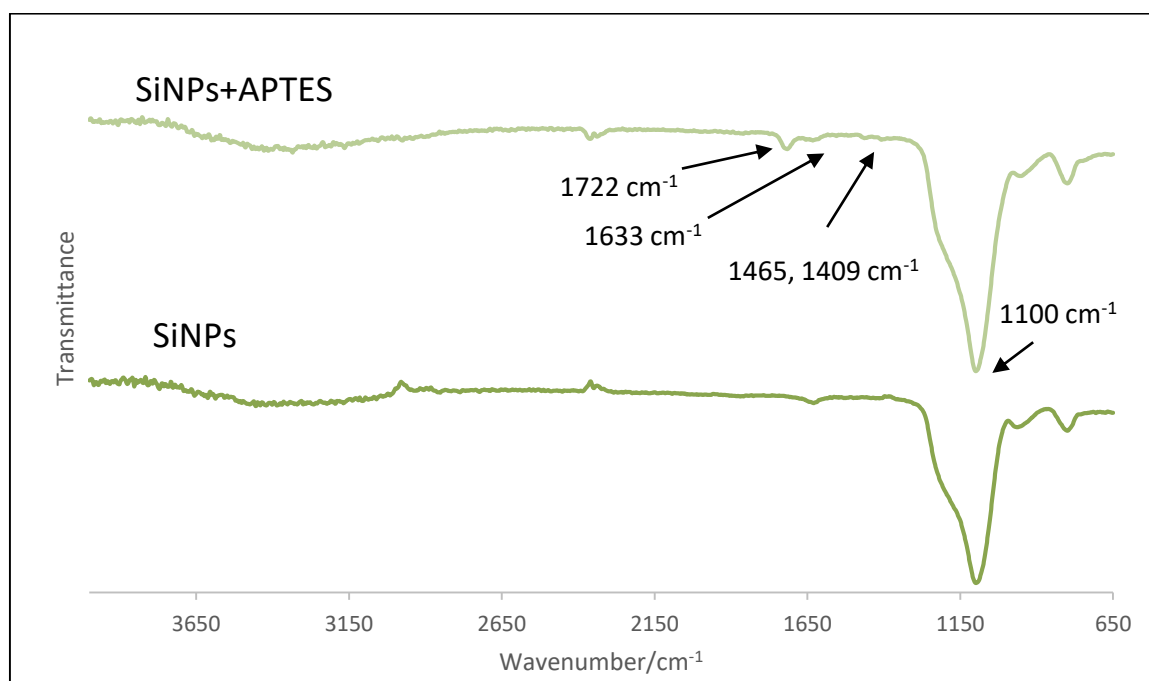
Figure 3-17. *A Comparison of IR Spectra of SiNPs and SiNPs Modified with APTES*

Figure 3-18 shows a comparison of the spectra of SiNPs and SiNP+APTES modified with glutaraldehyde. The spectrum of the silica-APTES-glutaraldehyde particles showed peaks at 1716 cm^{-1}, which may indicate the C=O stretch of an unsaturated aldehyde and at ~2960 cm^{-1}, which may indicate the C-H stretch of an

alkane. This data supports the successful attachment of glutaraldehyde to the to the surface of the APTES functionalized SiNPs.
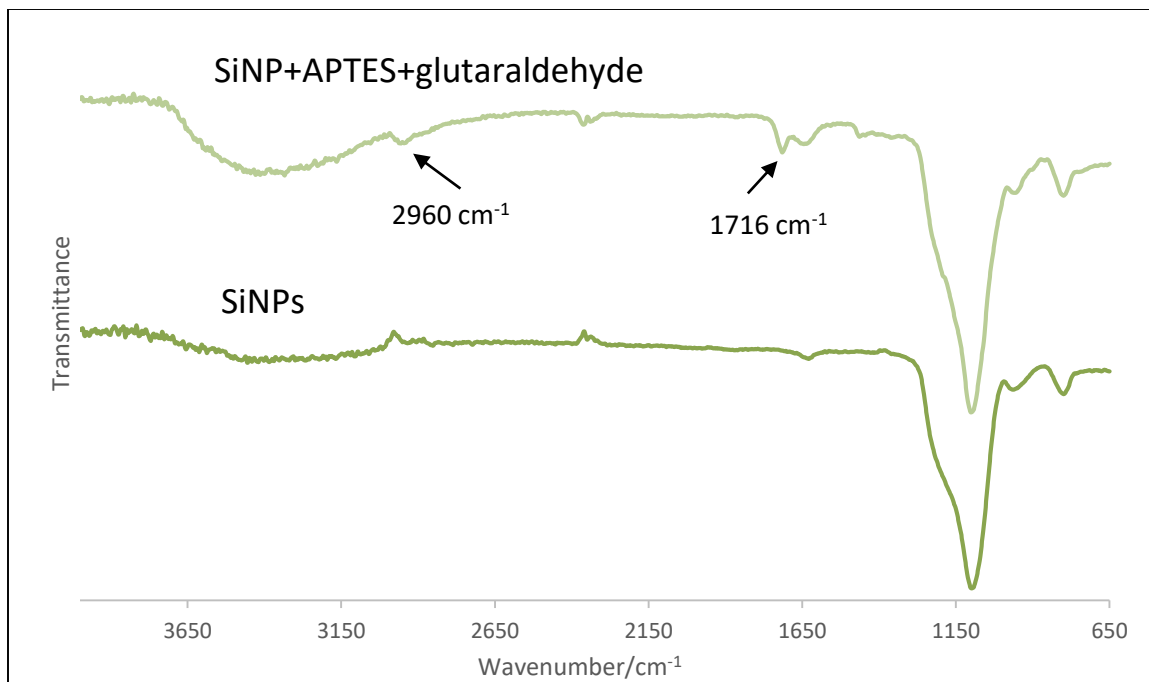
Figure 3-18. *Comparison of FTIR Spectra of SiNPs and SiNPs+APTES+Glutaraldehyde*

Figure 3-19 shows the spectrum of SiNPs in comparison to the final product of SAGN NPS after functionalization with neutral red. The SAGN spectrum shows the addition of peaks at 1621, 1490, 1319 and 1182 cm^{-1}, which may be from the C=C stretch of aromatic carbons found in the neutral red molecule. The spectrum also showed a small peak at 3326 cm^{-1}, which may be from the N-H stretch of a 2^0 amine, supporting the addition of neutral red to the aldehyde functional group by covalent binding to its primary amine, producing an imine bond, which was reduced to a 2^0 amine with sodium borohydride.
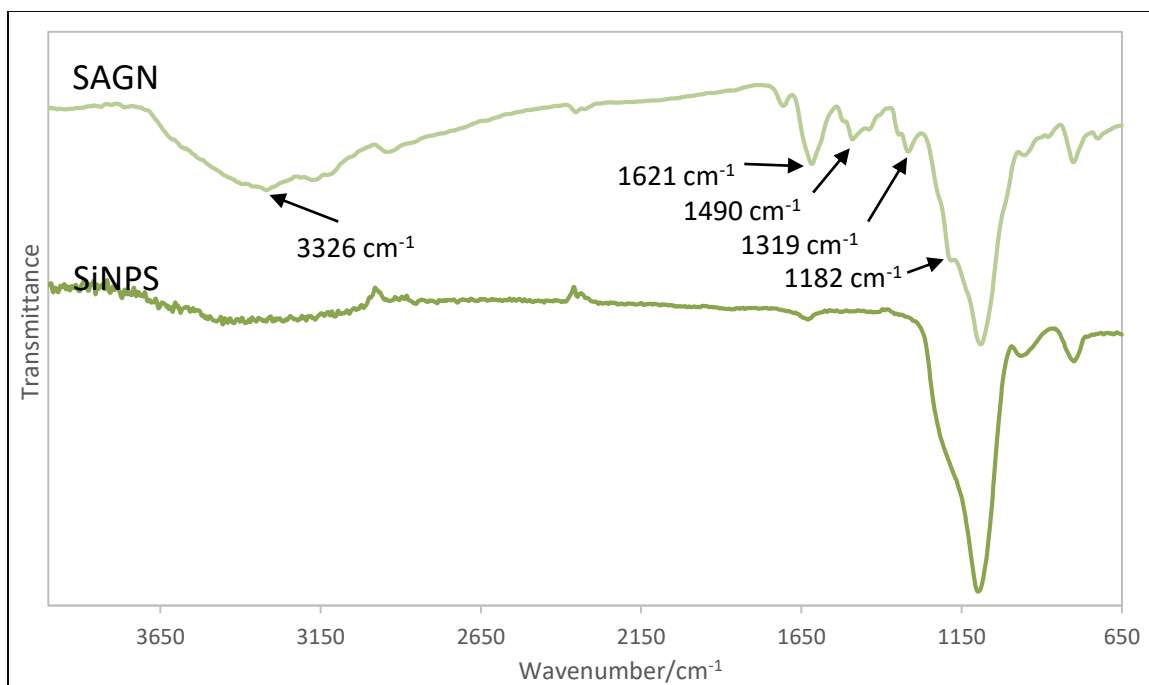
Figure 3-19. *A Comparison of IR Spectra of SiNPS with SAGN*

The graph in Figure 3-20 shows FTIR data recorded the reagents and for each stage of the synthesis of the HAGN. The first spectrum is of the HNTs. The second spectrum is of the HNTs after functionalization with APTES to provide an amine group.
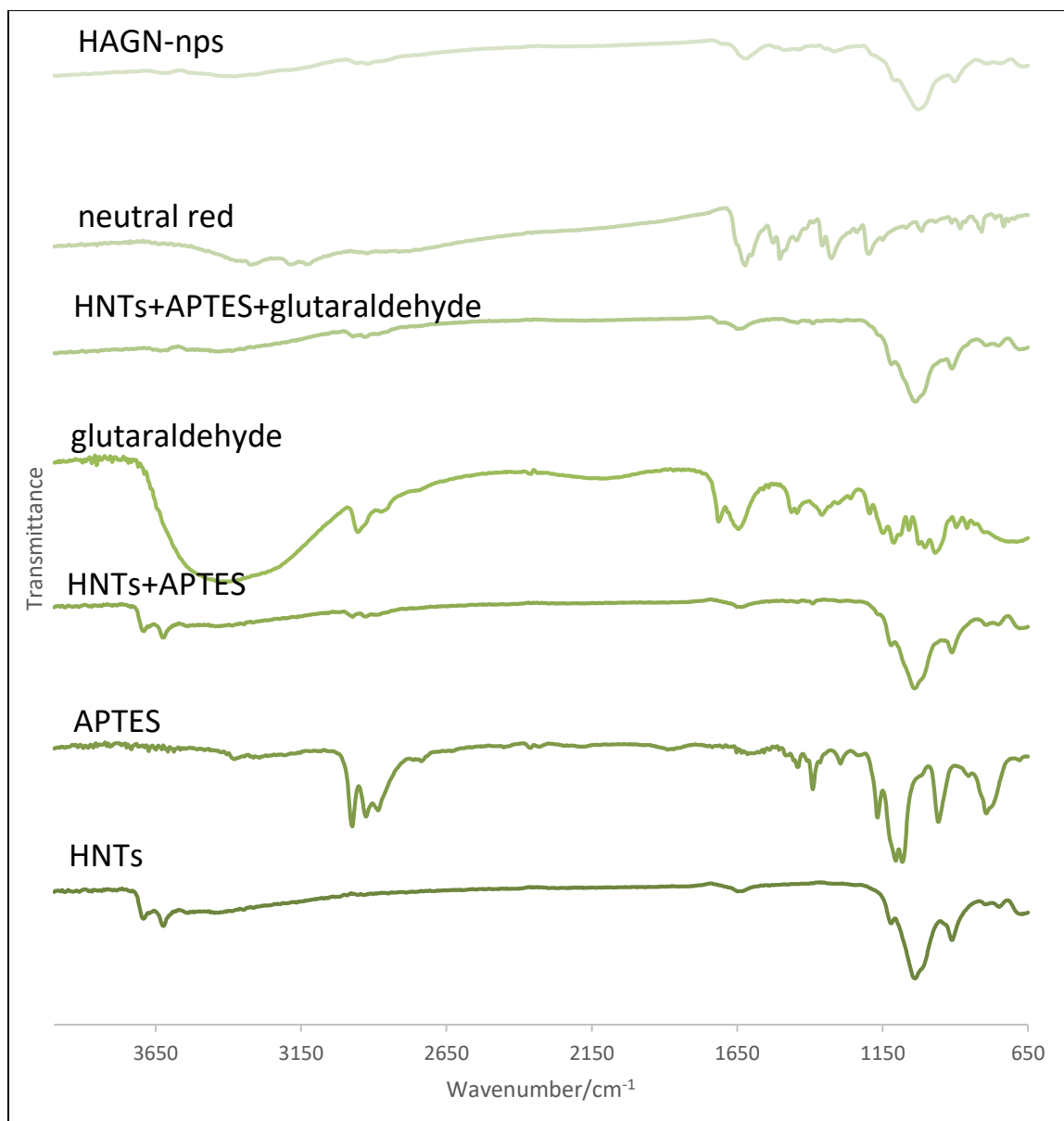
Figure 3-20. *A Comparison of IR Spectra of Layers of HAGN*

A comparison of the HNTs -APTES with unmodified HNTs can be seen in Figure 3-21. The two spectra both show a strong peak at ~1037 representing the Si-O stretch of silica. The spectrum of the HNTs -APTES does not show a discernable peak in the range of 355-3200, which would indicate an N-H stretch. The HNT-APTES show peaks at 2969 and 2929 cm^{-1} which may indicate the presence of alkanes from APTES. As with

the SiNPs, common protocols were followed when reacting the particles with APTES. Although in comparison to the SiNP spectra, the HNTs FTIR spectra is more supportive of addition of a propylamine moiety from APTES. However, this data would suggest that the protocols may be modified by increasing the amount of the reagent or reaction time. As with SiNPs, the lack of a sharp peak may be due to the relatively small percentage of amine groups that were bound to the surface of the particle. The presence of a stronger peak for alkanes may be due to the four alkanes ($-CH_2-CH_2-CH_2-CH_2-NH_2$) in the propyl group of APTES.
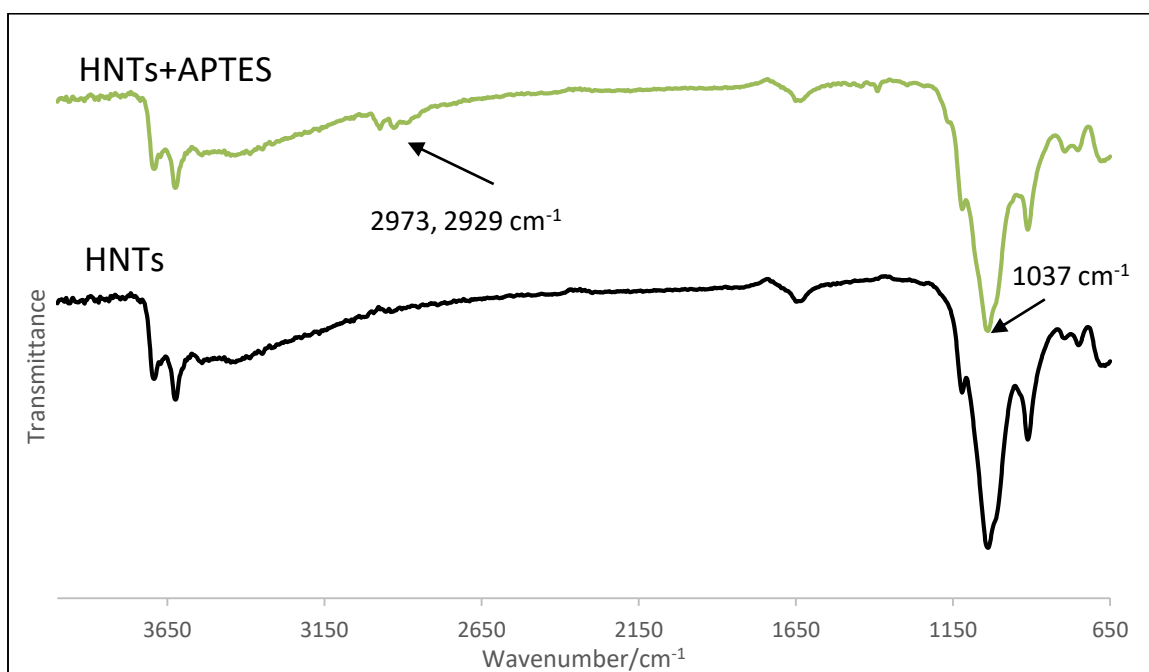
Figure 3-21. *A Comparison of IR Spectra for HNTS and HNTS Functionalized with APTES*

The spectra in Figure 3-22 shows the comparison of unmodified HNTs with HNT-APTES modified with glutaraldehyde. The halloysite-APTES-glutaraldehyde particles showed a small peak at 1708 cm^{-1}. which may indicate the C=O bending of an

aldehyde from glutaraldehyde. The peaks at 2969 and 2929 cm^{-1} may be from C-H

stretching. This data may support the successful attachment of glutaraldehyde to the to

the surface of the particle after reaction with glutaraldehyde.
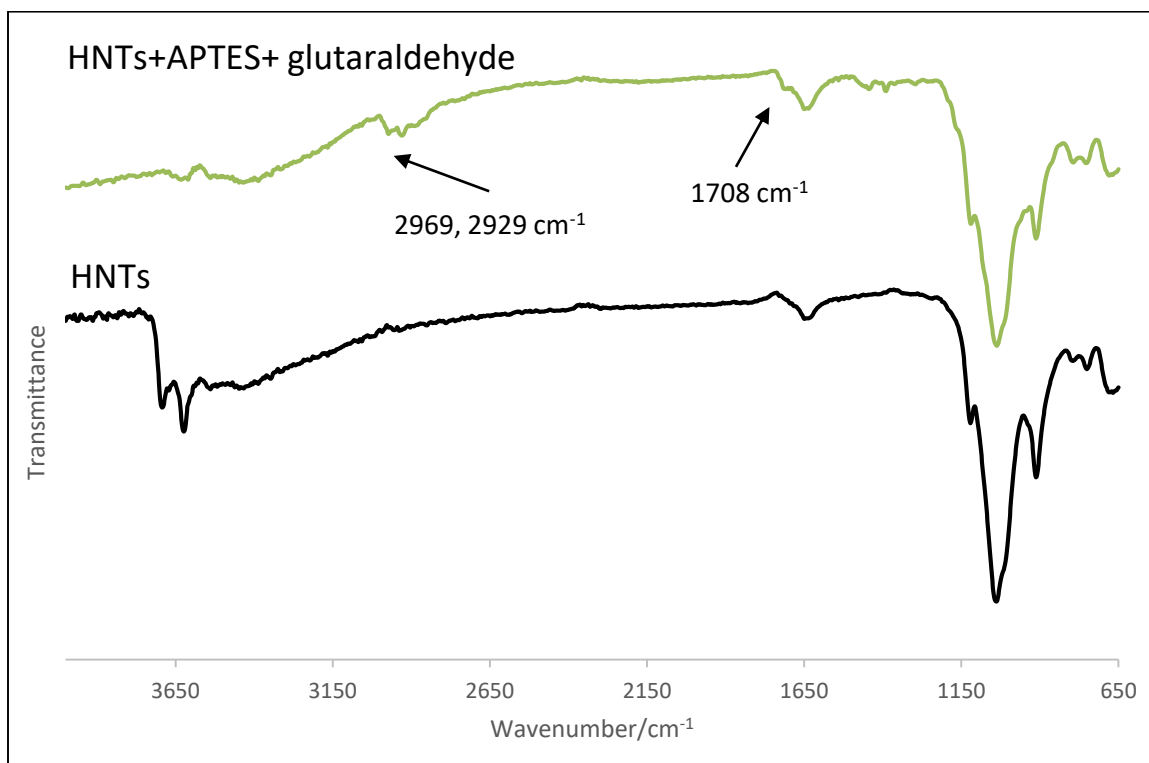
Figure 3-22. *Comparison of IR Spectra for HNTS and HNTS-+APTES+Glutaraldehyde*

Figure 3-23 shows the spectrum of SiNPs in comparison to the final product of

HAGN after functionalization with neutral red. The HAGN spectrum shows the addition

of peaks at 1469 and 1317 cm^{-1}, which may be from the C-H bending of alkenes found in

the neutral red molecule. A peak at 1697 cm^{-1} may be from N-H bending of an imine.
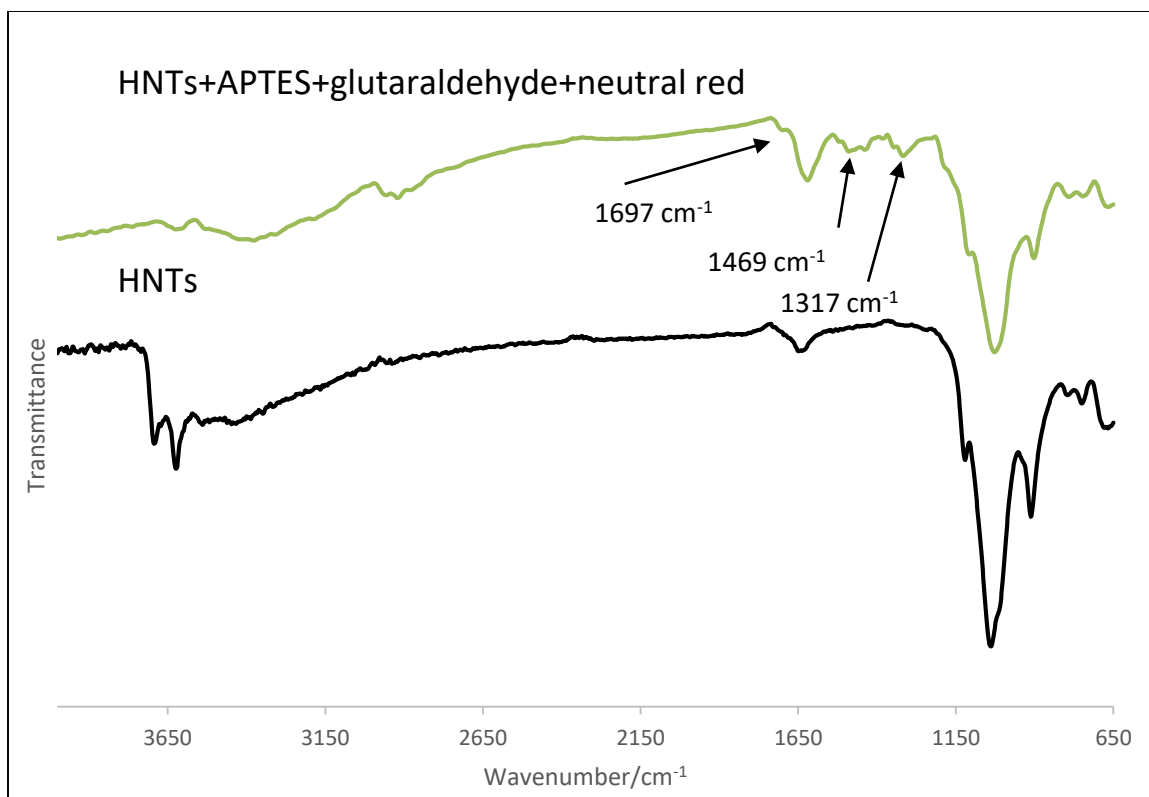
Figure 3-23. *A Comparison of IR Spectra for HNTs and HAGN*

3.4.5 UV-Vis Spectroscopy

Measuring the spectroscopic data for the nanoparticles in solution presented difficulty. UV-vis spectrophotometers are not well suited for observing nanoparticles for a variety of reasons such as the difficulty establishing a suitable blank or background and reflection and scattering of light by the particles in suspension. The reflectance and absorption spectra of the particles in suspension were recorded by using a cuvette set up that allowed collection at a 90^0 angle as seen in Figure 3-24. Collection at 180^0 from the source was not favorable because the signal of the light source overpowered the signal of the sample.
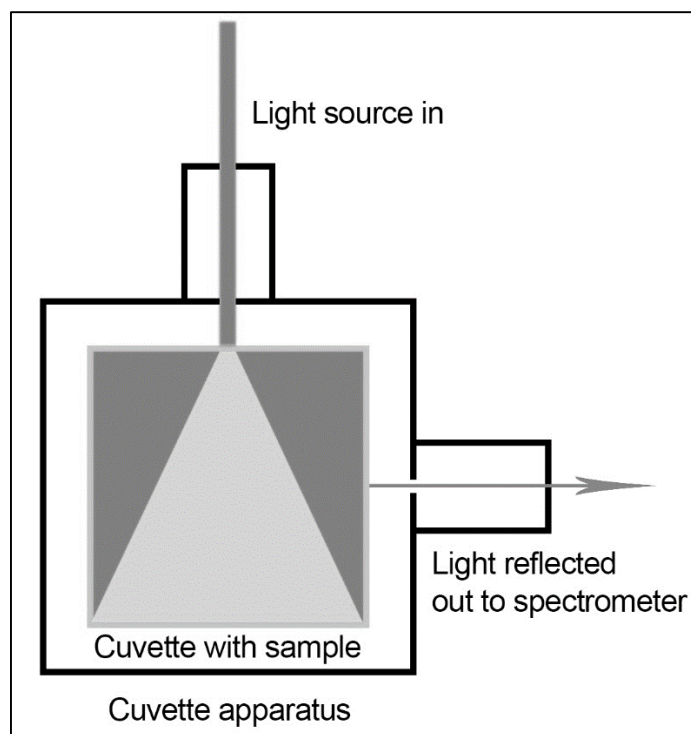
Figure 3-24. *A Diagram of the Cuvette Set Up Used to Collect Spectrophotometric Data for the Various NPs*

Neutral red is common pH sensitive dye that has a pK_a of 6.8 (Qui 209). A series

of dye solutions were prepared at a range of pH values from 5.0-8.0 and the absorption

spectra were measured with a UV-vis spectrometer as seen in Figure 3-25. It was found

that peaks at 448 and 532 nm were responsive to changes in pH values. In a basic

solution, neutral red has a yellow color and in acidic solutions it has a blueish red color.

At 448 nm, which is a blue hue, the absorbance peak is highest with basic pH values of

neutral red. This correlates with the reflectance of a yellow hue of the basic solutions

since an absorbance peak in the blue range would be expected from a yellowish

substance. The peak increases in intensity as the pH value increases or becomes more

basic. At 532 nm, which is a green hue, the peak increases as pH value decreases or

becomes more acidic. The hue of the neutral red solution at acidic values is red, giving

the expectation of an absorbance peak in the spectral band in this range.
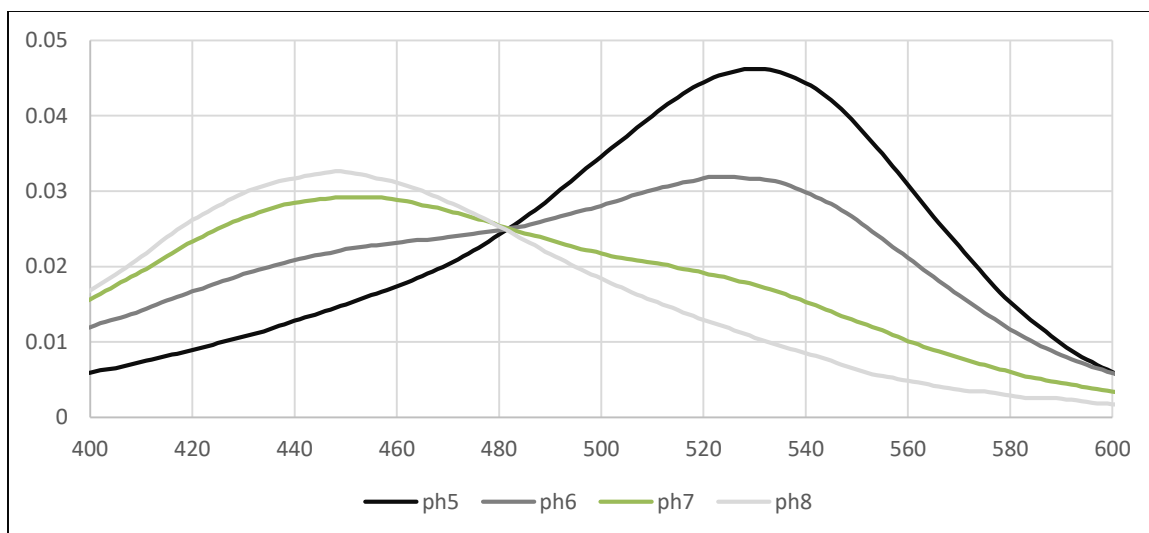
Figure 3-25. UV-Vis Absorption Spectra of Neutral Red at Ph Values 5-8 Showing Peaks at 448 nm and 532 nm

The particles were dispersed in two series of pH buffer solutions. The first series

of solutions covered a broad pH range of pH ~1 to 14, in increments of one pH value

giving a total of fourteen samples. A second series of solutions covered a near neutral

range of pH 6.0 to 8.0, in increments of 0.2 pH value giving a total of eleven samples.

The ratio of peak height of the spectral bands at 580 and 460 nm was performed for each

series of solutions.

Figure 3-26 shows the graph of peak height ratios for SAGN-np in pH solutions

ranging from 1.30 to 13.40. A steady increase in value is shown as pH value increases

from low pH to higher pH values. is shown in Figure 3-26. The relationship of the ratio to

changes in pH is linear and has a positive slope showing a positive correlation with

increase in ratio value to the increase in pH values.
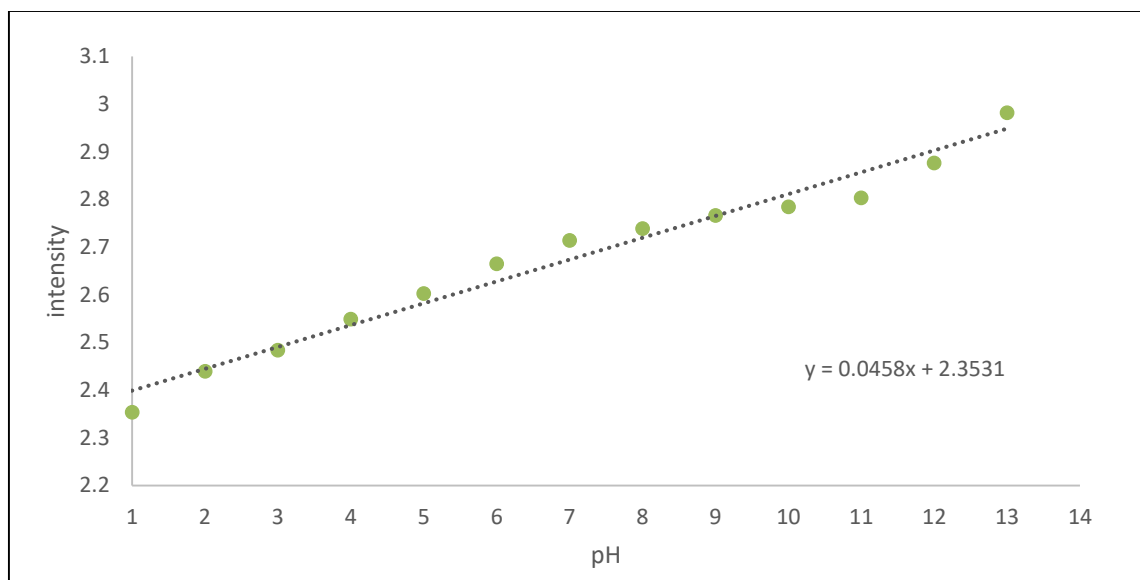
Figure 3-26. *A Graph of the Ratio of SAGN Peak Intensity vs. pH Showing the Relationship Between Peak Intensity and Ph Value for a pH Range of 1.40 to 13.40*

In Figure 3-27, the spectra taken were of SAGN- in solutions ranging from pH 1.40 to 13.40. The spectra show two spectral bands at `450-490 nm and from ~510 to 680 nm. Measurement of peaks at 460 nm, corresponding to a blue reflectance peak, and 580, corresponding to a yellow-orange reflection peak showed clear responsivity to changes in pH values. At low pH values, protonated neutral red is a blueish red. At basic pH values it is deprotonated and has a yellow-orange hue. The spectral band at 450-490 nm would be expected to decrease as the pH value increased. The spectral band at 510-580 nm and would be expected to increase as the pH value increased. This relationship is supported with the data collected at the peaks at 460 and 580 nm.
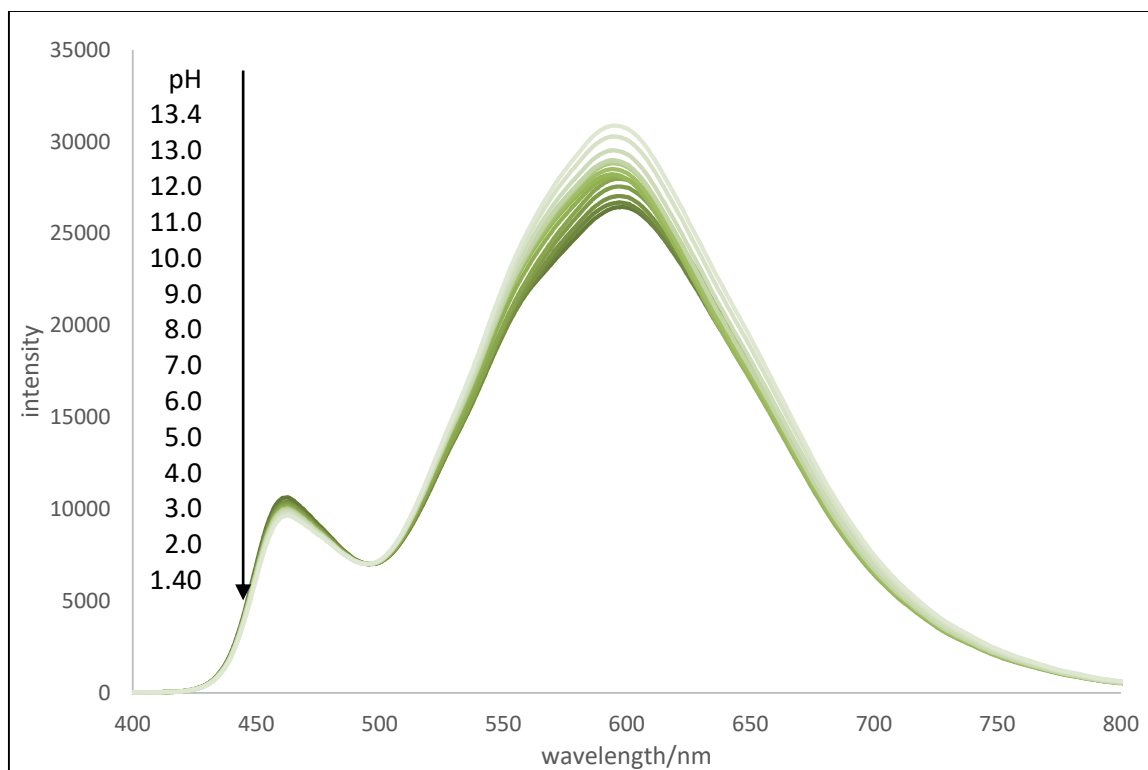
Figure 3-27. *A Comparison of Reflectance Spectra of SAGN in Aqueous Buffer Solutions Ranging from pH 1.40 to 13.40 Showing Spectral Bands and Peaks*

Figure 3-28 shows a magnification of the spectral band of 450-490 nm. This graph shows a decrease in intensity at 460 nm as pH value increases. Figure 3-29 shows the spectral band from 510-680 nm. This graph shows an increase in intensity at 580 nm as the pH value increases.
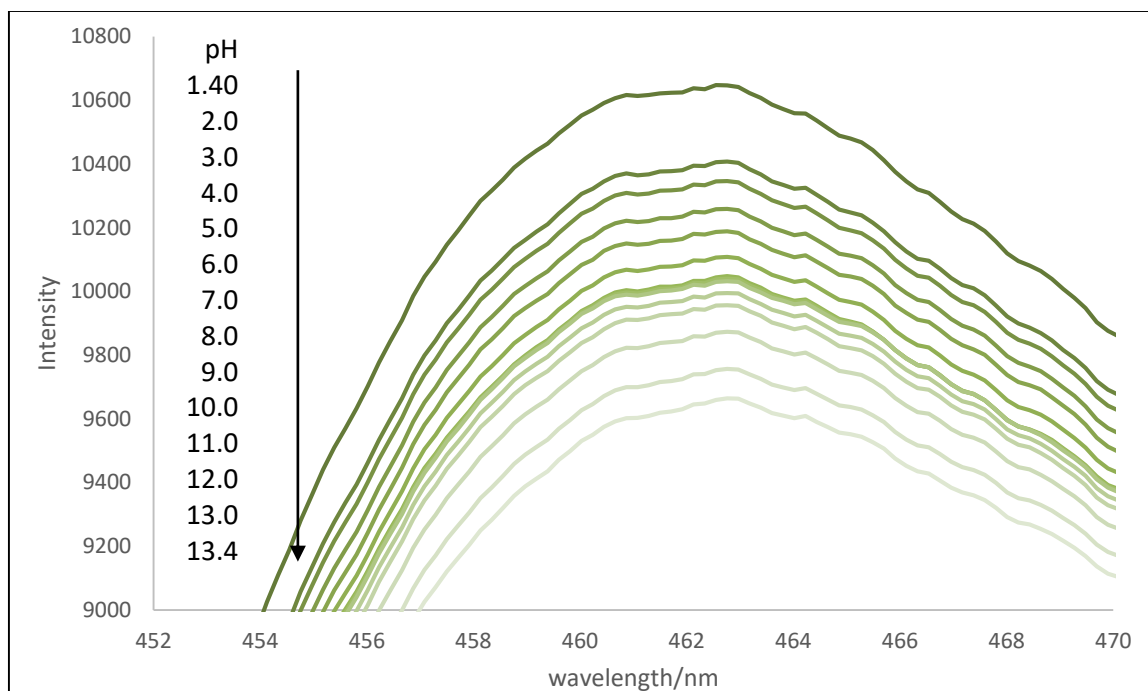
Figure 3-28. *A Magnification of the Reflectance Spectra of SAGN from Figure 3-27 Showing the Change in Intensity in the Spectral Band at ~450-490 nm*
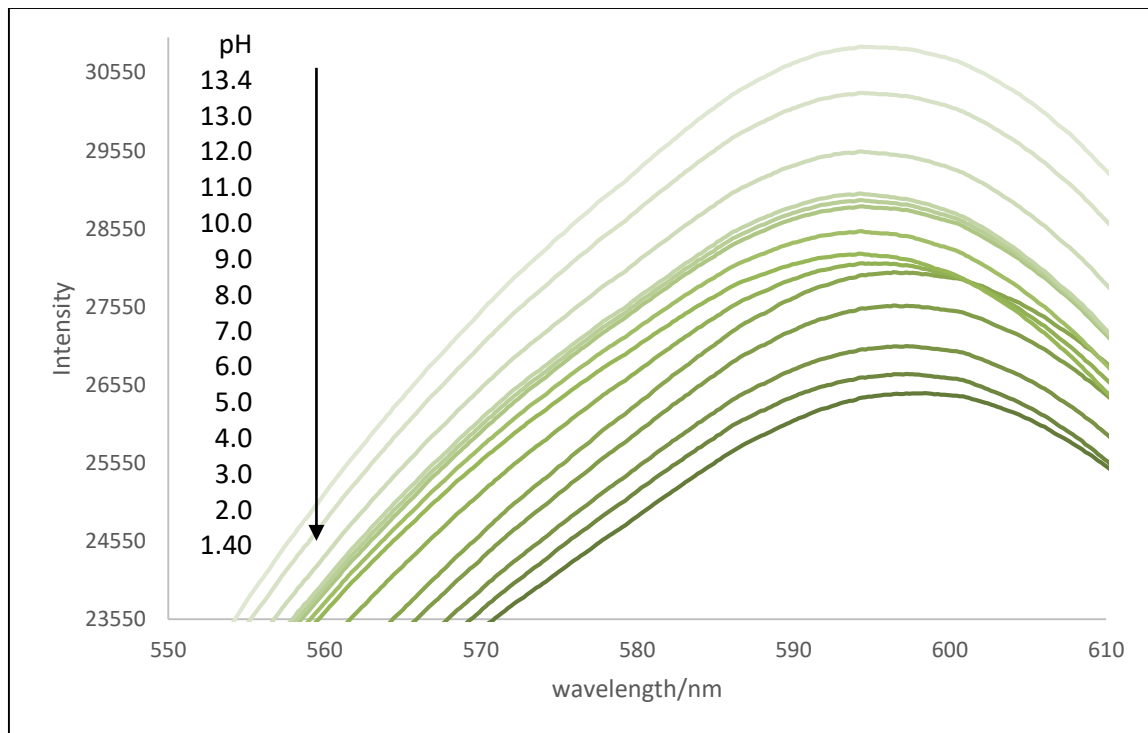
Figure 3-29. *The Reflectance Spectra of SAGN from Figure 3-27 Showing the Change in Intensity in the Spectral Band at ~510-680 nm*

The protocol was repeated for the neutral range of pH 6.0 to 8.0. The same pattern of the ratio of peaks 580 and 460 was seen in the smaller changed in pH values. The graph ratio of peak height of the peaks of the spectral bands of 580 and 460 nm is shown in Figure 3-30. The relationship of the ratio to changes in pH is linear and has a positive slope showing a positive correlation with increase in ratio value to the increase in pH values.
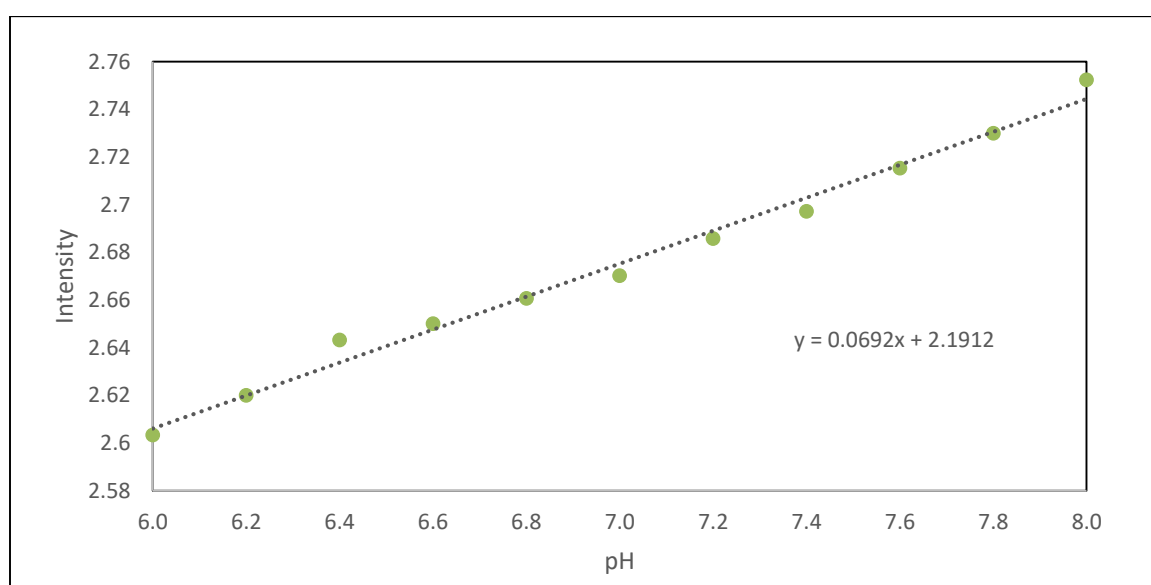
Figure 3-30. *A Graph of the Ratio of Peak Intensity of SAGN Showing the Relationship to pH Value for a PH Range of 6.0 to 8.0*

In Figure 3-31, the spectra taken were of particles in solutions ranging from pH 6.0 to 8.0 in increments of one. The spectra show the same two spectral bands at `450-490 nm and from ~510 to 680 nm. Figure 3-32 shows a magnification of the spectral band of 450-490 nm. This graph shows a decrease in intensity at 460 nm as pH value increases. Figure 3-33 shows the spectral band from 510-680 nm. This graph shows an increase in intensity at 580 nm as the pH value increases.
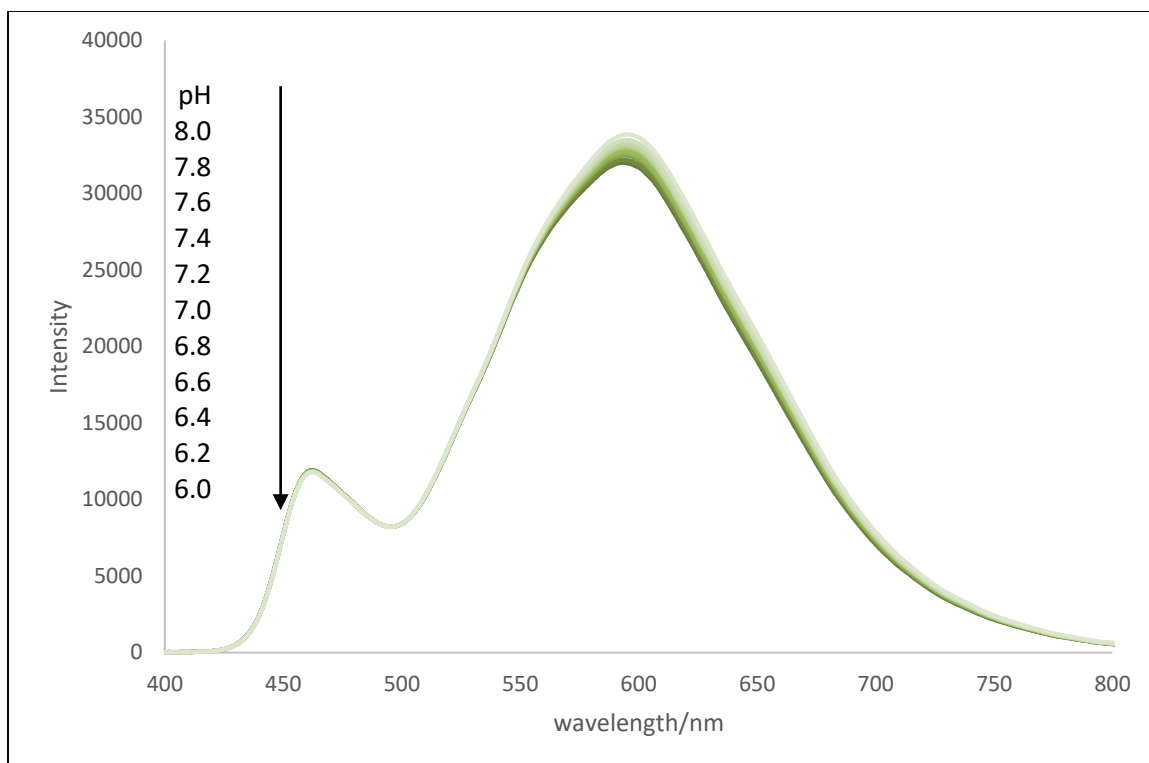
Figure 3-31. *A Comparison of Reflectance Spectra of SAGN in Aqueous Buffer Solutions Ranging from pH 6.0-8.0 Showing Spectral Bands and Peaks*
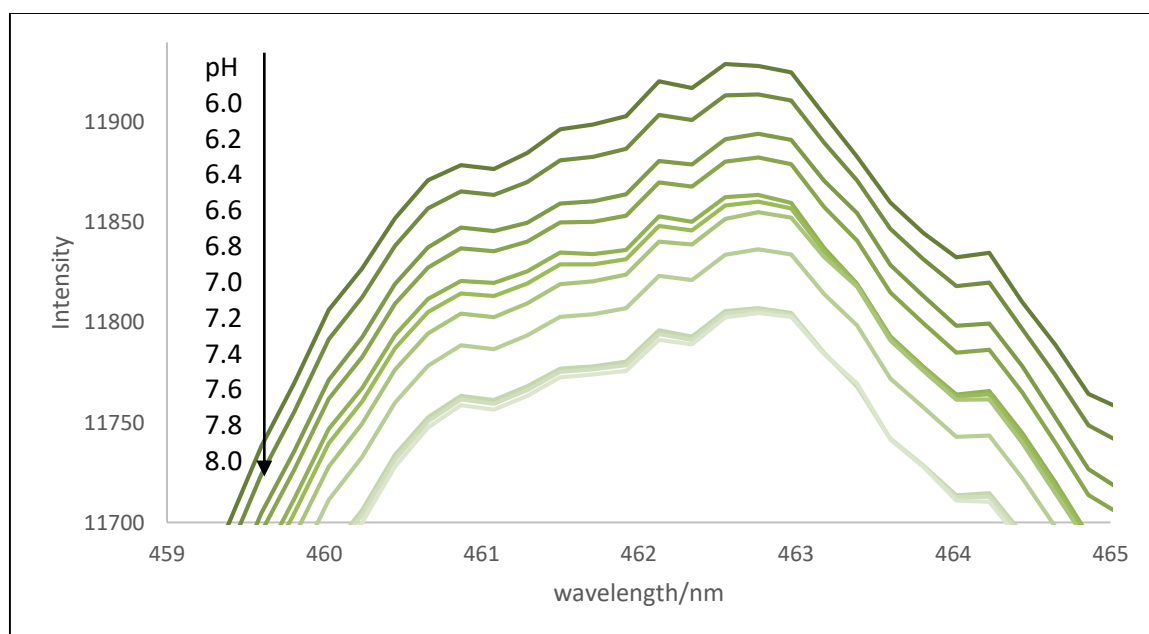
Figure 3-32. *A Magnification of the Reflectance Spectra of SAGN from Figure 3-31 Showing the Change in Intensity in the Spectral Band at ~450-490 nm*
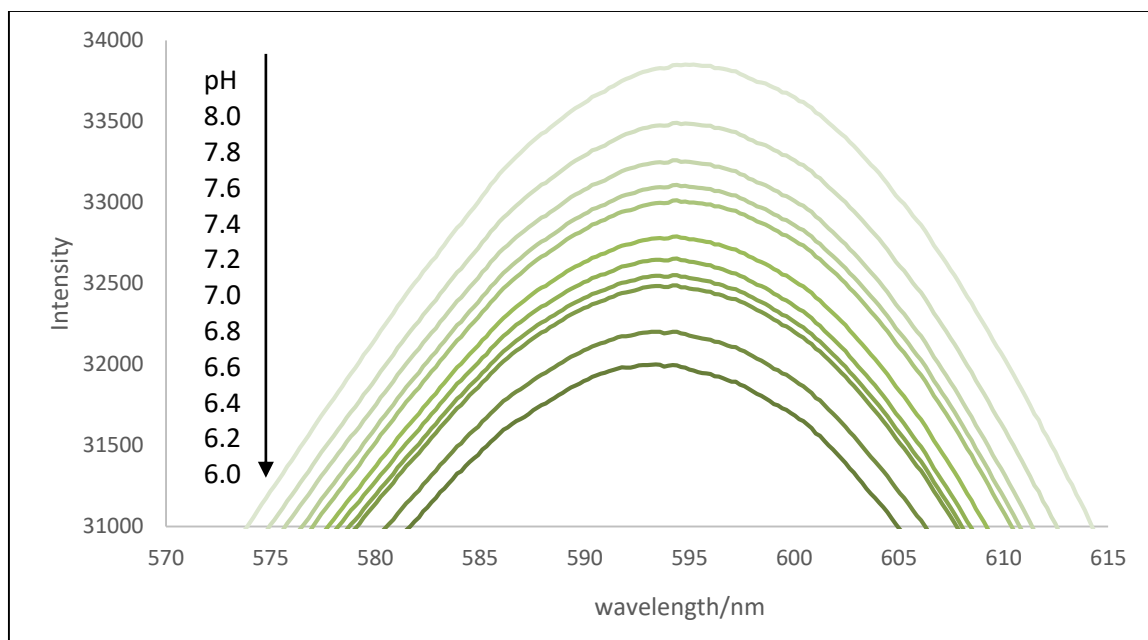
Figure 3-33. *A Magnification of the Reflectance Spectra of SAGN from Figure 3-27 Showing the Change in Intensity in the Spectral Band at ~510-680 nm*

The HAGN were dispersed in a series of pH buffer solutions in a broad pH range of 1.40 to 13.30 and a near normal range of pH 6.0 to 8.0. At the acidic pH values of 1.40 and 2.0 and the basic pH values of 13.0 and 13.4, the spectra were indistinguishable and so the spectra at 1.39 and 13.4 were not included. The spectra show two peaks at 460 nm, corresponding to a blue reflectance peak, and 580, corresponding to a yellow reflectance peak as can be seen in Figure 3-35.

Figure 3-34 shows the graph of peak height ratios for SAGN in pH solutions ranging from 1.30 to 13.40. A steady increase in value is shown as pH value increases from low, acidic pH to higher, basic pH values. The relationship of the ratio to changes in pH is linear and has a positive slope showing a positive correlation with increase in ratio value to the increase in pH values.
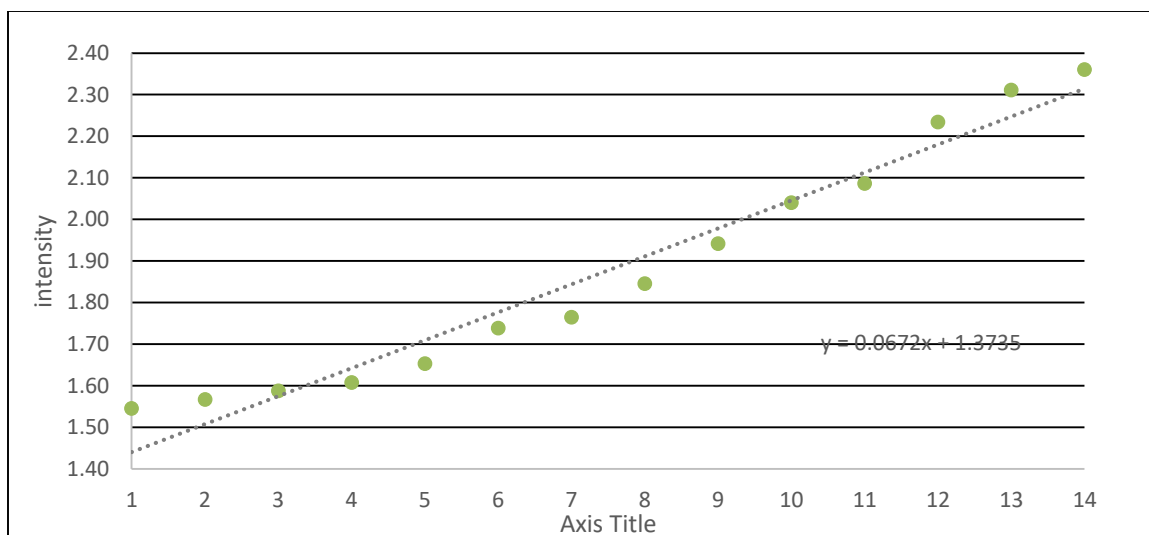
Figure 3-34. *This Graph of the Ratio of Peak Intensity of HAGN Shows the Relationship to pH Value for a pH Range of 1.40 to 13.40*
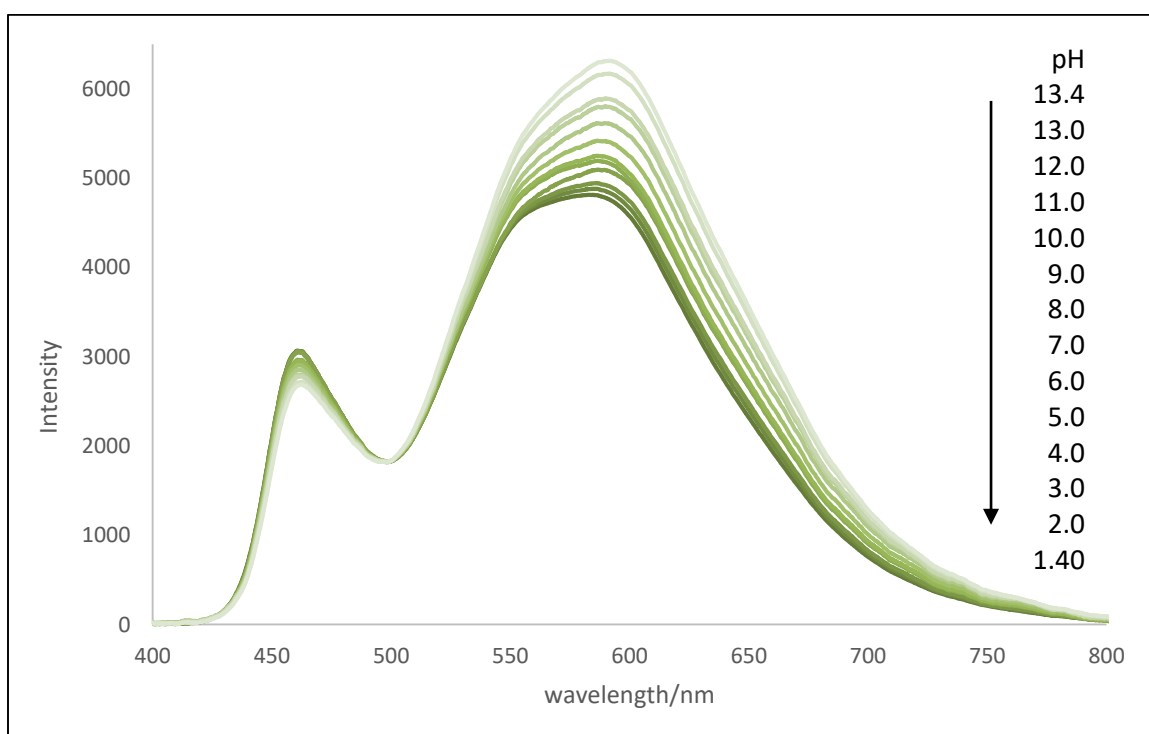
Figure 3-35. *A Comparison of Reflectance Spectra of HAGN in Aqueous Buffer Solutions Ranging from pH 2.0 to 13.0 Showing Peaks and 460 nm and 580 nm*

Figure 3-36 shows a magnification of the reflectance band of 450-490 nm. This graph shows a decrease in intensity at 460 nm as pH value increases. Figure 3-37 shows the magnification of the reflectance band at 580 nm. The graph shows an increase in intensity at 580 nm as the pH value increases.
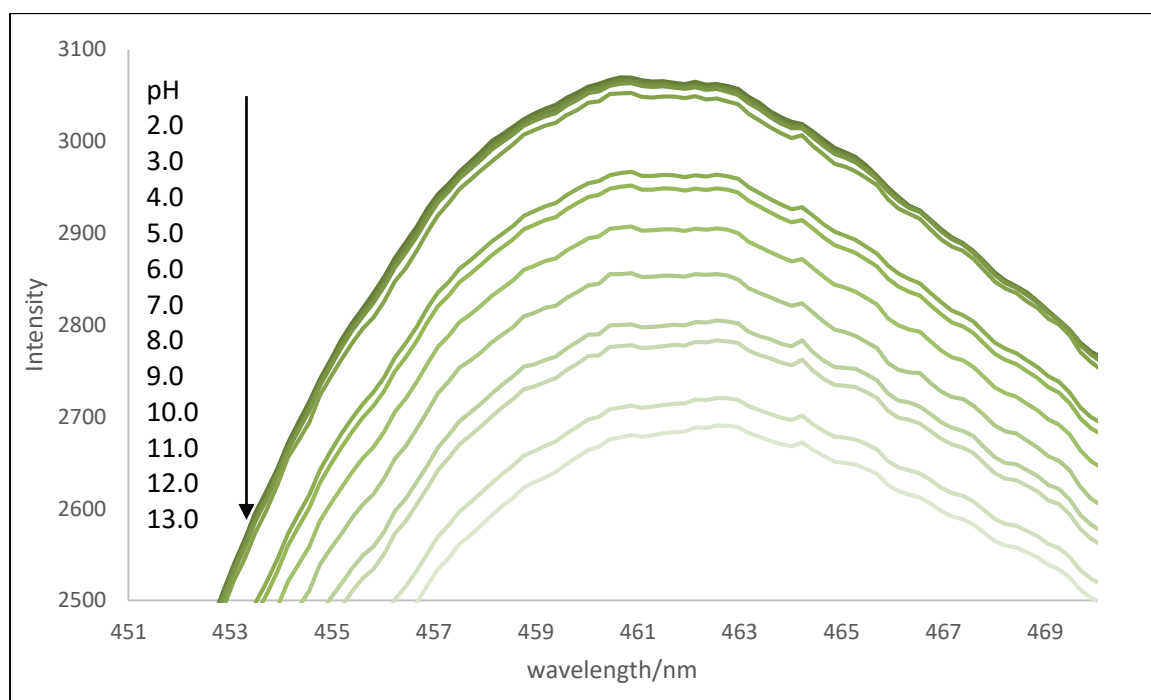
Figure 3-36. *A Magnification of the Reflectance Spectra of HAGN from Figure 3-27 Showing the Change in Intensity in the Spectral Band at 459-465 nm*
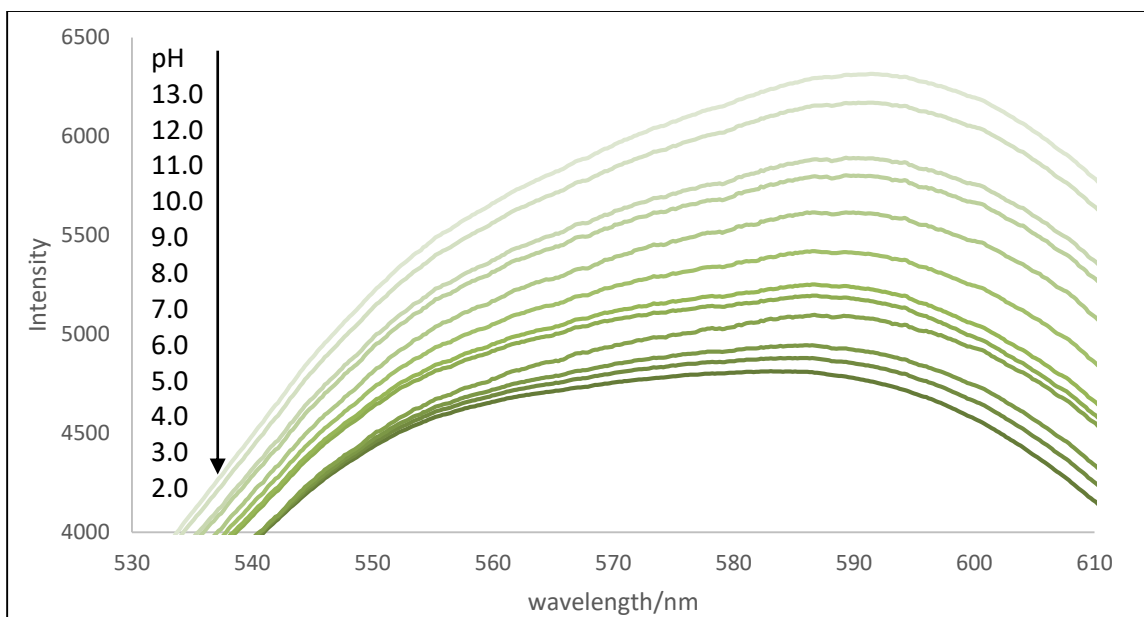
Figure 3-37. *A Magnification of the Reflectance Spectra of HAGN from Figure 3-27 Showing the Change in Intensity in the Spectral Band at 510-680 nm*

The protocol was repeated for the neutral range of pH 6.0 to 8.0 with the HAGN. The same pattern of the ratio of peaks 580 and 460 was seen in the smaller changed in pH values. The graph ratio of peak height of the peaks of the spectral bands of 580 and 460 nm is shown in Figure 3-38. The relationship of the ratio to changes in pH is linear and has a positive slope showing a positive correlation with increase in ratio value to the increase in pH values.
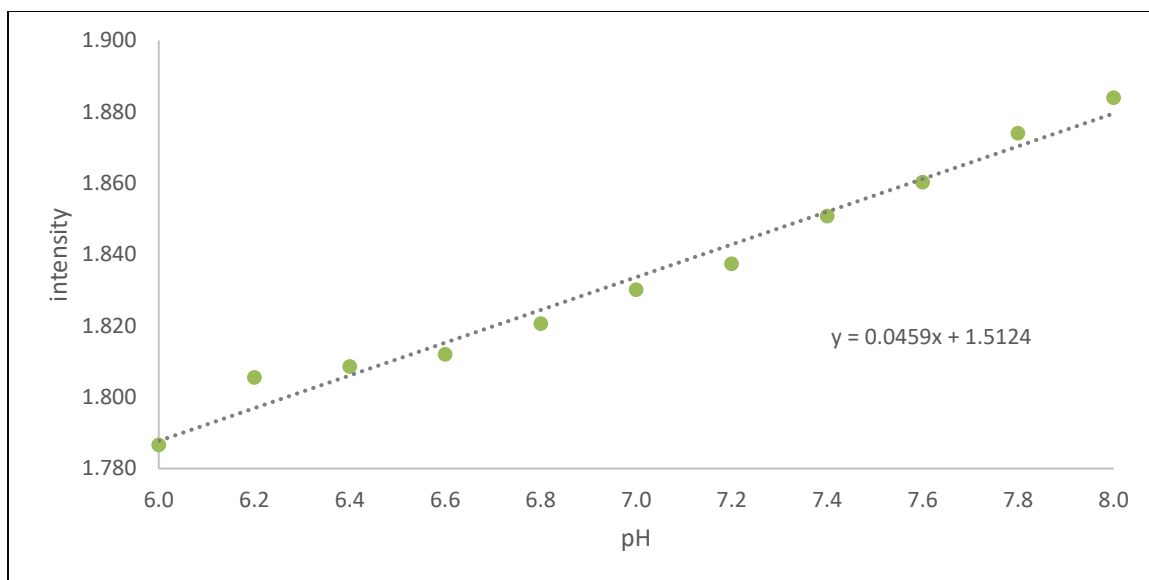
Figure 3-38. *This Graph Shows the Ratio of the Peak Intensity of HAGN at 580 and 460 Nm for the Ph Range of 6.0 to 8.0*

In Figure 3-39, the spectra taken were of particles in solutions ranging from pH 6.0 to 8.0 in increments of one. The spectra show the same two spectral bands at `450-490 nm and from ~510 to 680 nm. Figure 3-40 shows a magnification of the spectral band of 450-490 nm. This graph shows a decrease in intensity at 460 nm as pH value increases. Figure 3-41 shows a magnification of the spectra at the spectral band of 510-680 nm. This graph shows the increase in intensity at 580 nm as the pH value increases.
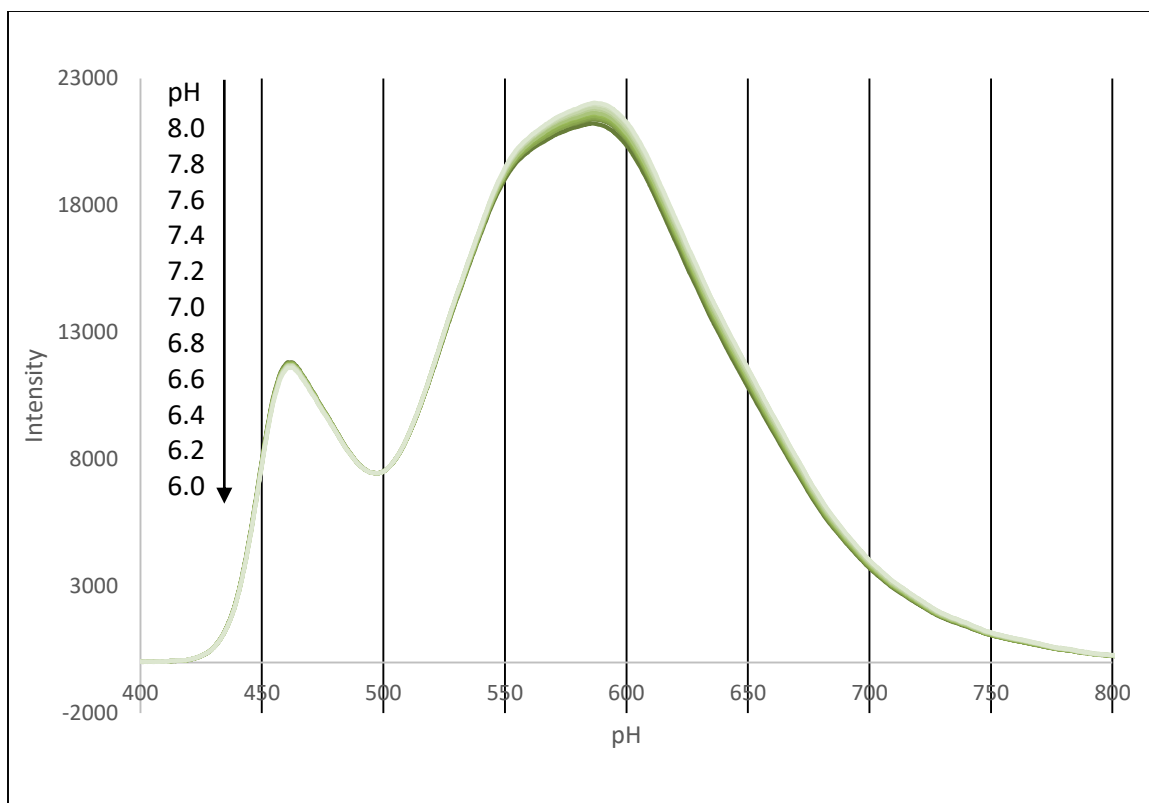
Figure 3-39. *A Comparison of Reflectance Spectra of HAGN in Aqueous Buffer Solutions Ranging from pH 6.0-8.0 Showing Reflectance Bands at 450-490 nm and 510-680 nm and Peaks at 460 nm and 580 nm*
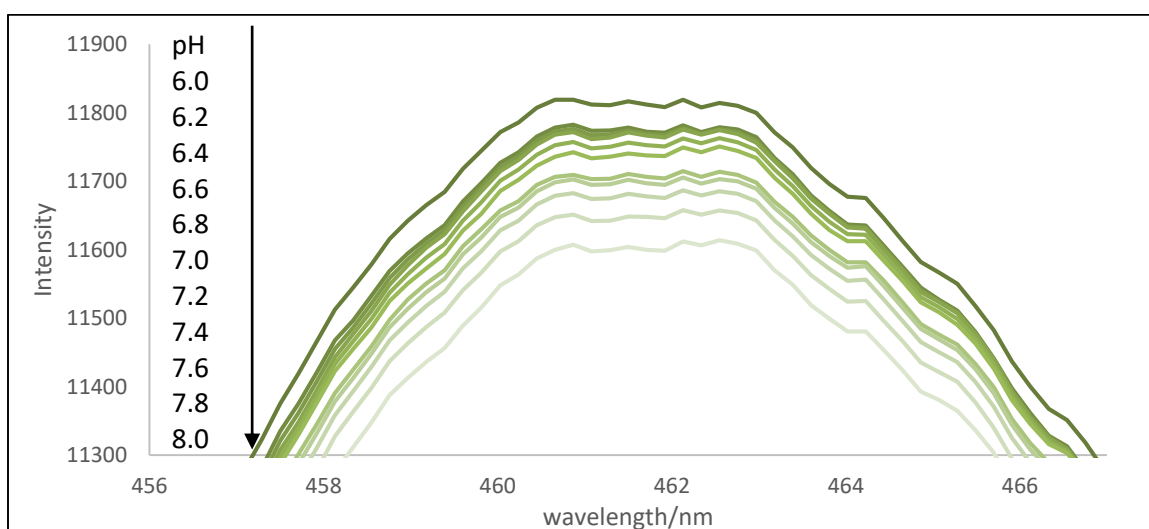
Figure 3-40. *A Magnification of the Comparison of Reflectance Spectra of HAGN in Aqueous Buffer Solutions Ranging from pH 6.0-8.0 at a Range of 460-462 nm*
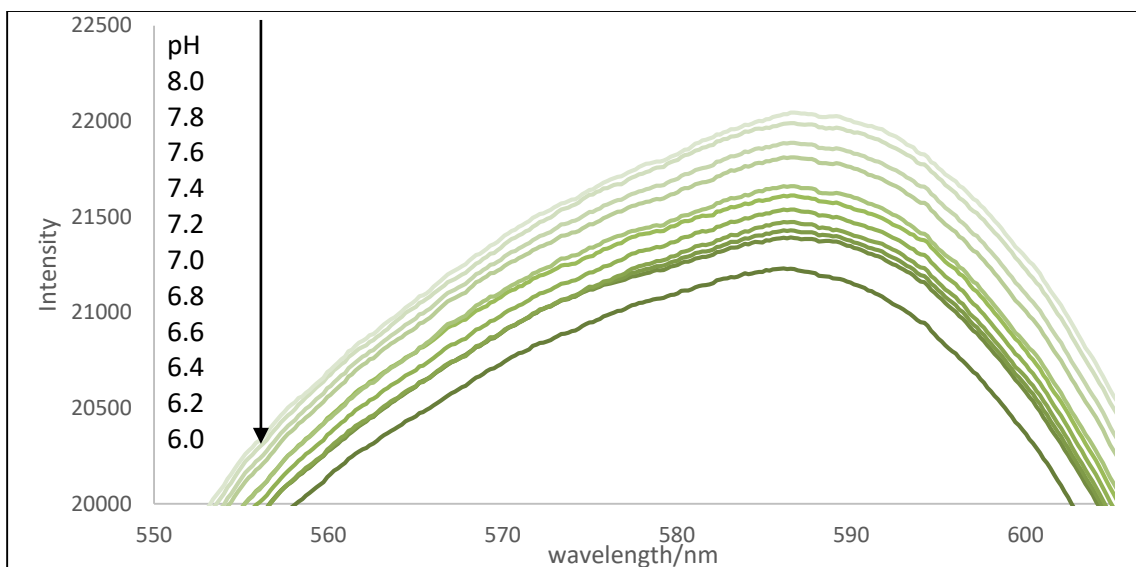
Figure 3-41. *A Magnification of the Comparison of Reflectance Spectra of HAGN in Aqueous Buffer Solutions Ranging from pH 6.0-8.0 at a Range of 580-600 nm, Increasing in Intensity as the pH Value Decreases*

.

CHAPTER 4

PREPARATION OF HALOCHROMIC IONOPHORE FUNCTIONALIZED SILICA AND HALLOYSITE CORE NANOPARTICLES WITH AN ORGANOSILANE COUPLING AGENT

4.1   Introduction

As previously stated in the preceding chapter, halochromic dyes have significant scientific relevance. Methods of preventing direct interaction of chemical sensors and study materials is a subject of concern in the laboratory. In the previous chapter, a method of covalently binding neutral red, a halochromic dye, to either SiNPs or HNTs was studied. In this chapter, an alternate synthesis protocol will be discussed where the number of steps of synthesis is reduced by using a silane functionalized with an aldehyde instead of an amine. This will allow the elimination of the previously used glutaraldehyde step.

Triethoxysilylbutyraldehyde (TSB), seen in Figure 4-1, is an organosilane crosslinking agent used to functionalize surfaces with an aldehyde group. The silanol groups will hydrolyze with silica surfaces or nanoparticles forming a silica bond, leaving the organic aldehyde functional group for further intended use. Aldehydes easily react with amines in mild aqueous environments. In this study, SiNPs and HNTs, both of which contain silica, were used as inorganic cores. The reaction scheme can be seen in Figure 4-2. TSB was added to the nanoparticles to generate aldehyde functional groups

on the surfaces. Neutral red can then be attached to the aldehyde under mildly basic

conditions. At an acidic pH, the primary amine would be protonated, and a reaction

would be less favored. A basic pH was used to facilitate the reaction of the aldehyde with

the primary amine group of the NR dye.
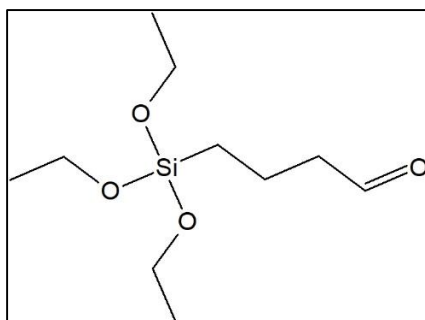
Figure 4-1. *Triethoxysilylbutyraldehyde (TSB)*

After the NR was covalently bound to the particles, the imine bond was changed

to a more stable 2^0 amine bond by reduction with sodium borohydride. This protocol

produced nanoparticles with either SiNP or HNT cores with covalently bound NR dye.

The NR moiety maintained its sensitivity to pH, as the primary amine is not responsible

for its halochromic response.
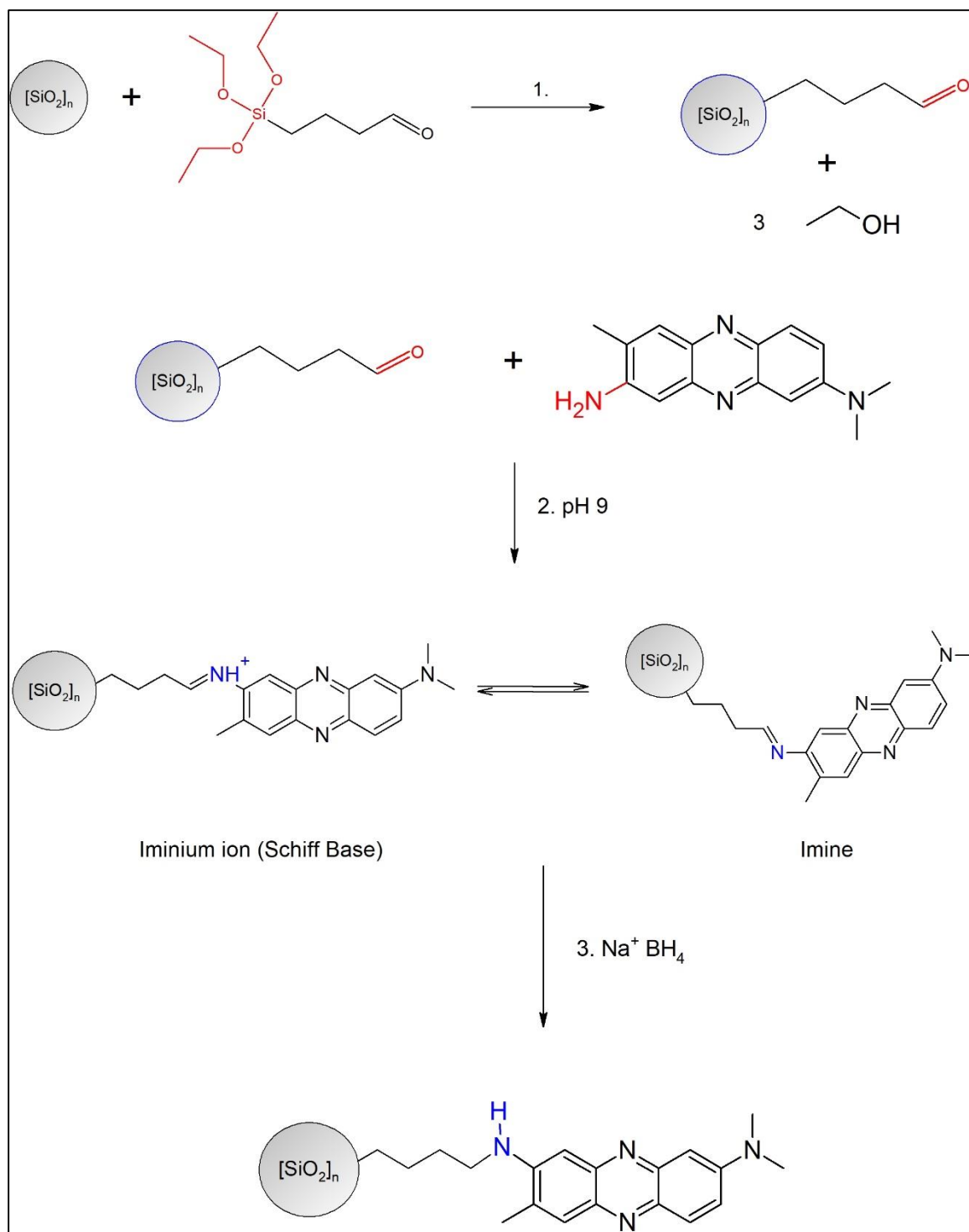
Figure 4-2. *The Reaction Scheme for the Preparation of STNR or HTNR*

The protocol has an advantage in being shorter and using less and fewer reagents than the previous method in Chapter 3. The previous protocol used a covalent binding scheme that used and amine-aldehyde-aldehyde-amine structure to attach the NR dye to the surface of nanoparticles. This protocol simplifies this into a direct aldehyde to amine reaction by using TSB to provide an aldehyde, instead of APTES to provide an amine. Although TSB is substantially more expensive than the widely used APTES, the shorter protocol can be more cost effective by conserving materials. The time to synthesis the particles is shorter as well, as only three steps are required to prepare the final products of silica-TSB-neutral red nanoparticles (STNR) and halloysite-TSB-neutral red nanotubes (HTNR).

Following NP formation, they were tested for durability and leaching. Washing with ethanol, 0.1M HCl and 0.1M NaOH showed no evidence of leaching. This protocol shortened the previous synthesis and produced reliable and pH sensitive nanoparticles.

4.2   Experimental

4.2.1   Materials and Reagents

The SiNP cores were purchased from US Research Nanomaterials. The HNTs were purchased from Sigma Aldrich. The reagent TSB (99.0%), was purchased from Geleste. The reagents neutral red (98.0%) and sodium borohydride (99.0%) were purchased from Sigma Aldrich. The solvents and other chemicals toluene (99.5%), methanol (95.27%), isopropyl alcohol (95.27%), glacial acetic acid (99.0%), sodium hydroxide (97%) and phosphate buffered saline TAB (99.0%) were purchased from Sigma Aldrich and Fischer Scientific.

4.2.2   Protocol

The protocol was developed to be used with either SiNPs or aluminosilicate HNTs. The functionalization occurs upon the silica surface of the nanoparticles or the silica outer layer of the HNTs.

1. The HNTs and SiNPs were dried at 150^0C for 24 hours prior to use. A sample of 200 mg of HNTs or SiNPs were mixed with 50 mL of methanol and sonicated for 10 minutes to separate and disperse the particles.

2. 100μL of TSB was added to the solution and it was stirred at room temperature for 12 hours.

3. The particles were washed by centrifugation. The precipitate was removed and resuspended in methanol with a vortex mixer. This was repeated three times to remove unreacted TSB.

4. The aldehyde functionalized particles were resuspended in 50 mL of methanol. The solution was adjusted to pH 9.0 with 2M ethanolic sodium hydroxide.

5. 100 mg of neutral red was dissolved in 2 mL of ethanol and slowly added to the solution with stirring. The solution was stirred for 6 hours and then washed three times with methanol by the previous method of centrifugation and resuspending the precipitate by vortex mixer to remove unreacted neutral red.

6. The neutral red functionalized particles were resuspended in 50 mL of methanol and rapidly stirred.

7. A solution of sodium borohydride was freshly prepared by mixing 2.5 mg of sodium borohydride with 5 mL of isopropyl alcohol. The $NaBH_4$ solution was rapidly added to the nanoparticle solution and stirred for 15 minutes.

8. 50 mL of DI H_2O was quickly added to the solution to quench the unreacted $NaBH_4$.

9. The particles were washed with methanol two times and DI H_2O two times and resuspended in DI H_2O or dried in an air hood for further use.

4.3   Instrumentation

The absorption/reflection spectra of the samples were obtained with an Ocean Optics USB4000 spectroscope using a StellarNet LED driver equipped with a white LED. The spectra were recorded and analyzed with Ocean View spectroscopic software. The FTIR spectra were performed on a Thermo Scientific IR100 IR spectrometer. DLS and zeta potential measurements were taken on a Brookhaven Instruments Zeta Plus analyzer. FESEM images were obtained with a Hitachi S-4800 field emission scanning electron microscope. All photographic images were taken with a Nikon D60 and processed with Photoshop.

4.4   Results and Discussion

4.4.1   Images

After synthesis with the previously described protocols, the nanoparticles were dispersed into buffered solutions at a concentration of 0.1 mg/ml. The buffered solutions were adjusted to a range of pH levels prior to the addition of the particles. Two series of solutions were prepared. One series contained a wide range of pH values from ~1.0 to

~13.50 in increments of one, giving fourteen solutions in total. The second series of buffer solutions prepared was in a range near neutral, from pH 6.0 to 8.0 in increments of 0.2, giving eleven solutions in total.

After addition of the particles, minor adjustments to the pH of each solution was made with 0.01M NaOH or 0.01M HCl. The particles exhibited rapid color change when added to the solutions. The color change was apparent to visual observation, but the particle solutions were additionally measured with a spectrometer. The particles showed a good dispersion in the aqueous buffer solutions. The dispersion was seen to persist for the duration of the measurements. Samples left overnight exhibited some settling of nanoparticles to the bottom of the vessel.

The SiNP core particles can be seen in Figures 4-3 and 4-4. In the first images, The STNR are shown in a pH range of 1.35 to 13.3. They exhibit a distinct color change and dispersibility in the aqueous buffer solutions. In the second image, the STNR are shown in a pH range near neutral, from 6.0 to 8.0. A color change is still apparent as well as dispersibility in water.

Figure 4-3. *STNR in Aqueous Buffer Solution Ranging from p 1.35 to 13.30 (Top Row: pH 1.40, 2.0, 3.0, 4.0, 5.0, 6.0, Middle Row: pH 7.0, 8.0, 9.0, 10.0, 11.0, 12.0, Bottom Row: pH 13.0, 13.30)*
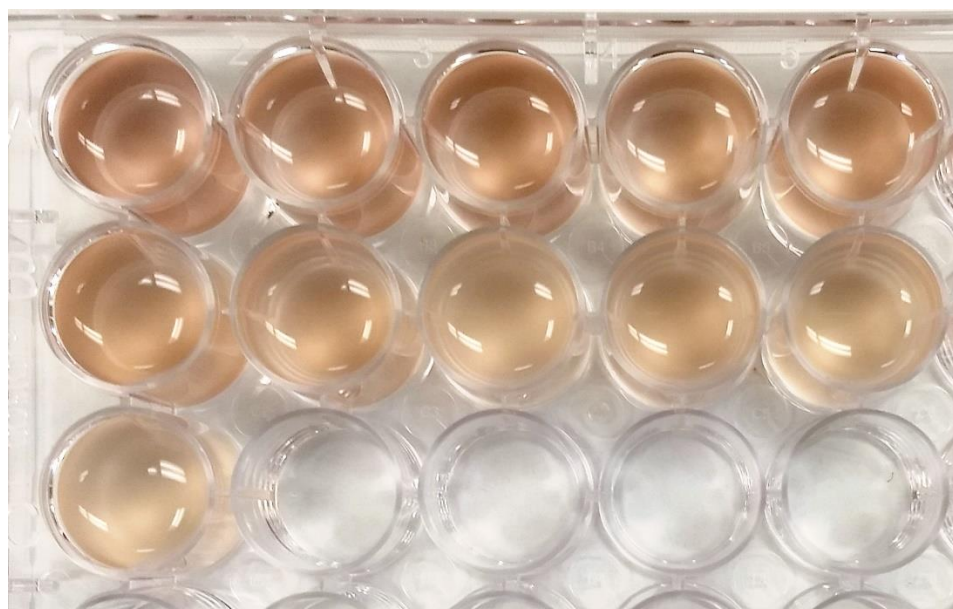
Figure 4-4. *STNR in Aqueous Aqueous Buffer Solution Ranging from pH 6.0 to 8.0 (Top Row: pH 6.0, 6.2, 6.4, 6.6, 6.8, Middle Row: pH 7.0, 7.2, 7.4, 7.6, 7.8, Bottom Row: pH 8.0)*

The HTNR were prepared according to the previously written protocol. In Figure 4-5, they can be seen after addition to a series of pH solutions from pH 1.40 to 13.40. The

HTNR show a strong color change apparent to visual observation and dispersibility in the aqueous buffer solutions. In Figure 4-6, the HTNR are shown in a pH range near neutral of 6.0 to 8.0. They show color change and dispersibility in water.

Figure 4-5. *HTNR in Aqueous Buffer Solution Ranging from p 1.40 to 13.35 (Top Row: pH 1.4, 2.0, 3.0, 4.0, 5.0, 6.0, Middle Row: pH 7.0, 8.0, 9.0, 10.0, 11.0, 12.0, Bottom Row: pH 13.0, 13.35*
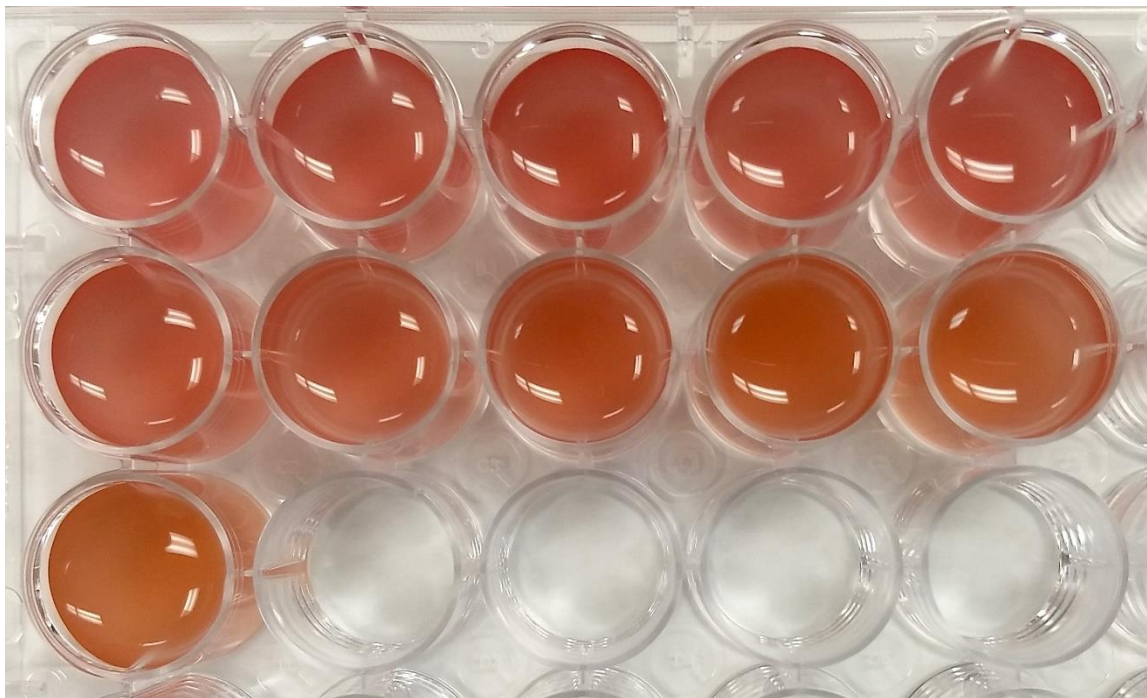
Figure 4-6. *Halloysite TSB-NR Nanoparticles in Aqueous Buffer Solution Ranging from pH 6.0 to 8.0 (Top Row: pH 6.0, 6.2, 6.4, 6.6, 6.8, Middle Row: pH 7.0, 7.2, 7.4, 7.6, 7.8, Bottom Row: pH 8.0)*

4.4.2   FESEM

Samples were prepared for FESEM processing by a previously described method in this study in Chapter 3. Unmodified SiNPs can be seen in Figure 4-7. They appear as clusters of spherical particles. The clumping may be due to the drying process as they were prepared for SEM imaging. SiNPs functionalized with TSB can be seen in Figure 4-8.

There is no change in surface appearance and morphology. This was expected as the TSB layer is thin in comparison to the size of the particles. The final product of SiNP-TSB-Neutral Red (STNR) can be seen in Figure 4-9. The appearance of the particles shows no change in characteristics in the SEM image, but visually the particles exhibited a red color, indicating the dye functionalization. The chart in Figure 4-10 shows a change

in size during the successive steps of the protocol. This may be due to the formation of clusters of different shapes which will affect DLS measurements or may be due to loss of smaller particles during the washing and purification steps of the protocol.
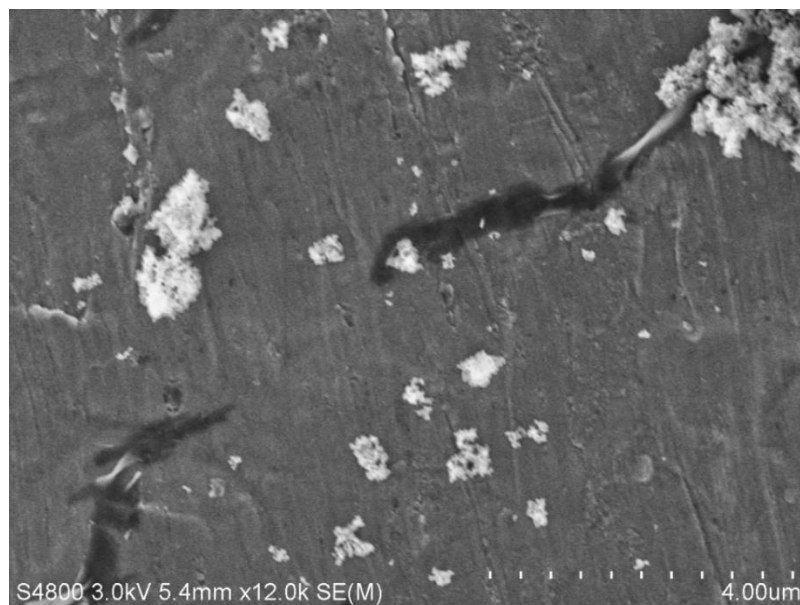
Figure 4-7. *SiNPs Showing Clusters of Dried Particles*
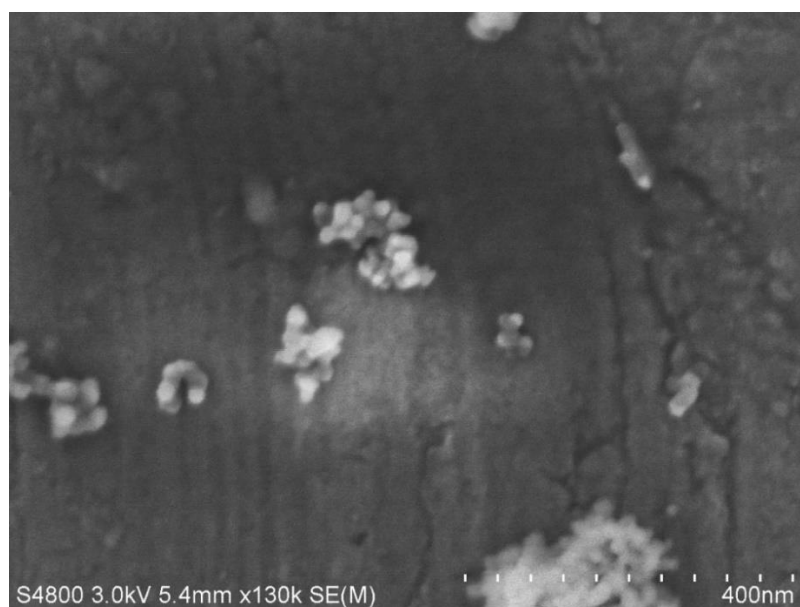
Figure 4-8. *SiNPs Functionalized with TSB*
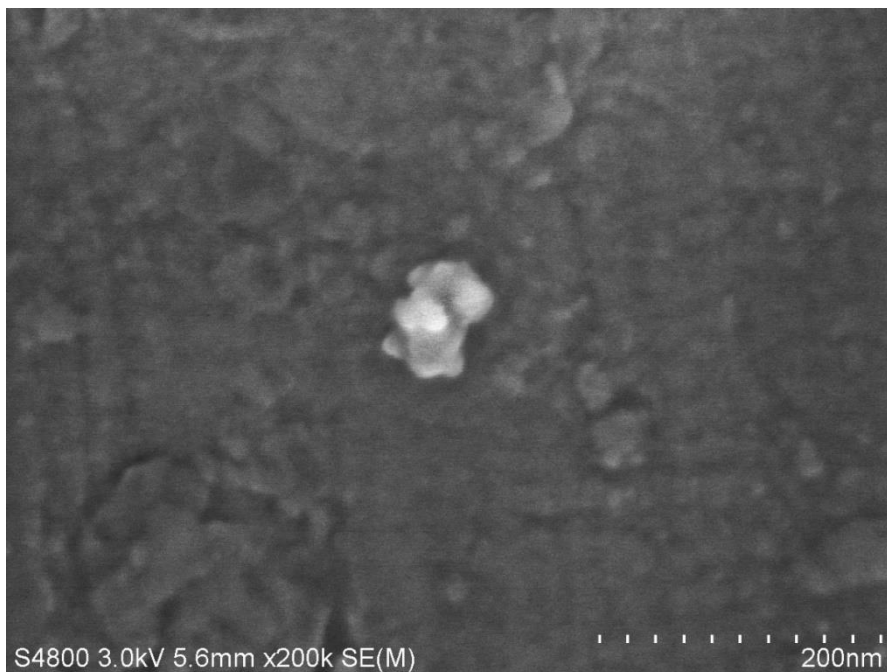
Figure 4-9. *SiNPs Functionalized with TSB and Neutral Red*

The halloysite core samples were prepared by the previously described procedure for SiNPs with no modifications to the protocol. The nanotubes were measured and showed a greater variability in size with compared with the SiNPs. This may be due to HNTs are a naturally produced material where SiNPs are synthesized using the well-known Stöber process that has been shown to reliably produce monodispersive particles.

The HNT based particles showed the same trend as the SiNPs. The halloysite surface features showed little change in observed characteristics, supporting the conclusion that the functional layers were thin. Unmodified HNTs can be seen in Figure 4-10. Figure 4-11 shows HNTs modified with TSB. Figure 4-12 shows the final product of HNT-TSB-Neutral red nanotubes (HTNR). No changes in surface features or morphology are noted in images of the progressive stages.
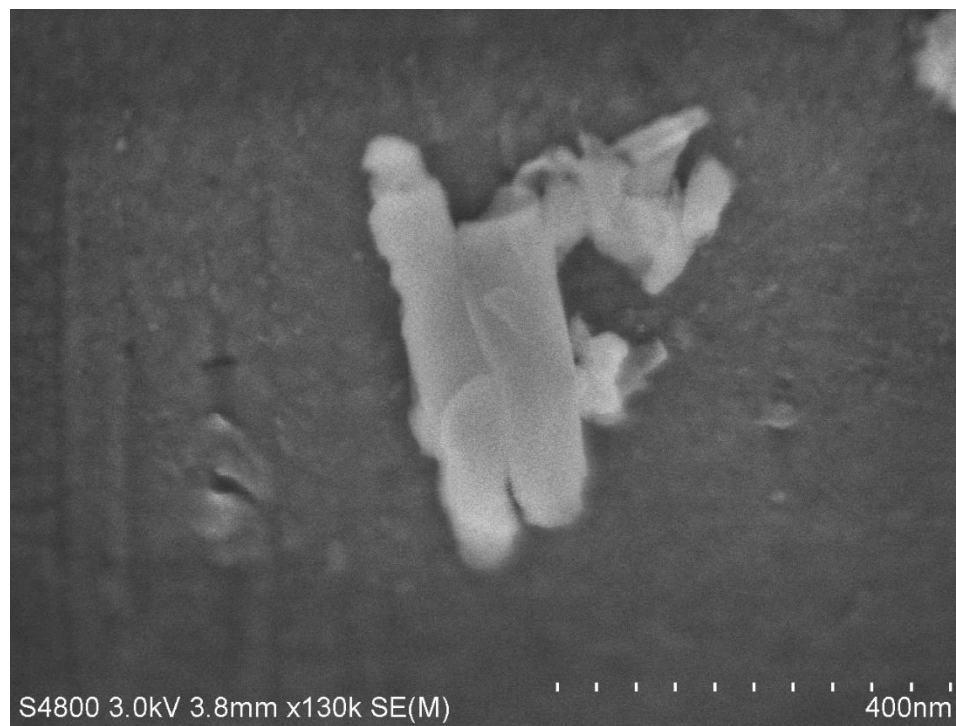
Figure 4-10. *Unmodified HNTs*

Figure 4-11. *HNTs Functionalized with TSB*
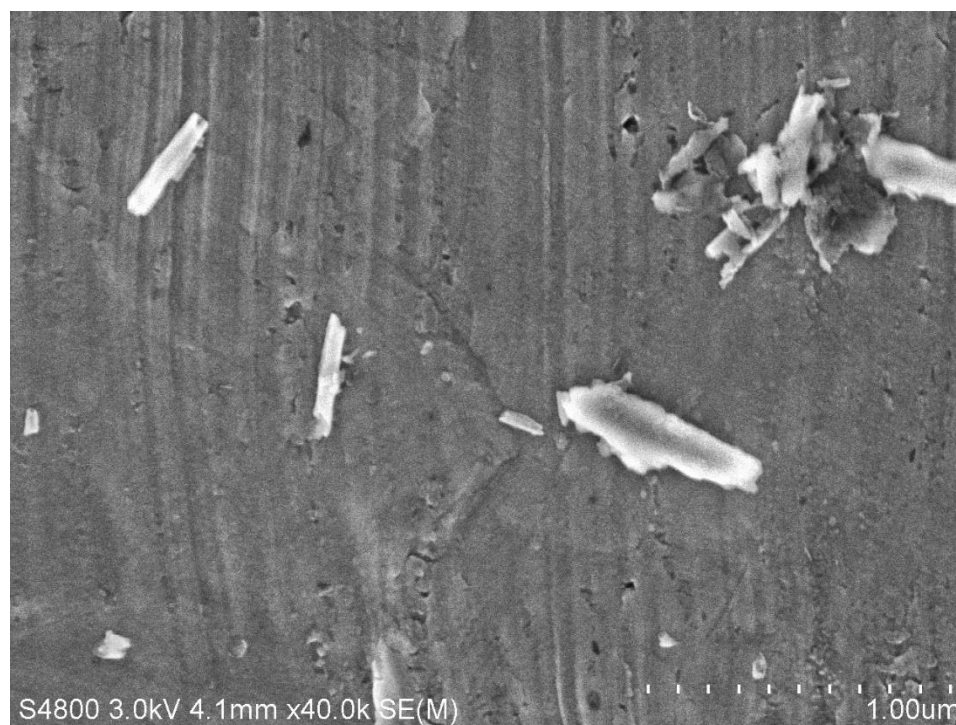
Figure 4-12. *HNTs Functionalized with TSB Neutral Red*

4.4.3   DLS

The particles were measured with DLS using a previously described protocol. The particles showed a change in size with each layer added. This was seen in both the SiNP and HNT based particles. The sizes of the stages of the protocol for the SiNPs can be seen in Figure 4-13 and for the HNTs in Figure 4-14. The changes in size may be due to the loss of smaller particles during the washing stages of the protocol. The SiNPs show a 21.88% increase while the HNTs show a 14.11% increase in size. This is supportive of the conclusion that the smaller particles where lost during washing and purification.
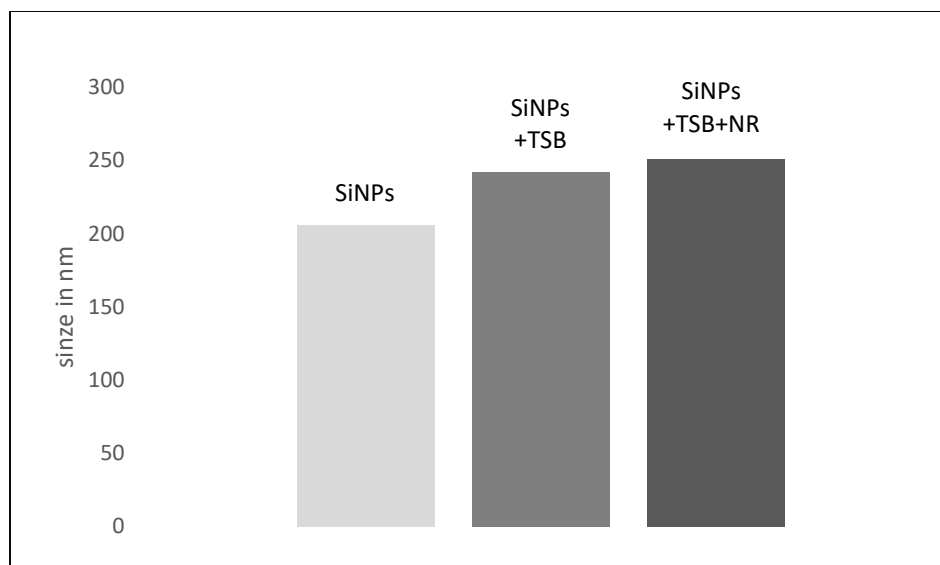
Figure 4-13. *DLS Data Comparing the Sizes of Component Particles in the Synthesis of STNR*
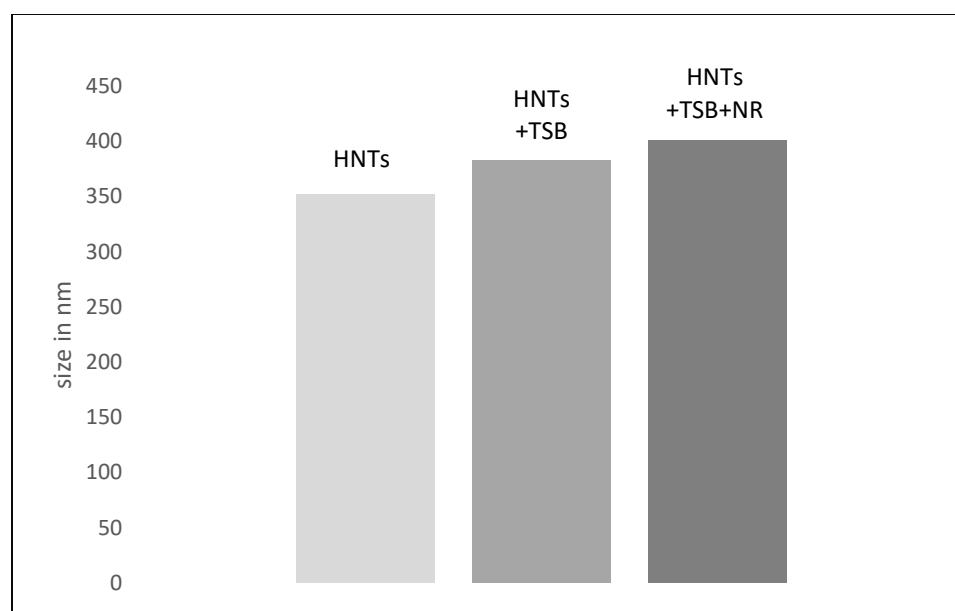
Figure 4-14. *DLS Data Comparing the Sizes of Component Particles in the Synthesis of HTNR*

4.4.4 FTIR

The spectra recorded for each stage of the synthesis of the silica based STNR can be seen in Figure 4-15. The first spectrum is of SiNPs and shows a peak at 1089 cm-[1]

which may indicate the Si-O stretch of silica. The spectra of the reagents TSB and NR are labeled in Figure 4-5.
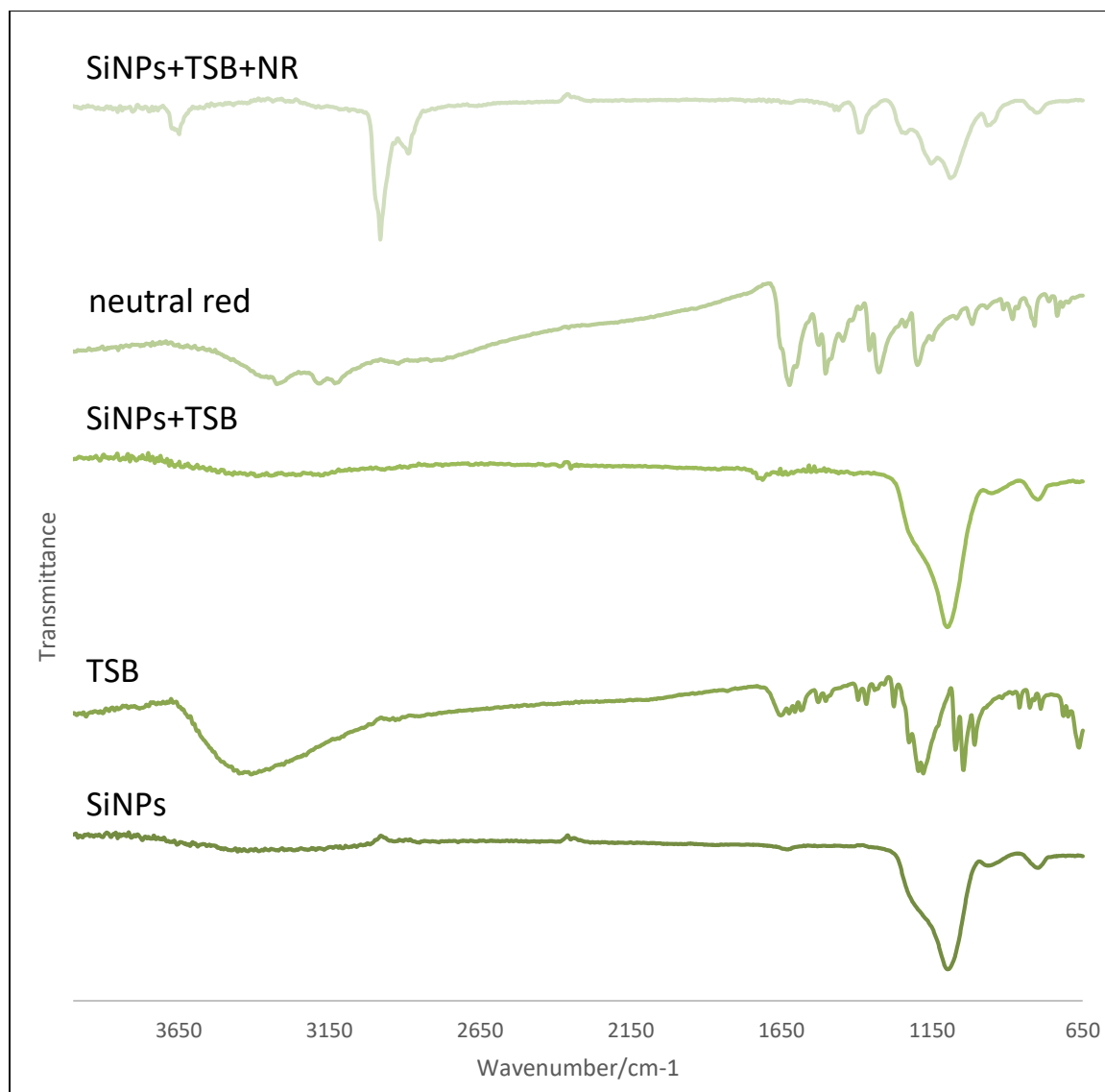
Figure 4-15. *A Comparison of FTIR Spectra of STNR Showing the Effect upon Spectra with the Addition of a Functional Group Layer*

Figure 4-16 shows a comparison of unmodified SiNPs in comparison to SiNPs functionalized with TSB to provide an aldehyde functional group. The spectrum of the Si-TSB particles was shown to have a peaks at 1710 and 1724 cm^{-1} which may correlate

to the C=O stretch for aldehydes. This data may support the successful reaction of TSB to the silica surface.
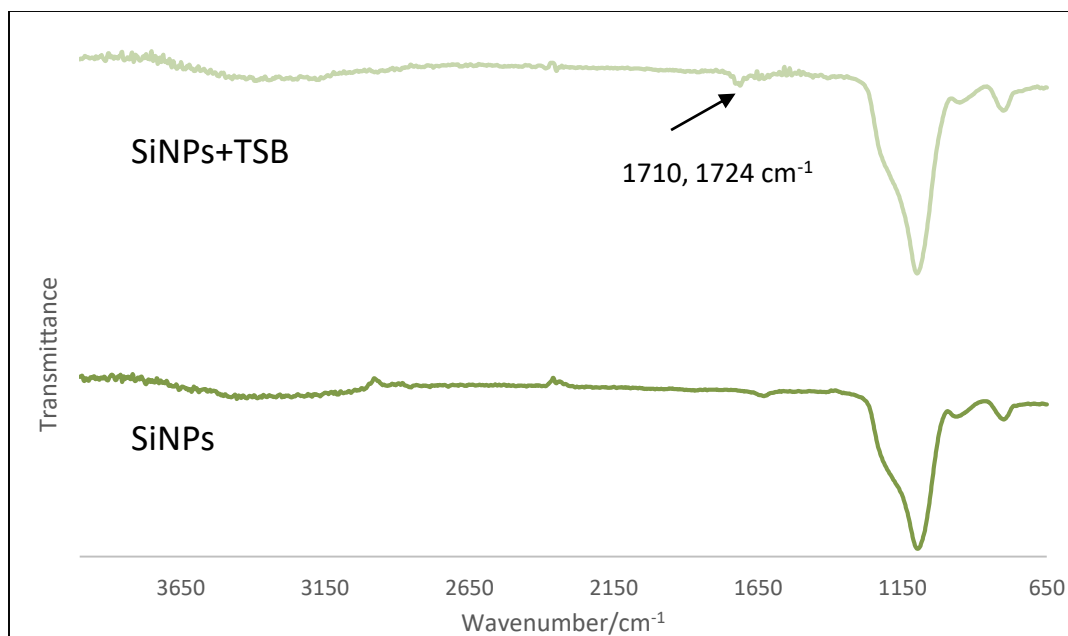
Figure 4-16. *A Comparison of the FTIR of SiNPs with SiNPS+TSB*

The fifth spectrum is of the final particle, STNR, with NR bound to the aldehyde group that was added previously, in comparison to SiNPs as seen in Figure 4-17. The STNR particle showed peaks at 1461, 1390, 1236 and 1151 cm^{-1}, which may be from the C=C stretch of aromatic carbons such as found in neutral red. Peaks are found at 2981 and 2981 cm^{-1} which may be from the C-H stretch of alkanes found in the NR molecule and TSB. The spectrum also contained a peak at 3648 cm^{-1}, which may be from the N-H stretch of a 2^0 amine produced after the aldehyde-amine reaction which was reduced with sodium borohydride to an amine. This data may support the covalent binding of the dye to the surface of the particle.
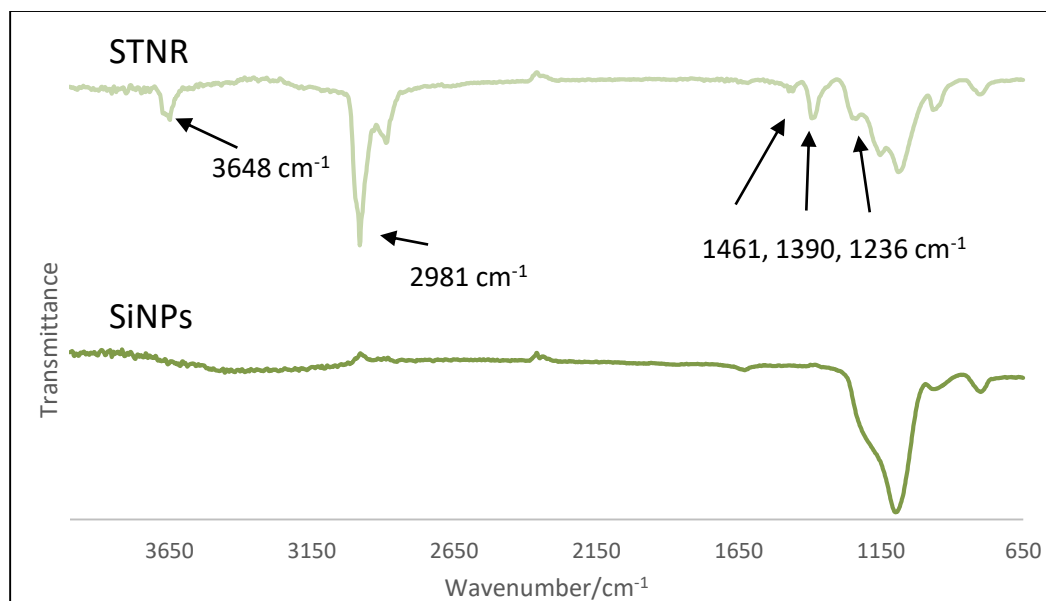
Figure 4-17. *A Comparison of the FTIR Spectra of STNR with SiNPs*

The graph in Figure 4-18 shows the FTIR spectra recorded for each stage of the synthesis of the halloysite based HTNR. The first spectrum is of unmodified HNTs and shows a peak at 1035 cm^{-1} indicative of the Si-O stretch of aluminosilicate. The second and fourth spectra are of the reagents TSB and NR.
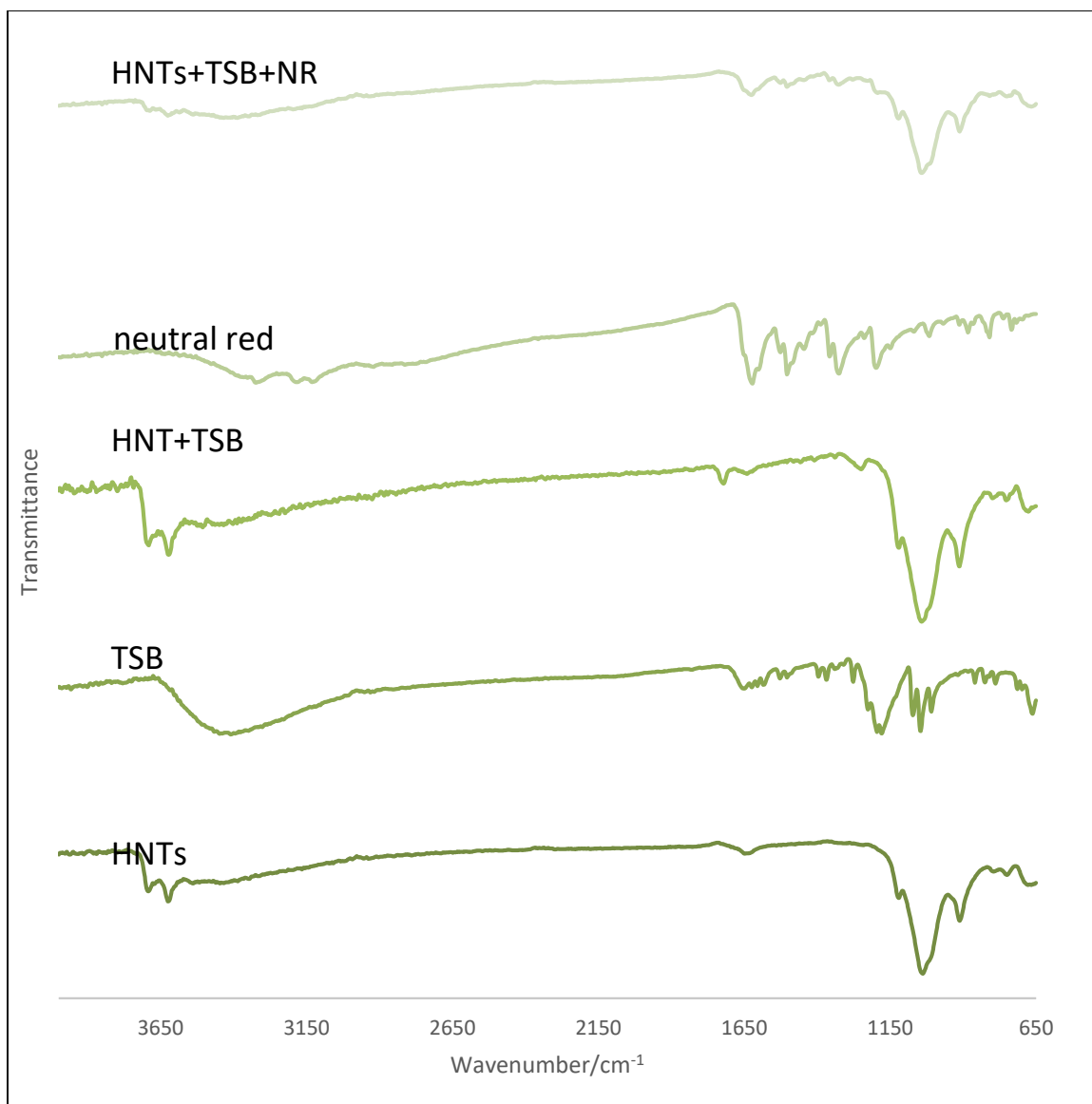
Figure 4-18. *A Comparison of FTIR Spectra of HTNR Showing the Effect on Spectra with the Addition of a Functional Group Layer*

The third spectrum of the HTNs after functionalization with TSB to provide an aldehyde group can be seen in Figure 4-19 in comparison with the spectrum of unmodified HNTs. The spectrum shows a peak at 1720 cm^{-1} that may be from the C=O stretch of an aldehyde group from TSB. This data may support the successful reaction of TSB to the silica surface.
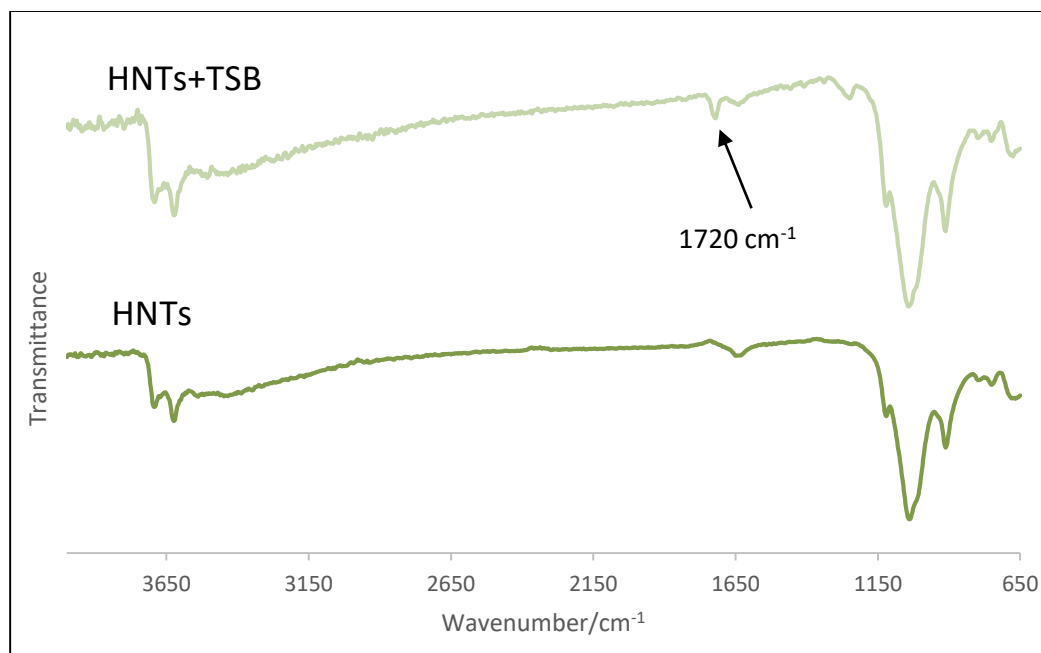
Figure 4-19. *A Comparison of FTIR Spectra of HNTs Modified with TSB with Unmodified HNTs*

The HAGN particle spectrum is shown in Figure 4-20 in comparison with HNTs. Peaks can be seen at 1623, 1502 and 1324 cm^{-1}, which may be from the C-H stretch of carbon bonds such as found in neutral red. The peak at 1632 cm-1 may be from the imine bond formed between the aldehyde of TSB and the amine of NR. This data may support the covalent binding of the dye to the surface of the particle.
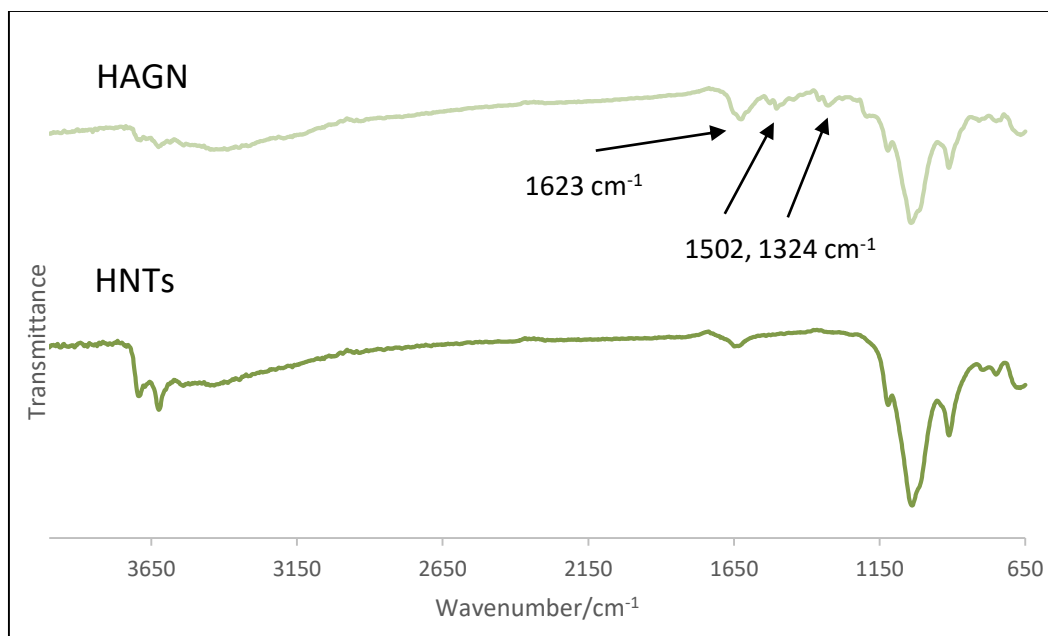
Figure 4-20. *A Comparison of FTIR Spectra of the Final HTNR in Comparison to HNTs*

4.4.5   UV-Vis Spectroscopy

The particles were dispersed in a series of pH buffer solutions in a broad pH range

of 1.35 to 13.30 and a near normal range of pH 6.0 to 8.0. The spectral band shows two

regions that respond to changes in pH: 450-480 nm 550 to 650. Within the spectral band

two peaks at 460 nm, corresponding to a blue reflection peak, and 580, corresponding to

a yellow reflection peak, have shown the highest responsivity to pH changes. At acidic

pH values, neutral red is a blueish red and at basic pH values it is yellow. The red phase

would corelate to a blue reflection peak and would be expected to decrease as the pH

value increased. The yellow phase would correlate to a yellow-orange reflection peak and

would be expected to increase as the pH value increased. This relationship is supported

with the data collected. The STNR had a stable relationship between pH value and the

increase and decrease of the peaks at 460 and 580 nm from pH values 2-13.

The graph of spectral peak ratios can be seen in Figure 4-21. It shows that the 580 nm peak has a positive correlation with rise in pH value. The relationship is linear and shows a positive correlation with the increase in pH values.
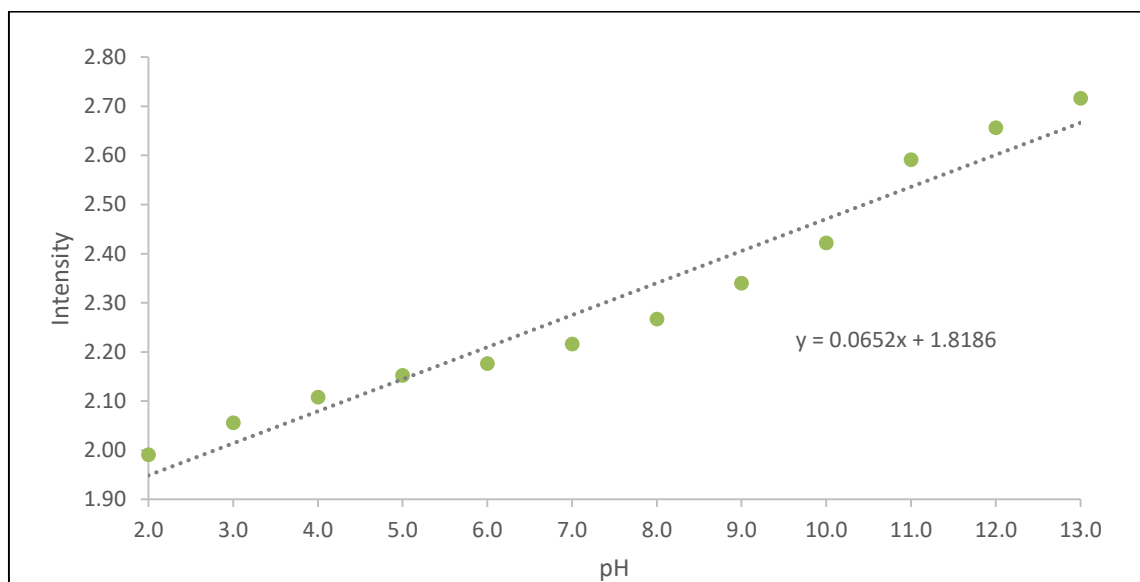
Figure 4-21. *This Graph of STNR Shows the Relationship Between the Ratio of Peak Intensity and pH Value at the Peaks of 460 and 580 nm*

In Figure 4-22, the spectra of STNR dispersed in buffered pH solutions can be seen. The solutions ranged from pH 2.0 to 13.0. The spectra for pH values 1.35 and 13.35 were taken, but they were identical to the spectra for pH 2.0 and 13.0 respectively. The spectra for 1.35 and 13.35 were not included. The data supports this method only in a pH range of 2.0 to 13.0. The spectra show two spectral bands at 450-490 nm and from 510-680 nm. Measurement of peaks at 460 nm and 580 nm showed clear responsivity to changes in pH values.
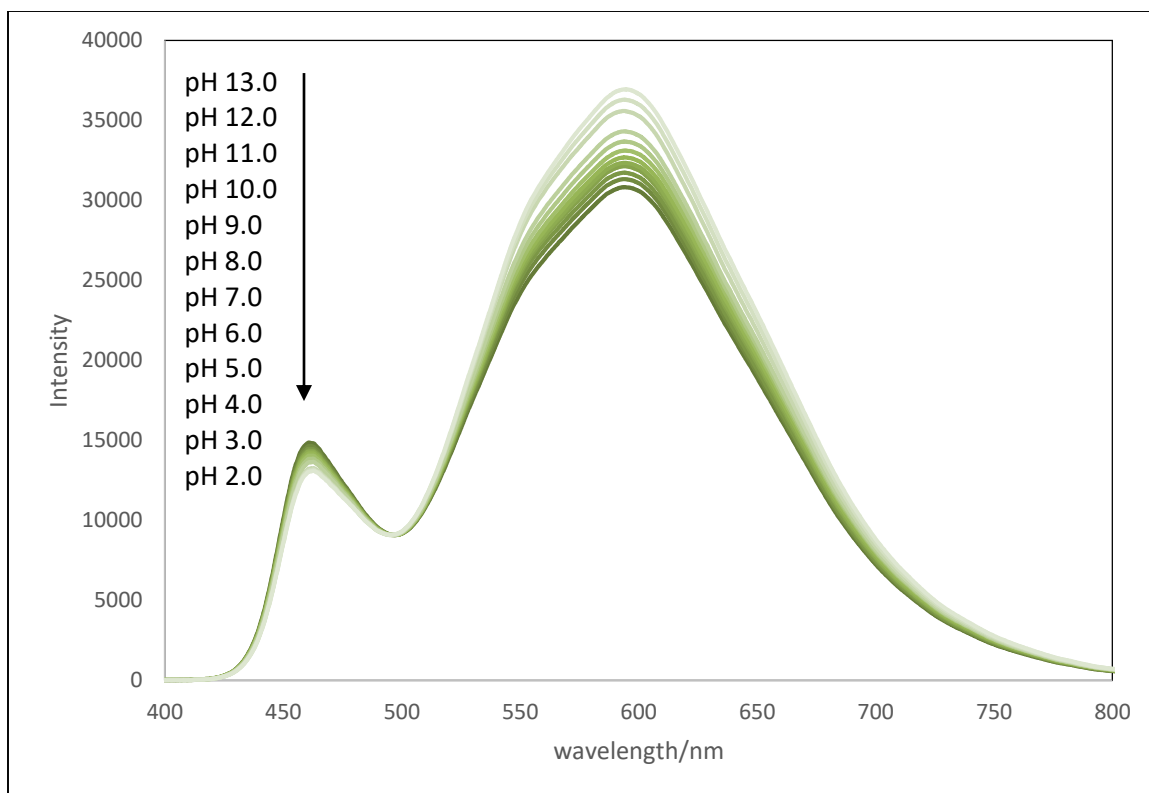
Figure 4-22. *A Comparison of Reflectance Spectra of STNR in Aqueous Buffer Solutions Ranging from pH 2.0 to 13.0 Showing Bands at 450-490 nm and 510-580 nm with Peaks and 460 nm and 580 nm*

At acidic pH values, the protonated neutral red has a blueish red hue and at basic pH values the deprotonated form has a yellowish orange color. As can be seen in Figure 4-23, the intensity of the peak at 460 nm was found to decrease as pH values increased, correlating with the change in ratio of the protonated and deprotonated species.
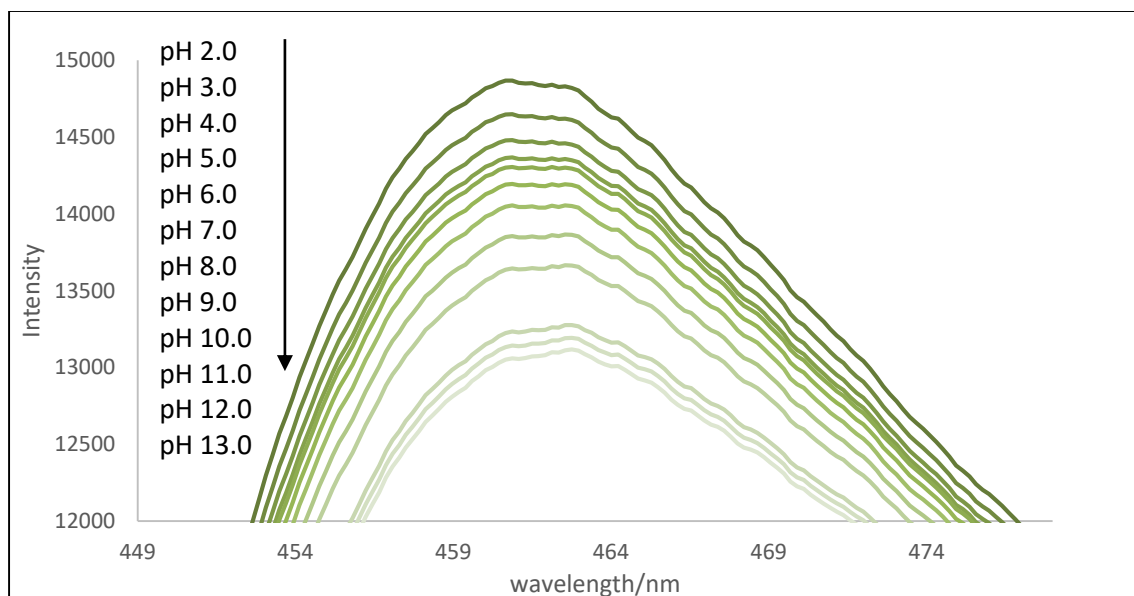
Figure 4-23. *A Magnification of the Reflectance Spectra of STNR from pH 2.0 to 13.0 Showing the Band at 450 to 490 nm*

As can be seen in Figure 4-24, the intensity of the peak at 580 nm was found to increase as pH values decreased, correlating with the change in ratio of the protonated and deprotonated species. This shows a direct relationship between the peak intensity at 580 nm and increase in pH values.
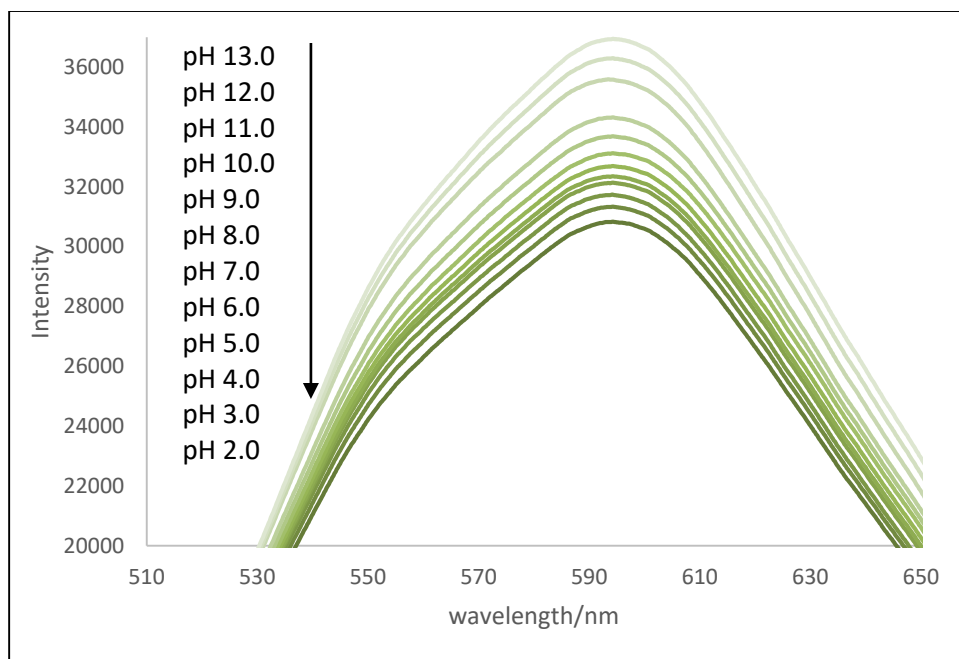
Figure 4-24. *A Magnification of the Reflectance Spectra of STNR from pH 2.0 to 13.0 Showing the Band at 510 to 680 nm*

The protocol was repeated for the neutral range of pH 6.0 to 8.0. The same pattern of the ratio of peaks 580 and 460 was seen in the smaller changed in pH values. The graph ratio of peak height of the peaks of the spectral bands of 580 and 460 nm is shown in Figure 4-25. The relationship of the ratio to changes in pH is linear and has a positive slope showing a positive correlation with increase in ratio value to the increase in pH values.
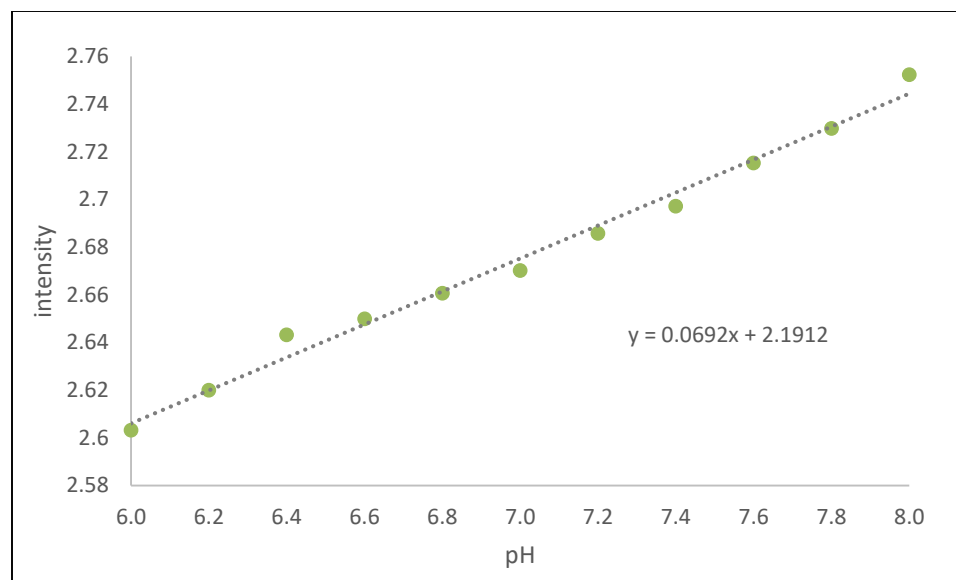
Figure 4-25. *This Graph of STNR Shows the Relationship Between the Ratio of Peak Intensity and pH Value for a pH Range of 6.0 to 8.0*

In Figure 4-26, the spectra taken were of particles in solutions ranging from pH 6.0 to 8.0 in increments of one for eleven samples. The spectra show the same two spectral bands at `450-490 nm and from ~510 to 680 nm. Figure 4-27 shows a magnification of the spectral band of 450-490 nm. This graph shows a decrease in intensity at 460 nm as pH value increases. Figure 4-28 shows the spectral band from 510-680 nm. This graph shows an increase in intensity at 580 nm as the pH value increases.
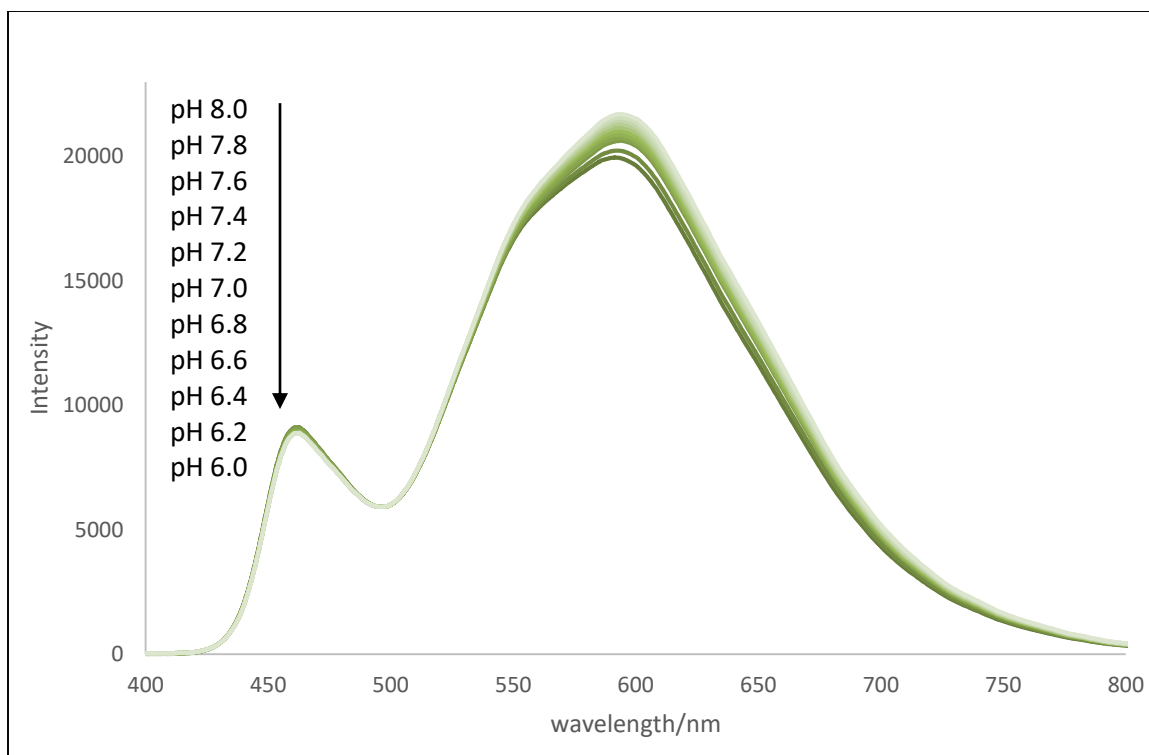
Figure 4-26. *A Comparison of Reflectance Spectra of STNR in Aqueous Buffer Solutions Ranging from pH 6.0-8.0 Showing Peaks and 460 nm and 580 nm*
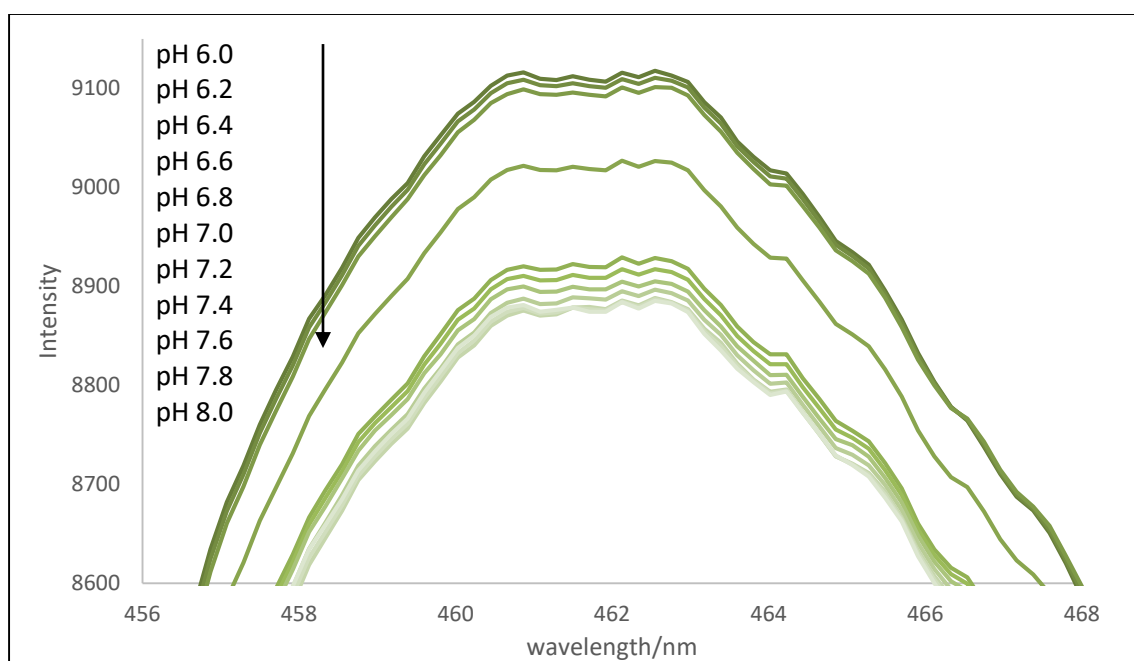
Figure 4-27. *A Magnification of Reflectance Spectra of STNR in Aqueous Buffer Solutions Ranging from pH 6.0-8.0 Showing the Band at 450-490 Nm*
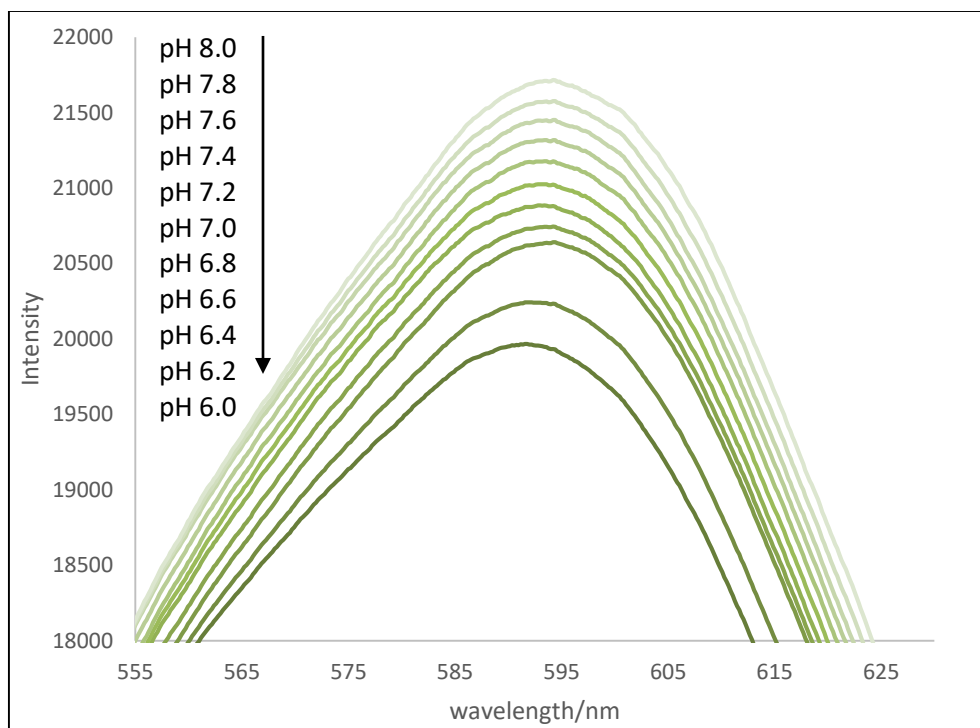
Figure 4-28. *A Magnification of the Reflectance Spectra of STNR from pH 6.0-8.0 Showing the Band at 510-680 nm*

In the same manner as the STNR, the HTNR particles were dispersed in a series of pH buffer solutions in a broad pH range of 1.40 to 13.40 and a near normal range of pH 6.0 to 8.0. The graph ratio of peak height of the peaks of the spectral bands of 580 and 460 nm is shown in Figure 4-29. The relationship of the ratio to changes in pH is linear and has a positive slope showing a positive correlation with increase in ratio value to the increase in pH values.
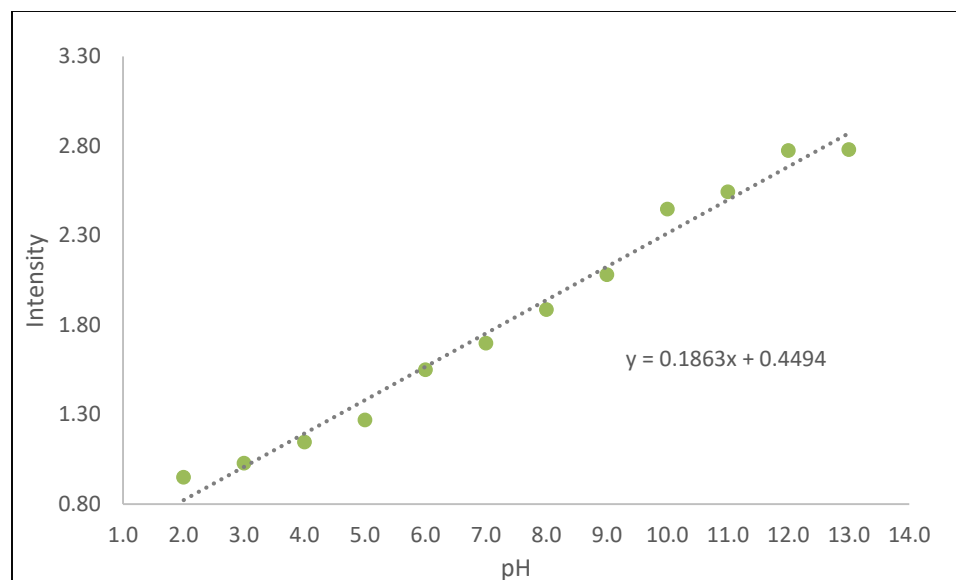
Figure 4-29. *This Graph of HTNR Shows the Relationship Between the Ratio of Peak Intensity and pH Value*

Figure 4-30 shows the spectra of the HTNR in a pH range of 2.0 to 13.0. The spectra show two spectral bands between 450-480 nm and 520-620 nm with at peaks at 460 nm, corresponding to a blue reflection peak, and 580 nm, corresponding to a yellow reflection peak. These peaks correlate with the blueish red hue of protonated NR and with the yellowish orange of the deprotonated state. The 460 nm peak intensity decreases as pH value increases and the 580 nm peak intensity increases along with pH values.
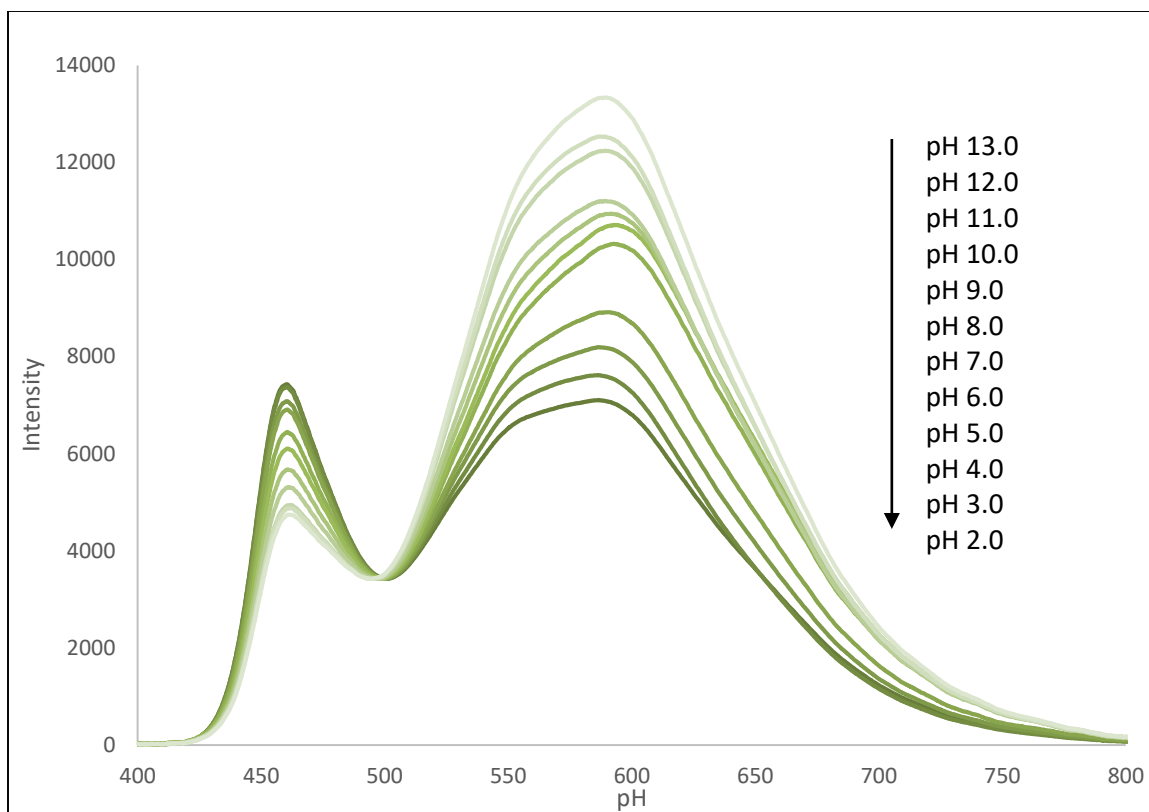
Figure 4-30. *A Comparison of Reflectance Spectra of HTNR in Aqueous Buffer Solutions Ranging from pH 2.0 to 12.0*

Figure 4-31 shows a magnification of the spectral band of 450-490 nm. This graph shows a decrease in intensity at 460 nm as pH value increases. Figure 4-32 shows the spectral band from 510-680 nm. The graph shows an increase in intensity at 580 nm as the pH value increases.
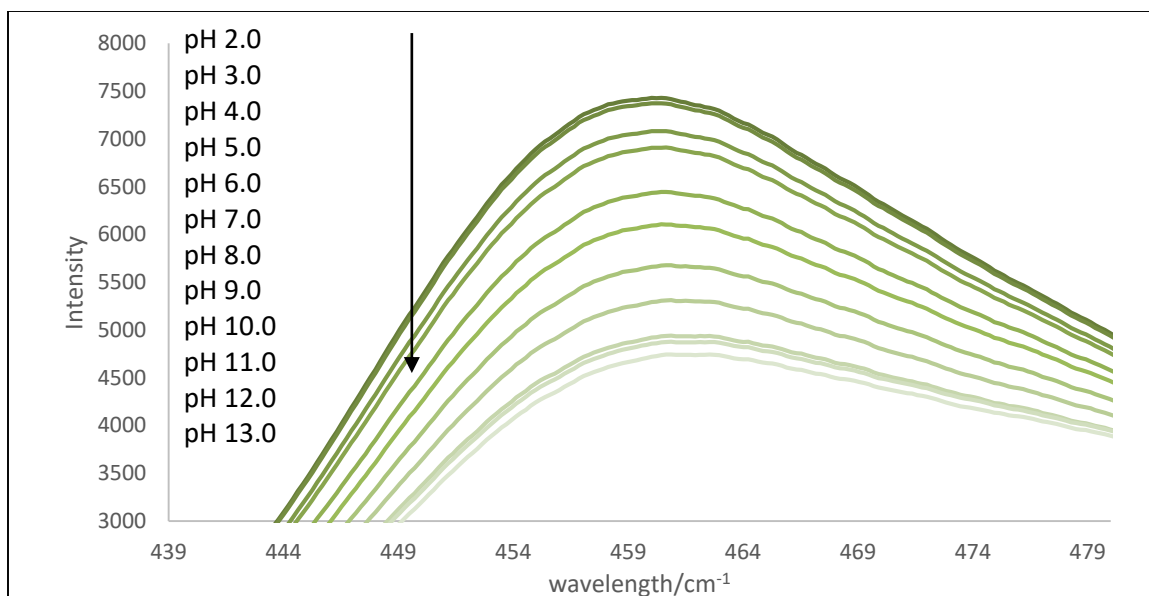
Figure 4-31. *A Magnification of Reflectance Spectra of HTNR from pH 6.0-8.0 Showing the Band from 450-490 nm*
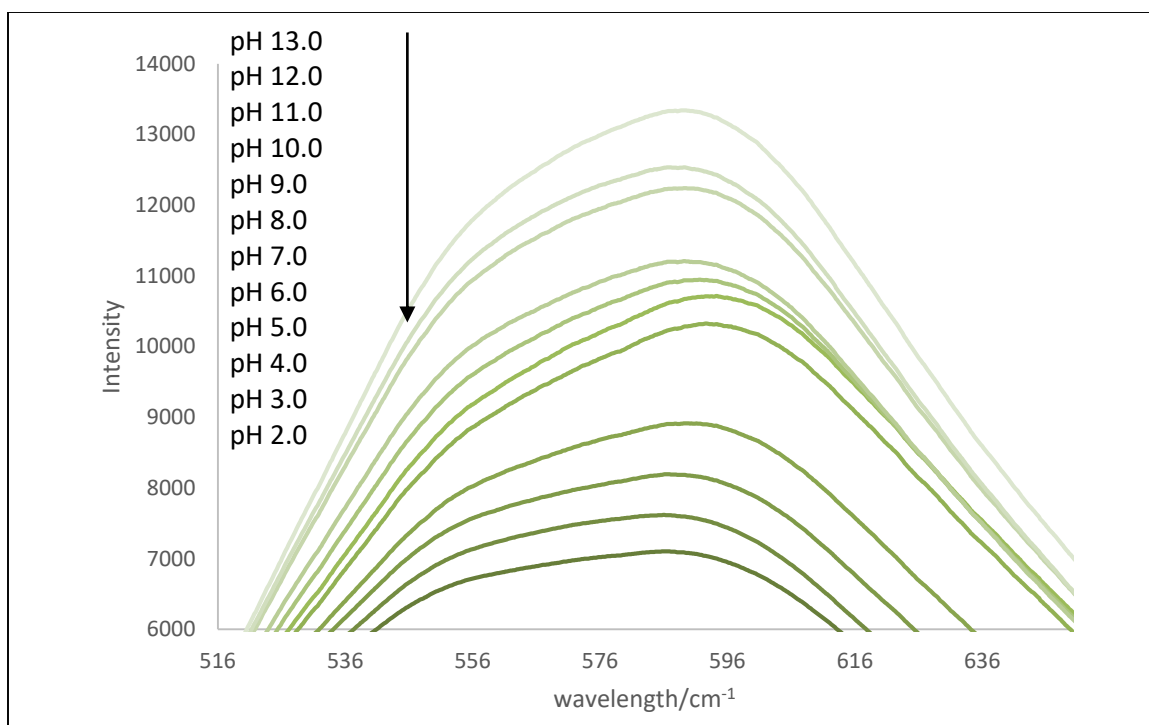
Figure 4-32. *A Magnification of the Reflectance Spectra of HTNR from pH 6.0-8.0 Showing the Band at 510-580 nm*

The protocol was repeated for the neutral range of pH 6.0 to 8.0 with the HTNR. The same pattern of the ratio of peaks 580 and 460 was seen in the smaller changed in pH values. The graph ratio of peak height of the peaks of the spectral bands of 580 and 460 nm is shown in Figure 4-33. The relationship of the ratio to changes in pH is linear and has a positive slope showing a positive correlation with increase in ratio value to the increase in pH values.
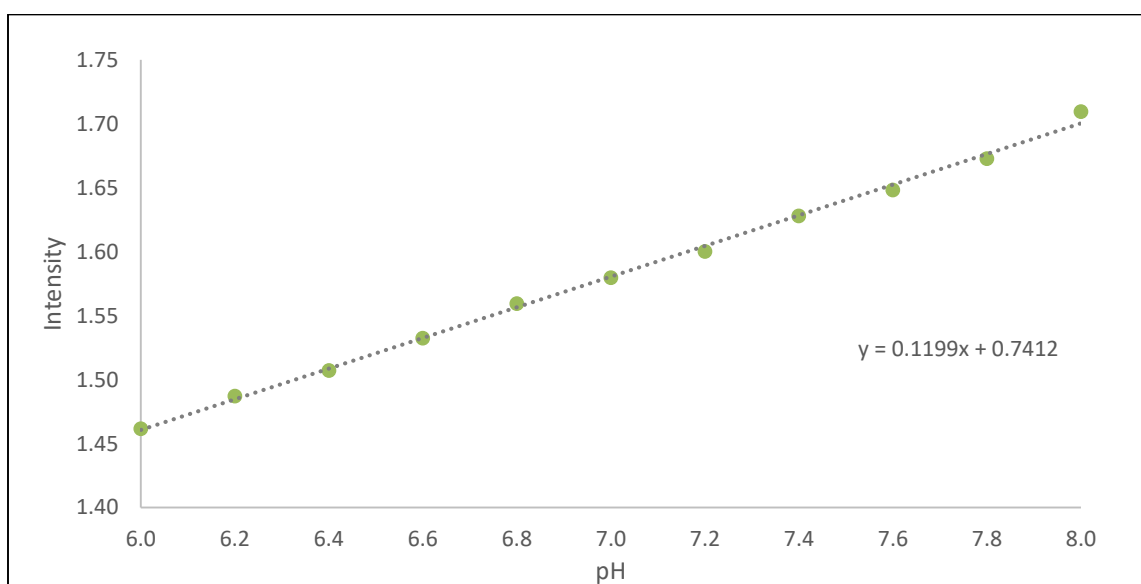
Figure 4-33. *This Graph of HTNR Shows the Relationship Between the Ratio of Peak Intensity and pH Value for a pH Range of 6.0 to 8.0*

In Figure 4-34, the spectra taken were of particles in solutions ranging from pH 6.0 to 8.0 in increments of one. The spectra show the same two spectral bands at `450-490 nm and from ~510 to 680 nm. Figure 4-35 shows a magnification of the spectral band of 450-490 nm. This graph shows a decrease in intensity at 460 nm as pH value increases. Figure 4-36 shows the spectral band from 510-680 nm. This graph shows an increase in intensity at 580 nm as the pH value increases.
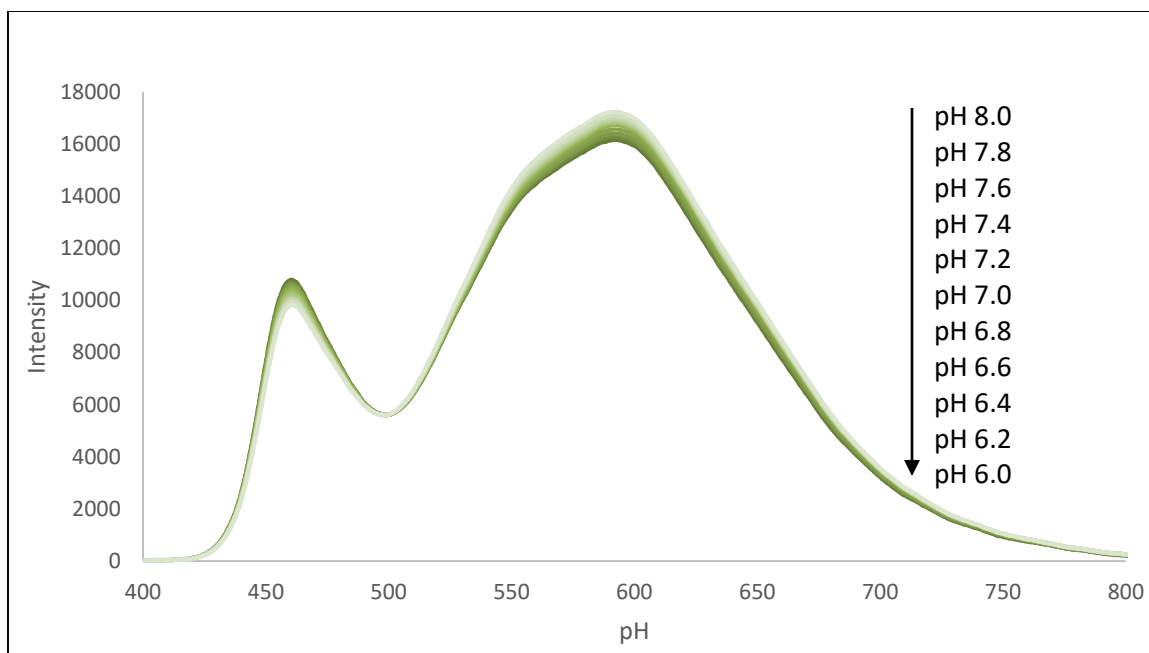
Figure 4-34. *A Comparison of Reflectance Spectra of HTNR in Aqueous Buffer Solutions Ranging from Ph 6.0-8.0*
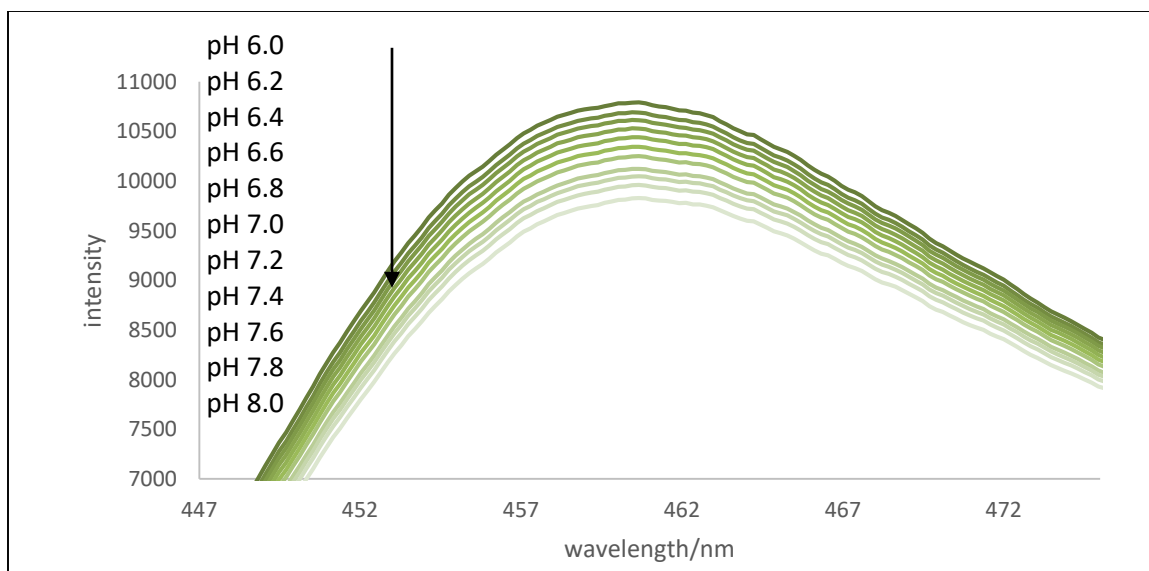
Figure 4-35. *A Magnification of Reflectance Spectra of HTNR from pH 6.0-8.0 Showing the Band at 450-490 nm*
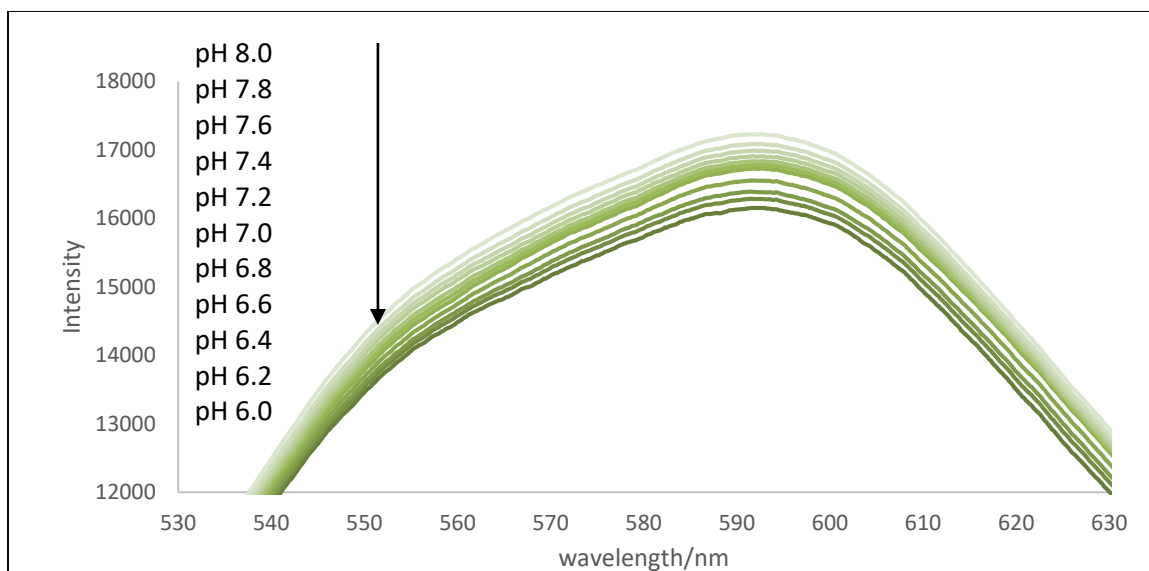
Figure 4-36. *A Magnification of Reflectance Spectra of HTNR from pH 6.0-8.0 Showing the Band at 510-580 nm*

CHAPTER 5

SYNTHESIS AND CHARACTERIZATION OF ONE-POT METHOD FOR SILICA-HALOCHROMIC DYE NANOPARTICLES

5.1   Introduction

The previous particles studied here used SiNP or HNT cores that were

functionalized with neutral red. This chapter explores a third type of particle that was

formed directly from TSB and a halochromic dye. TSB (see Figure 4-1) is an

organosilane crosslinking agent with an aldehyde functional group. The dyes used were

neutral red and Nile blue, which both have amine functionality. The amine group of the

dye was crosslinked with the aldehyde group of TSB forming an imine bond. This was

reduced to a secondary amine, forming a more stable bond. This one-pot synthesis

created pH sensitive NPs from a covalently bound silane-dye matrix. The first attempts to

synthesize this type of NP were unsuccessful. Hypothetically TSB should be capable of

forming a silane network and subsequently, NPs. However, the attempts using TSB and

neutral red only did not produce particles. In the initial experiments the reagents did not

react or produced an oily solution that contained no particles. This was confirmed by

DLS measurement (0.0 nm, 0.0 polydispersity) and by FESEM of samples of the dried

solution. Particles were produced when small amounts of tetraethoxysilane (TEOS), seen

in Figure 5-1, and ammonia (NH_4) were added, in a modification borrowed from the

Stöber process The resulting nanoparticles were spherical and dispersive in water.
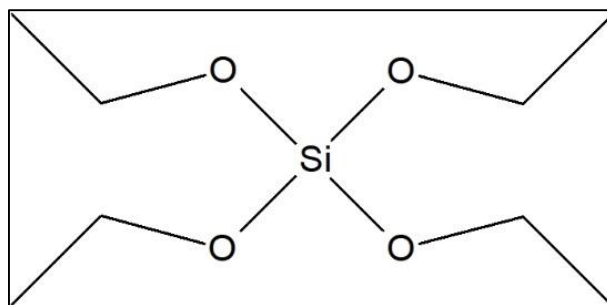
Figure 5-1. *Tetraethoxysilane (TEOS) an Ester Silicate and Organosilane Precursor*

The process was repeated using Nile blue, a halochromic dye with a pK_a of ~10, as seen in Figure 5-2. Nile blue was selected because it has a 2^0 amine group that would be suitable for the aldehyde-amine reaction. The higher pK_a of Nile blue also made it a comparison to neutral red which has a lover pK_a value of 6.8.
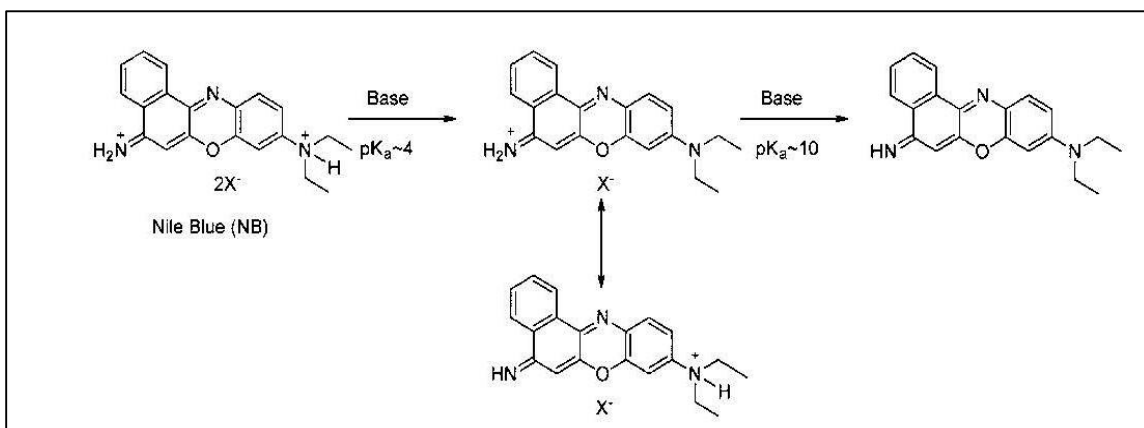
Figure 5-2. *Nile Blue pK_as at Stages of Protonation and Deprotonation (Madsen 2013)*

The synthesis produced NPs with both the neutral red and Nile blue. The NPs were highly responsive to changes in pH even at low concentrations. The organosilane-neutral red nanoparticles (OSNR) were sensitive in a near neutral pH range and showed a visually observable colorimetric change. Similarly, the organosilane-Nile blue nanoparticles (OSNB) showed a color change at a range of pH 10.0-12.0 observable to

the bare eye. Analysis of spectra showed that both the OSNR and OSNB could be used for sensing pH in a broad range by observing the changes in the spectral bands of the protonated and deprotonated states of the respective dyes.

The reaction scheme can be seen in Figure 5-3 and shows the progressive stages of the synthesis. The first step of the protocol involved the reaction of the aldehyde group of TSB with the secondary amines of the halochromic dyes, neutral red or Nile blue. The pH values of the reaction solutions were adjusted to basic values of pH 10 to reduce protonation and to shift the reaction towards the outcome of aldehyde to secondary amine bonding.

As stated previously in this study, the aldehyde-amine reaction produces an imine bond that is reversible with an iminium ion. The final step of the protocol was a treatment with sodium borohydride to reduce the imine bond to a more stable secondary amine bond. The neutral red moiety was still pH sensitive as the molecule was covalently bound via its primary amine functional group, not the tertiary amine that is responsible for its halochromic response. The Nile Blue moiety maintained pH sensitivity due to the covalent binding of the TSB to the secondary amine and a shift to the tertiary amine becoming the site of protonation. This aspect of the Nile blue molecule has been investigated before (Madsen 2013).
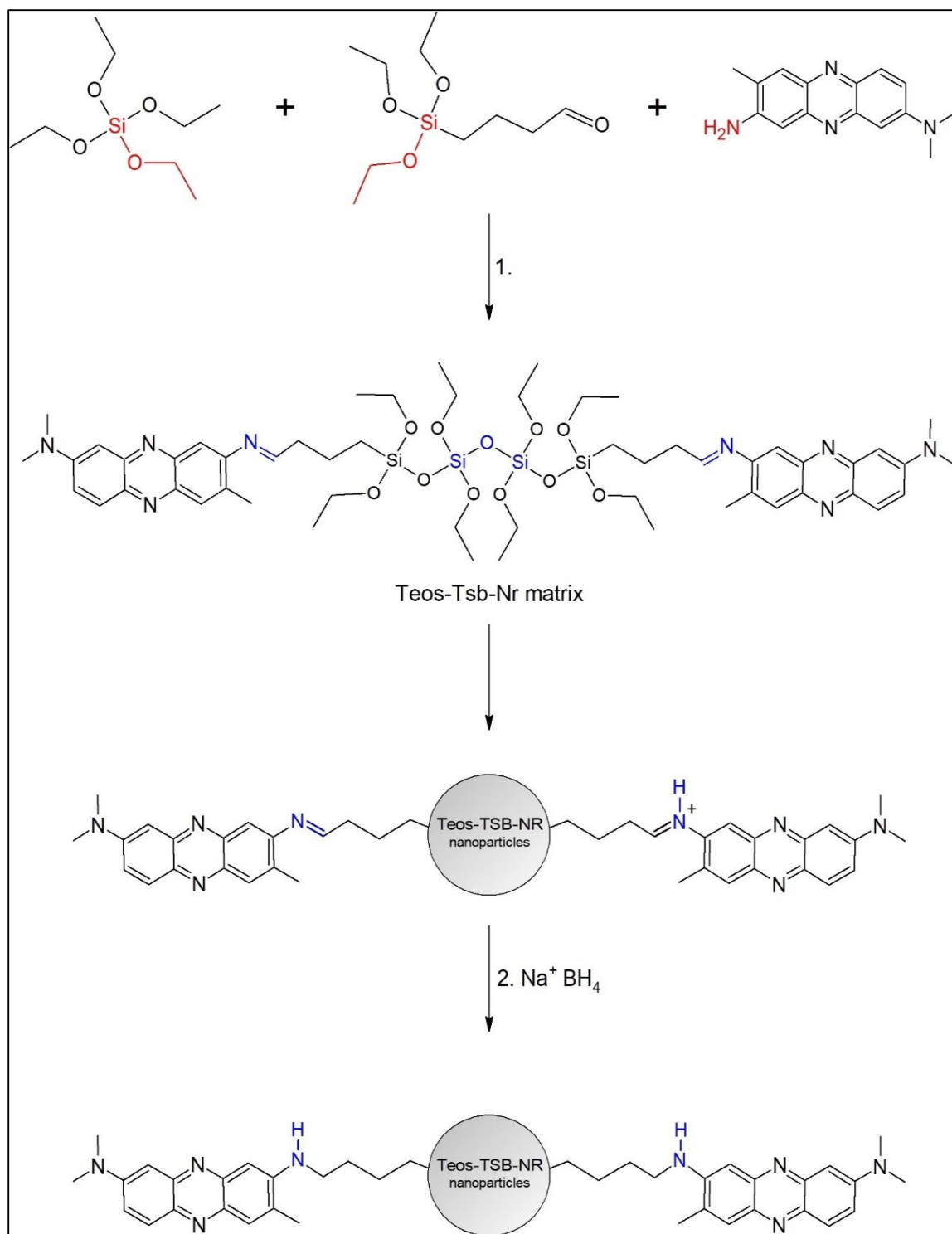
Figure 5-3. *The Reaction Scheme for OSNR and OSNB*

To test stability and resistance to leaching, the dye functionalized particles were washed in a variety of organic solvents and pH buffered solutions. There was no leaching when the particles were washed with ethanol, methanol, 0.1M HCl or 0.1M NaOH. The particles remained color stable and dispersive in aqueous solutions. The FTIR spectra of the particles were observed and the reflectance and absorption spectra were measured using an Ocean Optics spectrometer. The particles exhibited reliable changed in peak intensity of spectral bands when exposed to a broad range of pH solutions from ~1.5 to ~13.5 in range.

This protocol produced color stable and pH responsive nanoparticles than are sensitive to changes of pH in a broad and narrow range. The nanoparticles are water soluble and highly dispersive. Both series of particles have shown a tendency to progressively aggregate into larger particles when stored in aqueous solutions. Further areas of study could investigate the inclusion of a capping strategy into the protocols to stabilize the tendency of the particles to aggregate. This aspect may also be opportunity for further research into its suitability as a thin film coating or other sol-gel applications.

5.2   Experimental

5.2.1   Material and Reagents

The reaction scheme and protocols are identical for either neutral red or Nile blue. The reagent triethoxysilylbutyraldehyde (TSB) (99.0%), was purchased from Geleste. The reagents tetraethoxysilane (TEOS) (99.0%), neutral red (98.0%), Nile blue (99.0%) and sodium borohydride (99.0%) were purchased from Sigma Aldrich. The solvents and other chemicals, toluene (99.5%), ethanol (95.27%), isopropyl alcohol (95.27%), glacial

acetic acid (99.0%), sodium hydroxide (97%) and phosphate buffer (99.0%) were purchased from Sigma Aldrich and Fischer Scientific.

5.2.2 Protocol

The protocol was developed to be used with both of the polyamine dyes used in the study: Nile blue or neutral red. All steps are identical for either dye.

1. 50 mL of 95% ethanol was added to a round bottom flask.

2. 10 mg of neutral red or 10 mg of Nile blue was dissolved into 2 mL of ethanol and was slowly added to the stirring solution.

3. The pH of the solution was adjusted to ~pH 9.5 with 2M ethanolic sodium hydroxide.

4. 10 μL of TSB was added to the solution and it was stirred for 2 hours.

5. 10 μL of TEOS was added to the solution along with 5 μL of 2M ammonia. After these additions, the solution was stirred rapidly for 24 hours.

6. A solution was freshly prepared of 2.5 mg of sodium borohydride dissolved in 5 mL of isopropyl alcohol. The $NaBH_4$ solution was quickly added and the solution was stirred for 15 minutes.

7. 50 mL of DI H_2O was added to the solution to quench the unreacted $NaBH_4$.

8. The particles were washed with ethanol twice and DI H_2O twice by centrifugation, removing the supernatant and resuspending the precipitate by mixing with a vortex mixer. This was done to remove unreacted reagents. The NPS were either resuspended in ethanol or dried for further use.

The particles were synthesized following the protocol as written previously. The NPs were made with neutral red or Nile blue. The protocol was sufficient for

incorporation of either dye as NR and NB have similar solubilities and both contain an amine group suitable for reaction with an aldehyde. After synthesis, the particles were suspended in 0.01M phosphate buffer at pH 7.0 for storage. Particles that were used for FTIR or SEM were dried after the final wash.

5.3   Instrumentation

The absorption/reflection spectra of the samples were obtained with an Ocean Optics USB4000 spectroscope using a StellarNet LED driver equipped with a white LED. The spectra were recorded and analyzed with Ocean View spectroscopic software. The FTIR spectra were performed on a Thermo Scientific IR100 IR spectrometer. DLS and zeta potential measurements were taken on a Brookhaven Instruments Zeta Plus analyzer. FESEM images were obtained with an Hitachi S-4800 field emission scanning electron microscope. All photographic images were taken with a Nikon D60 and processed with Photoshop.

5.4   Results and Discussion

5.4.1   Images

After preparation using the previously described protocols, the OSNR and OSNB were dispersed in were dispersed into buffered solutions at a concentration of 0.1 mg/ml. The buffered solutions were adjusted to a range of pH levels prior to the addition of the particles. Two series of solutions were prepared. One series contained a range of pH values from 1.5 to 13.50 in increments of one, giving fourteen solutions in total. This was to show colorimetric change over a broad pH range.

The nanoparticle pH solutions for this range can be seen in Figures 5-4 and 5-5 for neutral red. After the OSNR were added to the solutions, adjustments were made with 0.01M NaOH or 0.01M HCl. The range of pH solutions is from 1.48 to 13.40 in increments of one. The particles exhibited rapid color change when added to the solutions. The color change was apparent to visual observation, but the particle solutions were measured with an Ocean Optics spectrometer. The particles showed a good dispersion in the aqueous buffer solutions. The dispersion was seen to persist for the duration of the measurements.

Figure 5-4. *OSNR in Aqueous Buffer Solutions Form pH 1.48 (Far Left) to 13.40 (Far Right) Showing Color Change and Dispersion*

Figure 5-5. *OSNR in Aqueous Buffer Solutions Form pH 1.48 to 13.40 Showing Color Change and Dispersion. (Top Row: pH 1.48, 2.0, 3.0, 4.0, 5.0, 6.0, Middle Row: pH 7.0, 8.0, 9.0, 10.0, 11.0, 12.0, Bottom Row: pH 13.0, 13.40)*

The silica-dye matrix particles containing Nile blue were synthesized by the same protocol as the neutral red particles. Both dyes are halochromic, have similar solubilities and have an amine groups suitable for conjugation with an aldehyde group. The particles were dispersed into buffered solutions at a range of pH values from 1.5 to 13.3 as seen in Figures 5-6 and 5-7. The particles showed a colorimetric change that was rapid and reversible. The OSNB showed a visually discernable color change in the pH range of 11 to 13. The pK_a of Nile blue is ~10, so the OSNB exhibit a bathochromic shift in pK_a. The spectrometer data was able to determine peak changes in a broader range of pH 2 to 13.
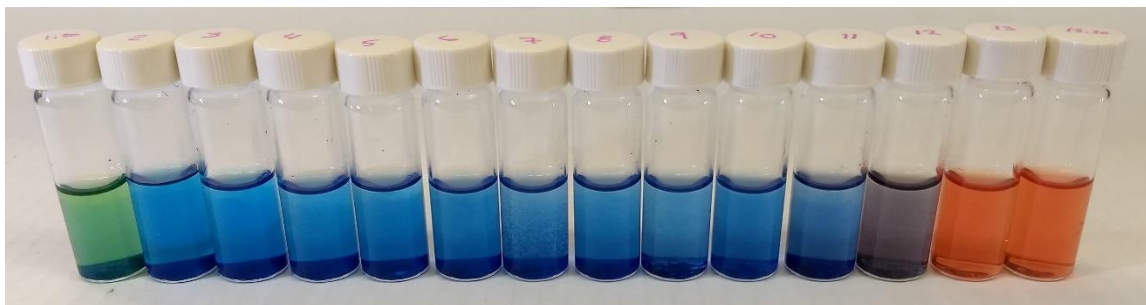
Figure 5-6. *OSNB in Aqueous Buffer Solutions Form pH 1.5 (Far Right) to 13.30 (Far Left) Showing Color Change and Dispersion*

Figure 5-7. *OSNB in Aqueous Buffer Solutions Form pH 1.5 to 13.30 Showing Color Change and Dispersion (Top Row: pH 1.5, 2.0, 3.0, 4.0, 5.0, 6.0, Middle Row: pH 7.0, 8.0, 9.0, 10.0, 11.0, 12.0, Bottom Row: pH 13.0, 13.3)*

5.4.2　　　FESEM

The particles were prepared for FESEM as described previously by dilution, sonication and drying on aluminum foil. Figure 5-8 shows an aggregate composed of material produced by the reaction of TSB with neutral red. No particles were produced. The oily material was prepared for SEM as previously described. No identifiable particles can be seen. In further attempts, the protocol was modified by the addition of TEOS and

ammonia and spherical nanoparticles were formed. Figure 5-9 shows OSNR. The NPs are spherical but have a range of sizes and are not monodispersive.
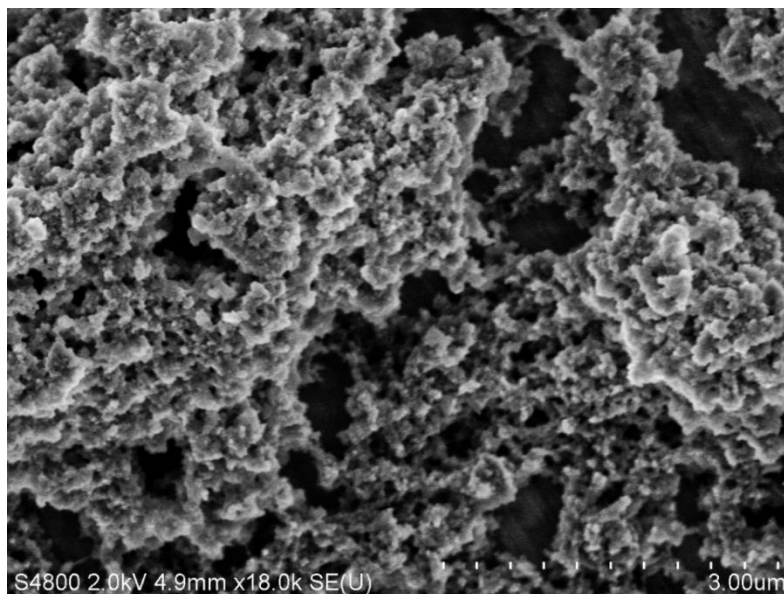
Figure 5-8. *Aggregate Formed After Drying an Unsuccessful Reaction of TSB and Neutral Red; Particles Were Not Formed*

Figure 5-9. *OSNR: The Addition of TEOS Led to the Growth of Spherical Nanoparticles*

In Figure 5-10 OSNB can be seen. These particles were synthesized with Nile blue using the TEOS modified protocol that was developed using neutral red. The particles were not monodispersive or uniform in shape. Clusters of aggregate were also formed, much more so than seen with the neutral red particles.
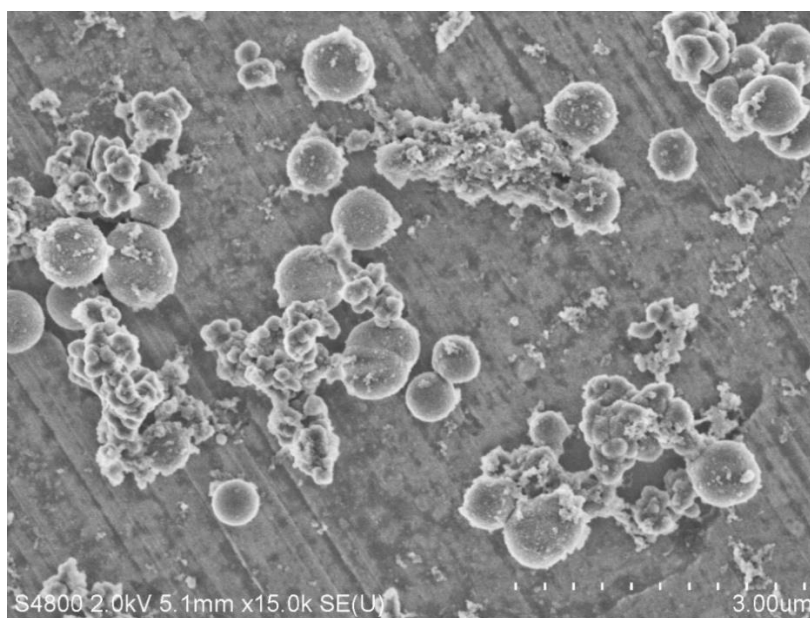
Figure 5-10. *OSNB Showing Spherical Particles of a Range of Diameters and Clusters of Aggregate*

5.4.3 DLS

The particles were measured with DLS. The SMNR and SMNB particles showed similar diameter and polydispersity. The SMNR were measured at 569.2 nm in diameter with a polydispersity of 0.25. The OSNB were measured at 593.5 nm with a polydispersity of 0.11.

5.4.4 FTIR

The spectra recorded in Figure 5-11 show the reagents and OSNR. The graph shows FTIR data recorded for the reagents that were used in the synthesis: TEOS, TSB and neutral red, as well as the final OSNR.
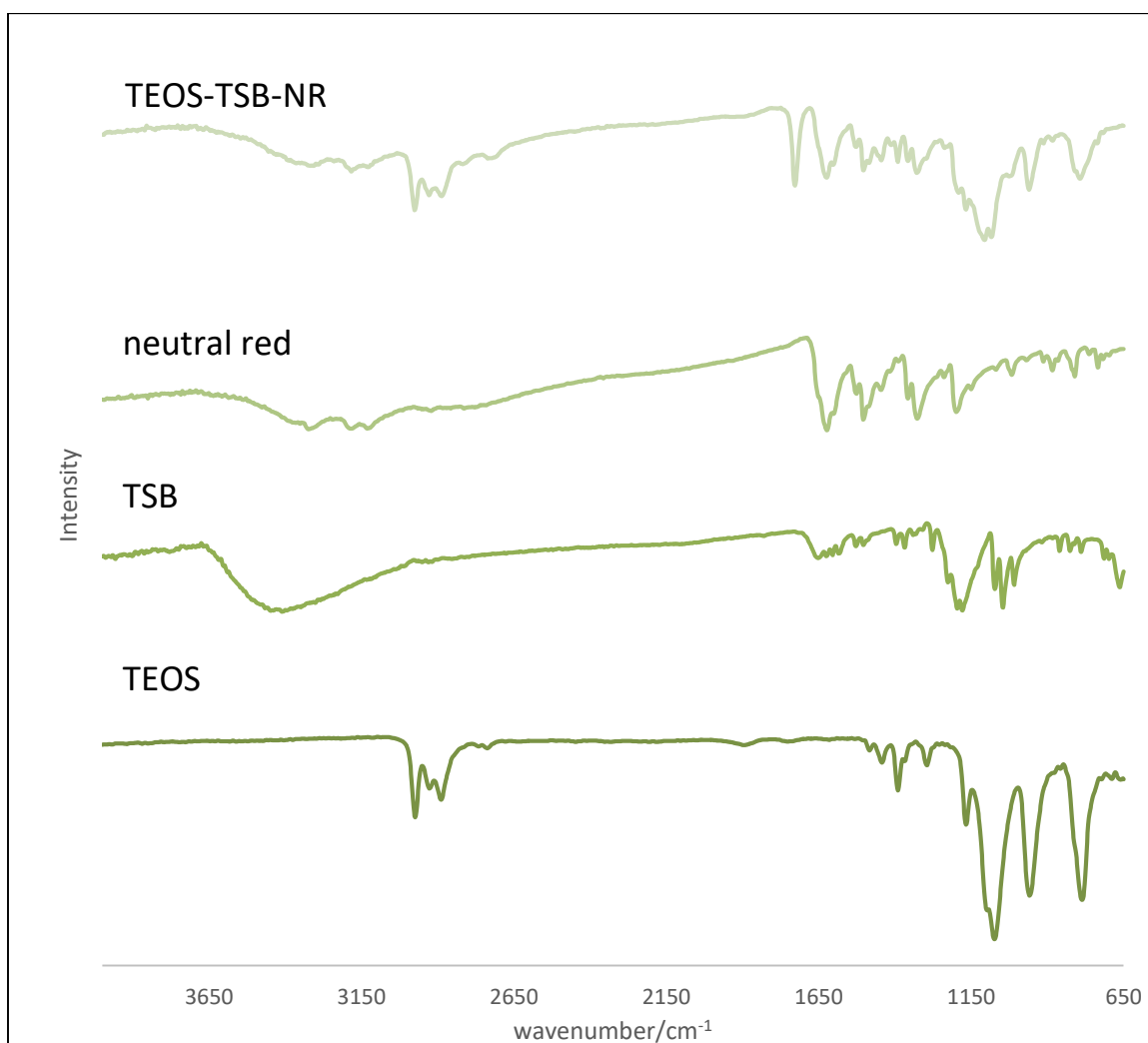
Figure 5-11. *A Comparison of FTIR Spectra of OSNR and Component Reagents*

The spectrum for the SMNR NPs can be seen in Figure 5-12. It shows a peak at 1105 cm^{-1} which is indicative of the Si-O stretch of silica. Peaks seen at 1625 and 1502 cm^{-1} may indicate the C=C stretch of alkenes from the neutral red molecule while peaks

at 2929 and 2886 cm^{-1} may be from alkenes from the butyl group of TSB. A peak at 1727

cm^{-1} may indicate the imine formed from the aldehyde amine reaction.
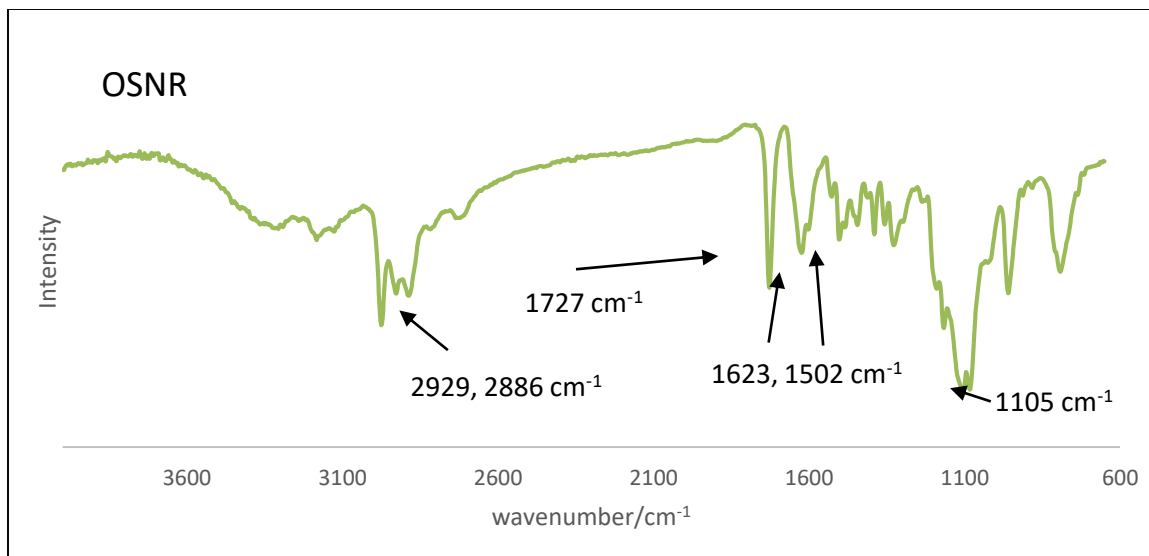
Figure 5-12. *FTIR Spectra of the OSNR*

The spectra for comparison of the reagents and OSNB can be seen in Figure 5-13.

The graph shows the FTIR spectra recorded for the reagents, TEOS, TSB, Nile blue dye,

and final particle of the organosilane-dye particles.
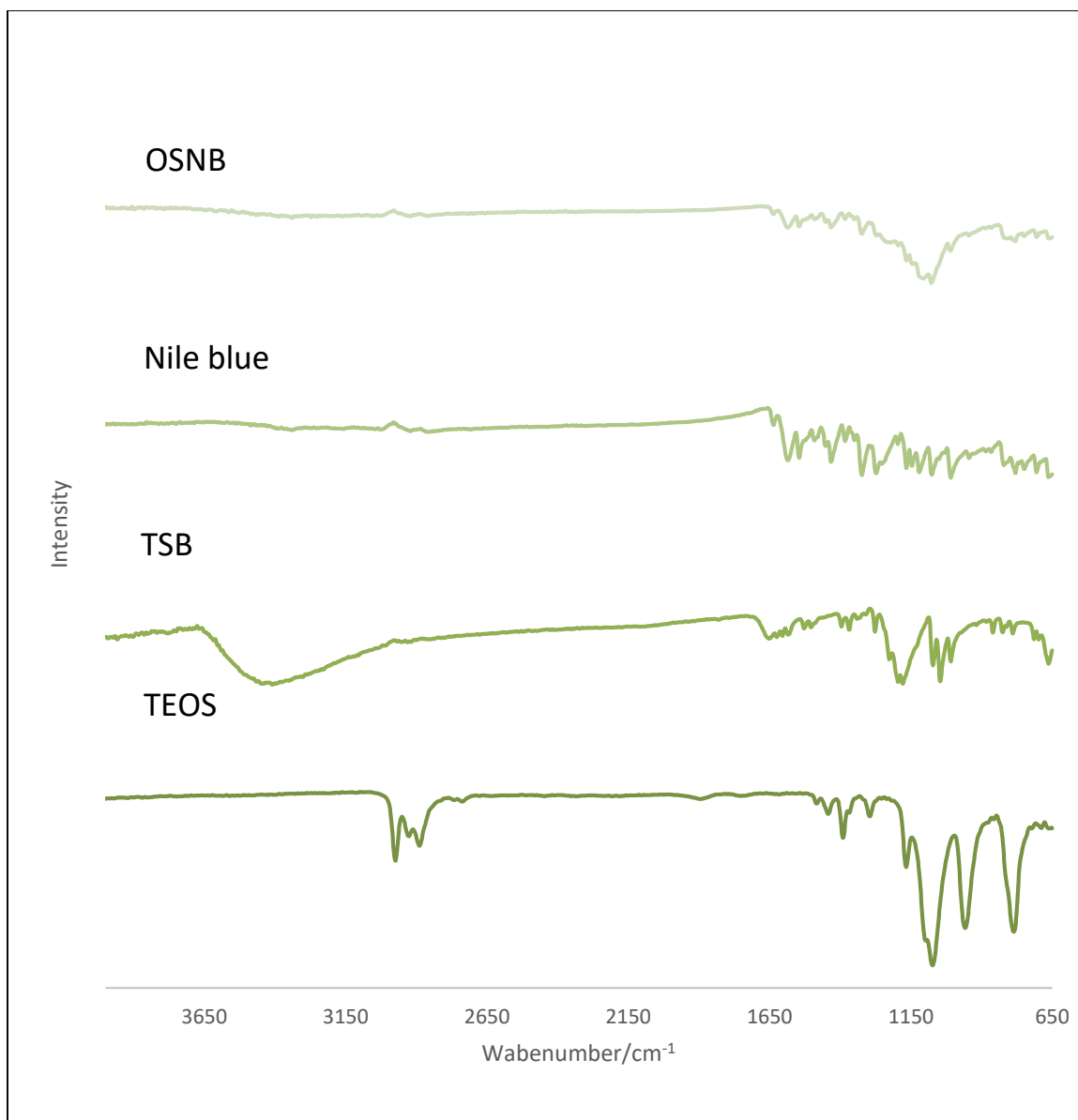
Figure 5-13. *A Comparison of the FTIR Spectra of the OSNB and Component Reagents*

The spectrum for the OSNB can be seen in Figure 5-14. The spectrum shows a peak at 1078 cm^{-1} that may indicate the Si-O stretch of silica. The peaks seen at 1582 and 1544 cm^{-1} may indicate the C=C stretch of alkenes from the Nile blue molecule. The peaks seen at 2854 and 2919 cm^{-1} may indicate the alkanes from the butyl group of TSB.
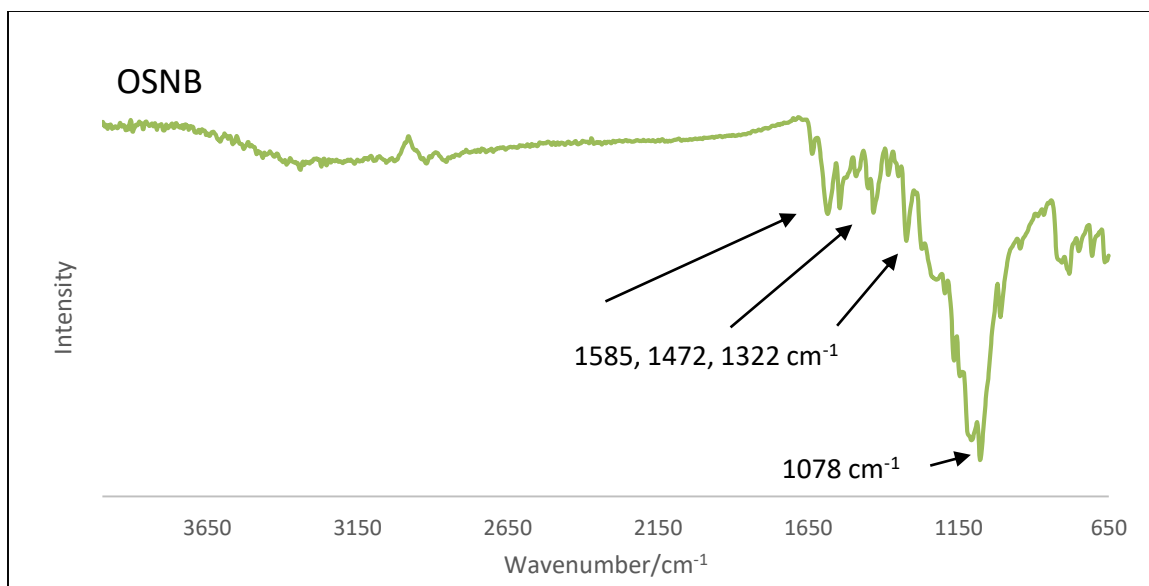
Figure 5-14. *FTIR Spectra of the OSNB*

5.4.5 UV-Vis Spectroscopy

The OSNR were dispersed in a series of pH buffer solutions in a broad pH range of 1.50 to 13.40 in increments of one for a total of fourteen solutions. The spectra show two spectral bands from 450-490 nm and 510-680 nm with peaks at 460 nm and 580 nm. The graph of ratio of these peaks can be seen in Figure 5-15. The value is shown to increase as the pH value increases exhibiting a positive correlation.
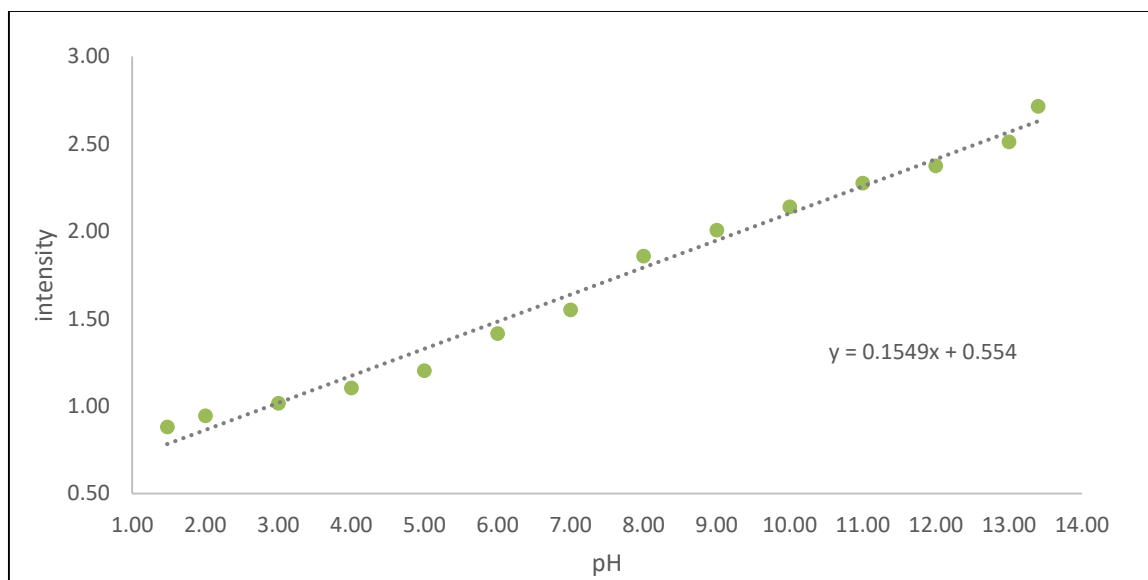
Figure 5-15. *The Graph of OSNR Showing the Relationship between the Ratio of Peak Intensity and pH Value*

The graph of the spectra of the OSNR dispersed in pH solutions can be seen in Figure 5-16. Two spectral bands can be seen from ~450 to 490 nm and ~510 to 680 nm. The spectral band at 450-490 nm corresponds to the blueish red color of the protonated species of neutral red. This region decreases in intensity as pH increases. The 510-680 nm spectral peak corresponds to the orangish yellow of the deprotonated species of the dye. This region increases in intensity as pH increases. The two peaks at 460 and 580 nm were seen to correlate most strongly to changes in pH value. The peak at 460 nm was found to decrease as pH values increased. The peak at 580 nm was found to increase as pH values increased (Figure 5-15).
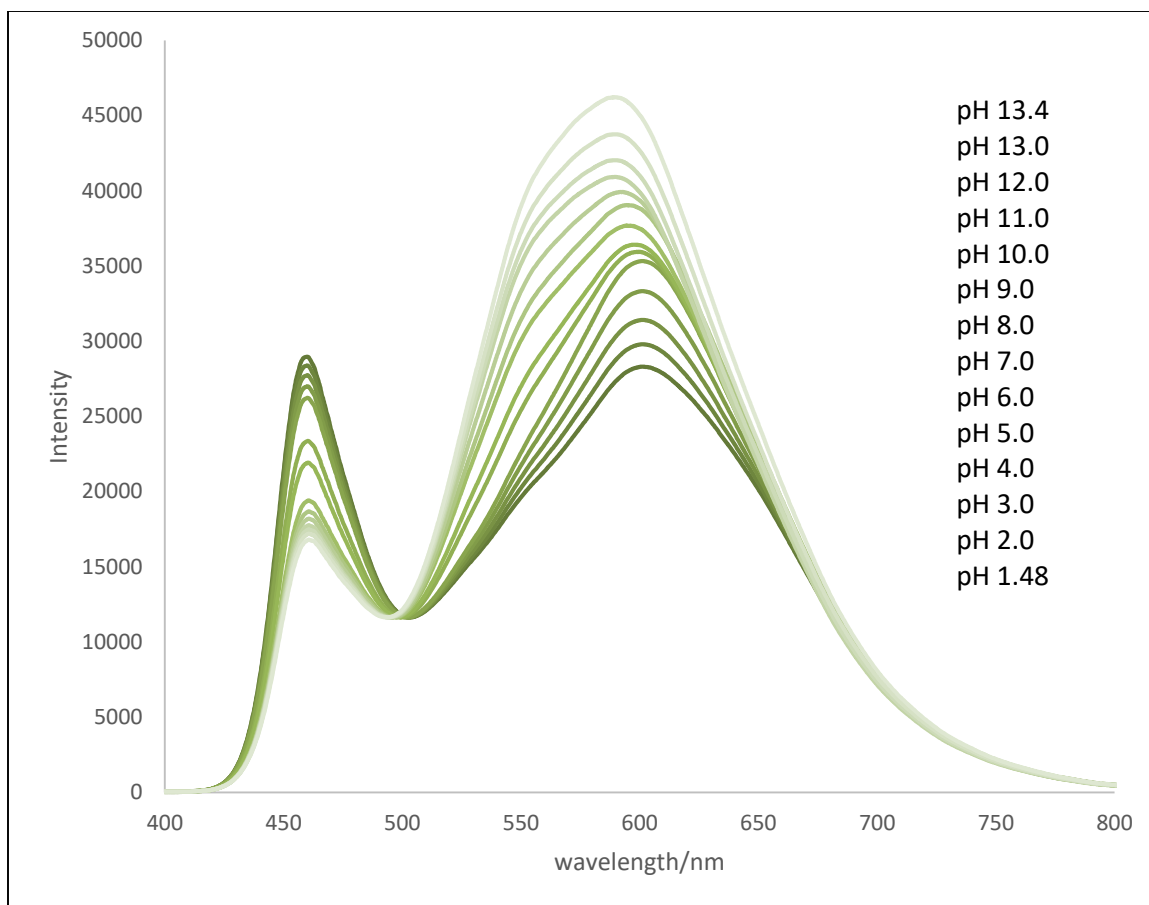
Figure 5-16. *SMNR in a Range of pH Solutions From 2.0 to 13.0*

The OSNB were dispersed in a series of pH buffer solutions in a broad pH range of 1.5 to 13.3. The spectrum for pH 1.5 is not included in the analysis because of its different reflectance values. The fully protonated species of Nile blue is green, and the absorbance and reflectance spectra do not support broad range pH sensitivity. The spectrum for pH 13.3 is identical to that of pH 12 and is not included for that reason. The absorbance and reflectance spectra were recorded. The spectra show spectral bands from 450 to 490 nm, 500 to 550 nm and 576 to 620 nm. Peaks at 463 and 540 nm were shown to decrease as pH values increased. A peak at 596 nm was shown to reliably increase as pH values increase.

Figure 5-17 shows the ratio of the peaks at 463 nm and 596 nm, corresponding to the protonated and deprotonated states of the Nile blue moiety of the OSNB. The ratio increases as pH values increase. The relationship is not liner do the larger change in values at the pH range of 11.0 to 13.0. Within the range of pH 2.0 to 11.0 the graph is linear. In Figure 5-18, a similar relationship can be seen in the graph of the ratio between the peak at 540 nm and 596 nm. Both peaks at 463 and 540 nm were seen to correlate to the protonated state of Nile blue and its characteristic blue color. The peak at 596 correlated to the fully unprotonated species with an orangish red color. The relationship between the two protonated peaks and the one deprotonated peak is stable for either ratio.
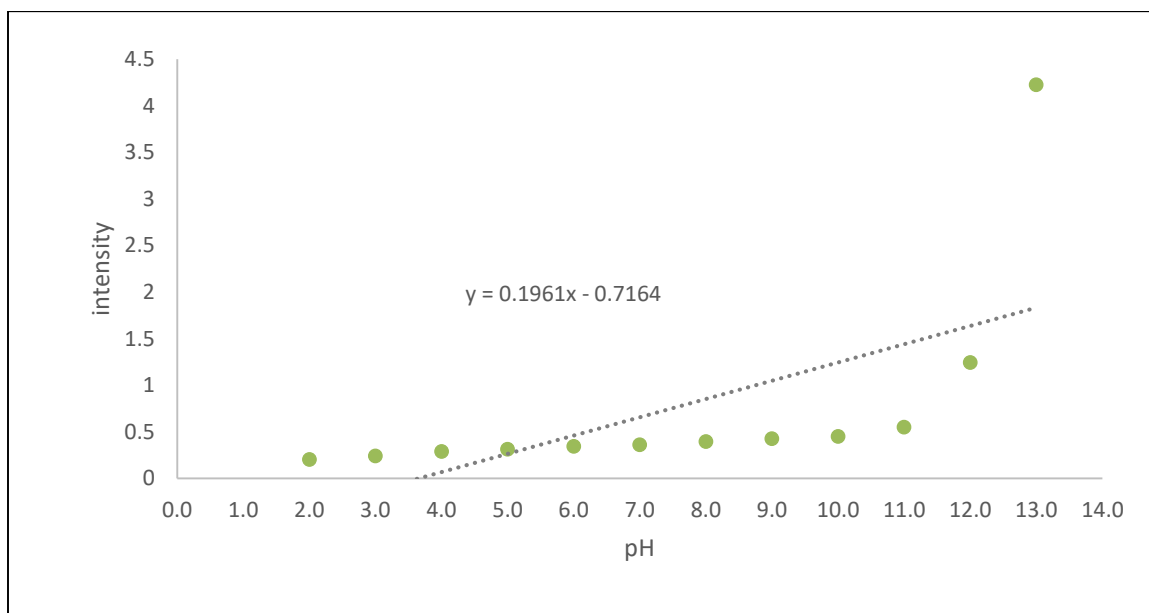
Figure 5-17. *The Graph of OSNB Showing the Relationship Between the Ratio of Peak Intensity and pH Value*
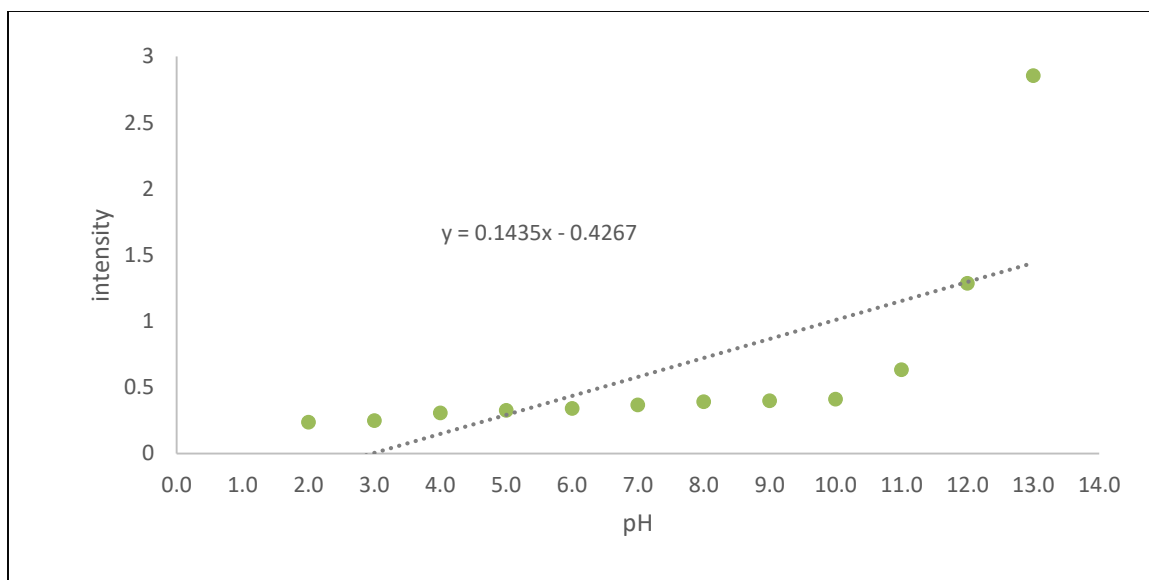
Figure 5-18. *A Graph of the Ratio Between Peaks at 540 and 596 nm for OSNB*

The spectra of the OSNB in a range of pH solutions can be seen in Figure 5-19. It shows spectral bands from 450 to 490 nm with a peak at 463 nm, corresponding to a blue reflectance peak, and a spectral band from 500 to 550 nm with a peak at 540 nm corresponding to a green reflectance peak.
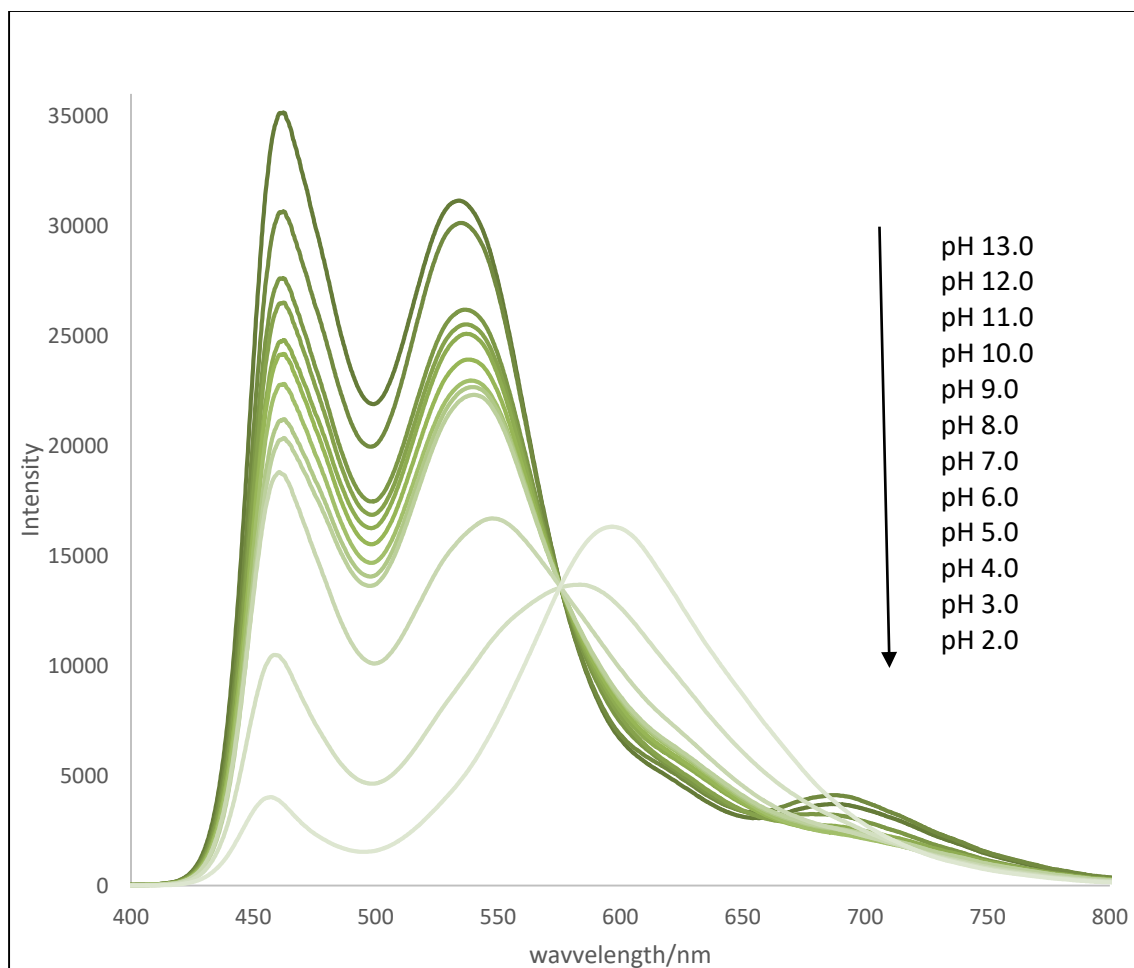
Figure 5-19. *Reflectance Spectra for OSNB from pH 2.0 to 13.0 Showing Spectral Bands and Peaks at 463, 540 and 596 nm*

These areas of the spectra correspond to the protonated species of Nile blue. Another spectral band is found at 576 to 620 nm with a peak at 596 nmn, corresponding to a red-orange reflectance peak and the deprotonated species. At pH values below 10.0, Nile blue exhibits a distinctive blue hue and at pH values above 11 it shows a red-orange hue. The 463 and 540 nm peaks decreased as pH value increased (from pH 2 to 13). The 596 nm peak increased as pH value increased (from pH 2.0 to 13.0). This relationship is supported with the data collected.

The spectra for pH 1.5 was not included because the relationship between the described peaks is not sufficient to describe their behavior as the particles took on a strong green color with different reflection spectra. The values for pH 13.3 were not included because they were indistinguishable from the values for pH 13.0.

CHAPTER 6

PREPARATION OF ALDEHYDE FUNCTIONALIZED SILICA AND HALLOYSITE NANOPARTICLES WITH NUCLEIC ACIDS ND NITROGENOUS BASES

6.1   Introduction

The previous chapters have studied the functionalization of inorganic nanoparticles with halochromic ionophore dyes. The method of attachment in each involved the reaction of an amine with an aldehyde, forming a covalent bond. The organosilane TSB is a crosslinking agent used to provide an aldehyde functional group to a silica surface. In Chapter 4, this study investigated the usefulness of functionalizing silica and aluminosilicate NPs with an aldehyde. Once prepared, the aldehyde functionalized NPs could present other opportunities for a variety of uses. This chapter of the study focuses on the covalent binding of nucleic acids to aldehyde functionalized inorganic NPs.

SiNPS and HNTs were used as cores for this study. The general reaction scheme can be seen in Figure 6-1. The protocol was able to be used for the attachment of adenine, a single nucleotide with a primary amine group and for DNA and RNA. Guanine and cytosine also have primary amines suitable for covalent bonding to aldehydes. The DNA and RNA samples were attached at 95^0C as the double stranded nucleic acids denature above that temperature.
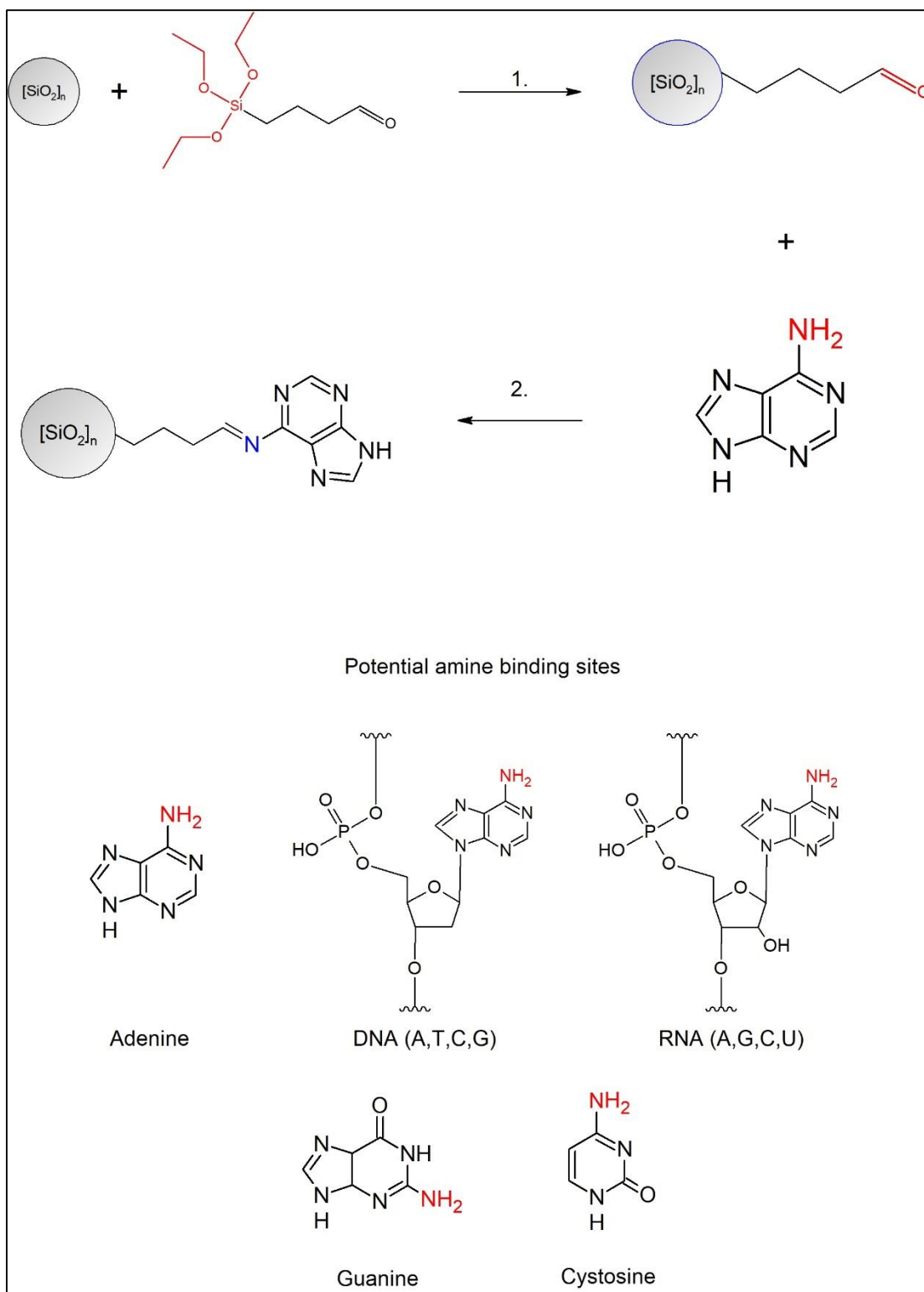
Figure 6-1. *The Reaction Scheme for the Modification of SiNPs, or HNTs, with TSB and Adenine, RNA or DNA*

6.2 Experimental

6.2.1   Materials and Reagents

The inorganic cores consisted of aluminosilicate HNTs or SiNPs. The SiNPs were purchased from US Research Nanomaterials. The HNTs were purchased from Sigma Aldrich. The reaction scheme and protocols are identical for either core. The reagent triethoxysilylbutyraldehyde (TSB) (99.0%), was purchased from Geleste. Ribonucleic acid (torula yeast) and deoxyribonucleic acid was purchased from Sigma-Aldrich. The solvents and other chemicals, methanol (95.0%), ethanol (95.0%), ammonia (17M), sodium hydroxide (99.0%) and saline phosphate buffer (99.0%) were purchased from Sigma Aldrich and Fischer Scientific.

6.2.2   Protocol

The protocol was developed to be used with either SiNPs or aluminosilicate HNTs. The functionalization occurs upon the silica surface of the nanoparticles or the silica outer layer of the HNTs. All steps are identical for either core. The reagents used to bind to the aldehyde were adenosine, yeast RNA and herring DNA. An identical protocol was used for all three reagents.

1. The HNTs and SiNPs were dried at 150^0C for 24 hours prior to use. 200 mg of either HNTs or SiNPs were mixed with 50 mL of methanol and sonicated for 10 minutes to separate and disperse the particles.

2. An aliquot of 100μL of TSB was added to the solution and it was stirred at room temperature 12 hours.

3. The particles were washed by centrifugation, removing the precipitate, resuspending it in methanol by stirring with a vortex mixer. This was repeated twice to remove unreacted TSB.

4. The aldehyde functionalized particles were resuspended in 50 mL of ethanol and magnetically stirred. The solution was heated to 90^0C.

5. The protocol differs between the use of adenine and DNA and RNA:

   5.1. A solution was freshly prepared of either 10 mg of DNA or10 mg of RNA dissolved in 10.0 mL of DI H_2O or

   5.2. A sample of 10 mg of adenosine was dissolved in 1.0 mL of 1M hydrochloric acid, then diluted with DI H_2O to 10 mL.

6. The nucleotide solution was slowly added to the warm stirring solution dropwise and the pH was adjusted to pH 9.0 with 2M ammonia.

7. The solution was refluxed at 90^0C for 2 hours.

8. The nucleotide particles were washed three times with ethanol to remove any unreacted reagents and resuspended in pH 7.0 aqueous phosphate buffered solution or dried for use in instrumental characterization.

6.3   Instrumentation

The particles were synthesized following the protocol as previously described. The particles were prepared with covalently bound adenine, DNA or RNA. The protocol used heat to denature the DNA and RNA into single strand conformations for binding to the nanoparticles. After synthesizing, the particles were resuspended in 0.01M phosphate buffer solution and frozen until use or dried for characterization studies. The particles were characterized with SEM, DLS, FTIR and TGA. SEM and DLS measurements both showed an increase in size after functionalization with nucleotides. IR spectra indicated that the nucleotides were bound to the particles. Thermogravitational analysis showed a change in response curves between the untreated core particles and the functionalized varieties.

6.4   Results and Discussion

6.4.1   FESEM

The SiNP core particles were prepared for SEM as previously noted. SiNPs

functionalized with TSB can be seen in Figure 6-2. They show no changes in morphology

from unmodified SiNPs. In Figure 6-3 SiNPs functionalized with adenine are shown. The

particles appear as aggregate clumps of smaller particles bound into clusters. Figures 6-4

and 6-5 show SiNPs functionalized with DNA and RNA respectively. The particles are

shown as aggregates or clusters of small nodule bound together with glue like material.
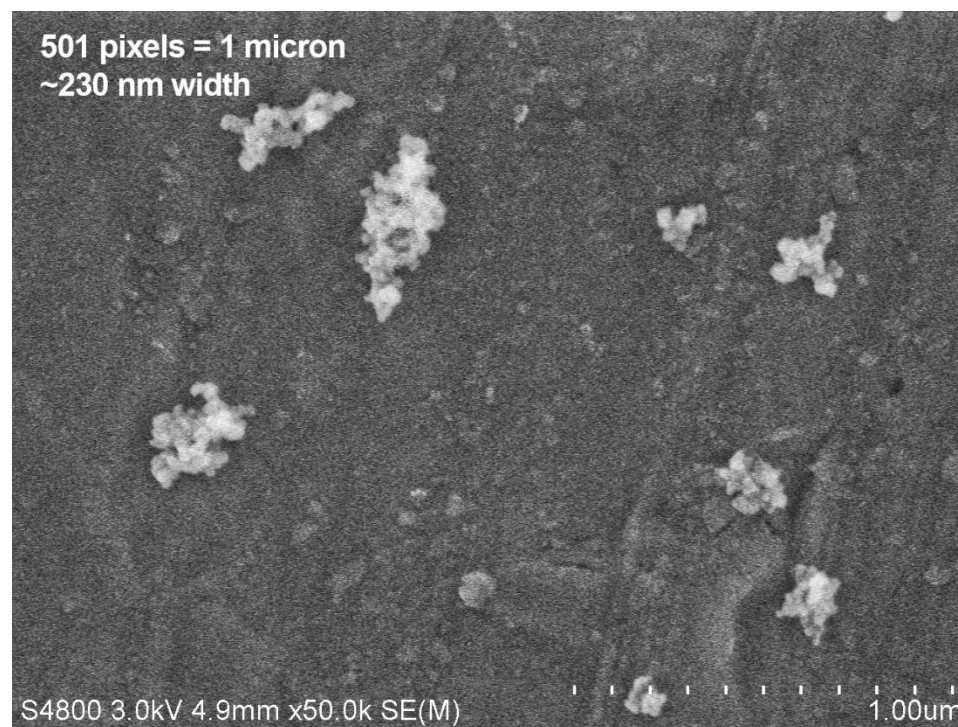
Figure 6-2. *SiNPs Functionalized with TSB*

Figure 6-3. *SiNPs Functionalized with TSB and Adenine*

353 pixels = 500 nm
~696 nm width
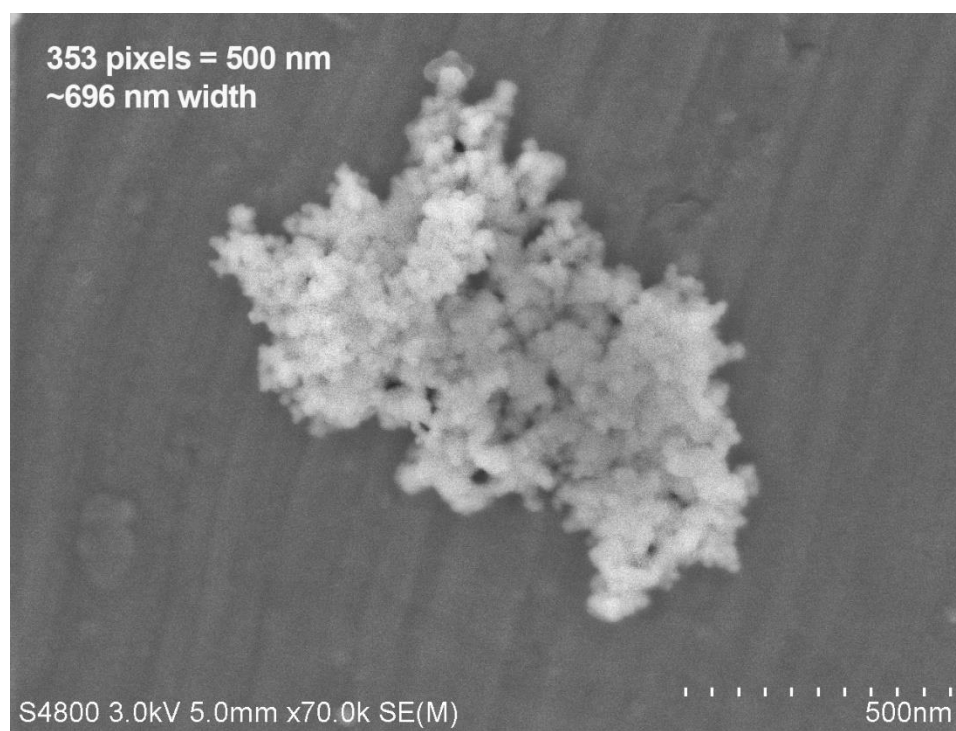
Figure 6-4. *SiNPs Functionalized with TSB and Single Strand DNA*
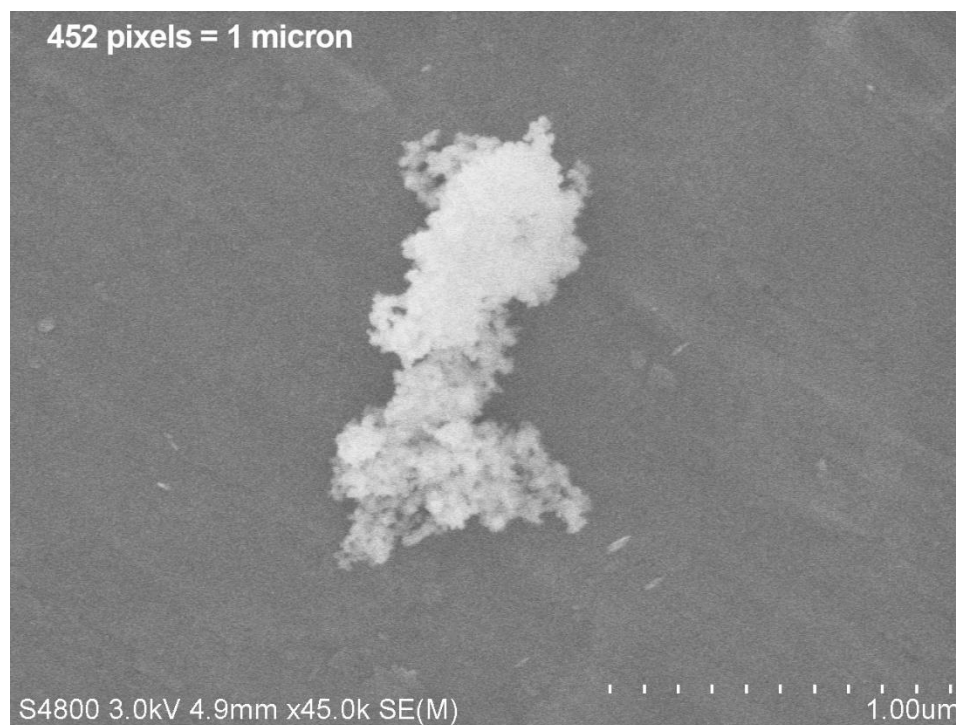
Figure 6-5. *SiNPs Functionalized with TSB and Single Strand RNA*

The HNT core particles were prepared for SEM as previously noted. HNTs functionalized with TSB can be seen in Figure 6-6. They show no changes in morphology from unmodified HNTs. In Figures 6-7, 6-8 and 6-9, HNTs functionalized with adenine, RNA and DNA respectively are shown. The nanotubes display no change in morphology or surface characteristics. This agrees with the expectation that the nucleic acids were a small percentage of the total mass of the particles and should not have caused changes in morphology.

Figure 6-6. *Halloysite Nanotubes Functionalized with TSB*
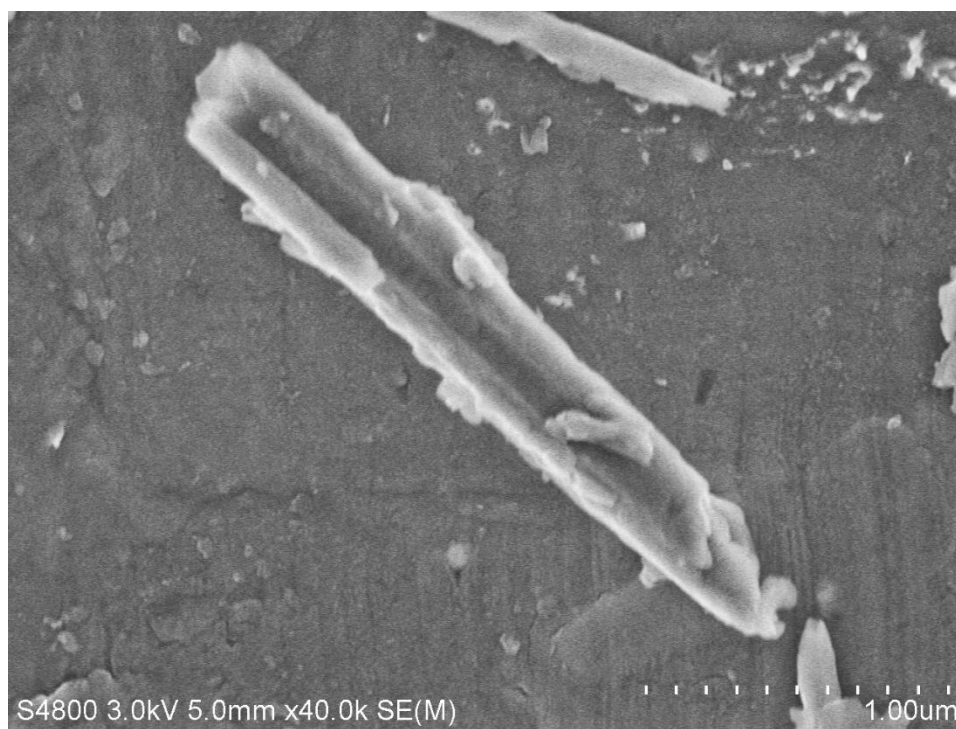
Figure 6-7. *Halloysite Nanotubes Functionalized with TSB and Adenine*
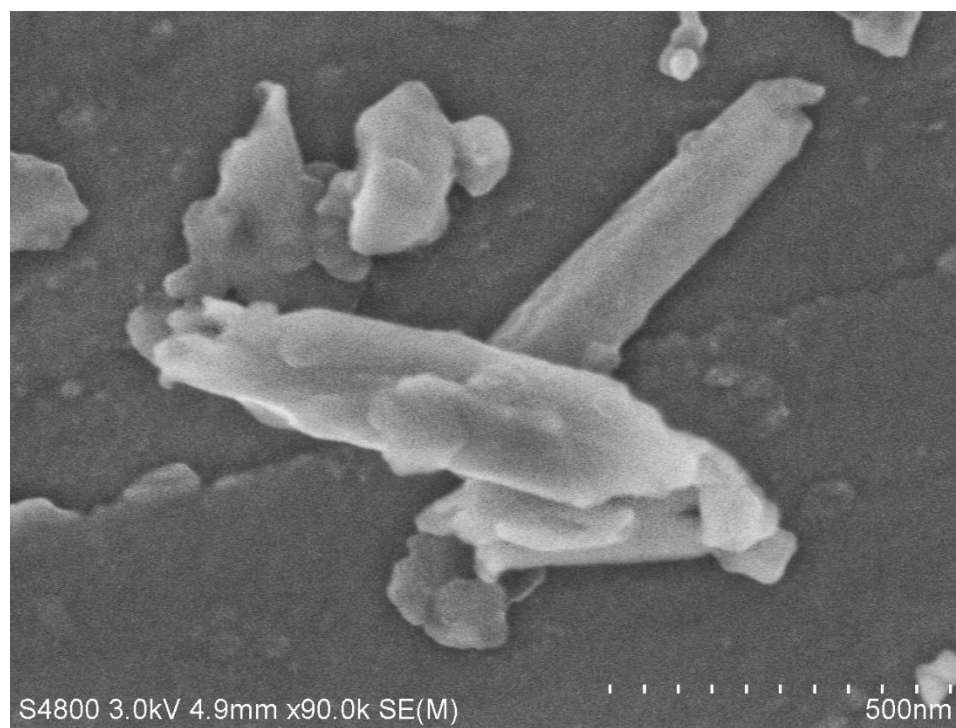
Figure 6-8. *Halloysite Nanotubes Functionalized with TSB and RNA*
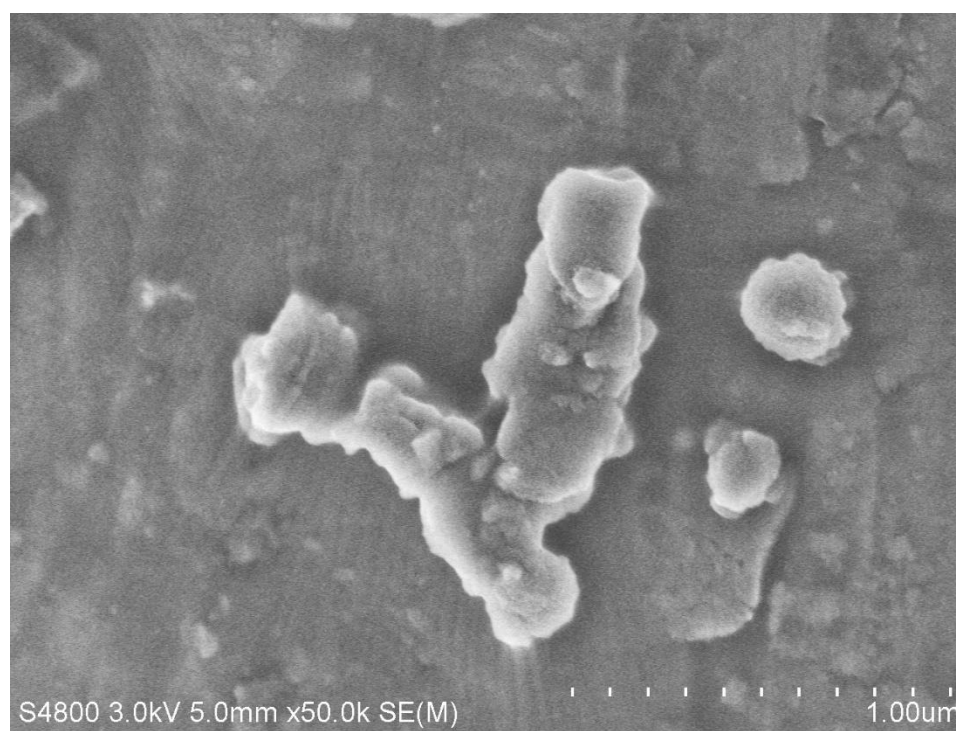
Figure 6-9. *Halloyite Nanotubes Functionalized with TSB and DNA*

6.4.2   **DLS**

The samples were prepared for DLS measurement by dilution in pH 7.0 phosphate buffer solution and sonicating for one minute to separate particles. A comparison of particle sizes after functionalization can be seen in Figures 6-10 and 6-11. The SiNP and HNT core particles showed in increase in size along with functionalization with nucleic acids. This may be from loss of smaller particles during the washing steps of the functionalization protocol or from the dilution steps of the DLS protocol. No changes in size were expected from the addition of the organic material to the surface of the particles.
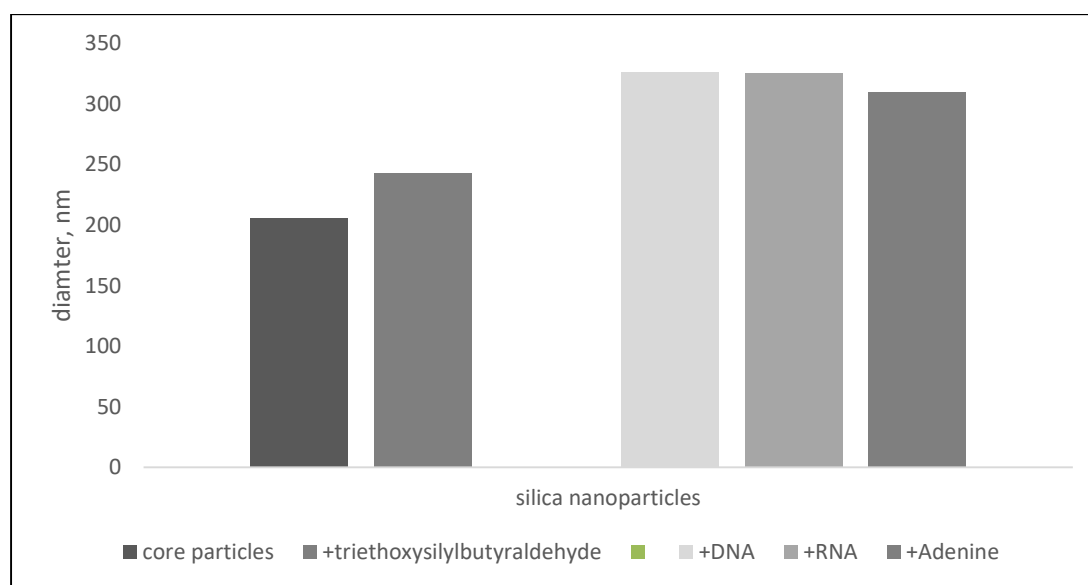
Figure 6-10. *DLS Data Showing a Comparison of Sizes of Sinp Core Particles at Stages of Synthesis*
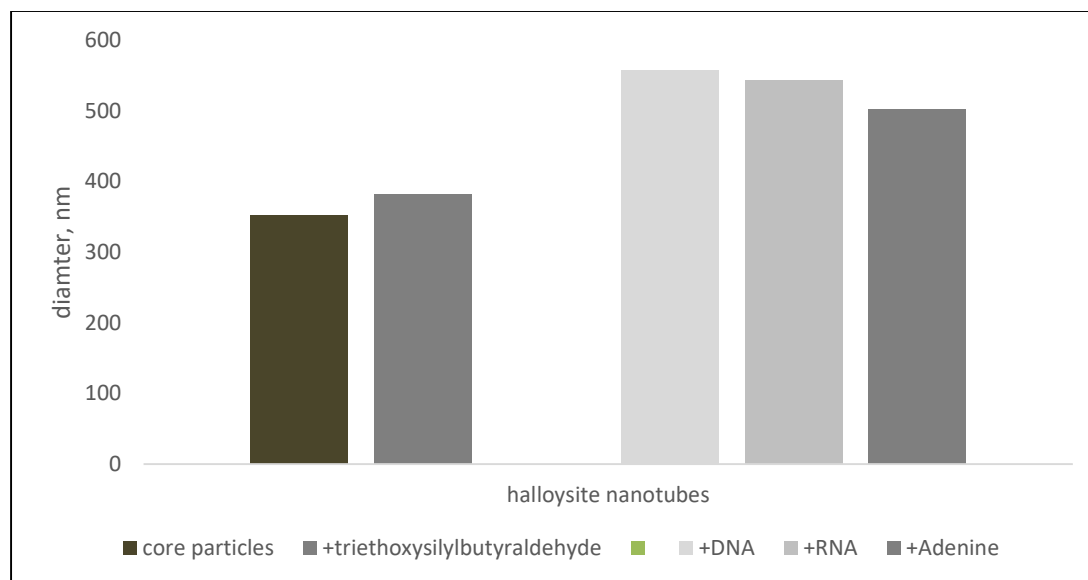
Figure 6-11. *DLS Data Showing a Comparison of Sizes of HNT Core Particles After Synthesis*

6.4.3 FTIR

The spectra in Figure 6-12 shows the OSNR in the stages of reaction in comparison to the reagents after reaction with adenine.
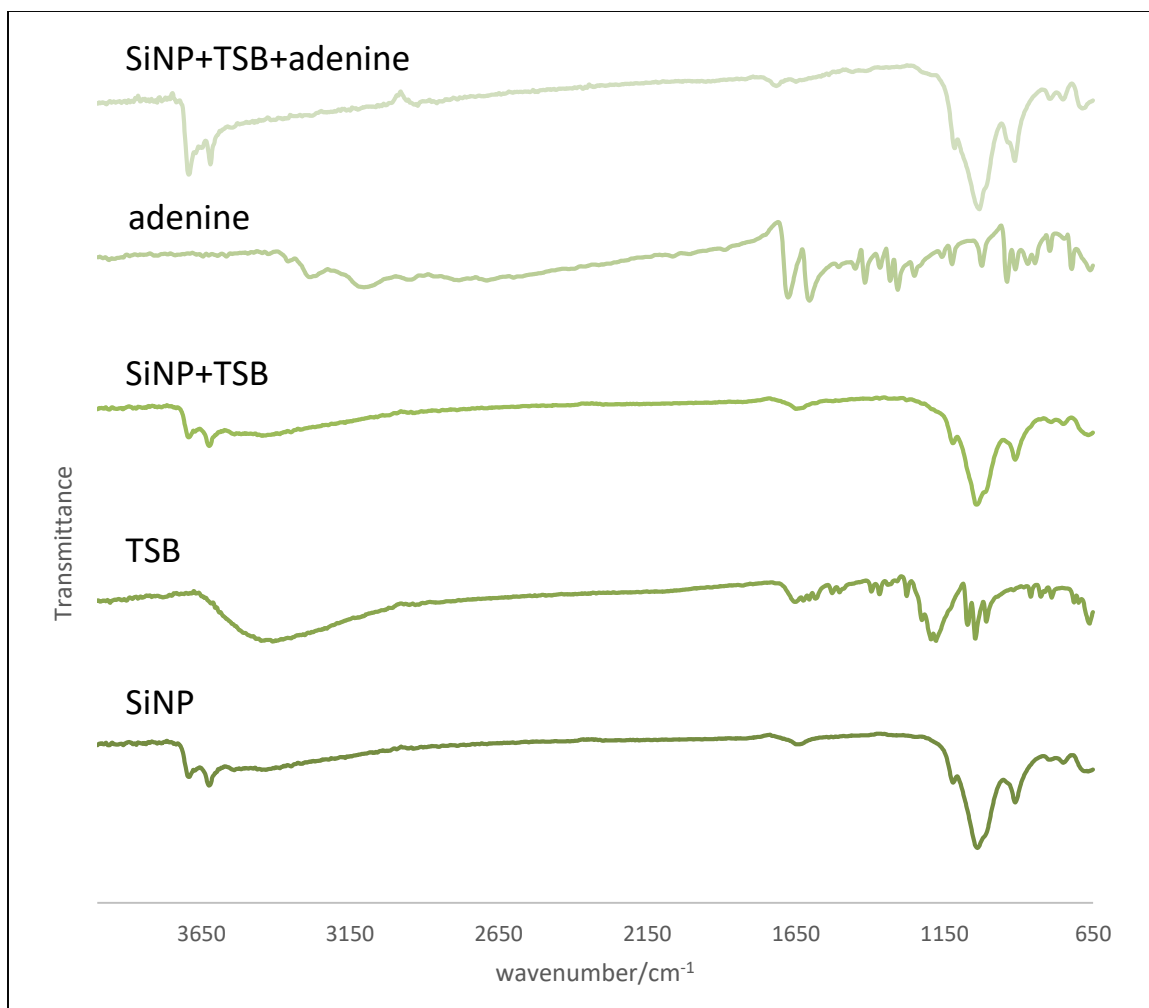
Figure 6-12. *A Comparison of FTIR Spectra of Subsequent Modification Layers to SiNP Cores with TSB and Adenine*

The spectrum in Figure 6-13 shows SiNPs after reaction with adenine. Peaks are found at 1619, 1463 and 1401 cm^{-1}, which may be from the C=C of alkenes found in adenine. The peak at 1714 cm^{-1} may be from the imine bond formed from the amine aldehyde reaction.
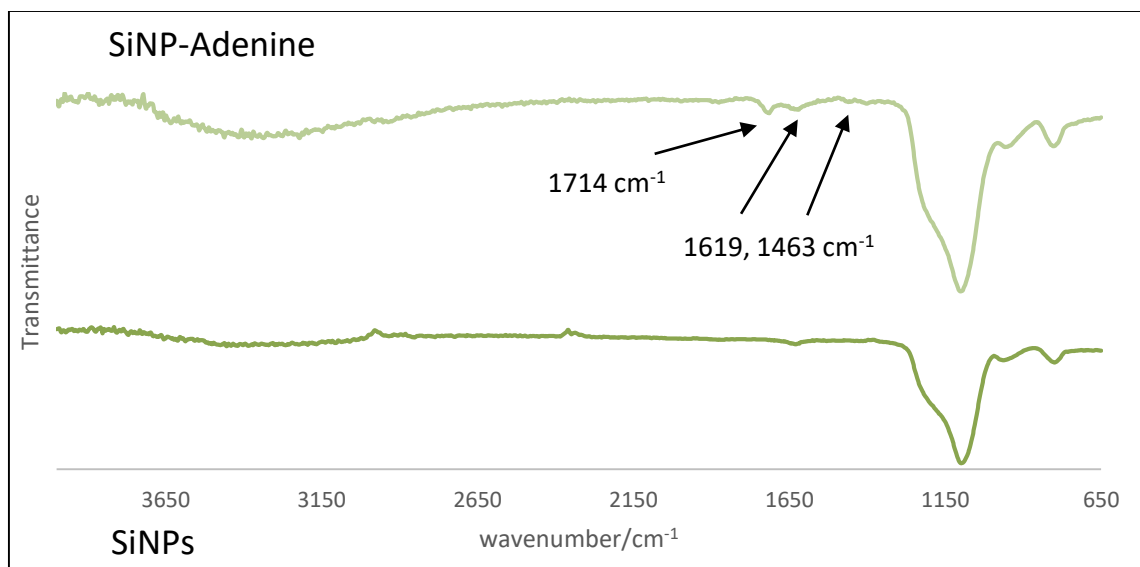
Figure 6-13. *A Comparison of FTIR Spectra of Subsequent Modification Layers to SiNP Cores with TSB and Adenine*

The spectra in Figure 6-14 shows a comparison of the FTIR of SiNPs with TSB and RNA in the stages of reaction in comparison to the reagents.
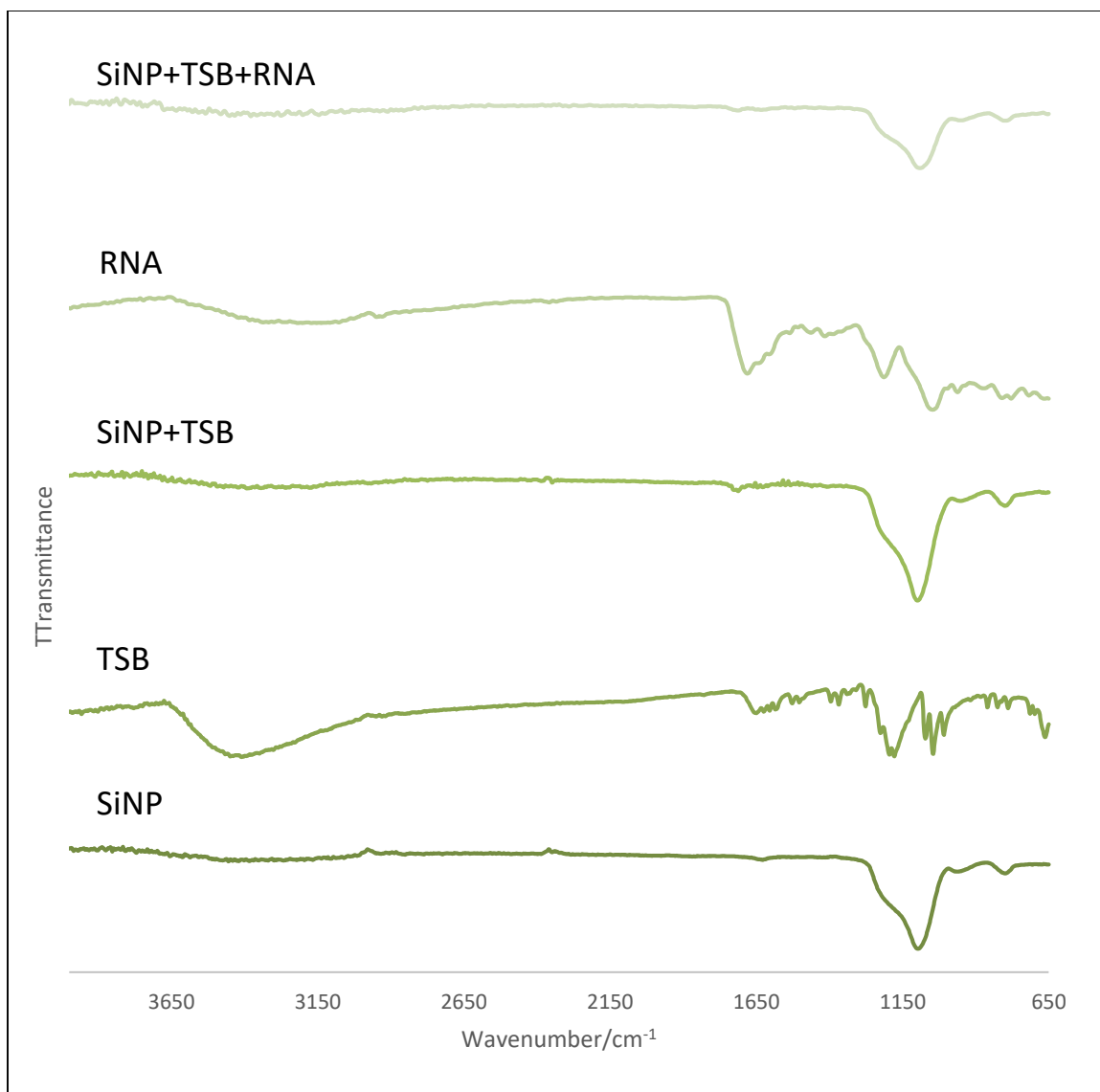
Figure 6-14. *A Comparison of FTIR Spectra of Subsequent Modification Layers to SiNP Cores with TSB and RNA*

The spectrum in Figure 6-15 shows SiNP-TSB NPs after reaction with RNA. A peak found at 1652 cm^{-1}, which may be from the C=C of the alkene found in RNA. The peak found at 1710 cm^{-1} may be from the imine bond formed from the amine aldehyde reaction.
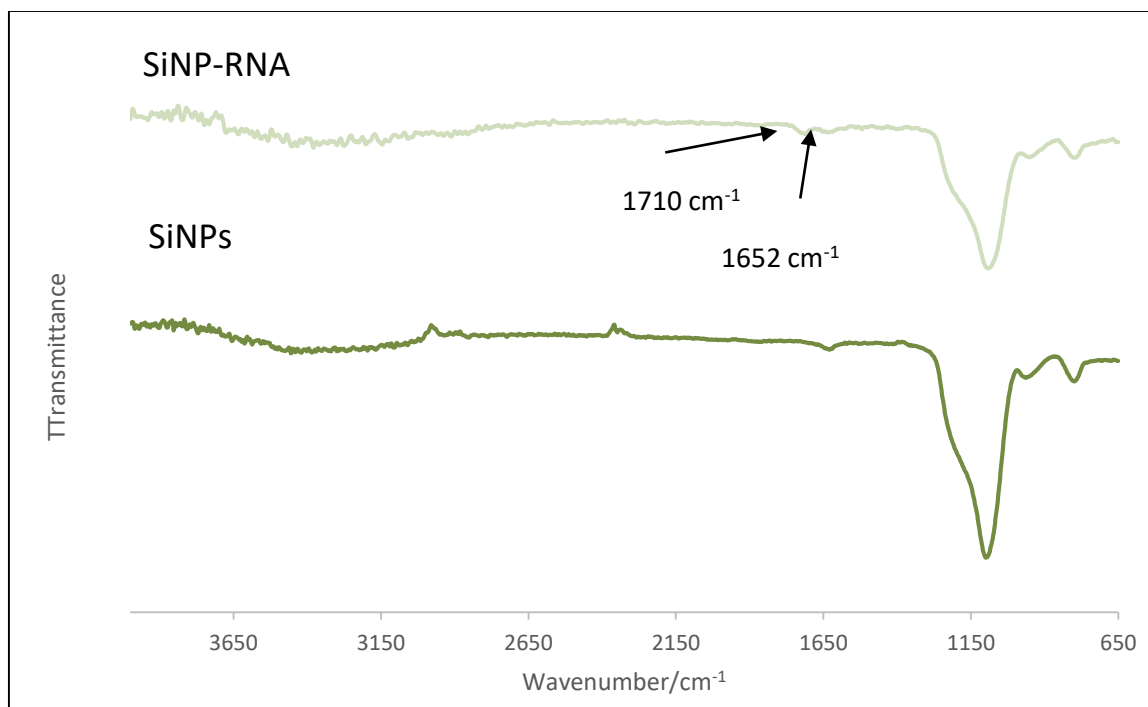
Figure 6-15. *A Comparison of FTIR Spectra of SiNPs After Modification with TSB and RNA*

As seen in Figure 6-16 the FTIR spectra shown were recorded for each stage of the synthesis of the DNA labeled particles. The first two spectra are for the reagents, silica NPs and TSB. The third spectrum is of silica NPs after reaction with TSB to provide aldehyde functional groups.
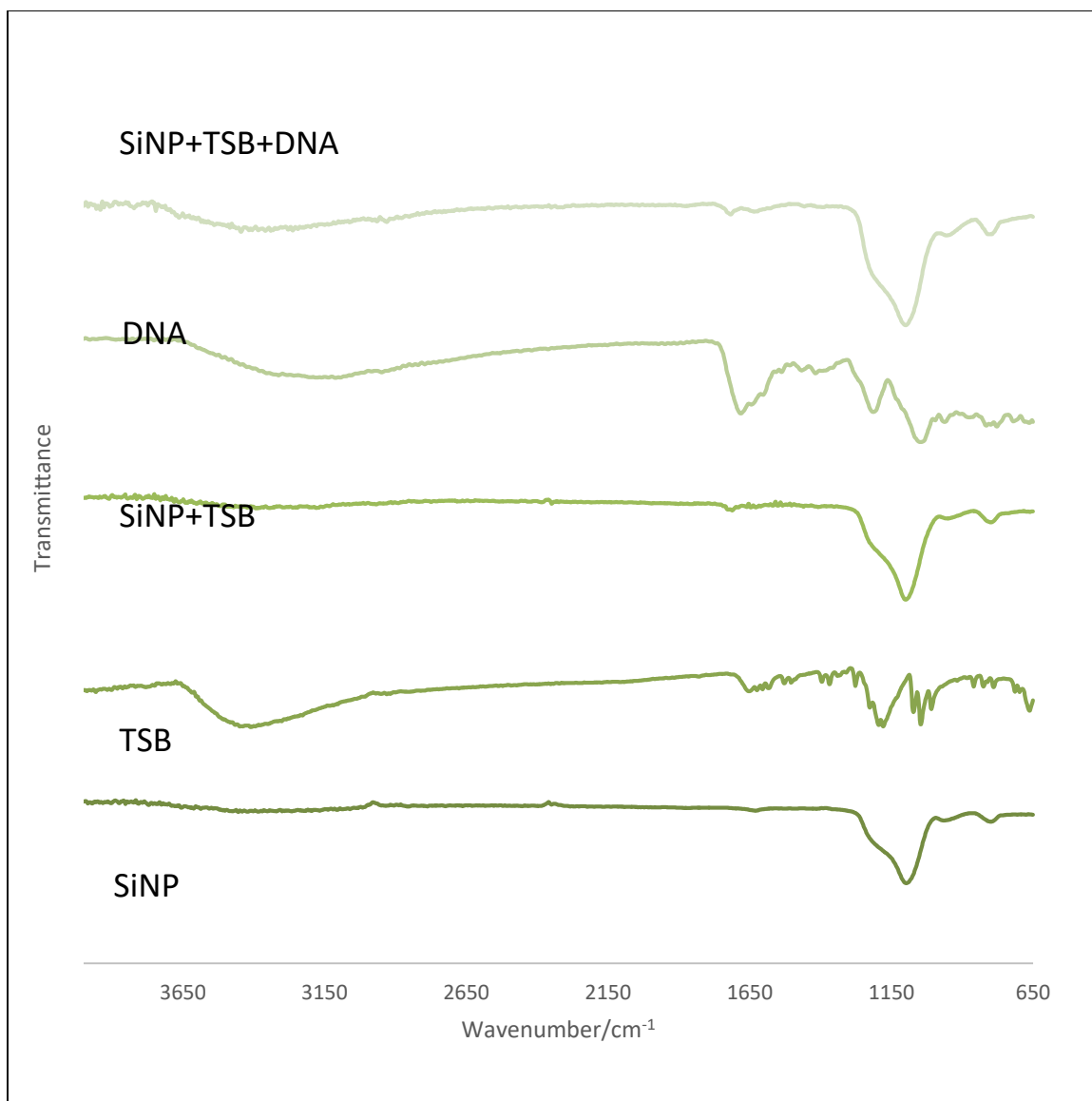
Figure 6-16. *A Comparison of FTIR Spectra of Subsequent Modification Layers to SiNPs with TSB and DNA*

The spectra shown in Figure 6-17 is of SiNPs after reaction with TSB then DNA. The peak found at 1621 cm^{-1} may be from the C=C of alkenes found in RNA. The peak found at 1714 cm^{-1} may be from the imine bond.
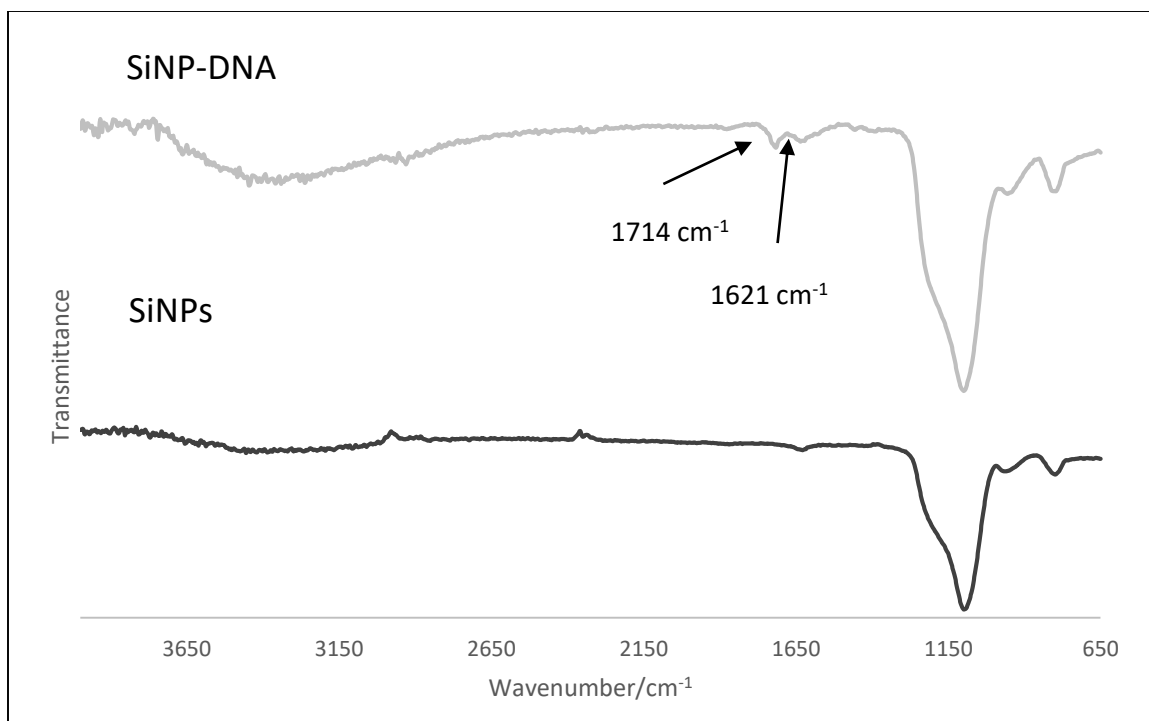
Figure 6-17. *A Comparison of FTIR Spectra of Si-TSB-DNA Particles to SiNPs*

The graph in Figure 6-18 shows the FTIR spectra recorded for each stage of the synthesis of the nucleotide labeled particles with adenine. The first two spectra are for the reagents, HNTs and TSB. The third spectrum is of HNTS after reaction with TSB to provide aldehyde functional groups.
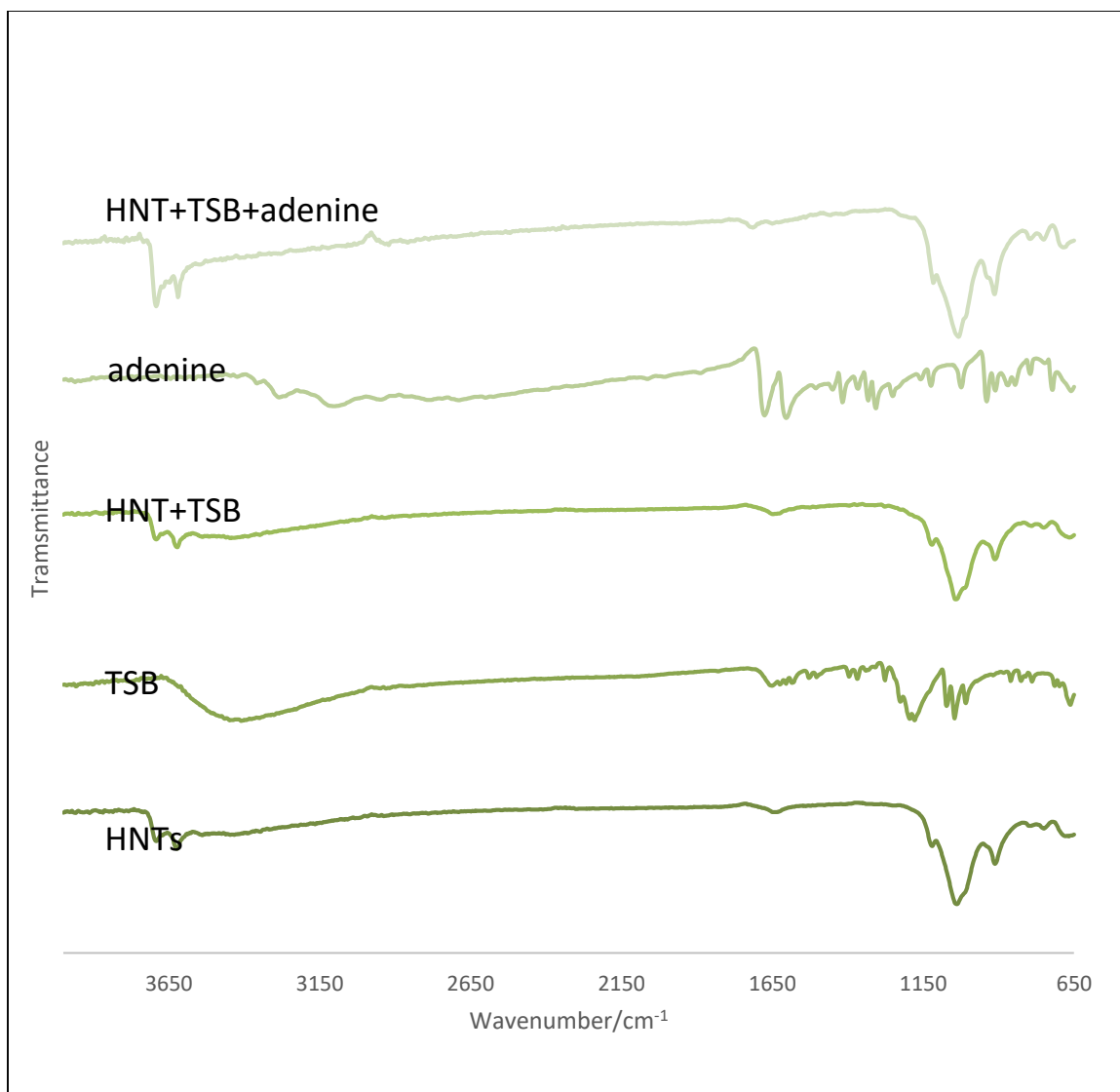
Figure 6-18. *A Comparison of FTIR Spectra of Subsequent Modification Layers to HNT Cores with TSB and Adenine*

The spectra shown in Figure 6-19 is of HNTs after reaction with TSB then adenine. The peak found at 1652 cm^{-1} may be from the C=C of alkenes found in adenine. The peak found at 1710 cm^{-1} may be from the imine bond.
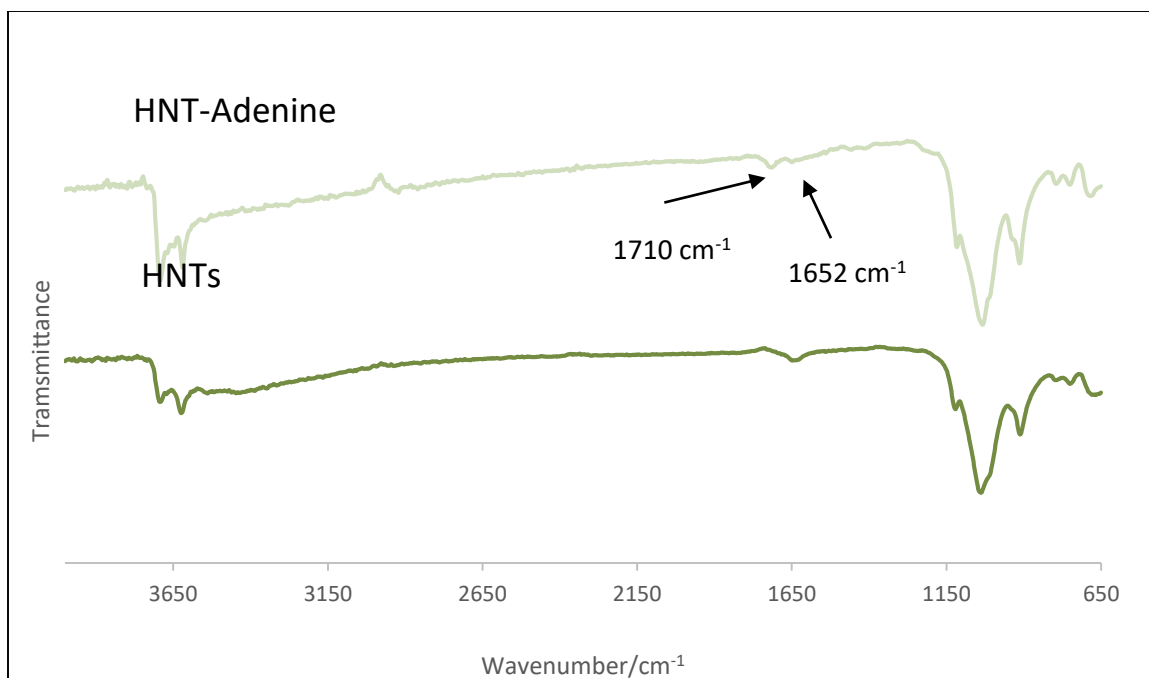
Figure 6-19. *A Comparison of FTIR Spectra of HNT-TSB-Adenine Particles to HNTs*

The graph in Figure 6-20 shows the FTIR spectra recorded for each stage of the synthesis of the nucleotide labeled particles with RNA. The first two spectra are for the reagents, SiNPs and TSB. The third spectra is of SiNPs after reaction with TSB to provide aldehyde functional groups.
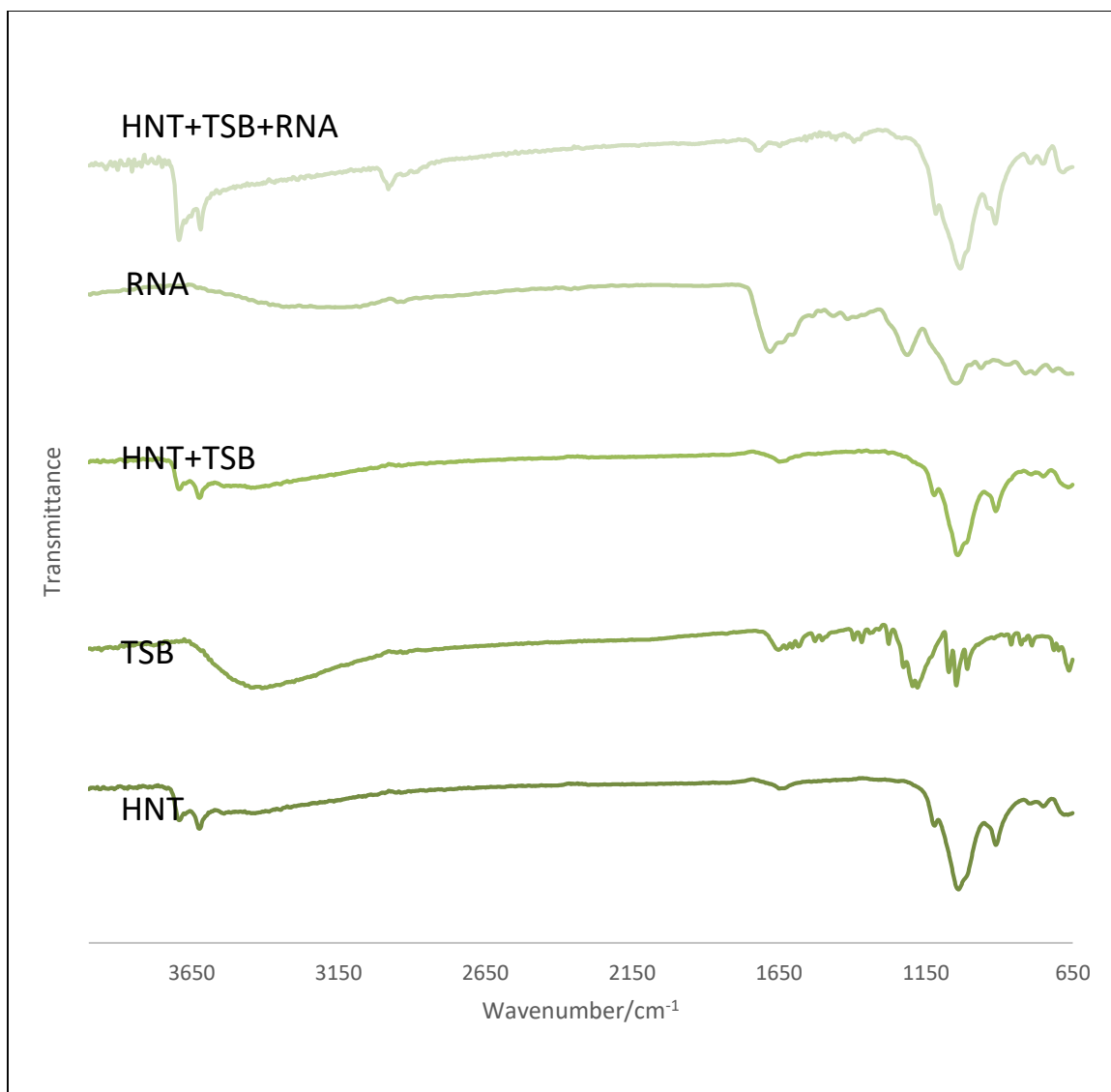
Figure 6-20. *A Comparison of FTIR Spectra of Subsequent Modification Layers to Silica NP Cores with TSB and RNA*

The spectrum shown in Figure 6-21 is of HNT-TSB NPs after reaction with RNA. A peak at 1716 cm^{-1} may be from the imine bond. Peaks found at 1455 and 1394 cm^{-1} may be from C=C stretching from RNA.
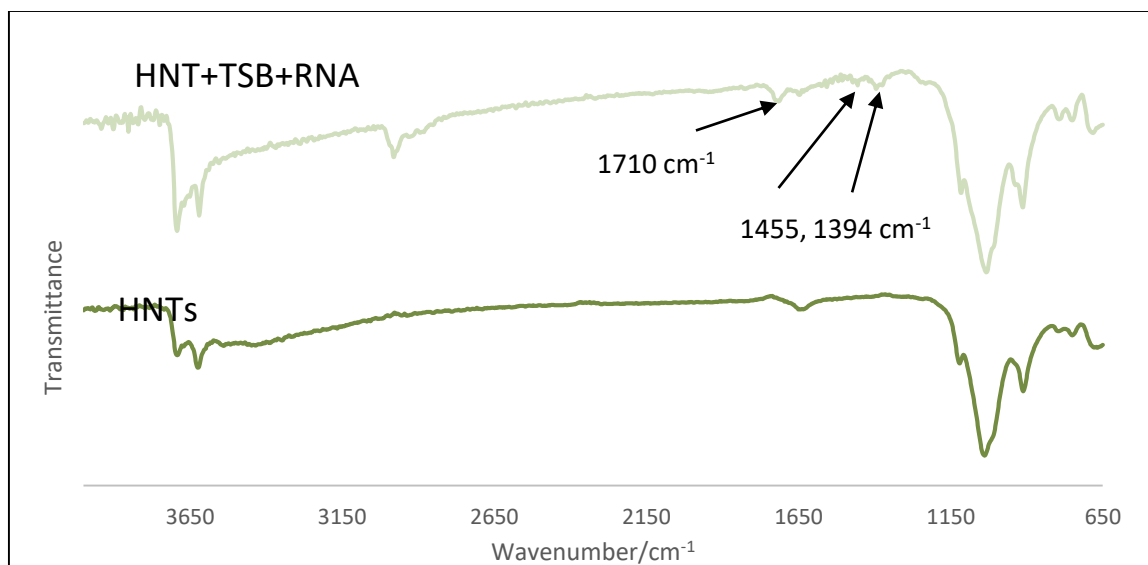
Figure 6-21. *A Comparison of FTIR Spectra of SiNPs to SiNPs Labeled with TSB+RNA*

The graph in Figure 6-22 shows the FTIR spectra recorded for each stage of the synthesis of the nucleotide labeled particles with DNA. The first two spectra are for the reagents, SiNPS and TSB. The third spectrum is of SiNPS after reaction with TSB to provide aldehyde functional groups.
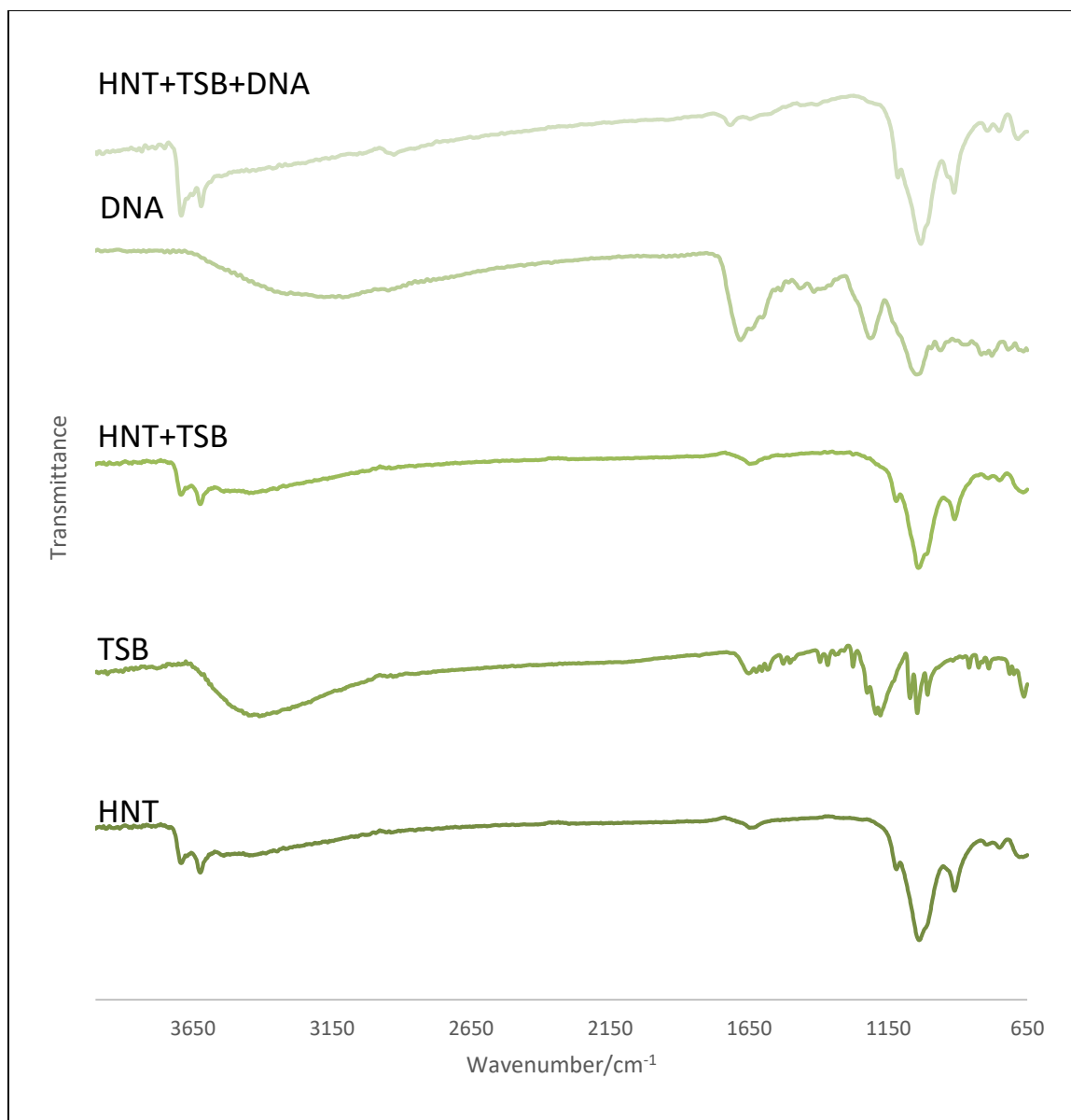
Figure 6-22. *A Comparison of FTIR Spectra of Subsequent Modification Layers to HNT Cores with TSB and DNA*

The spectrum shown in Figure 6-23 is of HNTs after reaction with TSB and DNA. Peaks found at 1448 and 1403 cm^{-1} may be from a C-H stretch of an alkene found in RNA. A peak at 1714 cm^{-1} may be from the imine bond.
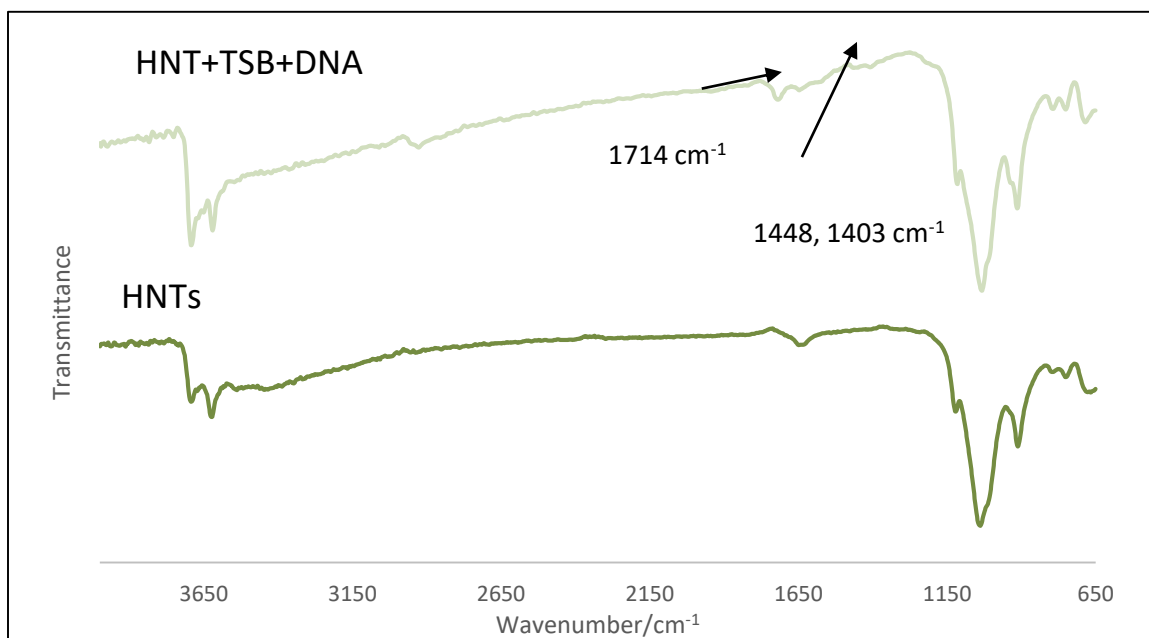
Figure 6-23. *A Comparison of FTIR Spectra of HNT-TSB-DNA Particles with HNTs*

6.4.4 Thermogravimetric Analysis

Thermogravimetric analysis (TGA) is an analytical method where the mass of the sample is measured over time with change in temperature. TGA can provide information about absorption, desorption and thermal degradation. It was used to analyze the nucleic acid loaded nanoparticles to verify that the nucleotides had been successfully bound to the particle surfaces. The changes in the curves of functionalized particles with the bare core and the reagents show a modification as successive layers are added to the nanoparticles.

The data for SiNPs is shown in comparison to particles functionalized with TSB and with the nucleic acid (DNA, RNA or adenine) reagent and the NA-functionalized particle. Figure 6-26 shows a graph of percent loss of mass for the SiNP cores.

Analysis of the TGA thermal degradation curves show that the SiNP core particles all exhibit a percent loss of mass. Data is shown in Figure 6-25 and Table 2-1 for SiNP-Adenine, Figure 6-26 and Table 6-1 for SiNP-RNA and Figure 6-27 and Table 6-2 for SiNP-DNA. The percent mass loss for SiNPs is 9.3%. This is likely largely due to loss of adsorbed water and a smaller amount of thermal loss of silica (SiO_2). DNA, RNA and adenine reagents show percent mass losses of 74.4, 73.6 and 98.2% respectively. This is probably due to thermal degradation of the organic reagents. The nucleic acid labeled particles show a percent loss of 18.0, 17.0 and 16.8% for SiNP-DNA, SiNP-RNA and SiNP-Adenine loaded particles. The difference between the loss of mass of the SiNPs and organically modified particles is 8.7, 7.7 and 7.5% for DNA, RNA and adenine loaded particles. The mass loss due to thermal degradation of organic matter on the SiNP cores would be 0.766, 0.369 and 0.440 mg for the DNA, RNA and adenine loaded particles. The graph in Figure 6-24 shows that the percent mass loss pattern of the nucleic acid labeled particles more closely resembles that of the silica NP core. This data supports the implication that the nucleic acids are a smaller percentage of total mass and form a thin coating.
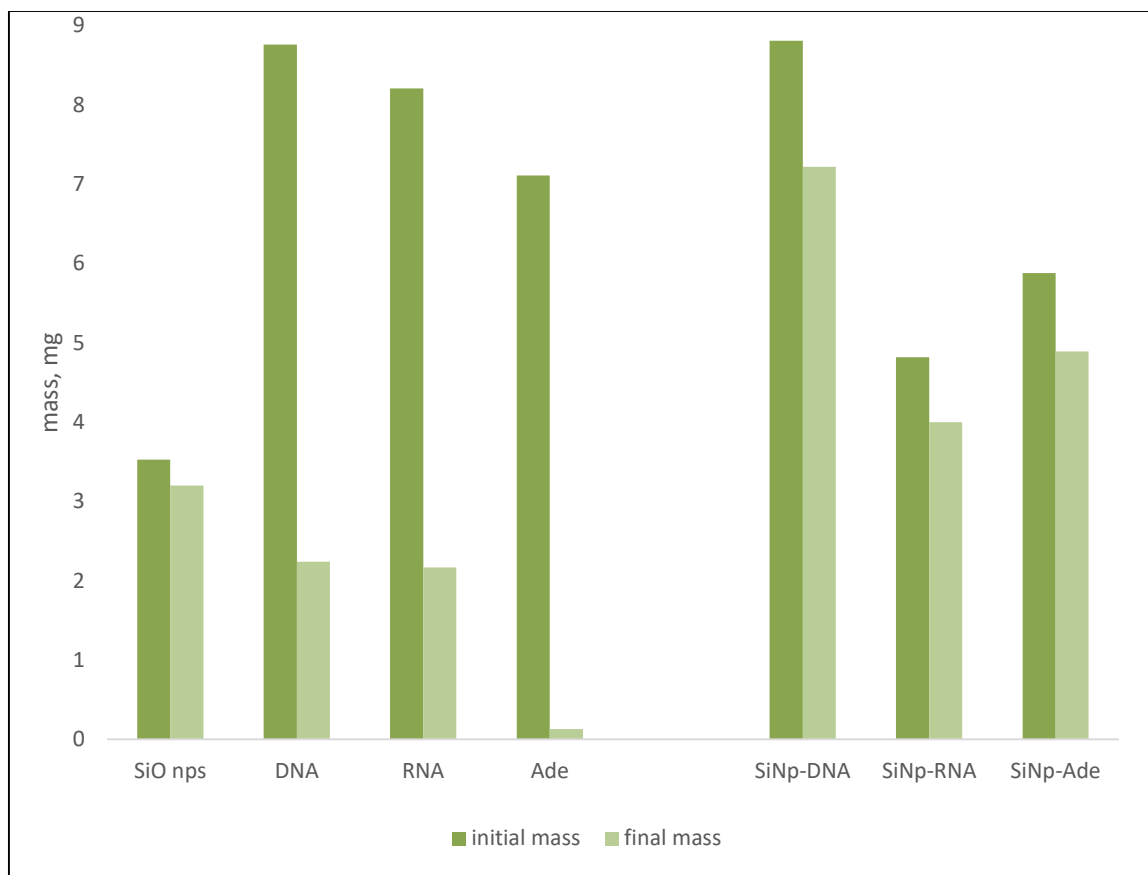
Figure 6-24. *A Graph of the Percent Loss of Mass of SiNP-TSB-Nucleic Acid Particles After TGA Analysis*
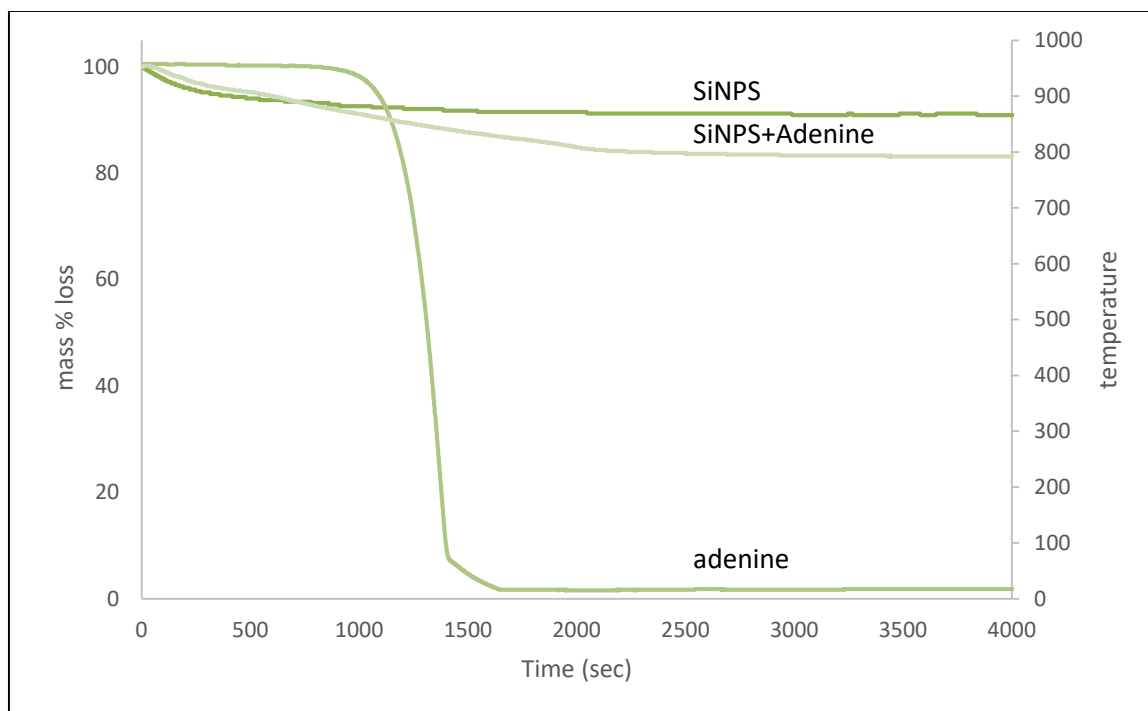
Figure 6-25. *A Comparison of TGA Data Showing Percent Mass Loss for SiNPs to Adenine and Adenine Loaded Particles*

Table 6-1. *TGA Data Showing Percent Loss of Mass of SiNPs, Adenine and Adenine Loaded SiNPs*

	initial mass	final mass	mass loss	% lost	% organic mass	organic mass lost (mg)
SiO nps	3.53	3.20	0.33	9.3%		
Adenine	7.11	0.13	6.98	98.2%		
SiNp-Ade	5.88	4.89	0.99	16.8%	7.5%	0.440
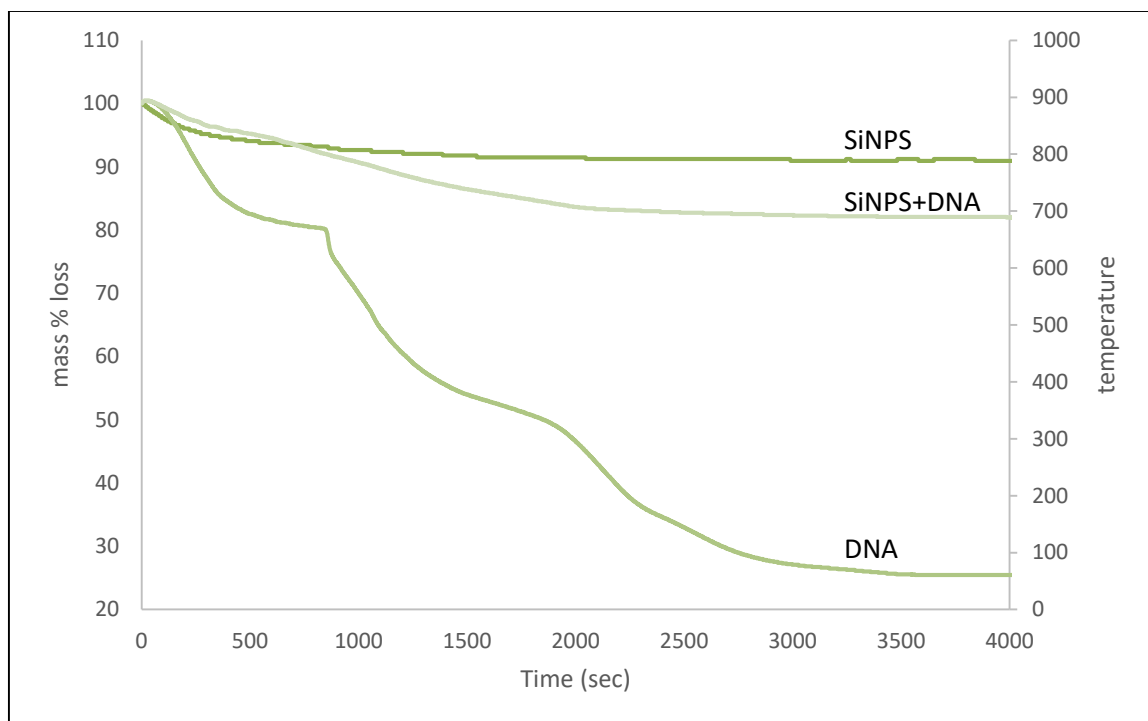
Figure 6-26. *A Comparison of TGA Data Showing Percent Mass Loss for SiNPs to DNA and DNA Loaded SiNPs*

Table 6-2. *TGA Data Showing Percent Loss of Mass of SiNPs, DNA and DNA Loaded SiNPs*

	initial mass	final mass	mass loss	% lost	% organic mass	organic mass lost (mg)
SiO nps	3.53	3.20	0.33	9.3%		
DNA	8.76	2.24	6.52	74.4%		
SiNp-DNA	8.81	7.22	1.59	18.0%	8.7%	0.766
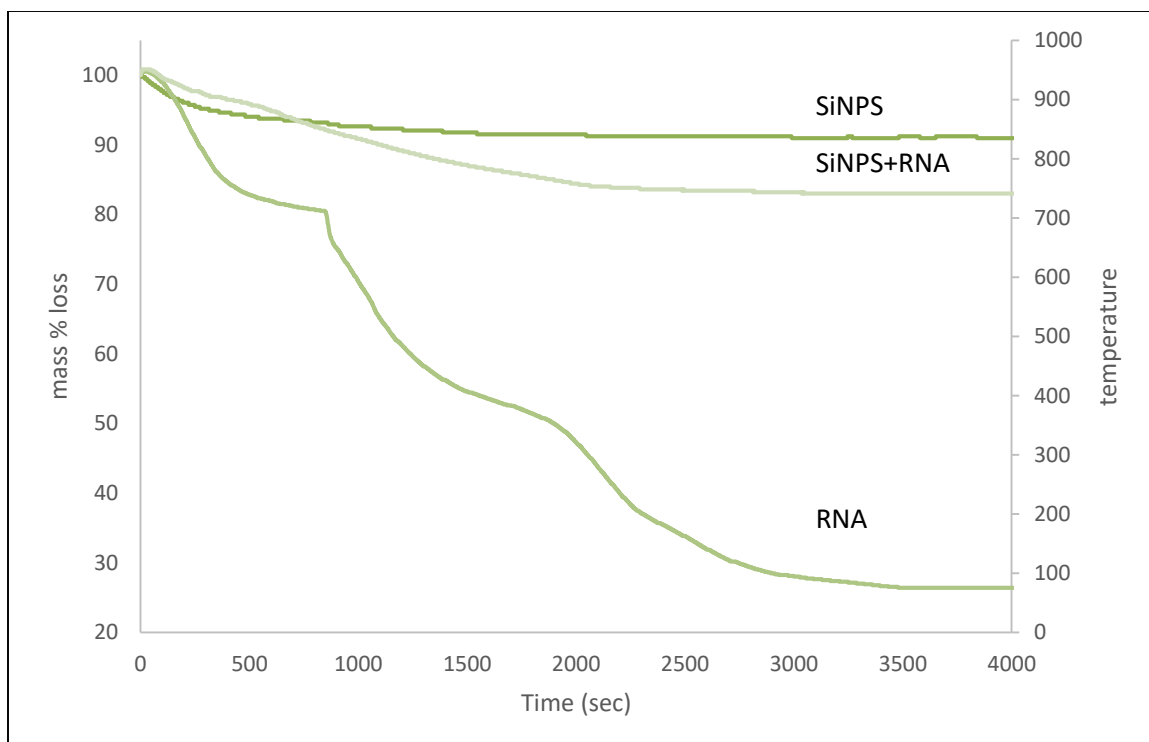
Figure 6-27. *A Comparison of TGA Data Showing Percent Mass Loss for SiNPs to RNA and RNA Loaded SiNPs*

Table 6-3. *TGA Data Showing Percent Loss of Mass of SiNPs, RNA and RNA Loaded SiNPs*

	initial mass	final mass	mass loss	% lost	% organic mass	organic mass lost (mg)
SiO nps	3.53	3.20	0.33	9.3%		
RNA	8.21	2.17	6.04	73.6%		
SiNp-RNA	4.82	4	0.82	17.0%	7.7%	0.369

Analysis of the TGA thermal degradation curves show that the HNTs have a percent mass loss of 19.4%. This is likely due to loss of adsorbed water. DNA, RNA and adenine show percent losses of 74.4, 73.6 and 98.2% respectively. This is probably due to thermal degradation of the organic reagents. The nucleic acid labeled particles all show a percent loss of mass. The DNA loaded HNTs lost 21.1, 21.4 and 20.1% for HNT-DNA,

HNT-RNA and HNT-Ade labeled particles. Data is shown in Figure 6-28 and Table 6-3 for HNT-Adenine, Figure 6-29 and Table 6-4 for HNT-RNA and Figure 6-30 and Table 6-5 for HNT-DNA The graph in Figure 6-27 shows that the percent loss pattern of the nucleic acid labeled particles more closely resembles that of the halloysite core, supporting the implication that the nucleic acids are a smaller percentage of total mass and form a thin coating. This data supports the description of nucleic acid labeled particles.

The data for HNTs is shown in comparison to particles functionalized with TSB and with the nucleic acid (DNA, RNA or adenine) reagent and the NA-functionalized particle. Figure 6-28 shows a graph of percent loss of mass for the HNT cores.

Analysis of the TGA thermal degradation curves show that the HNT core particles all exhibit a percent loss of mass. Data is shown in Figure 6-29 and Table 6-3 for HNT-Adenine, Figure 6-30 and Table 6-4 for HNT-RNA and Figure 6-31 and Table 6-5 for HNT-DNA. The percent mass loss for HNTs is 19.4%. This is likely largely due to loss of adsorbed water. DNA, RNA and adenine reagents show percent mass losses of 74.4, 73.6 and 98.2% respectively. This is probably due to thermal degradation of the organic reagents. The nucleic acid labeled particles show a percent loss of 21.1, 21.4 and 20.1% for HNT-DNA, HNT-RNA and HNT-Adenine loaded particles. The difference between the loss of mass of the SiNPs and organically modified particles is 1.7, 2.1 and 0.7% for DNA, RNA and adenine loaded particles. The mass loss due to thermal degradation of organic matter on the HNT cores would be 0.120, 0.148 and 0.047 mg for the DNA, RNA and adenine loaded particles. The graph in Figure 6-25 shows that the percent mass loss pattern of the nucleic acid labeled particles more closely resembles that of the silica

NP core. This data supports the implication that the nucleic acids are a smaller percentage of total mass and form a thin coating.

A comparison of the loss of organic mass from the SiNP and HNT core particles shows a greater loss from the SiNPs, an average of 7.97%. The HNTs show an average loss of organic matter of 1.5%. The organic matter is from the TSB and nucleic acids. The implication of the data is that the SiNP core particles contain more organic matter and are capable of binding a greater amount of nucleic acids.
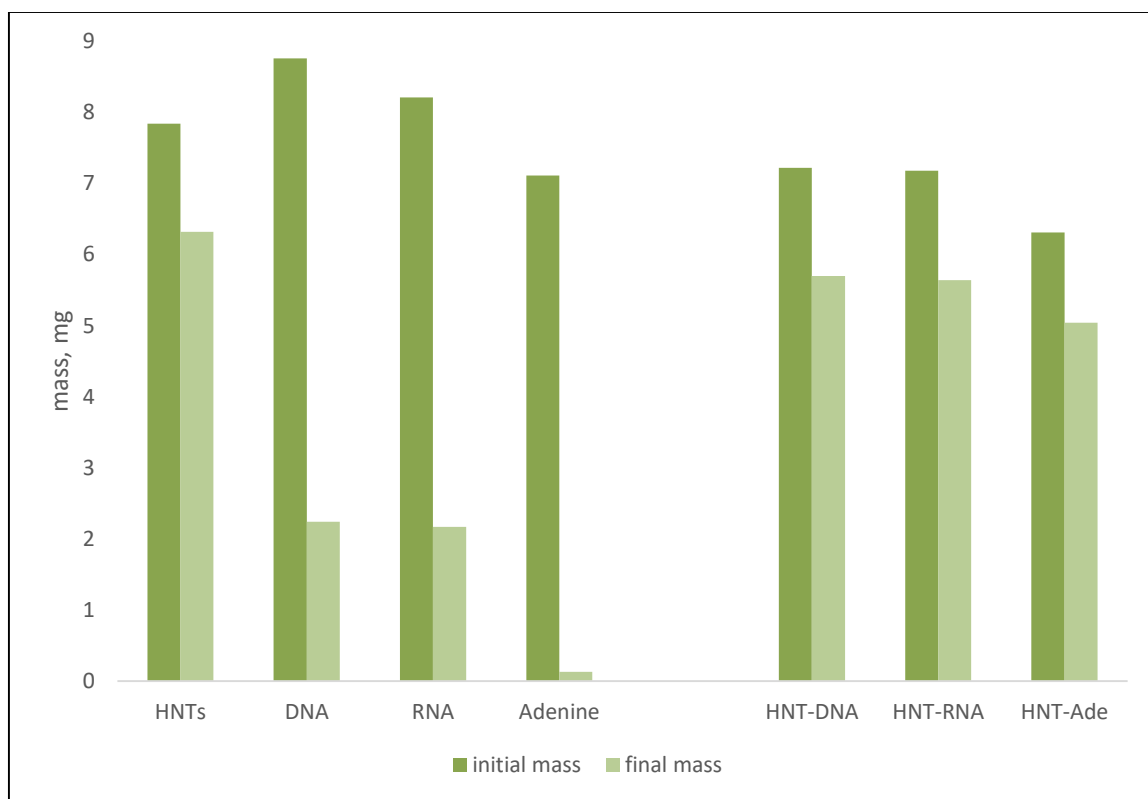
Figure 6-28. *A Graph of the Percent Loss of Mass of HNT-TSB-Nucleic Acid Particles*
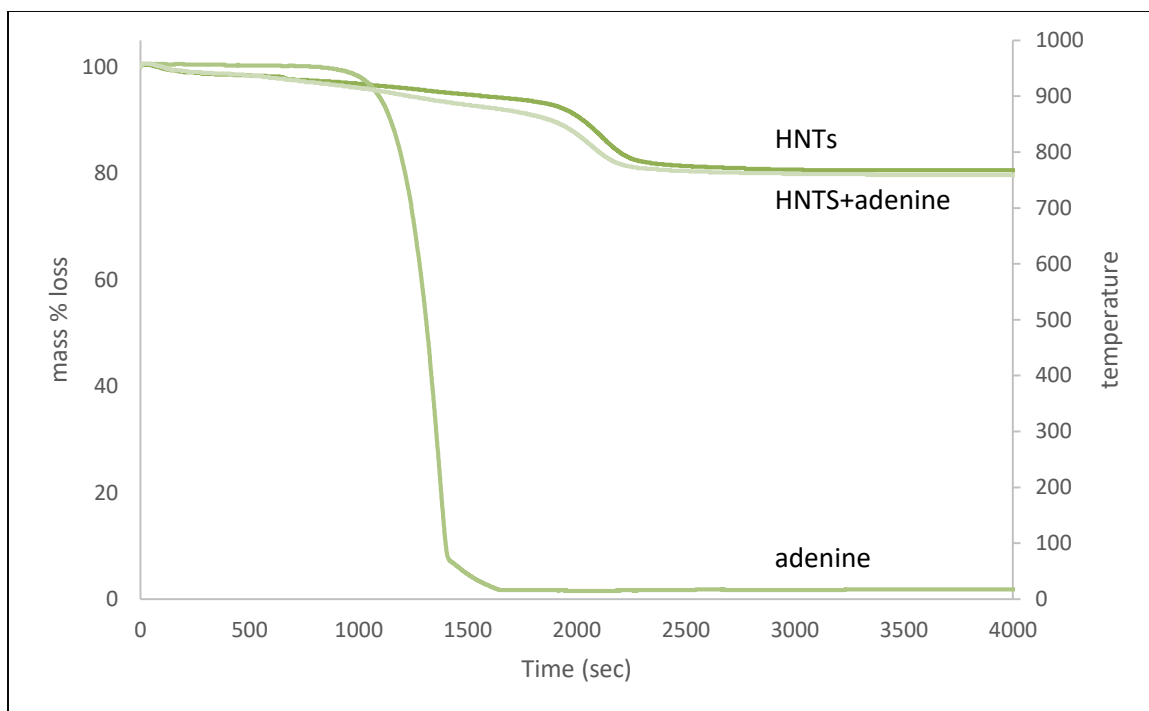
Figure 6-29. *A Comparison of TGA Data Showing Percent Mass Loss for HNTs to Adenine and Adenine Loaded HNTs*

Table 6-4. *TGA Data Showing Percent Loss of Mass of HNTs, Adenine and Adenine Loaded HNTs*

	initial mass	final mass	mass loss	% lost	% organic mass	organic mass lost (mg)
HNTs	7.84	6.32	1.52	19.4%		
Adenine	7.11	0.13	6.98	98.2%		
HNT-Ade	6.31	5.04	1.27	20.1%	0.7%	0.047
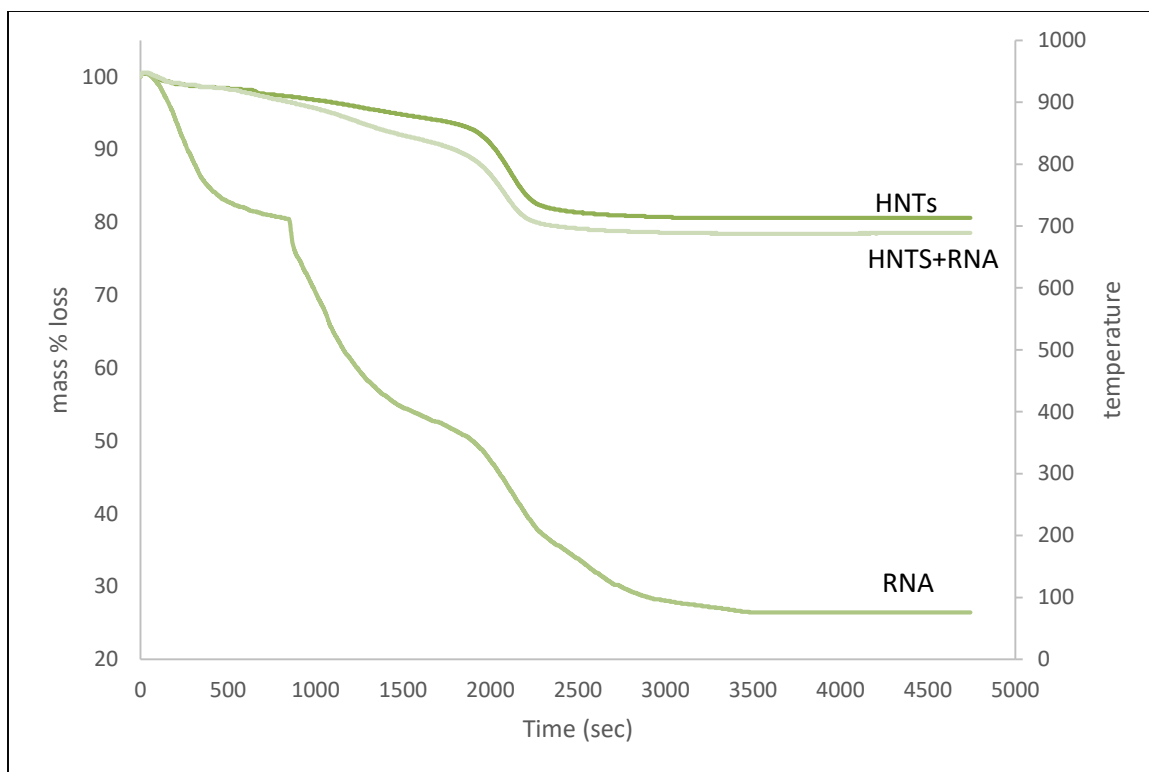
Figure 6-30. *A Comparison of TGA Data Showing Percent Mass Loss for HNTs to RNA and RNA loaded HNTs*

Table 6-5. *TGA Data Showing Percent Loss of Mass of HNTs, RNA and RNA Loaded HNTs*

	initial mass	final mass	mass loss	% lost	% organic mass	organic mass lost (mg)
HNTs	7.84	6.32	1.52	19.4%		
RNA	8.21	2.17	6.04	73.6%		
HNT-RNA	7.18	5.64	1.54	21.4%	2.1%	0.148
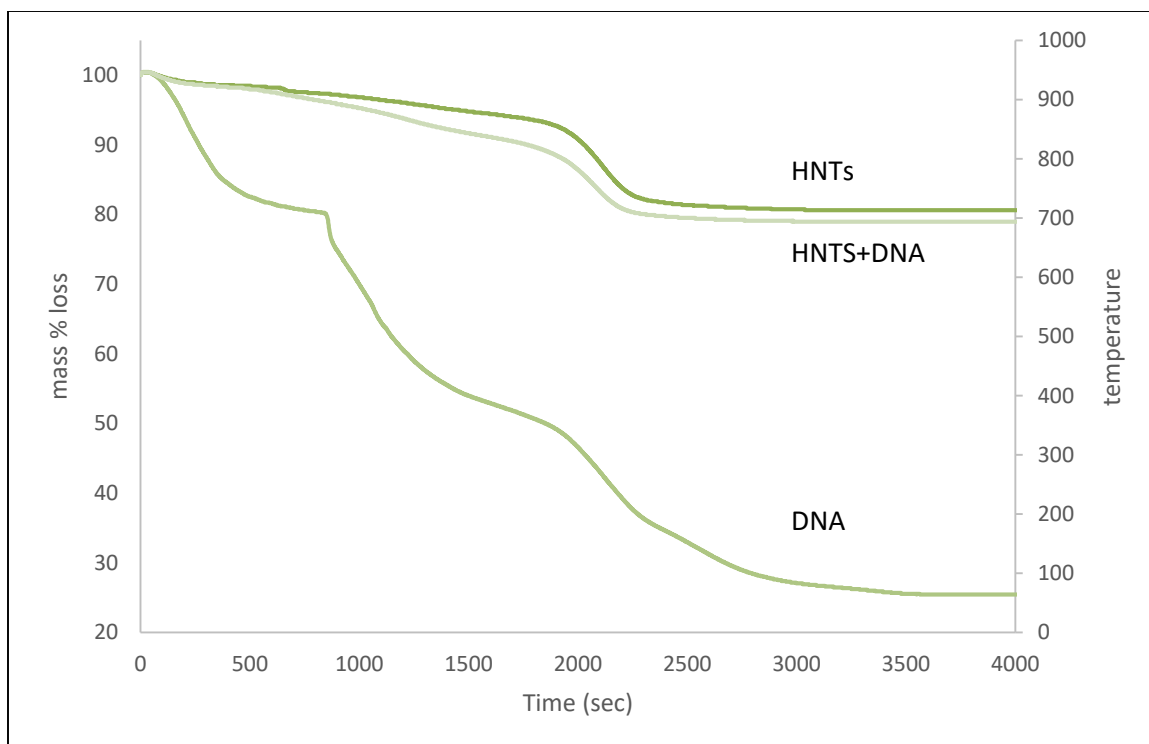
Figure 6-31. *A Comparison of TGA Data Showing Percent Mass Loss for HNTs to DNA and DNA Loaded HNTs*

Table 6-6. *TGA Data Showing Percent Loss of Mass for HNTs, DNA and DNA Loaded HNTs*

	initial mass	final mass	mass loss	% lost	% organic mass	organic mass lost (mg)
HNTs	7.84	6.32	1.52	19.4%		
DNA	8.76	2.24	6.52	74.4%		
HNT-DNA	7.22	5.70	1.52	21.1%	1.7%	0.120

CHAPTER 7

CONCLUSIONS

7.1   Conclusions

To summarize this study, four different types of nanoparticles were developed. The particles discussed in Chapters 3 and 4, SAGN/HAGN and STNR/HTNR, were variants that used aldehyde-amine covalent bonds to functionalize inorganic cores with the halochromic ionophore, neutral red. Covalently binding a sensor molecule to a NP substrate minimizes leaching and can prevent unwanted interaction with the study materials. Halochromic molecules are an alternative to fluorescent sensor molecules. They are less sensitive, but less prone to photobleaching and are more stable. These particles were synthesized using novel and facile protocols.

The SAGN/HAGN nps used APTES, an organosilane crosslinking agent with an amine functional group and glutaraldehyde, a dialdehyde crosslinking agent. Glutaraldehyde served as a bridge between the amine groups of APTES and NR. With a novel protocol, the STNR/HTNR nps shortened the synthesis by using TSB, an organosilane crosslinking agent with an aldehyde group. TSB provided an aldehyde group to the silica NP surfaces that was covalently bound to the NR directly.

This step eliminated the need for glutaraldehyde and produced a shorter protocol that used less reagents, but still produced stable and sensitive nps with a higher ratiometric response to changes in pH values.

The OSNR/OSNB nps described in Chapter 5 were synthesized with a protocol using an organosilane crosslinking agent, TSB, and the ionophores, NR and NB. This protocol produced organosilane-ionophore matrix based nanoparticles using a novel, facile, one-pot method. Both sensor molecules have amine groups suitable for binding to an aldehyde and similar solubilities, so the same protocol was able to be used for each. The NR and NB labeled particles were both shown to be sensitive to pH in a broad range with linear ratiometric responses.

The SiNP-NA and HNT-NA nps were synthesized with the novel reaction scheme using TSB to functionalize the silica NP surfaces. Nucleic acids are rapidly degraded inside cells or in an extracellular environment. Binding them to a NP substrate can prevent degradation and may serve as a delivery mechanism into cells or as a substrate for extra cellular activity. The basic protocol for these NPS was derived from the STNR/HTNR NPs. The aldehyde functional group was used to covalently bind nucleic acids, DNA or RNA, or the nitrogenous base, adenine, to the silica of the NP cores. This is a novel and facile protocol for functionalizing silica with nucleic acids.

The halochromic particles were shown to have a visual color change in the ranges of their pK_a's (~6.8, neutral red, ~10, Nile blue). It was shown that changes in the spectral bands of the halochromic dye functionalized NPs could be used to determine changes in pH in a wide range. Neutral red has spectral bands between 450-490 nm and 510-680 nm. At pH values <6.8, visually the NR labeled NPs exhibited a blueish red coloration. At higher more basic pH values, the NPs had an orangish yellow hue. The reflectance spectra were measured at 460 and 580 nm. These bands change in intensity with changes in pH. The intensity of the band at 460 nm decreases pH increases, showing a negative

correlation. The band 590 nm increases as pH values increase, showing a positive correlation.

The halochromic particles were found to have ratios between the bands at 460 and 580 nm. The graph of the ratio shows that the intensity increases along with an increase in pH level. In Figure 7-1, a comparison of the normalized ratio graphs for the neutral red functionalized NPs is shown. The most responsive of the particles are the halloysite based HTNR, followed by the organosilane matrix based OSNR. These particles showed a strong color change in a wide pH range. This effect was seen in Figure 4-5 for the HTNR and Figure 5-5 for the OSNR. The change in intensity for these two particles indicates a large sensitivity to changes in pH. The SiNP core particles show the least change in intensity with change in pH value. The glutaraldehyde based NPs, HAGN and SAGN, also show a smaller change in intensity. However, the slope is positive and linear, and the graph supports a positive correlation for all particles. The HTNR and OSNR may have a greater surface area and more dye moieties which enhance their sensitivity.
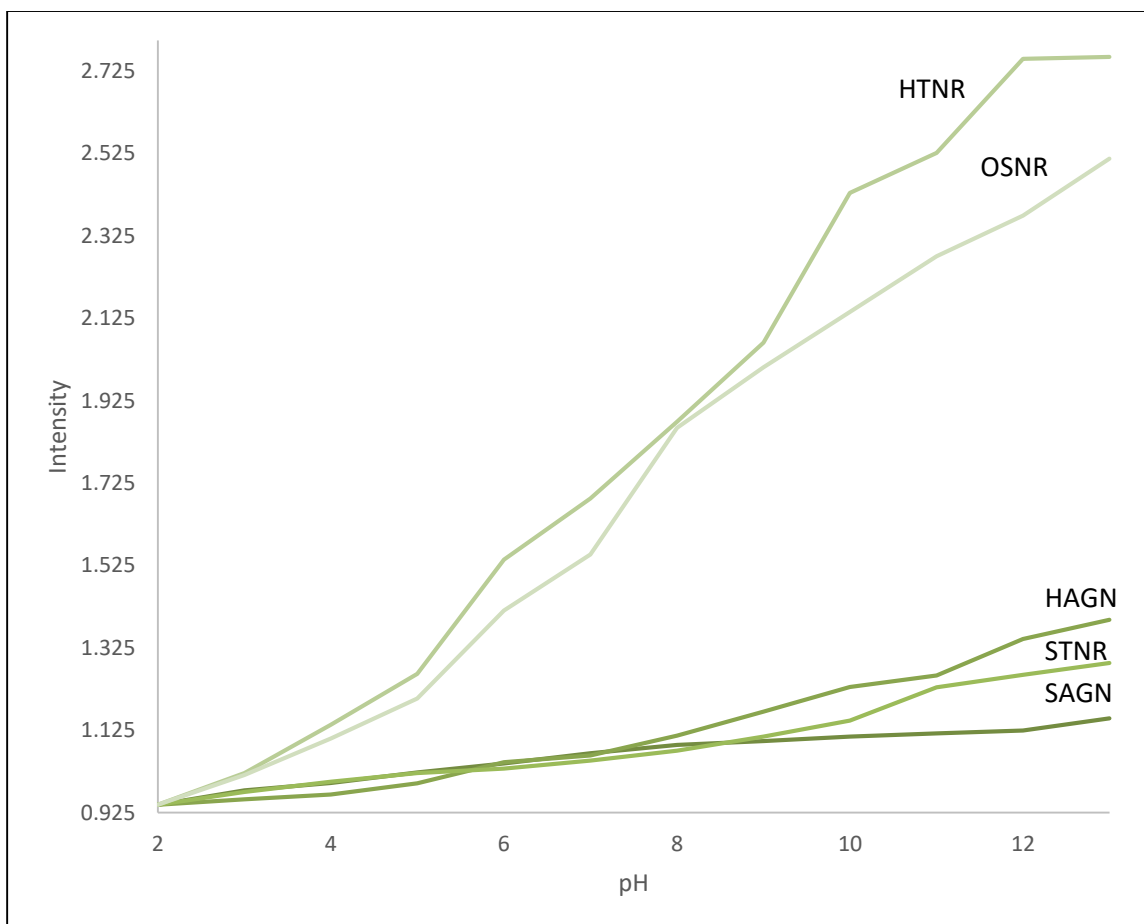
Figure 7-1. *A Comparison of the Intensity of Peak Ratios vs pH Response of the NR Functionalized NPs*

At low pH values, the blueish red protonated species of NR dominates. At high pH values the orangish red deprotonated species is more abundant. Measuring the changes in intensity of the bands at 460 and 590 nm showed a correlation with changes in pH. This method was reliable in measuring pH changes by recording the reflectance spectra. This method data expands the usefulness of the dye functionalized NPs.

The ionophores were bound to the particles using amine-aldehyde reactions that produce Schiff bases, which are reversible and less stable. The particles were treated with sodium borohydride to reduce the tertiary amine Schiff bases into secondary amines,

which are more stable. This process rendered the particles less prone to leaching and dye loss.

Another aspect that was investigated was the use of the reaction solution pH to manipulate surface charge and reduced particle aggregation. After the particles were labeled with amine functional groups ($-NH_2$), the reaction solution was decreased to a lower pH value, increasing the surface charge towards a positive value ($-NH_3^+$) so that the particles would be more likely to repel each other. Use of a dialdehyde such as glutaraldehyde could result in crosslinked particles of a large structure but charge based repulsion along with a careful stoichiometry in relation to reagent amounts, led to particles sufficiently coated with the reagent of interest and a low incidence of large particle aggregation.

7.2   Future Work

There are many possibilities for future work with these particles. The particles could possibly be incorporated into thin film polymer matrixes and investigated for responsiveness to pH. There are many issues of difficulty with use of pH sensitive films however. Other unsuccessful studies conducted have shown issues with sensitivity and reduced reaction time with proton flow through a membrane. The search for a suitable support polymer for proton sensitive materials would be a research project of its own. Another option would be to functionalize silica surfaces with the halochromic dyes. The protocols could be adapted into thin film coatings on larger substrates. Some preliminary work here did not show a heavy enough deposition of the dyes to support detection. Future work could focus on increasing surface area to increase dye loading possibly by

etching or by nanomanufacturing techniques such as sputtering or electrospinning a thin film substrate.

There are many methods to increase the surface area of NPs. These could include the use of mesoporous SiNPs or branched structures on the NP surfaces such as star or bottle brushes that could be used as supports for dye functionalization.

The organosilane coupling agents used in this study were APTES and TSB which provided an amine ($-NH_3$) or aldehyde ($-C=O$) functional groups. Other organosilanes are available that contain isocyanate ($-NCO$), thiol ($-SH$) , epoxy ($-C-O-C-$) or phosphonate ($-PO_3$) functional groups. Using these coupling agents would expand the repertoire of possible chemical reactions and increase the number of molecules that could be covalently bound to the surface or incorporated into the matrix of NPs.

Another aspect that could be investigated is the use of metals such as silver or gold as cores for silica NPs. This method has been shown to increase sensitivity of fluorescence based optical sensors by surface plasmon resonance (Amendola 2010). This would be an interesting avenue to explore. The SiNPs and HNTs loaded with silver or other metal nanoclusters could be investigated for functionalization with other halochromic dyes and studied for sensitivity, reversibility, reproducibility, and consistency.

Biological and cell studies could be investigated to determine the effect of the particles on cell cultures or tissues. Study of how the particles interact with cells could be a good area of study. The particles behavior and pH sensitivity could be studied microbiological studies. The particles could also be incorporated into thin films such as

hydrogels or in growth media such as agar and used in biological studies. This would provide information on their characteristics in a biological setting.

The fourth particles were developed using nucleic acids. The silica and aluminosilicate surfaces were functionalized with TSB, a more recently developed organosilanes crosslinking agent. TSB provided aldehyde groups suitable for attachment to nucleic acids. Nucleic acids can be used for many objectives such as substrates, enzymes or sensors. Coating nanoparticles with nucleic acids can accomplish these tasks or be investigated as a method of delivery of single-strand nucleic acids intracellularly. Living cells do not respond favorably to the presence of single strand DNA or RNA. Introduction of these into a cell presents difficulty and will result in digestion and degradation of the nucleic acid strands. Since SS-DNA or SS-RNA may be indicative of a viral infection, there is the risk of an immunological inflammation response as a tissue or cell responds to a possible viral vector. Nucleic acid labeled nanoparticles may be investigated for their suitability in delivering SS-DNA or SS-RNA into a cell. The attachment of the amine groups in cytosine, guanine, and adenine found in both DNA and RNA to an aldehyde produces a Shiff base which may be reversible in a lower pH environment or within a cell. Further investigation of this protocol for cell studies would be rewarding.

REFERENCES

[1] Abdullayev, E., Joshi, A., Wei, W., Zhao, Y., Lvov, Y. 2012. "Enlargement of halloysite clay nanotube lumen by selective etching of aluminum oxide." *ACS Nano.*

[2] Abdullayev, E., Price, R., Shchukin, D., Lvov, Y. 2009. "Halloysite tubes as nanocontainers for anticorrosion coating with benzotriazole." *ACS Appl. Mater. Interfaces* 1437-1443.

[3] Abdullayev, E., Sakakibara, K., Okamoto, K., Wei, W., Ariga, K., Lvov, Y. 2011. "Natural tubule clay template synthesis of silver nanorods for antibacterial composite coating." *ACS Applied Materials & Interfaces* 4040--6.

[4] Agotegaray, M., Lassalle, V. 2017. *Silica coated nanoparticles.* Springer Briefs in Molecular Science.

[5] Ahmed, F.R., Shoaib, M.H., Azhar, M., Um, S.H., Yousuf, R.I., Hashmi, S. and Dar, A.,. 2015. "In-vitro assessment of cytotoxicity of halloysite nanotubes agaisnt HepG2, HCT116 and human peripheral blood lymphocytes." *Colloids and Surfaces B: Biointerfaces* 50-55.

[6] Allen, D., Cooksey, C., Tsai, B. 2018. "Spectrophotometry." National Institute of Standards and Technology.

[7] Almeida, J. P., A. L. Chen, A. Foster, and R. Drezek. 2011. "In vivo biodistribution of nanoparticles." *Nanomedicine* 815-35.

[8] Amendola, V., Bakr, O., Stellacci, F. 2010. "A study of the surface plasmon resonanace of silver nanoparticles by the discrete dipole approximation method: effect of shape, size, structure, and assembly." *Plamonics* 85-97.

[9] Arkles, B. 1977. "Tailoring surfaces with silanes." *CHEMTECH* 766-78.

[10] Bahdra, Sambhu. 2009. "Progress in preparation, processing and applications of polyaniline." *Progress in Polymer Science* 783-810.

[11] Bamfield, P., Hutchings, M. 2010. *Chromic phenomena.* Cambridge: RSC Publishing.

[12] Bates. T., Hildebrand, F., Swineford, A. 1950. "Morphology and structure of endellite and halloysite." 463-84.

[13]   Baxter, I., Cother, L., Dupuy, C. 1997. "Hydrogen bonding to silanols." *Electronic Conference on Organometallic Chemistry.*

[14]   Bellucci, D., Sola, A., Anesi, A., Salvatori, R., Chiarini, L. 2015. "Bioactive glass/hydroxyapatite composites: Mechanical properties and biological evaluation." *Mater Sci Eng C Mater Biol Appl.*

[15]   Berthier, P. 1826. "Analyse de l'halloysite." *Ann Chim Phys Vol 32* 332-335.

[16]   Bertolino, V., Cavallaro, G., Lazzara, G., Milioto, S., Parisi, F. 2017. "Biopolymer-targeted adsorption onto halloysite nanotubes in aqueous media." *Langmuir.*

[17]   Bertotti, G. 1998. *Hysteresis in magnetism: For physicists, materials scientists, and engineers.* Academic Press.

[18]   Bin Mu, Mingfei Zhao, Peng Liu. 2008. "Halloysite nanotubes grafted hyperbranched (co)polymers via surface-initiated self-condensing vinyl (co)polymerization." *J Nanopart Res* 831-838.

[19]   Boissière, C., Larbot, A., Van der Lee, A., Kooyman, P., Prouzet, E. 2000. "A new synthesis of mesoporous msu-x silica controlled by a two step pathway." *Chemistry of Materials* 2902-2913.

[20]   Bottino, M.C., Batarseh, G., Palasuk, J., Alkatheeri, M.S., Windsor, L.J. and Platt, J.A.,. 2013. "Nanotubemodified modified dentin adhesive - Physiochemical and dentin bonding characterizations." *Dental Materials* 1158-1165.

[21]   Brindley, George W. 1952. "Structural mineralogy of clays." *Clays and Clay Minerals 1* 33-43.

[22]   2016. "A Non-invasive fluorescence-based oxygen sensor and platform for studying cell responses to metabolic agents in real-time."

[23]   Burns, A., Ow, H,. Wiesner, U. 2006. "Fluorescent core-shell silica nanoparticles: towards "lab on a particle" architectures for nanobiotechnology." *Chem Soc Rev 35* 1028-1042.

[24]   Cairns, Donald. 2008. *Essentials of pharmaceutical chemistry.* London: Pharmaceutical Press.

[25]   Carlisle, E.M. 1986. "Silicon as an essential trace element in animal nutrition." *Ciba Foundation Symposium* 123-39.

[26]   Carlisle, E.M. 1986. "Silicon biochemstry." *Ciba Foundation Symposium* 123-139.

[27] Cataldo, S., Lazzara, G., Massaro, M., Muratore, N,, Pettignano, A., Riela, S. 2018. "Functionalized halloysite nanotubes for enhanced removal of lead(II) ions from aqueous solutions." *Applied Clay Science* 87-95.

[28] Cavallaro, G., Lazzara, G., Milioto, S. 2012. "Exploiting the colloidal stability and solubilization ability of clay nanotubes/ionic surfactant hybrid nanomaterials." *The Journal of Physical Chemistry C.*

[29] Cavallaro, G., Lazzara, G., Milioto, S., Palmisano, G., Parisi, F. 2014. "Halloysite nanotube with fluorinated lumen: Non-foaming nanocontainer for storage and controlled release of oxygen in aqueous media." *Journal of Colloid and Interface Science.*

[30] Cavallaro, G., Lazzara, G., Milioto, S., Parisi, F. 2015. "Hydrophobically modified halloysite nanotubes as reverse micelles for water-in-oil emulsion." *Langmuir* 7472-8.

[31] Chang, P., Xie, Y,, Wu, D., Ma, X. 2011. "Amylose wrapped halloysite nanotubes." *Carbohydrate Polymers* 1426-9.

[32] Chen, F., Hableel, G., Zhao, E., Jokerst, J. 2018. "Multifunctional nanomedicine with silica: role of silica in nanoparticles for theranostic, imaging, and drug monitoring." *Journal of Colloidal and Interface Science.*

[33] Ćirić-Marjanović, G. 2010. *Polyaniline nanostructures, in nanostructured conductive polymers.* Chichester: John Wiley & Sons.

[34] Ciriminna, M., Pagliaro, R. 2009. "Organofluoro-silica xerogels as high-performance optical oxygen sensors." *Analyst* 1531-5.

[35] De Silva, R., Pasbakhsh, P., Lee, S., Kit, A. 2015. "ZnO deposited/encapsulated halloysite–poly(lactic acid) (PLA) nanocomposites for high performance packaging films with improved mechanical and antimicrobial properties." *Applied Clay Science* 10-20.

[36] Guo, B., Jia, D. 2010. "Newly emerging applications of halloysite nanotubes: A review." *Polym Int*. 574-582.

[37] Eklund, S.E. 2003. "Modification of the CytosensorTM microphysiometer to simultaneously measure extracellular acidification and oxygen consumption rates." *Analytica Chemica* 93-101.

[38] Elsabahy, M., Wooley, K. 2013. "Cytokines as biomarkers of nanoparticle immunotoxicity." *Chemical Society Reviews* 5552-5576.

[39] Feng, K., Hung, G., Liu, J., Li, M., Zhou, C., Liu, M. 2018. "Fabrication of high performance superhydrophobic coatings by spray-coating of polysiloxane modified halloysite nanotubes." *Chemical Engineering Journal* 744-54.

[40]   Fernandez, L.D., Lara, E., Mitchell, E.A. 2015. "Checklist, diversity and distribution of testate amoebae in Chile." *Eur J Protistol* 409-24.

[41]   Flörke, Otto W. et al. 2008. *Ullmann's encyclopedia of industrial chemistry.* Wiley VCH.

[42]   Fu, H., Wang Y., Li, X., Chen, W. 2016. "Synthesis of vegetable oil-based waterborne polyurethane/silver-halloysite antibacterial nanocomposites." *Composites Science and Technology* 86-93.

[43]   Gao, B., Ding, S., Kargbo, O., Wang, Y., Sun, Y., Cosnier S. 2013. "Enhanced electrochemiluminescence of peroxydisulfate by electrodeposited Au nanoparticles and its biosensing application via integrating biocatalytic precipitation using self-assembly bi-enzymes." *Journal of Electroanalytical Chemistry* 9-13.

[44]   Garcia-Garcia, D., Ferri, J., Ripoll, L., Hidalgo, M., Lopez-Martinez, J., Balart, R. 2017. "Characterization of selectively etched halloysite nanotubes by acid treatment." *Applied Surface Science* 616-25.

[45]   Garrett, P. 1992. *Defoaming: theory and industrial applications Vol 45.* New York: CRC Press: 1992.

[46]   Griffith, J. and Orgel, L. 1957. "Ligand Field Theory." *Rev Chem Soc* 381-383.

[47]   Grist, S.M. 2010. "Optical oxygen sensors for applications in microfluidic cell culture." *Sensors* 9286-316.

[48]   Guimarães, L., Enyashin, A., Seifert, G., Duarte, H. 2010. "Structural, electrical and mechanical properies of single-walled halloysite nanotube models." *J. Phys. Chem* 11358-11363.

[49]   Hashemifard, S., Ismail, A., Matsuura T. 2011. "Mixed matrix membrane incorporated with large pore size halloysite nanotubes (HNT) as filler for gas separation." *Journal of Colloid and Interface Science* 359-70.

[50]   Hollas, M. 2004. *Modern Spectroscopy.* Hoboken: John Wiley & Sons.

[51]   Holleman, A. F., Wiberg, E. 2001. *Inorganic Chemistry.* San Diego/Berlin: Academic Press/De Gruyter.

[52]   Hornung, V., Bauernfeind, F., Halle, A. 2008. "Silica crystals and aluminum salts activate the NALP3 inflammasome through phagosomal destabilization." *Nature Immunology* 847-856.

[53]   Hu, Y., Chen, J., Li, X., Su, Y., Huang, S., Li, Y., Liu, H., Xu, J. and Zhong, S. ,. 2017. "Multifunctional halloysite nanotubes for targeted delivery and controlled release of doxorubicin in -vitro and in-vivo studies." *Nanotechonology* 1-40.

[54]   Hu, Y., Chen, Li, Sun, Huang, Li, Liu, Xu, Zhong. 2017. "Multifunctional halloysite nanotubes for targeted delivery and controlled release of doxorubicin in-vitro and in-vivo studies." *Nanotechnology 28.*

[55]   Ibrahim, G., Isloor, A., Moslehyani, A., Ismail, A. 2017. "Bio-inspired, fouling resistant, tannic acid functionalized halloysite nanotube reinforced polysulfone loose nanofiltration hollow fiber membranes for efficient dye and salt separation." *Journal of Water Process Engineering* 138-48.

[56]   Iler, R. K. 1979. *The chemistry of silica.* Plenum Press.

[57]   Jiang. L., Zhang, C., Wei, J., Tjiu, W., Pan, J., Chen, Y,, et al. 2014. "Surface modifications of halloysite nanotubes with superparamagnetic Fe3O4 nanoparticles and carbonaceous layers for efficient adsorption of dyes in water treatment." *Chemical Research in Chinese Universities* 971-7.

[58]   Johnston, C., Driscoll, K., Finkelstein, J. 2000. "Pulmonary chemokine and mutagenic responses in rats after subchronic inhalation of amorphous and crystalline silica." *Toxicol Sci* 405-413.

[59]   Jokerst, J. V., T. Lobovkina, R. N. Zare, and S. S. Gambhir. 2011. "Nanoparticle PEGylation for imaging and therapy." *Nanomedicine* 715-728.

[60]   Jugdaohsingh, R. 2007. "Silicon and bone health." *The Journal of Nutrition, Health and Aging* 99-110.

[61]   Kamble, R., Ghag, M., Gaikawad, S. 2012. "Halloysite nanotubes and applications: A review." *Journal of Advanced Scientific Research, 2012, 3(2)* 25-29.

[62]   Kang, E.T. 1996. "The protonation-deprotonation hysteresis in polyaniline." *Polymer* 925-929.

[63]   Kang, Z., Liu, Y., Lee, S. 2010. "Small-sized silicon nanoparticles: New nanolights and nanocatalysts." *Nanoscale.*

[64]   Kerr, Paul F. 1952. "Formation and occurrence of clay minerals." *Clays and Clay Minerals* 19-32.

[65]   Koivisto, A.J., et al.,. 2018. "Occupational exposure during handling and loading of halloysite nanotubes – A case study of counting nanofibers. ." *NanoImpact* 153-160.

[66] Kolbe, Gerhard. 1956. *Das komplexchemische verhalten der kieselsäure.* Jena: Friedrich-Schiller Universitat Jena.

[67] Kreft, S., Kreft, M. 2009. "Quantification of dichromatism: a characteristic of color in transparent materials." *Journal of the Optical Society of America* 1576-181.

[68] Kryuchkova, M., Danilushkina, A., Lvov, Y. and Fakhrullin, R. ,. 2016. "Evaluation of toxicity of nanoclays and graphene oxide in vivo: A Paramecium caudatum study. ." *Environmental Sciences: Nano* 442-452.

[69] Kui, Steven. 2013. "Robust phosphorescent platinum(ii) complexes containing tetradentate ONCN ligands." *Chemistry, European Journal.*

[70] Labbaf, S., O. Tsigkou, K. H. Müller, M. M. Stevens, A. E. Porter, and J. R. Jones. 2011. "Spherical bioactive glass particles and their interaction with human mesenchymal stem cells in vitro." *Biomaterials* 1010-1018.

[71] Li, C., Liu, J,. 2009. "A general synthesis approach toward halloysite-based composite nanotube." *Journal of Applied Polymer Science* 2647–55.

[72] Li, X. et al. 2012. "Study on the Adsorption Mechanism of DNA with Mesoporous Silica Nanoparticles in Aqueous solution." *Langmuir.*

[73] Lin, W., Huang, Y., Zhou, X. 2006. "In vitro toxicity of silica nanoparticles in human lung cells." *Toxicology and Applied Pharmacology.*

[74] Lin, Y. S., Hurley, K. R., & Haynes, C. L. (. 2012. "Critical considerations in the biomedical use of mesoporous silica nanoparticles." *Journal of Physical Chemistry Letters* 364-374.

[75] Liu, M., Guo, B., Du, M., Cai, X. 2007. "Properties of halloysited nanotube-epoxy resin hybrids and the interfacial reactions in the systems." *Nanotechnology.*

[76] Liu, T., L. Li, X. Teng, X. Huang, H. Liu, D. Chen, J. Ren, J. He, and F. Tang. 2011. "Single and repeated dose toxicity of mesoporous hollow silica nanoparticles in intravenously exposed mice." *Biomaterials* 1657-1668.

[77] Long, Z. et al. 2017. "Polyethyleneimine grafted short halloysite nanotubes for gene delivery." *Materials Science and Engineering: C.*

[78] Luo, P. et al. 2011. "Preparation and characterization of silane coupling agent modified halloysite for cr(VI) removal." *Ind Eng Chem Res* 10246-52.

[79] Lvov, Y., Shchukin, D., Mohwald, H, Price, R. 2008. "Halloysite clay nanotubes for controlled release of protective agents." *J Phys Chem C* 958-964.

[80]   Lvov, Y., Shchukin, D., Mohwald, H., Price, R. 2008. "Halloysite clay nanotubes for controlled release of protective agents." *ACS Nano.*

[81]   Lvov, Y.M., DeVilliers, M.M. and Fakhrullin, R.F. ,. 2016. "The application of halloysite tubule nanoclay in drug delivery." *Expert Opin. Drug. Deliv* 977-986.

[82]   MacDiarmid, A. 1986. *Synthetic metals* 193.

[83]   MacDiarmid, Alan. 1995. "Secondary doping in polyaniline." *Synthetic Metals* 85-92.

[84]   Madsen, J., Canton, I., Warren, N. et al. 2013. "Nile blue based nanosized pH sensors for simultaneous far-red and near-infrared live bioimaging." *Journal of the American Chemical Society.*

[85]   Maleki, A., Hajizadeh, Z., Firouzi-Haji, R. 2018. "Eco-friendly functionalization of magnetic halloysite nanotube with SO3H for synthesis of dihydropyrimidinones." *Microporous and Mesoporous Materials* 46-53.

[86]   Mao, Y., Daniel, L.N., Whittaker, N., Saffiotti, U. 1994. "DNA binding to cyrstalline silica characterized by fourier transform infrared spectroscopy." *Enviorn Health Perspect.*

[87]   Massaro, M. et al. 2016. "Direct chemical grafted curcumin on halloysite nanotubes as dual-responsive prodrug for pharmacological applications." *Colloids and Surfaces B: Biointerfaces* 505-13.

[88]   Massaro, M. et al. 2018. "Functionalized halloysite nanotubes: Efficient carrier systems for antifungine drugs." *Applied Clay Science* 186-92.

[89]   McDiarmid. 1987. "Polyaniline: A new concept in conducting polymers." *Synthetic Metals.*

[90]   McNeil, S.E. 2005. "Nanotechnology for the biologist." *Journal of Leukocyte Biology* 585-594.

[91]   Meyer, A., Sandler, D., Freeman, L. 2017. "Pesticide exposure and risk of rheumatoid arthritis among licensed male pesticide applicators in the agricultural health study." *Environ Health Perspect.*

[92]   Mills, D., Lvov, Y.M. 2015. Ceramic nanotube composites with sustained drug release capability for implants, bone repair and regenaration,. United States Patent

[93]   Zhao, M. and Liu, P. 2008. "Halloysite nanotubes grafted hypebranched (co)polymers via surface-initiated self-condensing vinyl (co)polyerization." *J Nanopart Res* 831-838.

[94]   Muller, W.E et all. 2011. *the unique invention of the siliceous sponges: Their enzymatically made biosilica skeleton.* Berlin: Springer.

[95]   Nascimento, Gustavo M. Do. 2010. "Spectroscopy of polyaniline nanofibers." In *Nanofibers*, by Ashok Kumar. InTech.

[96]   Nassau, K. 1983. *The physics of chemistry and color.* New York: John Wiley & Sons.

[97]   Nicholson, J. 2002. *The chemistry of medical and dental materials.* Royal Society of Chemistry.

[98]   Ninfa, A., Ballou, D. 2004. *Fundamental laboratory approaches for biochemistry and biotechnology.* Hoboken: Wiley.

[99]   Ortiz-Quiñonez, J.L., C Vega-Verduga, D Díaz, and I Zumeta-Dubé. 2018. "Transformation of bismuth and β-Bi2O3 nanoparticles into (BiO)2CO3 and (BiO)4(OH)2CO3 by capturing CO2: The role of halloysite nanotubes and "sunlight" on the crystal shape and size." *Crystal Growth and Design* 4334-4346.

[100] Ouyang, J., et al. 2016. "Radical guided selective loading of silver nanoparticles at interior lumen and out surface of halloysite nanotubes." *Materials & Design.*

[101] Papke, Keith G. 1971. "Halloysite deposits in the Terraced Hills, Washoe County, Nevada." *Clays and Clay Minerals* 71-74.

[102] Park, J.-H., L. Gu, G. v. Maltzahn, E. Ruoslahti, S. N. Bhatia, and M. J. Sailor. 2009. "Biodegradable luminescent porous silicon nanoparticles for in vivo applications." *Nat Mater* 331-6.

[103] Pauling, L. 1939. "The theory of the color of dyes." *Proc Natl Acad Sci USA* 577-585.

[104] Peng Yuan, Peter DS, Zongwen Liu, Malcolm ER Green, James MHook, Sarah J et al. 2008. "Halloysite nanotubes and applications: A review." *Phys. Chem*. 15742-15751.

[105] Pitchford. S. 2001. " Ligand Characterization Using Microphysiometry."*Neuroscience*. 7-17.

[106] Pohaku-Mitchell, K., Liberman, A., Kummel, A. C., Trogler, W. C. 2012. "Iron(III)-doped, silica nanoshells: A biodegradable form of silica." *Journal of the American Chemical Society* 13997-14003.

[107] Price, R., Gaber, B., Lvov, Y. 2001. "In-vitro release characteristics of tetracycline HCL, khellin and nicotinamide adenine dinucleotide from halloysite." *J Microencapsul* 713-722.

[108]   Qui, R., Yin, S. et al. 2009. "Synthesis and structure of air-stable cationic organobismuth complex and its use as a highly efficient catalyst for direct diastereoselective Mannich reaction in water." *Royal Society of Chemistry.*

[109]   Rawtani, D., Agrawal, Y. 2012. "Multifarious applications of halloysite nanotubes: A review." *Rev Adv Mater Sci* 282–95.

[110]   Reffitt, D. M., Jugdaohsingh, R., Thompson, R. P. H. 1999. "Silicic acid: Its gastrointestinal uptake and urinary excretion in man and effects on aluminium excretion." *Journal of Inorganic Biochemistry* 141-47.

[111]   Rieter, W., Kim, J., Taylor, K., An, H., Lin, W., Tarrant, T., Lin, W. 2007. "Hybrid silica nanoparticles for multimodal imaging." *Angewandte Chemie.*

[112]   Rimsza, J., Jones, R., Criscenti, L. 2018. "Interaction of NaOH solutions with silica surfaces." *Journal of Colloid and Interface Science* 128-37.

[113]   Robson, Harry E. 1976. Synthetic halloysites as hydrocarbon conversion catalysts. USA Patent US4098676.

[114]   Rondeau, V., Jacqmin-Gadda, H., Commenges, D., Helmer, C. 2008. "Aluminum and silica in water and the risk of alzheimer's disease or congnitive decline: Findings from 15-year follow up of the PAQUID cohort." *American Journal of Epidemiology* 489-96.

[115]   Ronkainen, N., Halsall, H., Heineman, W. 2010. "Electrochemical biosensors." *Chemical Society Reviews* 1747-1763.

[116]   Rosi, N., Thaxton, S., Mirkin, C. 2004. "Control of nanoparticle assembly by using dna-modified diatom templates." *Angewandte Chemie International 43* 5500-5503.

[117]   Ruiz-Hitzky, E., Aranda, P., Darder, M. and Rytwo, G. ,. 2010. "Hybrid materials based on clays for environmental and biomedical application." *Journal of Materials Chemistry,* 9306-9321.

[118]   S.E. Gratton, P.A. Ropp, P.D. Pohlhaus, J.C. Luft, V.J. Madden, M.E. Napier. 2008. "The effect of particle design on cellular internalization pathways." *Proc. Natl. Acad. Sci. U. S. A. 105* 11613–11618.

[119]   Sabnis, R. 2007. *Handbook of acid-base indicators.* CRC Press: Boca Raton.

[120]   Sakiewicz, P., M. Lutynski, J. Soltys, and A Pytlinski. 2016. "Purification of halloysite by magnetic separation." *Physiochemical Problems of Mineral Processing* 991-1001.

[121]   Sanchez-Ballester N.M., Ramesh GV, Tanabe T, Koudelkova E, Liu J, Shrestha LK, et al. 2015. "Activated interiors of clay nanotubes for agglomeration-tolerant automotive exhaust remediation." *Journal of Materials Chemistry A* 6614-9.

[122]   Shamsi MH, Geckeler KE. 2008. "The first biopolymer-wrapped non-carbon nanotubes." *Nanotechnology.*

[123]   Shamsi, M.H., Geckeler, K.E. 2008. "The first biopolymer-wrapped non-carbon nanotubes." *Nanotechnology.*

[124]   Shao, L, et al. 2017. "A highly sensitive ascorbic acid sensor based on hierarchical polyaniline coated halloysite nanotubes prepared by electrophoretic depositio." *Electrochimica Acta.*

[125]   Shi, Y., Tian, Z., Zhang, Y., Shen, H. and Jia, N. ,. 2011. "Functionalized halloysite nanotube-based for intracellular delivery of antisense oligonucleotides." *Nanoscale Research Letters* 1-7.

[126]   Sileika, T. et al. 2013. "Colorless multifunctional coatings inspired by polyphenols found in tea, chocolate, and wine." *Angew Chem Int Ed Engl* 10766-70.

[127]   Skoog, D., Holler, F., Crouch, S. 2007. *Principles of intrumental analysis.* Belmont, CA: Thomson Brooks Cole.

[128]   Solomon, Sally. 2012. "Synthesis and study of silver nanoparticles." *Journal of Chemical Education, ACS Publications.*

[129]   Spyrnskyy, M., Niedojadlo, J., Buszewisk, B. 2011. "Structural features of natural and acids modified chrysotile nanotubes." *Journal of Physics and Chemistry of Solids* 1015-1026.

[130]   Stöber, W., Bohn, E. 1968. "Controlled growth of monodispersive silica spheres in the micron size range." *Colloid Interface Sci* 62.

[131]   Stöber, W., Fink, A., Bohn, E. 1968. "Controlled growth of monodispersive silica spheres in the micron size range." *Journal of Colloid and Interface Science* 62-69.

[132]   Sun, P. et al. 2015. "Effective activation of halloysite nanotubes by piranha solution for amine modification via silane coupling chemistry." *RSC Advances* 52916-25.

[133]   Tada, K., Onoda, M. 2005. "Electrophoretic deposition through colloidal suspension: A way to obtain nanostructured conjugated polymer film." *Synth. Met. 152* 341–344.

[134] Tamada, O., Gibbs, G., Boisen, M., Rimstidt, J. 2012. "Silica dissolution catalyzed by NaOH: Reaction kinetics and energy barriers simulated by quantum mechanical strategies." *Journal of Mineralogical and Petrological Sciences* 87-89.

[135] Tanaka, K., Kitamura, K. 2008. "Multi-modal F NMR probe using perfluorinated cubic silsesquioxane-coated silica nanoparticles for monitoring enzymatic activity." *Chem Commun* 6176-6178.

[136] Tang, L., Gabrielson, N. P., Uckun, F. M., Fan, T. M., & Cheng, J. 2013. "Size dependent tumor penetration and in vivo efficacy of monodisperse drug–silica nanoconjugates." *Molecular Pharmaeutics* 883-892.

[137] Thanawala, K., Khanna, A., Singh Raman, R., Bohm, S. 2015. "Smart anti-corrosive self-healing coatings using halloysite nanotubew as host for entrapment of corrosion inhibitors." *Corrosion & Prevention.* Paper 17.

[138] Thevenot, D., Toth, K., Durst, R., Wilson, G. 2001. "Electrochemical biosensors: Recommended definitions and classification." *Analytical Letters* 634-659.

[139] Tsai, C.., C.. Chen, Y. Hung, F.. Chang, and C.. Mou. 2009. "Monoclonal antibody-functionalized mesoporous silica nanoparticles (MSN)for selective targeting breast cancer cells." *Journal of Materials Chemistry* 5737-5743.

[140] Tully, J., Yendluri, R. and Lvov, Y.,. 2015. "Halloysite clay nanotubes for enzyme immobilization." *Biomacromolecules* 615-621.

[141] Tzamalis, G. 2003. "Applicability of the localization-interaction model to magnetoconductivity studies of polyaniline films at the metal-insulator boundary." *Physical Review B.*

[142] Updike, S.J. 1967. "The enzyme electrode." *Nature* 986-988.

[143] Vallet-Regi, M., Ragel, C., Salinas, A. 2003. "Glasses with medical applications." *European Journal of Inorganic Chemstry* 1029-1042.

[144] Vallet-Regí, M., Salinas, A. J., & Arcos, D. 2006. "From the bioactive glasses to the star gels." *Journal of Materials Science: Materials in Medicine* 1011-1017.

[145] Veerabadran, N., Mongayt, D., Torchilin, V., Price, R., Lvov, Y. 2009. "Organized shells on clay nanotubes for controlled release of macromolecules." *Macromolecular Rapid Communications* 99-103.

[146] Vergaro, V. et al. 2010. *Biomacromolecules* 820-826.

[147] Vinokurov, V. et al. 2017. "Formation of metal clusters in halloysite clay nanotubes." *Science and Technology of Advanced Materials* 147.

[148]   Wan, Y., Zhao, D. 2007. "On the controllable soft-templating approach to mesoporous silicates." *Chem. Rev.* 2821-2860.

[149]   Wang R, Jiang G, Ding Y, Wang Y, Sun X, Wang X, et al. 2011. "Photocatalytic activity of heterostructures based on TiO2 and halloysite nanotubes." *ACS Applied Materials & Interfaces* 4154-8.

[150]   Wang, L, et al. 2013. "Halloysite nanotube supported ru nanocatalysts synthesized by the inclusion of preformed ru nanoparticles for preferential oxidation of CO in H2 rich atmosphere." *The Journal of Physical Chemistry C* 4141-51.

[151]   Wang, Q., et al. 2014. "Adsorption and release of ofloxacin from acid- and heat-treated halloysite." *Colloids and Surfaces B: Biointerfaces* 51-9.

[152]   Wang, Y. et al. 2015. "Mesoporous silica nanoparticles in drug delivery and biomedical applications." *Nanomedicine: Nanotechnology, Biology and Medicine* 313-327.

[153]   Wang, Y., Sun, L., Jiang, T., Zhang, J., Zhang, C., Sun, C., et al. 2014. "The investigation of MCM-48-type and MCM-41-type mesoporous silica as oral solid dispersion carriers for water insoluble cilostazol." *Drug Development and Industrial Pharmacy.*

[154]   Wei, J.H. 2007. "Conductance switching, hysteresis, and magnetoresistance in organic semiconductors." *Organic Electronics* 487-497.

[155]   Wei, Q., Amin, D., Messersmith, P. 2015. "Polymer directed self-assembly of pH responsive antioxidant nanoparticles." *Langmuir 31.*

[156]   Williams, S., Davies, P., Allender, C. 2013. "Controlling the nanoscale patterning of AuNPs on silicon surfaces." *Nanomaterials* 192-203.

[157]   Wilson, M.J. 1999. "The origin and formation of clay minerals in soils: Past present and future perspectives." *Clay Minerals 34* 7-25.

[158]   Wu, S. H., Mou, C. Y., & Lin, H. P. 2013. "Synthesis of mesoporous silica nanoparticles." *Chemical Society Reviews* 3862-3875.

[159]   Wu, S., Qiu, M., Guo, B,, Zhang, L., Lvov, Y. 2017. "Nanodot-loaded clay nanotubes as green and sustained radical scavengers for elastomer." *ACS Sustainable Chemistry & Engineering.*

[160]   Yah, W.O., Xu, H., Soejima, H., Ma, W., Lvov, Y., Takahara, A. 2012. "Biomimetic dopamine derivative for selective polymer modification of halloysite nanotube lumen." *Journal of the American Chemical Society.*

[161]   Yang, S., et al. 2014. "New insight into PEO modified inner surface of HNTs and its nano-confinement within nanotube." *Journal of Materials Science.*

[162]   Yang, Y. Zhang, and J. Ouyang,. 2016. "Physicochemical Properties of Halloysite." *Developments in Clay Science* 67 - 91.

[163]   Yeh, T. et al. 2006. "Highly sensitive optical fiber oxygen sensor using Pt(II) complex embedded in sol-gel matrices." *Sensors and Actuators B.*

[164]   Yendluri, R., Otto, D.P., De Villiers, M.M. and Vinokurov, V.,. 2017. "Application of halloysite clay nanotubes as a pharmaceutical excipient." *International Journal of Pharmaceutics* 287-273.

[165]   Yu, H. et al. 2014. "Improving the antifouling property of polyethersulfone ultrafiltration membrane by incorporation of dextran grafted halloysite nanotubes." *Chemical Engineering Journal* 322-8.

[166]   Yuan P, Southon PD, Liu Z, Kepert CJ. 2012. "Organosilane functionalization of halloysite nanotubes for enhanced loading and controlled release." *Nanotechnology* 7216-26.

[167]   Yuan P., Tan D., Annabi-Bergaya F. 2015. "Properties and applications of halloysite nanotubes: recent research advances and future prospects." *Applied Clay Science* 112-113, 75-93.

[168]   Yuan, P., Southon, P., Liu, Z., Green, M., hook, J., Antill, S., Kepert, C. 2008. "Functionalization of halloysite clay nanotubes by grafting with γ-Aminopropyltriethoxysilane." *J. Phys. Chem. C* 15742–15751.

[169]   Yuri ML, Dmitry GS, Helmuth M, Ronald R. 2008. Halloysite nanotubes and applications: A review. *ASC Nano* 814-820.

[170]   Zeng. S., Reyes, C,, Liu. J,. 2014. "Facile hydroxylation of halloysite nanotubes for epoxy nanocomposite applications." 6519-28.

[171]   Zeng. X., Wang, Q. 2017. "Catalytically active silver nanoparticles loaded in the lumen of halloysite nanotubes via electrostatic interactions." *Journal of Materials Science.*

[172]   Zhang Y, Yang H. 2012. "Co3O4 nanoparticles on the surface of halloysite nanotubes." *Physics and Chemistry of Minerals* 789-95.

[173]   Zhang, H. Y., D. R. Dunphy, X. M. Jiang, H. Meng, B. B. Sun, D. Tarn, M. Xue, X. Wang, and S. J. Lin. 2012. "Processing pathway dependence of amorphous silica nanoparticle toxicity: colloidal vs pyrolytic." *Journal of the American Chemical Society* 15790-15804.

[174]   Zhang, S., Du, Z., Li, G. 2011. *Anal Chem* 7531-41.

[175]   Zhang, Y., Gao, R., Liu, M., Shi, B., Shan, A. and Cheng, B.,. 2015. "Use of modified halloysite nanotubes in the feed reduces the toxic effects of zearalenone on sow reproduction and piglet development." *Theriogenology* 932-941.

[176]   Zhao, D., J. Feng, Q. Huo, N. Melosh, G. H. Fredrickson, B. F. Chmelka, and G. D. Stucky. 1998. "Triblock copolymer syntheses of mesoporous silica with periodic 50 to 300 angstrom pores." *Science* 548-552.

[177]   Zhao, X., Bagwe, R., Tan, W. 2004. "Development of organic-dye-doped silica nanoparticles in a reverse microemulsion." *Advanced Materials* 173-176.

[178]   Zollinger, H. 2003. *Color chemistry: Synthesis, properties and applications of organic dyes and pigments.* Weihham: Wiley-VCH.

[179]   Zou, M,, Du, M., Zhu, H., Xu, C., Fu, Y. 2012. "Green synthesis of halloysite nanotubes supported Ag nanoparticles for photocatalytic decomposition of methylene blue." *Journal of Physics D: Applied Physics.*